



**HAL**  
open science

# Anderson Localization in high dimensional lattices

Elena Tarquini

► **To cite this version:**

Elena Tarquini. Anderson Localization in high dimensional lattices. Condensed Matter [cond-mat]. Université Paris Saclay (COMUE), 2016. English. NNT : 2016SACLS540 . tel-01727220

**HAL Id: tel-01727220**

**<https://theses.hal.science/tel-01727220>**

Submitted on 9 Mar 2018

**HAL** is a multi-disciplinary open access archive for the deposit and dissemination of scientific research documents, whether they are published or not. The documents may come from teaching and research institutions in France or abroad, or from public or private research centers.

L'archive ouverte pluridisciplinaire **HAL**, est destinée au dépôt et à la diffusion de documents scientifiques de niveau recherche, publiés ou non, émanant des établissements d'enseignement et de recherche français ou étrangers, des laboratoires publics ou privés.

NNT : 2016SACLS540

THÈSE DE DOCTORAT  
DE L'UNIVERSITÉ PARIS-SACLAY  
PRÉPARÉE À L'UNIVERSITÉ PARIS-SUD

Ecole doctorale n°564  
Physique en Île-de-France  
Spécialité de doctorat : Physique

par

**MILLE ELENA TARQUINI**

Anderson Localization in high dimensional lattices

Thèse présentée et soutenue à Paris, le 12 Décembre 2016.

Composition du Jury :

M. ALBERTO ROSSO	Directeur de Recherche Université Paris-Saclay	(Président du jury)
M. VLADIMIR KRAVTSOV	Professional Staff P-5 ICTP (Trieste)	(Rapporteur)
M. YAN V. FYODOROV	Professor King's College London	(Rapporteur)
M. J.-PHILIPPE BOUCHAUD	Professeur CFM et École Polytechnique	(Examineur)
M. GABRIEL LEMARIÉ	Chargé de Recherche Université Paul Sabatier (Toulouse)	(Examineur)
M. GIULIO BIROLI	Directeur de Recherche IPhT - CEA (Saclay)	(Directeur de thèse)
M. MARCO TARZIA	Maître de Conférence LPTMC - Université Paris VI	(Invité)



# Contents

<b>Introduction</b>	<b>3</b>
<b>I The Anderson Localization Transition: introduction</b>	<b>1</b>
I.1 Disorder and Localization	1
I.2 Characteristics of the transition and localized states	5
I.3 Anderson Localization in one and two dimensions and weak localization	7
I.4 Scaling theory and field theory formulation	9
I.5 Anderson transition on the Bethe Lattice: mean field	12
I.6 Anderson Localization and Random Matrix Theory	13
I.7 Brief review on numerical results	17
I.8 Experiments on Localization	18
I.9 Open problems	21
I.9.1 Interactions and Many Body Localization	22
I.9.2 The problem of the intermediate phase	23
<b>II Overview on analytical techniques and known results</b>	<b>27</b>
II.1 Definitions	27
II.2 Cavity equations	29
II.2.1 On the Bethe Lattice	32
II.3 Supersymmetric method	34
II.4 Dyson Brownian motion model	43
<b>III Localization Transitions of Lévy Matrices</b>	<b>49</b>
III.1 Introduction and motivations	49
III.2 The recursion equation for the resolvent	52
III.3 The density of states	53
III.4 Computation of the mobility edge	57
III.4.1 The mapping to directed polymers in random media	61
III.5 Numerical check of the phase diagram	65
III.6 The problem of the intermediate phase: previous results	68
III.7 The Supersymmetric method applied to Lévy Matrices	71
III.7.1 Equation on $\mathbf{R}(\boldsymbol{\Sigma})$ with the supersymmetric method	73
III.8 The Dyson Brownian motion argument	74
III.9 Numerical results for $\mu \in (1, 2)$	76
III.10 Numerical results for $\mu \in (0, 1)$	80

III.10.1 Numerical results for $Q(G)$ . . . . .	84
III.10.2 Wavefunction statistics and multifractal spectrum . . . . .	88
III.11 Summary of the results . . . . .	96
<b>IV Critical properties of the Anderson model in high dimension</b>	<b>101</b>
IV.1 Numerical results in $d = 3, \dots, 6$ . . . . .	103
IV.1.1 Transport properties . . . . .	103
IV.1.2 Statistics of level spacings and of wave-functions coefficients . . .	110
IV.2 Strong Disorder RG . . . . .	116
IV.3 Summary of the results . . . . .	125
<b>Conclusion and perspectives</b>	<b>131</b>
<b>A Transfer Matrix, conductance and localization length</b>	<b>135</b>
A.1 Transfer Matrix and conductance . . . . .	135
A.2 Transfer Matrix and localization length . . . . .	137
<b>B Critical wave functions: multifractality</b>	<b>141</b>
<b>C The IPR in terms of the Green function</b>	<b>145</b>
<b>D The DoS of Sparse RM model with the supersymmetric method</b>	<b>147</b>
<b>E Meaning of the order parameter function</b>	<b>149</b>
<b>F The generalized central limit theorem</b>	<b>151</b>
<b>G Computation of the mobility edge of Lévy Matrices</b>	<b>153</b>
<b>List of Figures</b>	<b>159</b>
<b>Bibliography</b>	<b>167</b>
<b>Synthèse en français</b>	<b>179</b>

# Introduction

The study of transport properties of electrons in metals dates back to the classical Drude theory, based on the idea that free electrons were scattered by positive ions occupying lattice sites. The discovery of quantum mechanics and of the wave character of the electron led to a revision of such classical model: the electron is diffracted from an ideal crystal and the one-particle wave-functions are given by Bloch states [1]. Resistance, and thus finite conductivity, is due to the scattering of electrons with the imperfections in the crystal. The classical Drude model can still be used, but in the new picture the electron is not scattered by ions but by impurities. With this description, the mean free path of the diffusive motion of the electron is reduced when the concentration of the impurities is increased, and thus the conductivity is lowered. The discovery that, beyond a certain critical amount of disorder in the system, diffusion is not just reduced but it can be completely suppressed was due to Anderson [2] almost sixty years ago. Beyond a critical value of the disorder strength, the electron wave-function is no more an extended plane wave, but is a standing wave confined in space and exponentially localized around a center. The idea of Anderson was revolutionary at that time, and was at the origin of a new view of metal-insulator transition: the insulating phase in the Anderson model is not related to the filling of bands but to the formation of traps for the electron in the lattice due to the presence of disorder.

The phenomenon has been intensively studied during the last sixty years leading to important results: relatively early it was shown by Mott and Twose that in  $1d$  all states are localized independently of the strength of the disorder [3], as also confirmed by successive works [4, 5]. Yet, the theory of localization made a breakthrough during the 1970s, with the application of scaling arguments to the study of the Localization Transition [6, 7], and with the analytical solution of the problem on the Bethe Lattice due to Abou-Chacra, Anderson and Thouless [8]. The scaling theory of the Anderson Localization Transition received later solid basis with the field-theory formulation of the problem in terms of a non-linear  $\sigma$  model (NL $\sigma$ M) [9].

Numerical techniques have also given, and still give, a fundamental contribution to the comprehension of the phenomenon, providing a way to explore transport properties [10, 11, 12, 13], as well as statistical properties of the spectrum of the Hamiltonian [14, 15, 16, 17, 18, 19] and of wave-functions amplitudes [20, 21, 22, 23, 24, 25]. Anderson Localization is indeed a rich field of research presenting connection with the study of Random Matrices and chaos theory. The Hamiltonian of the Anderson model, a tight-binding model with on-site disorder, can be viewed as a random matrix, and standard Random Matrix Theory is conjectured to capture local properties of the spectrum in the delocalized phase, typically characterized by strong correlations

between eigenvalues, described by GOE (for orthogonal systems) level statistics. The localized phase is instead associated to Poisson level statistics. This analogy with the field of random matrices allows for a further connection with the concepts of ergodicity and quantum chaos: the conjectures of Barry and Tabor [26] and Bohigas, Giannoni and Smith [27] establish respectively that quantum integrable systems have Poissonian level statistics and quantum non-integrable, ergodic systems exhibit GOE level statistics: localization transition can be viewed in this sense not just as localization in the real space but also as localization in the configuration space. This idea is particularly important in the context of the study of Many Body Localization (MBL), an interesting new kind of phase transition between a high-temperature ergodic phase, in which we expect all the eigenstates to obey the Eigenstate Thermalization Hypothesis (ETH) [28], according to which each eigenstate is representative of the micro canonical ensemble, and a low-temperature non-ergodic phase, in which the ETH stops to hold and the dynamic conserves some memory of the local initial conditions. This phenomenon occurs in isolated interacting quantum systems, and in particular disorder electrons, but was also independently investigated in [29] to explain the quantum ergodicity transition of complex molecules. MBL can be thus interpreted as localization of the  $N$ -particles wave-function in the configuration space.

Almost sixty years later the seminal work of Anderson, the phenomenon of Anderson Localization remains an alive field of research with several unanswered issues. A good comprehension of the problem in low dimension has been obtained, with the identification of the lower critical dimension  $d_c = 2$  (for orthogonal spin independent systems), and with the perturbative renormalization group expansion in  $2 + \epsilon$  dimension. This method is however only relevant for the critical properties of the system in a small region near  $d = 2$ . The analytical study of the behavior in higher dimension is challenging, mainly because of the unconventional nature of the order parameter, the distribution of the local density of states. Anderson Localization has thus been largely studied numerically in  $d \geq 3$ , but due to the rapid increase of the running time required by the algorithms, its behavior is well understood only in  $d = 3$ , while there are very few results beyond  $d = 5$ . Important questions, like the existence of the higher critical dimension  $d_u$  remain thus unanswered.

The limit of infinite dimension can be understood by considering the Anderson model on tree-like structures, a problem which has been largely studied in literature and constitutes one of the few cases for which analytical results can be provided [30, 31, 32, 33, 34, 35, 36, 37]. The properties of the delocalized phase of this kind of models are however very unusual: in numerical simulations the system exhibits a strong non-ergodic behavior in a large region even far from the critical point. This anomalous behavior of the observables in the extended phase makes the analysis of the data highly non trivial, and had suggested the existence of an intermediate phase, which is delocalized but non-ergodic. It is really complicated to establish if such unusual behavior is the sign of a true intermediate phase transition, or the consequence of strong finite-size effects. The existence of an intermediate phase delocalized but non-ergodic has been advocated also in other random matrix models with long-range hopping as Lévy Matrices, whose entries are distributed independently with a heavy-tail law [38], and which are the subject of Chapter (III).

The study of the behavior of Anderson Localization in the limit of infinite dimen-

sion, and in particular the question of the existence of such intermediate phase is a particularly active field, which has produced a lot of works recently [39, 40, 41, 42, 43, 44, 45, 46]. The great interest on the subject is in part due to its connection with the study of Many Body Localization, where the existence of an intermediate delocalized non-ergodic phase has been advocated [47]. Indeed, in a pictorial view, the problem of  $N \gg 1$  interacting particles in a finite dimensional lattice can be interpreted as a one-particle localization problem on a very high dimensional lattice, which for spinless electrons consists in an  $N$ -dimensional hyper-cube of  $2^N$  sites [48, 29, 47]. This pictorial analogy can be done by thinking MBL as localization in the Fock space.

This thesis deals with the study of Anderson Transition in high dimension: on one hand we study a random matrix model, the Lévy Matrices, which is related to the large connectivity limit of Anderson model on tree-like structures, and thus on the infinite  $d$  limit of Anderson Localization. On the other hand we consider the tight-binding Anderson model with on-site disorder on hyper-cubic lattices of dimension  $d = 3, \dots, 6$ , and we perform a detailed numerical study in order to better understand the critical properties of the system in high dimension and to provide new ideas to develop novel analytical approaches to tackle this problem.

Chapter (I) is dedicated to a general introduction on Anderson Localization: we explain the characteristics of the phenomenon and we propose a brief historical review of the main results, both analytical and numerical. We conclude describing the open problems, focusing in particular on the issue of the existence of the intermediate phase in the limit of infinite dimensionality. In Chapter (II) we present some of the analytical techniques used to study Anderson Localization and RMs: in particular, we describe the techniques we have used in our analysis of Lévy Matrices. Chapter (III) is dedicated to the study of Lévy Matrices: after an introduction which explains the motivations and the relation with tree-like structures, we derive one of main results of our analysis, which is an exact equation for the mobility edge. We focus then on the problem of the intermediate phase, open since the seminal work of [38]. We present in particular our arguments based on the supersymmetric method and on the Dyson Brownian motion techniques, which support the idea that the delocalized phase of Lévy Matrices is ergodic. In the last part of Chapter (III) we show our numerical results, which on one hand agree with the analytical ones, and on the other hand help to understand the mechanism which generates the large crossover region in which the system behaves as if it was in an intermediate extended non-ergodic phase. Finally, Chapter (IV) is dedicated to a detailed numerical study of the critical properties of the Anderson model in dimensions from 3 to 6 based on exact diagonalization and transfer matrix method and on an approximate Strong Disorder real space Renormalization Group (SDRG) approach, analyzing the statistics of eigenvalues and wave-functions coefficients, as well as transport properties. Our results support the idea that the upper critical dimension of Anderson Localization Transition is infinite. Moreover, in high dimension the transition seems to be governed by a strong disorder limit, as predicted by the supersymmetric approach, since the critical values of all observables smoothly approach the ones of the localized phase as the dimensionality is increased. Another indication for that is the fact that the SDRG method gives much more accurate results than the one based on the weak coupling limit ( $d + \epsilon$  expansion) for the critical parameters in  $d \geq 3$ . This picture could provide an interpretation of the unusual properties of the

delocalized phase of the system in the limit  $d \rightarrow \infty$ .

# Chapter I

## The Anderson Localization Transition: introduction

### I.1 Disorder and Localization

The Anderson Localization Transition is a metal-insulator transition induced by disorder.

When an electron propagates in a periodic potential, the interference of the reflected and the transmitted components of the wave-function generates bands and gaps in the electron energy spectrum [1]. For a certain energy in a band, if the density of states is nonzero, the corresponding electron wave-function spreads over the whole structure. In a real crystal, the scattering of the electron wave-function with impurities gives rise to resistance and finite conductivity. In the semiclassical framework [49], the behavior of electrons in a metal is diffusive, and can be described as a random walk: after each collision the electron loses memory of its preceding motion, and the density of particles  $n(r, t)$  follows, in this approximation, the equation

$$\frac{\partial n}{\partial t} = D \nabla^2 n, \quad (\text{I.1.1})$$

where  $D$  is the diffusion coefficient. The density  $n(r, t)$  can be interpreted as the density of particles, but also as the probability to find a particle in  $r$  at the instant  $t$ . If the electron starts at time  $t = 0$  from a certain point, the mean square displacement at time  $t$ , for sufficiently long time, is [50]

$$\langle r(t)^2 \rangle = 2Dt, \quad t \rightarrow \infty. \quad (\text{I.1.2})$$

From the above expression (I.1.2), introducing the mean free path  $l$  and the time between two successive collisions  $\tau$ , we can write for the diffusion constant

$$D = \frac{l^2}{2\tau} = \frac{v_F l}{2} = \frac{\hbar k_F l}{2m}, \quad (\text{I.1.3})$$

where  $v_F = \hbar k_F / m$  is the velocity of the electron at the Fermi surface,  $m$  is the mass of the electron and  $k_F$  is the Fermi wave vector.

When an electric field  $E$  is applied to the conductor, the electron receives momentum from the external field, and acquires a drift velocity: in this semiclassical

description, the particle is assumed to have a well defined momentum on a length scale of the mean free path  $l$ , and to lose it each time it is scattered from impurities. In equilibrium, the rate at which the electron is accelerated from the external field is equal to the rate at which it is scattered from impurities. Combining this description with the idea that electric current is carried only by electrons with an energy close to the Fermi energy  $E_F$ , and using the expression of the diffusion constant (I.1.3) we obtain for the conductivity

$$\sigma = e^2 D \rho(E_F), \quad (\text{I.1.4})$$

where  $e$  is the charge of the electron and  $\rho(E_F)$  the density of states at the Fermi surface. Within this picture, increasing the disorder of the system, i.e. the concentration of impurities, the conductivity decreases, being the mean free path of the electron reduced [51]. For strong disorder, one would expect however a finite value of  $\sigma$ . In his seminal paper [2] of 1958, Anderson suggested that, beyond a critical amount of disorder, the relation (I.1.4) breaks down, the electron is trapped and its diffusive motion comes to a complete halt. This idea was initially introduced in order to explain some experimental results obtained by the Feher's group [52], which showed anomalously long relaxation times of electron spins in doped semiconductors. In particular, Anderson suggested that, when the mean free path of the electron becomes smaller than its Fermi wavelength  $\lambda_F = 2\pi/k_F$ , instead of thinking electrons as extended waves with short lifetimes, they could be seen as spatially confined waves with long lifetimes. The wave-function  $\psi(r)$  of the electron is exponentially localized around a center  $r_0$ , over a distance  $\xi$ , called localization length, and we have

$$|\psi(r)|^2 \sim A \exp\left(-\frac{|r - r_0|}{\xi}\right). \quad (\text{I.1.5})$$

To explain how the phenomenon of localization can occur, Anderson used a tight-binding model in a disordered lattice, which has become the paradigmatic model in the study of localization phenomena. In the Anderson Model the electron feels a random potential  $\epsilon_i$  at each site  $i$  of the lattice, and it is able to hop to the neighboring sites thanks to the hopping energy term  $t$ . Electron-electron interactions are neglected. The Hamiltonian of the model is the following:

$$H = \sum_i \epsilon_i c_i^\dagger c_i - t \sum_{\langle i,j \rangle} c_i^\dagger c_j + h.c., \quad (\text{I.1.6})$$

where the random variables  $\epsilon_i$  are independently and identically distributed, for example with the following box distribution:

$$p(\epsilon_i) = \begin{cases} \frac{1}{W}, & \epsilon_i \in \left[-\frac{W}{2}, \frac{W}{2}\right] \\ 0 & \text{otherwise.} \end{cases} \quad (\text{I.1.7})$$

If  $W = 0$  the eigenfunctions of the model are the Bloch states, while in the opposite case, if  $t = 0$  the Hamiltonian is diagonal and each eigenstate is completely localized on one site of the lattice. What happens between these two extreme cases depends on the strength of the ratio  $W/t$ : if it is large, there is very few probability for the

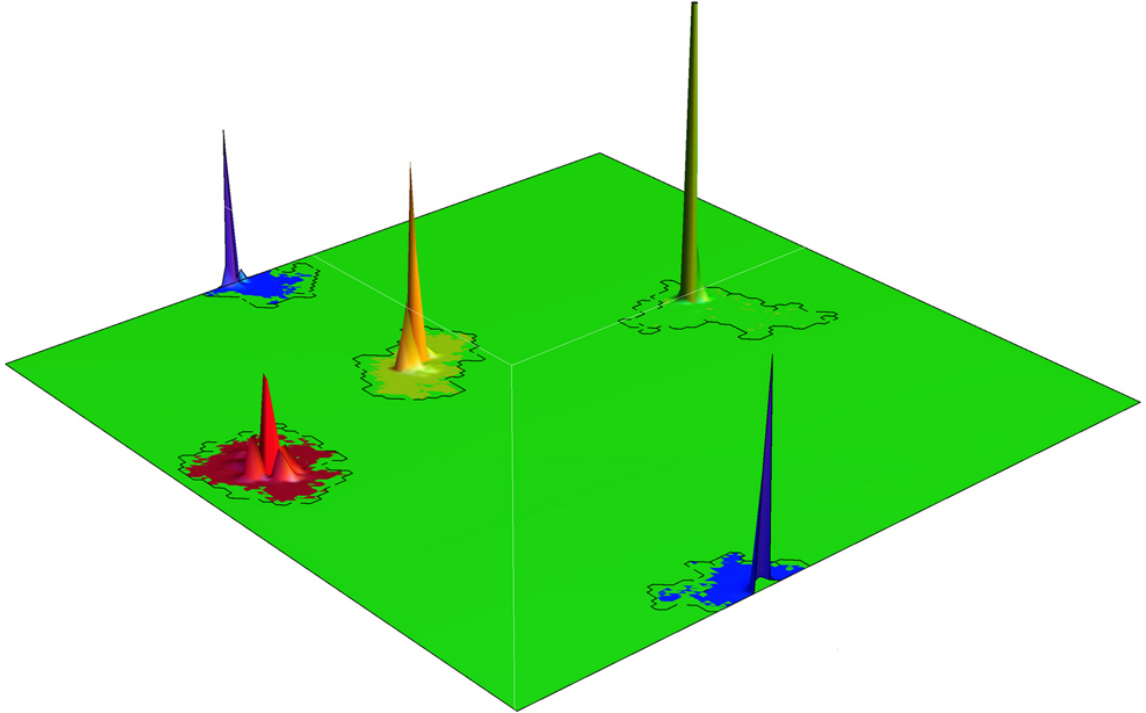


Figure I.1: The figure shows four localized wave-function for a disordered two dimensional material. The image is by Yang-Zhi Chou and Matthew Foster (Rice University) [53].

electron to find a level close in energy and spatially not too far, such that the overlap of the wave-functions at the corresponding sites is not negligible. To better understand this idea we can imagine to diagonalize a  $2 \times 2$  Hamiltonian, with diagonal terms  $\epsilon_1$  and  $\epsilon_2$  and hopping term  $t$ . It is easy to see in this case that the deviation of the eigenstates from the original on-site vectors is controlled by the ratio  $t/|\epsilon_1 - \epsilon_2|$  and the difference between the eigenvalues  $E_1$  and  $E_2$  is given by  $\sqrt{(\epsilon_1 - \epsilon_2)^2 + t^2}$ . Therefore, if  $|\epsilon_1 - \epsilon_2| \gg t$ , the eigenfunctions are close to the original on-site wave functions, while if  $|\epsilon_1 - \epsilon_2| \ll t$  we obtain two eigenstates in which the probability is shared between the sites (*resonance*). In the Anderson model we can thus imagine that, if the disorder is strong ( $W \gg t$ ), there will be few isolated resonances, and the wavefunctions are close to the on-site wavevectors. In this case the electron is trapped around a center, and its wave-function is given by the envelope (I.1.5). If on the contrary the hopping term is enough strong compared to the disorder, we will have many resonances which overlap and the system will have a metallic behavior.

Localized eigenstates are expected to appear in the tails of the energy spectrum. The first intuitive reason is that these states are originated from large random energies, and therefore one expects that they are more affected by the disorder than the states at the center of the spectrum. The second reason was suggested by Lifshitz [54]: as mentioned above, diffusive motion is possible if the wavelength  $\lambda_F$  of the electron is much

smaller than the mean free path  $l$ . Therefore, an intuitive criterion for localization is the condition

$$\lambda_F \sim l. \quad (\text{I.1.8})$$

Since the states belonging to the tails of the spectrum have a larger wavelength than those at the center, we expect localization to occur first in the tails. For each value of the disorder  $W$  there is a critical energy  $E_c$ , called *mobility edge*, which separates the localized states from the delocalized ones. In the case of the Anderson model the situation is qualitatively represented in figure (I.2): the density of states  $\rho(E)$  is symmetric and two mobility edges  $E_{c1}$  and  $E_{c2}$  separate, for each value of  $W$ , the localized states in the tails from the extended states in the central part of the spectrum. By varying the Fermi level  $E_F$  with respect to the mobility edge it is possible to obtain a metal-insulator transition at zero temperature: in particular, if  $E_F > E_{c1}$  the system behaves as a metal, as an insulator in the opposite case. There exists a critical value  $W_c$  of the disorder such that  $E_{c1} = E_{c2}$ , and all states in the spectrum are localized, as shown in figure (I.3). The intuition of Anderson and the discover of the mechanism of Anderson Localization has represented a breaking of the conventional diffusion picture: the insulator of Anderson is not related to the filling of bands but to the formation of traps for the electron in the lattice due to the presence of disorder.

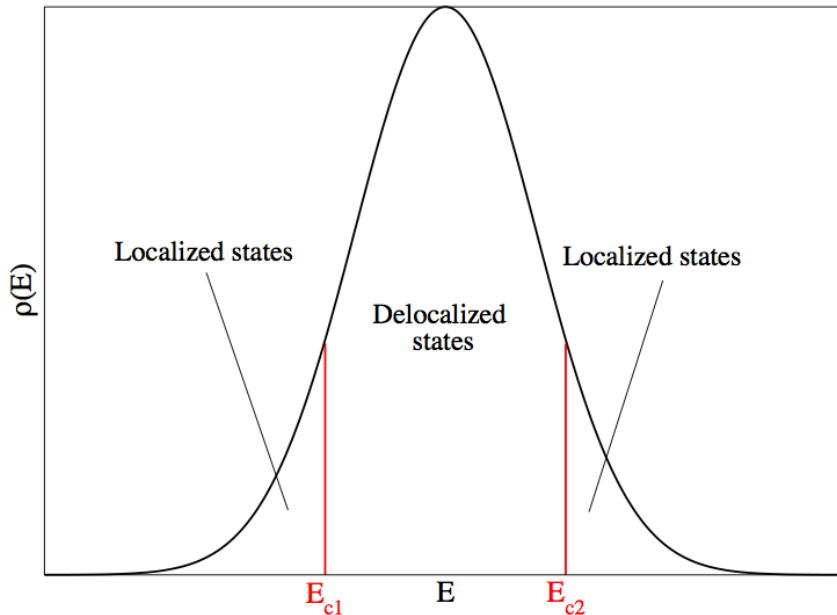


Figure I.2: The localized states appear first in the tails of the spectrum, as we expect intuitively. For a fixed value of the disorder  $W < W_c$ , by varying the Fermi energy with respect to the mobility edge, a metal-insulator transition occurs in the system.

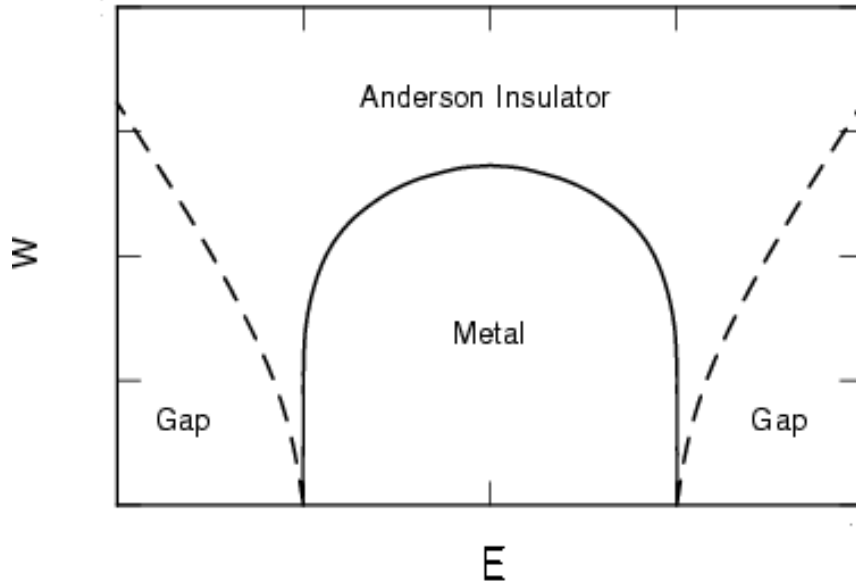


Figure I.3: Qualitative sketch of the phase diagram of the Anderson model in the  $W$ - $E$  plane. For each value of the disorder  $W$  there are two symmetric mobility edges, and when the disorder is increased over a critical value  $W_C$  all the spectrum is localized. The dashed lines indicate the boundaries of the spectrum, beyond which the density of states is zero.

## I.2 Characteristics of the transition and localized states

In his seminal work Anderson showed that quantum particles can be localized by a random potential even in a situation where classical particles would be delocalized. The intuitively way to understand this mechanism is to think about waves scattered by random centers: the probability  $P$  of propagation from a point to another one is obtained by summing over the amplitudes of all the possible paths between the two points, and taking the square of the complex value obtained [55]. In particular, we have an expression of the type

$$P = \left| \sum_i a_i e^{iS_i} \right|^2, \quad (\text{I.2.1})$$

where  $i$  runs over all the possible paths between the two points considered,  $S_i$  is the action of the  $i$ -th path and  $a_i$  the corresponding amplitude. Since we have to sum the different contributions before squaring, the probability  $P$  contains a certain number of interference terms in addition to the classical incoherent contributions given by the sum of the squares of the amplitudes, and we have an expression of the form

$$P = \left| \sum_i a_i \right|^2 + \sum_{i \neq j} a_i a_j^* e^{(S_i - S_j)}. \quad (\text{I.2.2})$$

The interference terms in equation (I.2.2) don't cancel each other if for example

the system has a time reversal symmetry such that the loops in the paths can be followed in a direction and also in the opposite one: in this case the probability to have backscattering, e.g. to return to the same point, results to be enhanced. In figure (I.4), for a wave which propagates from point A to point B and then goes back to A, a possible random path is represented, together with the same path traversed in the opposite direction: because of the constructive interference between these two paths, the probability from the propagating wave to return to point A is twice as large as it would have been if we had considered the classical incoherent contributions only. This mechanism, which can be a first, intuitive way to understand how localization can occur, is particularly relevant in low dimensions (*weak localization* [7, 56]), where the number of loops is larger. In particular, for a random walk in  $d = 1$  and  $d = 2$  the probability to return to the starting point is one (i.e. the random walk is recurrent), whereas this is not true for  $d \geq 3$ . Dimensions one and two play therefore a special role, and the quantum corrections to the conductivity (I.1.4) due to interference effects are in this case large no matter how weak the disorder is.

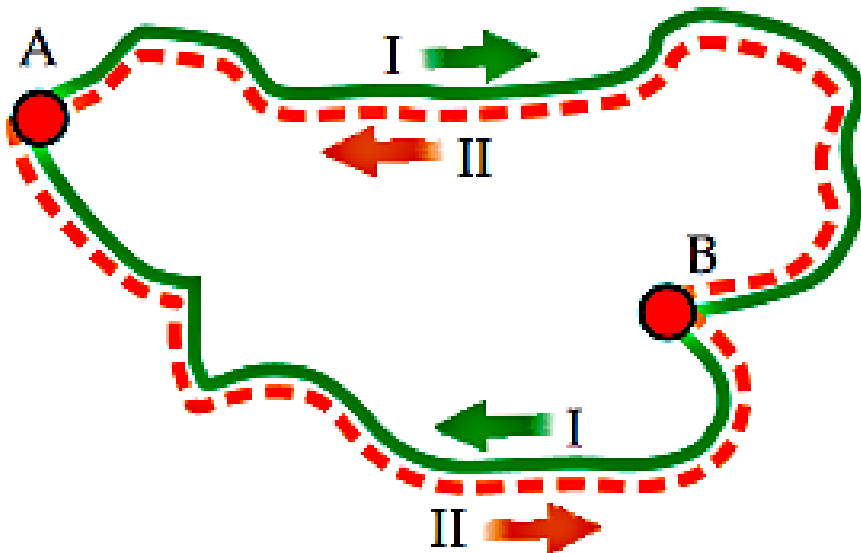


Figure I.4: The wave going from A to B interferes constructively with the one going from B to A: the interference effects enhance the probability of backscattering. The figure is taken from [57].

Localization can also be intuitively understood in the limit of strong disorder: as explained in the previous paragraph using the Anderson model as a reference, we expect that, where the random potential forms a deep well, the electron is trapped, and the overlap with adjacent orbitals is not sufficient to delocalize the particle: the wave-function is therefore exponentially localized as in (I.1.5). If we reduce the disorder, we can ask if the wave-functions of the particles eventually become delocalized. As we will explain in the next section, the transition occurs for  $d > 2$  in spinless systems with time-

reversal symmetry (orthogonal systems): it is a continuous quantum phase transition, i.e. a transition at zero temperature. The identification of an order parameter for the Anderson Localization Transition is not an easy task: the first attempts to describe the transition with the language of field theory would suggest to use the expectation value of the local density of states (DoS), but it results in fact not critical. As we will see in Chapter (II), the distribution of the local DoS develops heavy tails in the localized phase: therefore, the good quantity to consider in order to distinguish between localized and extended states is the typical value of such distribution (see figure (I.5)). In other words, in a region of the spectrum corresponding to localized eigenstates, the Hamiltonian has a point spectrum [58]. The average density of states can be regular and smooth, but the local density of states varies a lot, being zero almost everywhere and large in correspondence of few resonances: this is due to the fact that in the localized regime just few sites contribute with a weight of order one to a certain eigenstate, while the contribution of the others can be exponentially small. On the contrary, in the delocalized regime the spectrum is absolutely continuous and the typical value of the local density of states is of the same order as the average value: each site contributes to a certain eigenstate with a weight which is of the same order as all the other sites. Another characteristic of localized states is the insensitivity to boundary conditions, and in general to what happens far from the localization center of the state we consider, a feature which has often been used in numerical analysis [59, 60, 61].

The formal definitions of the quantities which allow one to discriminate between localized and extended states and to quantitatively study the transition are given in section (II.1). Even if the identification of an order parameter for the Localization Transition is not trivial, the phenomenon can be described in terms of scaling arguments, as we will see in much detail in section (I.4): in this picture, the localization length  $\xi$  defined in (I.1.5) plays the role of a characteristic length scale going to infinity as the critical point is approached. In particular, if the transition is studied from the insulating side, we consider the scaling of  $\xi$ :

$$\xi \propto (W - W_c)^{-\nu}, \quad (\text{I.2.3})$$

while, starting from the metallic phase, a central role is played by the scaling of the conductivity  $\sigma$ :

$$\sigma \propto (W - W_c)^{-s}. \quad (\text{I.2.4})$$

We will see in section (I.4) how scaling arguments have been justified providing a field theory formulation of Anderson Localization Transition and we will present a brief historical review on the field.

### I.3 Anderson Localization in one and two dimensions and weak localization

As Anderson had suggested in his seminal work, all states in a one-dimensional chain are localized. The proof of this result is attributed to Mott and Twose [3] and

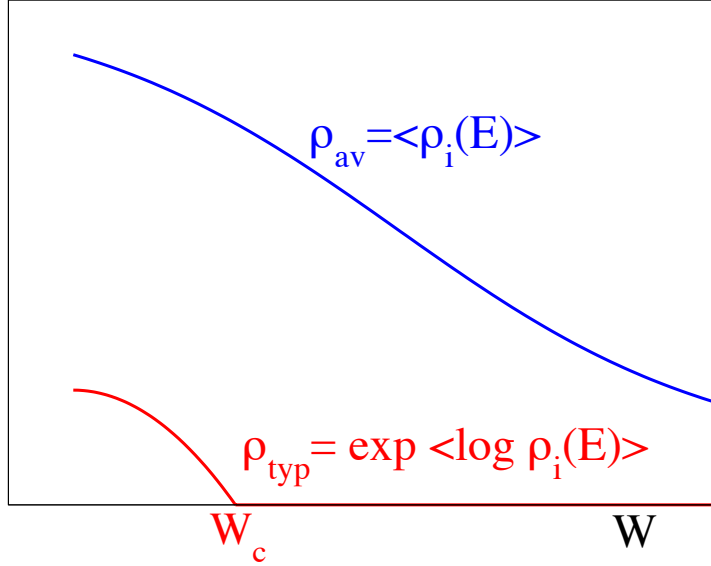


Figure I.5: The average value of the local density of states  $\langle \rho_i \rangle$  can not be used as order parameter for Anderson Localization: as shown in blue in the plot, this quantity is regular and finite in both the extended and the localized phase. Instead, since the local density of states develops heavy tails in the localized phase, its typical value is zero in the localized phase and finite in the extended one, as shown in red in the plot, and is actually the good order parameter to consider.

confirmed by other authors later [4, 5]. Indeed, as explained in Appendix (A), for one dimensional and quasi-one dimensional systems it is possible to compute the localization length through the transfer matrix method combined with results on the limiting behavior of products of random matrices [62, 63, 64, 65, 66]. In particular the localization length is identified with the inverse of the smallest positive Lyapunov exponent, which represents the slowest possible exponential increase of the wave-function in the thermodynamic limit [67]. As shown in Appendix (A), in one dimension calculations are particularly simple because the transfer matrix reduces to a  $2 \times 2$  matrix. Identifying the localization length as a limiting property of a product of random matrices is one of the way to prove that in a one dimensional disordered system all states are localized independently of the strength of the disorder [68, 69, 70].

Localization in higher dimensions was more complicated to solve: as we will see in section (I.4), the scaling theory shows that  $d = 2$  is the lower critical dimension for the Anderson Localization Transition<sup>1</sup>, therefore no metallic phase exists in two dimensional systems. Nonetheless, the diffusive regime, i.e. the diffusive propagation of the electron in the sample, can be obtained in 2d systems and in weakly disordered quasi one dimensional systems, if the size  $L$  does not exceed the localization length  $\xi$ .

<sup>1</sup>This is true for spinless systems with time-reversal symmetry and spin-independent hopping.

Indeed, in two dimensions the localization length is extremely large for small disorder (of orders of  $10^6$  lattice sites for  $W = 1$ ), diverging exponentially for  $W \rightarrow 0$ : for this reason, in many simulations and experiments the system behaves for all purposes as if it was delocalized, and this has been at the origin of a debate for long time, since various works, analyzing too small systems, identified the Anderson transition also in two dimensions [71]. In thin wires and weakly disordered metallic films it is thus possible to observe a diffusive regime, and the only sign of localization can be found in anomalies with respect to the classical behavior (I.1.4): such effect is the consequence of the quantum interference processes explained in section (I.2), which lead to important corrections to the classical conductivity known as *weak localization corrections*. As we have seen in section (I.2), in the quantum case the interference terms enhance the probability of backscattering: since the number of loops is larger in low dimensional systems, weak localization effects become particularly important in this case. In two dimensions, the weak localization corrections to the conductivity are negative and depend logarithmically on the system size [7, 72, 73]. In order to study the dependence of these corrections on the temperature we have to replace the geometrical system size by an effective system size  $L_\phi$  (the phase coherence length) [74, 75, 76, 77] representing the mean distance between successive inelastic scattering events and given by

$$L_\phi^2 = D \tau_\phi, \quad (\text{I.3.1})$$

with  $\tau_\phi$  the phase coherence time. This quantity is usually introduced phenomenologically, assuming that it depends on the temperature as  $\tau_\phi \propto T^{-p}$  ( $p = O(1)$ ): the value of  $p$  can be obtained by fitting experimental data (see for example Ref. [78]). Proceeding in this way, at low temperature we obtain logarithmic corrections to the conductivity with the temperature, which have been observed in experiments with films [79, 80].

Negative corrections to the conductivity as an effect of the enhanced backscattering are present in systems with time reversal symmetry. If a strong magnetic field is applied to the system, the time reversal symmetry is broken: on each closed loop the electron acquires a phase which depends on the length of the loop. The sum over all loops leads in the end to the cancellation of all these contributions and no corrections to the classical conductivity is present. Finally, we mention for completeness the case of systems with time reversal symmetry and spin dependent hopping between neighboring sites (symplectic models), where the quantum corrections to the conductivity change the sign, leading to an enhancement with respect to the classical conductivity with the system size (weak anti-localization corrections).

## I.4 Scaling theory and field theory formulation

Anderson showed that the localization transition strongly depends on the dimension of the system, and he suggested that in a one-dimensional chain all states should be localized. As we have mentioned in section (I.3), this was successively proved by Mott and Twose [3], but localization in higher dimensions was more complicated to solve.

The success of scaling arguments in describing continuous phase transitions in other

fields of statistical physics [81] suggested that the same type of arguments could be used in the study of the Anderson Localization Transition. As pointed out in section (I.2), unlike other quantum phase transitions, for the Anderson Localization Transition it is not easy to identify an order parameter; nonetheless, it exists a length scale  $\xi$  going to infinity as the transition is approached. The first to propose a description of the phenomenon in terms of scaling properties was Wegner [6], while the scaling theory was formulated in [7]. The order parameter [59] used to develop the theory is a dimensionless conductance  $g$ , which is a measure of the sensitivity of the system to a change of the boundary conditions. We define the Thouless conductance  $g_T$  as

$$g_T = \frac{e^2}{h} \frac{\langle \delta E \rangle}{\Delta E}, \quad (\text{I.4.1})$$

where  $\langle \delta E \rangle$  is the average change in eigenenergy which corresponds to a change in the boundary condition, and  $\Delta E$  is the mean distance between two subsequent level in energy. It was shown in [59] that, if  $E$  belongs to the metallic part of the spectrum, then  $g_T = \sigma L^{d-2}$ . This behavior relates the definition (I.4.1) to the Landauer conductance, as explained in Appendix (A). The quantity  $g = g_T/(e^2/h)$  is dimensionless, and it is the only parameter used to describe the transition in scaling theory. The fundamental assumption is that the length dependence of the conductance is given only by the conductance itself, thus we have:

$$\frac{\partial \log g}{\partial \log L} = \beta(g). \quad (\text{I.4.2})$$

The relation (I.4.2) is supposed to hold for  $L$  large enough, such that the microscopic details of the model become irrelevant. We consider now the limits  $g \rightarrow \infty$  and  $g \rightarrow 0$ . As mentioned above, in the limit of large conductance, from considerations on the diffusive motion of the electron, and using the relation (I.1.4), we have  $g = \sigma L^{d-2}$ , and thus

$$\beta(g) = d - 2, \quad g \rightarrow \infty. \quad (\text{I.4.3})$$

In the opposite limit  $g \rightarrow 0$ , we have localization, and the conductance decreases exponentially with the system size. As a consequence we have

$$\beta(g) = \log g, \quad g \rightarrow 0. \quad (\text{I.4.4})$$

Assuming that  $\beta(g)$  is a monotonous function, the interpolation between the two limits gives the behavior shown in figure (I.6): for  $d < 2$  the function  $\beta(g)$  is always negative, so the conductance decreases with the system size for each initial value  $g_0$ . Therefore, for  $d < 2$  there is no phase transition. For  $d = 2$ , we have to compute the first correction to the conductance as a function of  $L$ , in order to determine if  $\beta(g)$  is positive or negative: the computation shows that  $\beta(g) < 0$  for all  $g$ , and thus all states are localized for  $d = 2$ , as we have anticipated in section (I.3), assuming that  $\beta(g)$  is a monotonic function of  $g$ . These corrections to the conductance are the weak localization corrections in the diffusive regime discussed in section (I.3). For  $d > 2$  there is a critical point  $g_c$  such that  $\beta(g_c) = 0$ , and thus the conductance remains constant with the system size. This is an unstable fixed point of the renormalization

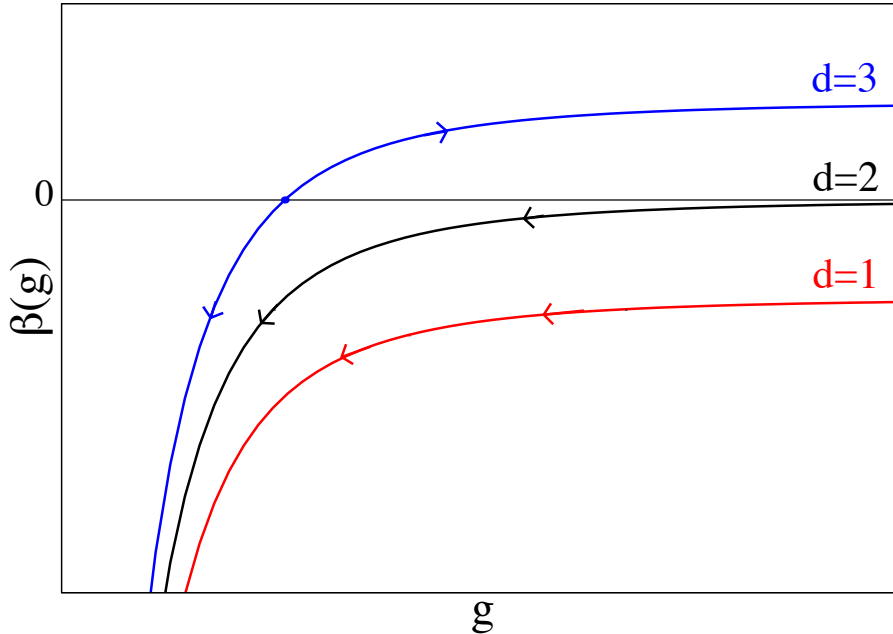


Figure I.6: Renormalization flow for  $d = 1$ ,  $d = 2$  and  $d = 3$ . For  $d < 2$  the function  $\beta(g)$  is always negative and thus there is no phase transition. For  $d = 3$  there is a fixed point  $g_c$  where  $\beta(g_c) = 0$ : this value  $g_c$  is associated to the mobility edge.

flow: if we start from  $g = g_c + \delta g$ , the system, for  $L \rightarrow \infty$  develops into the metallic phase, while if we start from  $g = g_c - \delta g$  we fall into the localized regime.

The scaling theory of Anderson Transition represents a big step in the comprehension of the phenomenon. This picture received solid basis with the field-theory description of the transition in terms of a non-linear  $\sigma$  model (NL $\sigma$ M), introduced by Wegner [9]. However, this model is not exactly solvable in most of the cases of interest, as in  $d = 3$ . The original derivation of the  $\sigma$  model uses the replica trick in order to perform the average over the disorder [9, 82, 83, 84]. Later, an alternative supersymmetric formulation, obtained combining fermionic and bosonic degrees of freedom, was proposed by Efetov [85, 86, 87]: this formulation is equivalent to the previous one, based on the replica method, at the level of perturbation theory, but presents the advantage to allow a non-perturbative analysis which leads to results on the energy levels and eigenfunctions statistics. The supersymmetric method is presented in section (II.3), where we discuss the method in general and how it has been used to derive important results on the Bethe Lattice. We will then use this method in Chapter (III) to derive some properties of the level statistics of Lévy Matrices. Being  $d = 2$  the lower critical dimension of the NL $\sigma$ M, it is possible to perform a renormalization group analysis in

$d = 2 + \epsilon$  dimension. The flow  $\beta$  can be computed perturbatively near  $d = 2$  by expansion in the parameter  $t = 1/(2\pi g)$ , proportional to the inverse of the dimensionless conductance  $g$  [88, 89]. In particular, in terms of  $t$ , we have  $\beta(t) = -dt/d \log L$ , and, since for  $d = 2 + \epsilon$ , with  $\epsilon \ll 1$ ,  $t_c \sim \epsilon$ , the function  $\beta(t)$  can be expanded in powers of  $t$ , leading to

$$\beta(t) = \epsilon t + 2t^2 - 12\zeta(3)t^5 + O(t^6). \quad (\text{I.4.5})$$

The critical point can be obtained from  $\beta(t_c) = 0$ , and the critical exponents  $\nu$  defined in (I.2.3) from  $\nu = -1/\beta'(t_c)$ . The  $\epsilon$  expansion gives numerically accurate values for the transition point and the critical exponents only in the limit  $\epsilon \rightarrow 0$ : this has been verified by numerical simulations on fractals with dimensionality slightly higher than two [90]. However, even at five loops, it fails in estimating the critical properties in 3 dimensions ( $\epsilon = 1$ ): the result at two loops obtained for the exponent of the localization length is  $\nu = 1$  while numeric simulations give  $\nu \simeq 1.58 \pm 0.01$  (here we report the most precise estimate, obtained in [91, 92, 14, 15, 16, 17, 18, 19, 20, 21]). The computation at five loops gives an even worse estimation of  $\nu \simeq 0.67$ . The  $\epsilon$  expansion remains however an important tool for the comprehension of the qualitative properties of the localization transition. For example it is able to capture an important feature of the Anderson Transition at criticality: the multifractality of wave functions. At the critical point the normalized measure  $|\psi|^2$  is indeed characterized by strong fluctuations, and there exists an infinite set of critical exponents describing the anomalous scaling of the moments of this distribution [93, 94] (for a quantitative description of the multifractal behavior at the Anderson critical point see Appendix (B)). The  $\epsilon$  expansion is able to reproduce this behavior [95], and also to give results quite in agreement with numerical simulations for the multifractal exponents [96]. We conclude this section stressing that the results presented are valid for orthogonal systems, e.g. systems with time-reversal symmetry and spin-independent hopping (the classification of symmetries and universality classes in connection with Random Matrix Theory is presented in section (I.6)). The scaling theory, with its field-theory formulation, can be applied to other symmetry classes: we mention here that symplectic systems present a truly metallic regime for  $d = 2$  [97, 98].

## 1.5 Anderson transition on the Bethe Lattice: mean field

The first analytical result obtained for the Anderson Localization Transition was the one of Abou-Chacra, Anderson and Thouless [8] who provided an analytical solution of the Anderson model on the Bethe Lattice, a graph without loops, where each node is connected to a fixed number  $k+1$  of nodes. The analysis in [8] was based on the approach originally used by Anderson in its seminal work [2], where the localization of electron eigenfunctions for strong disorder (or in the tails of the energy spectrum) was shown starting from a perturbative expansion in powers of the hopping term for the self-energy. With this technique the authors found a self-consistent equation leading to the mobility edge, showing thus that loops are not necessary to localize the electron. As we will see in Chapter (II), it is the hierarchical structure of the Bethe Lattice which makes the problem analytically tractable. Even if there exist other models pre-

senting a localization transition which are analytically tractable, such as for example the Power Law Random Banded model (PRBM) [99, 100, 101, 102] or the generalized Rosenzweig-Porter random matrix model [103, 104], the Anderson Model on the Bethe Lattice plays a special role in the study of the Localization Transition. Since in such a structure the number of sites at a certain distance from a given site grows exponentially with the distance itself, the Bethe Lattice is generally interpreted as corresponding to infinite dimensionality. Statistical models defined on the Bethe Lattice usually show a critical behavior which coincides with the one displayed in mean field approximation, which is generally exact for infinite-range interactions (fully-connected models). For Anderson Localization Transition, due to the unusual nature of the order parameter, the study of the mean field behavior and of the fluctuations around is particularly complicated: the analysis of models defined on tree-like structures remains the best way to explore mean field properties and is the starting point for the attempt to understand the behavior in high dimension. As we will explain in section (I.9) and more in details in Chapter (II), the Anderson Transition on the Bethe Lattice has been largely studied in literature: in particular, the critical behavior has been explored with the supersymmetric method, (see section (II.3)), both in the version of the tight-binding Anderson model [30, 31, 32, 33] and in the one of the  $\sigma$ -model [34, 35, 36, 37]. In section (I.9) we will explain how some properties of the transition on the Bethe Lattice still remain unclear and how the problem has received renewed attention in the last years in connections with Many Body Localization.

## I.6 Anderson Localization and Random Matrix Theory

The study of Random Matrices (RMs) is an independent and rich field of research, intensively developed since the 1950s: it is concerned with the analysis of properties (such as the distribution of eigenvalues, the level statistics and some properties of the eigenvectors) of matrices with entries chosen randomly from various probability distributions. The study of RMs has begun with the application as statistical models for heavy nuclei atoms [105], and since this pioneering work, it gained importance in many areas of physics and also in other disciplines [106, 107, 108]. Some examples are diffusion in random graphs [109], [110], wireless communications [111], but also financial risk [112] and biology [113]. The reason for such versatility is that Random Matrix Theory (RMT) provides universal results, which are independent of the particular probability distribution of the random entries: only few features, determining the universality class, matter. The majority of results are available for the three Gaussian Wigner ensembles, including matrices with independent and identically distributed Gaussian random variables as elements. Depending on the symmetries of the problem we distinguish the Gaussian Orthogonal Ensemble (GOE), constituted by real symmetric matrices, the Gaussian Unitary Ensemble (GUE), which includes complex hermitian matrices, and the Gaussian Symplectic Ensemble (GSE), including quaternion self-dual matrices. In the case of Gaussian Ensembles, the rotational invariance allows to perform analytic computations for many quantities of interest. In particular, the joint probability distribution of the eigenvalues  $E_1, \dots, E_N$  can be obtained. In the GOE case, which corresponds to independent Gaussian entries with mean 0 and

variance of the off-diagonal elements which is half the variance of the diagonal ones, it takes the form

$$P(E_1, \dots, E_N) = C_{N,\beta} e^{-\beta W}, \quad (\text{I.6.1})$$

$$W = \frac{1}{2} \sum_{j=1}^N E_j^2 - \sum_{i<j} \log |E_i - E_j|, \quad (\text{I.6.2})$$

where  $\beta = 1$ . In the expression (I.6.1)  $\beta$  is actually a coefficient depending on the particular Gaussian ensemble considered, and in the GUE and GSE case takes the values 2 and 4 respectively. Due to the presence of the term  $\sum_{i<j} \log |E_i - E_j|$  in the potential (I.6.2), the eigenvalues of GOE matrices are strongly correlated random variables: it can be shown [106] that the product  $\prod_{i<j} |E_i - E_j|^\beta$ , which comes from the interaction term of the potential, can be written as a determinant containing “oscillator wave functions” (which can be expressed in terms of Hermite polynomials). Thanks to this property the  $n$ -points correlation functions can be expressed in terms of orthogonal polynomials, and in particular results for the density of states and for the level statistics are available. In the thermodynamic limit the density of states for the GOE ensemble converges to the *Wigner semicircle law*:

$$\rho_{N \rightarrow \infty}(E) \rightarrow \frac{1}{\sqrt{2N}} f\left(\frac{E}{\sqrt{2N}}\right), \quad (\text{I.6.3})$$

where

$$f(x) = \sqrt{1 - x^2}. \quad (\text{I.6.4})$$

The determinantal structure of the joint probability density of the eigenvalues also provides information on the level statistics: for example one quantity of interest is the probability distribution  $p(s)$  of the spacing between two subsequent eigenvalues  $s = N\rho(E_\alpha)(E_{\alpha+1} - E_\alpha)$ , or equivalently the 2-points correlation functions of eigenvalues [106]. For the Gaussian ensembles explicit calculations are possible for this quantity [114, 115], even if a final expression for the limiting correlation function is available only in the GUE case (*Dyson sine kernel*). The computation of such correlation functions is complicated, but, in general, a good approximation to the distribution  $p(s)$  is given by the so called Wigner surmise, whose most general form is

$$p(s) = a_\beta s^\beta \exp(-b_\beta s^2). \quad (\text{I.6.5})$$

In the expression (I.6.5)  $a_\beta$  and  $b_\beta$  are factors depending on the coefficient  $\beta$  depending on the ensemble. As we can see in the red curve represented in figure (I.7), the Wigner surmise takes account of the “level repulsion”, i.e. for the strong correlations between subsequent eigenvalues, characteristic of Gaussian ensembles: as a consequence, two subsequent eigenvalues cannot be arbitrarily close to each other, and  $p(s=0) = 0$ . In the figure the opposite situation is also represented (in black): it corresponds to independent eigenvalues, described by the Poisson statistics  $p(s) \propto \exp(-s)$ . Rotational invariance also assures in the Gaussian case that the eigenvectors are delocalized, i.e. for a  $N \times N$  matrix, they are uniformly distributed on

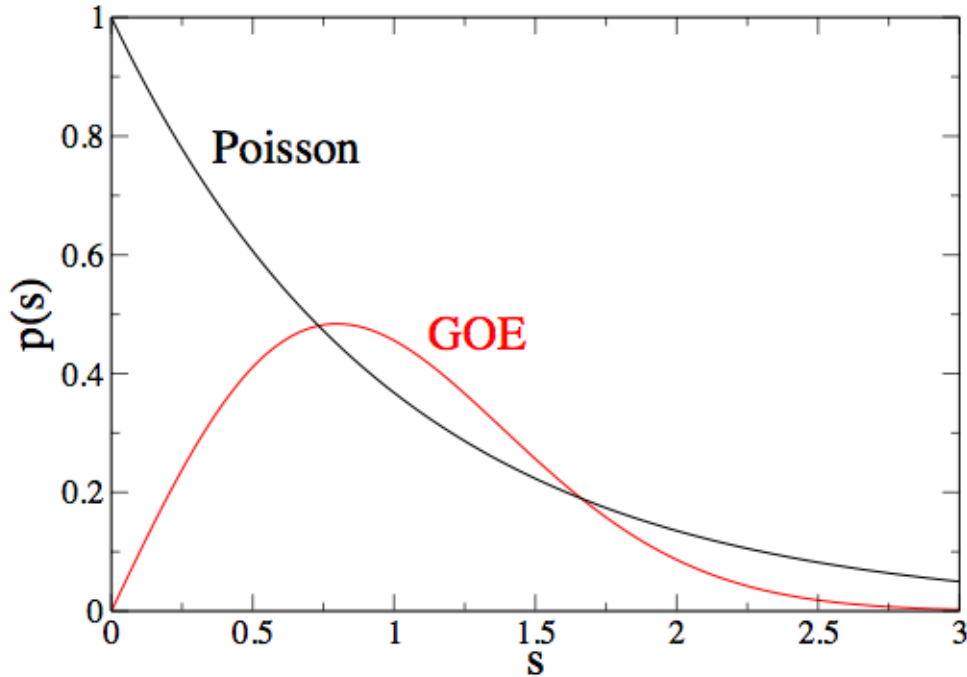


Figure I.7: The plot shows the level spacing distribution  $p(s)$  in the Poisson case and in the case of the Gaussian Orthogonal Ensemble ( $\beta = 1$ ). The two behaviors are typical of the localized phase and of the extended phase respectively.

the sphere  $S^{N-1}$ : the coordinate of the eigenvectors have smallest possible magnitude of order  $N^{-1/2}$ , up to logarithmic corrections.

A generally accepted idea, which makes RMT a field open to connections with different areas of research, is the universality conjecture: the local and global properties of the spectrum of the Gaussian ensembles, as well as the eigenvector properties, are believed to hold for a very large class of random matrices, in particular for general Wigner matrices [116], i.e. matrices with i.i.d. entries distributed with a generic distribution function with finite second moment. As we will explain in Chapter (II.4), this conjecture, with varying degrees of strength and generality, has been proved for some classes of Wigner matrices [117, 118, 119, 120, 121, 122, 123, 124, 125, 126], including matrices with i.i.d. entries generically distributed with a subexponential decay.

As mentioned above, RMT is an interesting field in its own, on a mathematical point of view, but lots of motivation comes from physical problems. In particular, the connection with the study of the Localization Transition in disordered systems is strong. Indeed, the Anderson Hamiltonian (I.1.6) can be interpreted as a random matrix, with a deterministic off-diagonal part  $T$  and a random on-site part  $H_0$ :

$$H = H_0 + T. \quad (\text{I.6.6})$$

The symmetry properties of the matrix are related to the physical problem: sym-

metric matrices represent systems with time-reversal invariance and spin independent hopping, hermitian matrices correspond to systems in which the time reversal invariance is broken, e.g. by a magnetic field, and symplectic matrices represent systems with time-reversal invariance and spin dependent hopping (i.e. the rotational invariance is broken). Using the analogy between RMs and the Anderson Hamiltonian, we can interpret Wigner matrices as representative of an Anderson Hamiltonian with fully connected interactions: in this case all the eigenvectors are delocalized, and the spectral properties, as explained above, are the same as in the Gaussian ensembles. Yet, the Anderson Hamiltonian (I.1.6) with nearest-neighbours interactions belongs to a more general universality class, composed by matrices with independent but non identically distributed entries with the form of a Schrödinger operator with random on-site potential. There exists a universality conjecture for random Schrödinger operators, which states that there are two different regimes depending on the energy and the disorder strength: in the strong disorder regime the eigenfunctions are localized and the level statistics are Poisson-like, while in the weak disorder regime the eigenfunctions are delocalized and the level statistics are the same as in the GOE case. Intuitively, it is easy to associate localization to Poisson statistics: we can think that, since each state is localized around a specific site, the corresponding eigenvalues are not correlated, and two subsequent levels can be arbitrary close to each other. On the contrary, in the delocalized phase we expect strong correlations between subsequent eigenvalues, and therefore the distance between two subsequent levels can not be zero. On a mathematical point of view, for the Anderson model in  $d \geq 3$  the localized regime at large disorder or near the spectral edges has been well understood [127, 128, 58]. It has been shown that the level statistics are Poisson-like [129] and that the eigenfunctions are exponentially localized with an upper bound on the localization length that diverges at the presumed transition point [130]. About the delocalized regime, delocalization has been established on the Bethe Lattice [131, 132, 133], corresponding to the infinite dimensional case. In finite dimension there are no rigorous results on the level statistics, but it is conjectured, as explained before, that in the thermodynamic limit the local correlation functions of the eigenvalue follow the GOE statistics. Based on this conjecture, the behavior of the local eigenvalue statistics is used as a tool to compute the phase diagram numerically. In particular, in Refs. [15, 16, 19, 134, 135] the transition in the level statistics has been studied in detail in finite- $d$  models: the methods used require in general the computation of the histogram of the distribution  $p(s)$ . More recently it has been suggested by V. Oganesyan and D. Huse [136] to characterize the correlations between adjacent gaps by the ratio

$$r = \frac{\min\{\delta_\alpha, \delta_{\alpha+1}\}}{\max\{\delta_\alpha, \delta_{\alpha+1}\}}, \quad (\text{I.6.7})$$

where  $\delta_\alpha = E_{\alpha+1} - E_\alpha \geq 0$ . The average value over the realizations of the disorder of this observable provides the same information as the distribution  $p(s)$ , and has well defined limits in the GOE and in the Poisson case, corresponding respectively to  $\langle r_{\text{GOE}} \rangle \simeq 0.53$  and  $\langle r_{\text{P}} \rangle \simeq 0.39$ .

Studying the localization transition from the point of view of Random Matrices also allows to establish a connection with the concepts of ergodicity and quantum chaos. In particular, the conjecture of Barry and Tabor [26] establishes that quantum

integrable systems have Poissonian level spacing statistics, and the one of Bohigas, Giannoni and Smith [27] states that quantum non-integrable, ergodic systems (chaotic systems) exhibit Wigner-Dyson level statistics. The idea behind this result is understandable in the semiclassical limit [137, 138]: for  $\hbar \rightarrow 0$ , the eigenstates of a quantum non-integrable system spreads over the whole configuration space, given by the micro canonical surface. This is the quantum analogous of ergodic classical systems, in which the micro canonical density of probability is uniform on regions with the same energy. In this sense, the localization transition can be viewed not just as localization of electrons in the real space, but also as localization in the configuration space. This aspect is particularly relevant in the field of Many Body Localization (MBL), the study of the Anderson Localization when interactions among electrons are taken into account. Indeed, in this case the concept of the localization transition as breaking of ergodicity and thermalization is particularly significant [139]. Some aspects of Many Body Localization Transition and the connections with the subjects of this theses will be presented in section (I.9.1).

## I.7 Brief review on numerical results

Despite almost sixty years of research in the field, the Anderson Localization Transition remains an interesting challenging problem: as we have seen in section (I.5), analytical results are available for the Anderson model on the Bethe Lattice and for few other models [99, 100, 101, 102, 103, 104]. The Anderson Model in finite dimension results instead to be still not analytically tractable away from the low dimensional limit, and much less is known in high dimension. As we will see in much details in section (I.9), one of the reason for that is unconventional nature of the order parameter, the distribution of the local density of states, which develops heavy tails in the localized phase. Moreover, there is no small parameter which allows one to study the problem perturbatively, except in a very small region near the lower critical dimension  $d_c = 2$ : indeed, already in  $d = 3$ , the critical disorder is of the same order as the typical bandwidth. This difficulty in treating the problem analytically has motivated the development of numerical techniques, which still results crucial for advances in the topic (see [71] and [61] for reviews on numerical results and methods).

The majority of numerical results has been obtained in three dimension, where scaling analysis of different observables for increasing system sizes has been performed using several numerical techniques. An important part of this analysis regards the study of observables describing transport properties, such as the conductivity or the localization length [10, 11, 12, 13, 140, 91, 92], using the transfer matrix method (see Appendix (A)). Another group of works [14, 15, 16, 17, 18, 19] analyzes observables related to the statistics of energy levels, which, as we have seen in section (I.6), connect the localization transition to RMT and quantum chaos. Also the analysis of wavefunction coefficients and of the multifractal nature of the states at criticality has been performed by different authors [20, 21, 22, 23, 24, 25]. In Ref. [141] the phase diagram in the energy-disorder plane has been also calculated. For the Anderson model with the Hamiltonian (I.1.6) describing spinless electrons with a box distributed on-site disorder, in the middle of the energy spectrum ( $E = 0$ ) a transition is found at a crit-

ical value of the disorder  $W_c \sim 16.5$ . At present, the most precise numerical estimate of the critical exponent  $\nu$ , defined by (I.2.3) and describing the critical behavior of the localization length  $\xi$  is  $\nu = 1.58 \pm 0.01$  [91, 92, 14, 15, 16, 17, 18, 19, 20, 21]. Numerical simulations of this model in three dimension [14, 15, 16, 17, 18, 19] agree with the conjecture explained in section (I.6): the level statistics is GOE-like in the delocalized phase, and thus the properties of the system are captured by RMT, and is Poisson-like in the localized phase, where wave-functions close in energy are exponentially localized on very distant sites and thus do not overlap. At the critical point the level statistics are not GOE nor Poisson-like [142], and are instead characterized by a universal distribution which depends on the dimensionality. Another feature of the critical point is the multifractal spectrum shown by the wave-function amplitudes [22, 23, 24, 25]: the critical eigenstates are not extended nor localized, with large fluctuations of wave-function amplitudes at all length scale. Details on the properties of the multifractal spectrum at the critical point of Anderson Localization Transition are presented in Appendix (B).

Accurate results in 4 and 5 dimensions have also been recently provided [143] through the study of transport properties only. There are however very few results on the level statistics above dimension three [144] and no results for transport properties for  $d > 5$ . The reason for that is the very fast increasing of the running time of numerical algorithms with the size of the system: for exact diagonalization such time increases as  $L^{3d}$  and for transfer matrix algorithms as  $L^{3d-2}$ . As we will see in section (I.9), this problem, besides the lack of analytical techniques, leaves some important questions unanswered, like the existence of an upper critical dimension  $d_u$  or the relation with the infinite  $d$  limit, corresponding to Anderson Localization on tree-like structures.

## I.8 Experiments on Localization

The phenomenon of localization has been observed in different types of systems, even if the first experimental verification of localization arrived around twenty years after the pioneering work of Anderson. A large group of experiments on the metal-insulator transition was realized around 1986. The systems considered were doped silicon Si:P [145] and persistent photoconductors [146]. The transition was studied looking at the conductivity and at the dielectric susceptibility, on both the insulating and the metallic side. The strength of disorder was controlled by varying the concentration of doping atoms in silicon or the concentration of the charge carriers by optical excitation in photoconductors. The results obtained for the critical exponent opened the problem known as the “exponent puzzle”: for the group of uncompensated semiconductors, like Si:P, the critical exponent is  $1/2$ , while for photoconductors and other amorphous solids the value obtained is close to one.

As mentioned in section (I.3), a group of experiments in the early 1980s showed the existence of weak localization, by observing the behavior of the resistance of weakly disordered metallic films: the anomalies revealed could be explained only by taking into account the quantum interference effects in the propagation of the electron wave function. Most of results are reported in the review of Bergmann [148]: in particular it

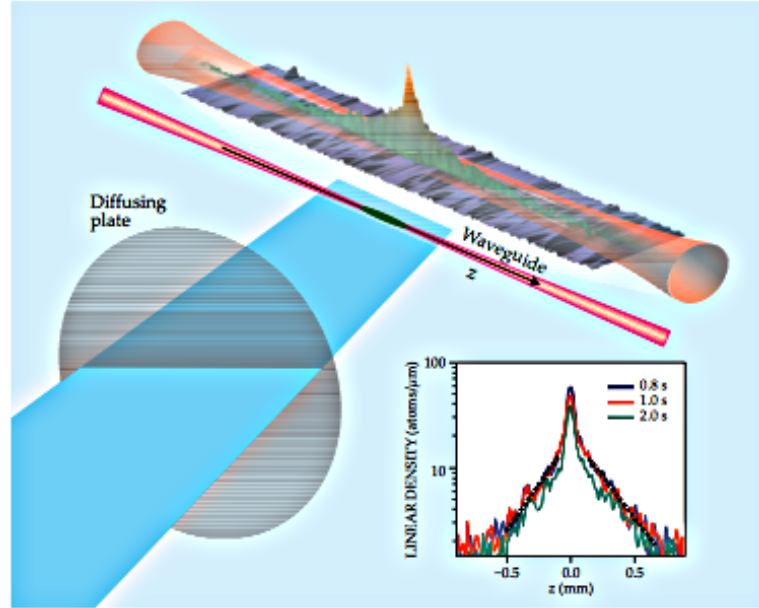


Figure I.8: Density profile of the atomic matter wave localized by a laser speckle. The waveguide confines the atoms transversely to the  $z$ -axis but they are free to travel along the  $z$  direction. A laser beam creates a disorder intensity pattern which varies along  $z$ . A small Bose-Einstein condensate, initially confined along  $z$  is released, and its expansion stops after about 0.5 s. The stationary density profile which emerges at 0.8, 1, and 2 s is plotted, confirming the localization. The image is by [147].

is interesting the observed logarithmic increase of the resistance with the temperature.

Localization Transition can also be observed in classical waves, such as light and acoustic waves [149, 150, 151, 152, 153]. One of the advantage of classical waves is that they don't interact with each other, and it is thus easier to control the experiment at room temperature. In addition to the conductance, it is then possible to study the behavior of other observables strongly influenced by localization, like the fluctuations of wave amplitude. In order to observe localization of light it is necessary to have a material which scatters light strongly enough, but at the same time avoiding absorption effects. A possibility is for example to use near-IR light scattered by a semiconductor with an electronic band gap higher than the frequency of light, such that the absorption is avoided, but with a high refractive index [154]. Other interesting experiments with classical waves were performed with acoustic waves, and in particular ultrasounds: using a point-like source on a three dimensional sample of aluminium, it has been recently observed in [155] the localization of the elastic energy in the transverse direction.

It is very difficult to obtain a clean observation of the Anderson localization in a crystal: as we have seen, the experiments are mainly based on the observation of modifications of bulk properties like conductivity and dielectric susceptibility, and one has no access to the electronic wave functions. It is then complicated to reduce interactions among electrons and the coupling with a thermal reservoir, which can

destroy localization. The most recent experiments on Anderson Localization have been performed using cold atoms: atoms cooled near absolute zero temperature have a large wavelength, of the order of fractions of a micron. Contrary to the case of electrons, the interactions can be controlled. The first observation of Anderson Localization using cold atoms relies on the analogy of Anderson Localization with a dynamical quantum system, the quantum kicked rotor, which is a paradigmatic model in quantum chaos. It models the behavior of a particle periodically kicked by a field, and is described by the Hamiltonian,

$$H = \frac{p^2}{2m} + K \cos \theta \sum_{n=-\infty}^{\infty} \delta(t - n), \quad (\text{I.8.1})$$

where  $m$  is the mass of the particle,  $p$  is the momentum,  $\theta$  is the angular position (we can imagine that the particle is constrained to move on a ring), and  $K$  is the strength of the kicks. In the classical version of the model, if  $K$  is strong enough the system is chaotic. It has been shown that in the quantum case the classical diffusion is suppressed by interference effects [156], and it has been discovered that this system can be mapped to the 1D Anderson model [157]. The first observation of Anderson Localization in 1D with atomic matter waves was possible thanks to the realization of the kicked rotor with laser-cooled atoms interacting with a pulsed standing wave [158].

Localization in one dimension was recently observed by two experimental groups, at Institut d'Optique (Palaiseau) and at the European Laboratory for Nonlinear Spectroscopy (Florence), who realized the experiment exposing a Bose-Einstein condensate to a laser speckle [147, 159, 160], which creates a controlled disorder. In these experiments, the atomic density profile is imaged as a function of time, and it has been found that disorder stops the expansion and leads to the formation of a stationary, exponentially localized wavefunction (see figure (I.8)).

A further step is to observe the localization transition in three dimensional systems. To this end, a generalization of the kicked rotor model which can be mapped to the 3D Anderson model has been considered [161]. The system is obtained by modulating the standing wave pulses with a set of two incommensurate frequencies  $\omega_2$  and  $\omega_3$ . The strength of the kicks  $K$  in equation (I.8.1) is thus replaced by

$$K(t) = K[1 + \epsilon \cos(\omega_2 t + \phi_2) \cos(\omega_3 t + \phi_3)], \quad (\text{I.8.2})$$

and the variable  $\theta$  is extended in the  $(-\infty, +\infty)$  range. This quasi periodic kicked rotor was recently realized experimentally [162], and with a careful analysis of the scaling properties of the dynamics the critical exponent  $\nu$  of the localization length has been determined: the value obtained is  $\nu = 1.4 \pm 0.3$ , compatible with the numerical results for the 3D Anderson model cited in the previous section. In Ref. [163], performing a numerical analysis of the quasiperiodic rotor, it was shown that this system actually belongs to the same universality class as the 3D Anderson model, since both models give the same critical exponent  $\nu$ . Localization of ultra cold atoms in 3d has also been recently observed in experiments using a disordered potential created by laser speckle [164, 165].

## I.9 Open problems

After almost sixty years, the study of Anderson Localization remains an interesting and active field, with various open questions. As we have seen in section (I.4), we have at present a good knowledge of what happens in low dimensional systems. The scaling theory, with its justification through field theory, is able to determine the lower critical dimension, which is two for orthogonal systems, and analytical results for the critical exponents have been obtained perturbatively in dimension  $d = 2 + \epsilon$ , with  $\epsilon \ll 1$ . Yet, the method of the perturbative expansion of the RG flow near  $d = 2$  fails in determining quantitatively the properties of the transition in three dimensions, where exact results for the critical exponents can be determined only numerically: the Anderson Model (and its corresponding field theory NL $\sigma$ M) is in general not soluble for  $d > 2$ , except for a narrow region near  $d = 2$ . The Anderson Localization Transition appears more complicated to treat than conventional critical phenomena. As described in section (I.2), the density of states does not distinguish between the localized and the extended phase, and one has to look at fluctuations of the imaginary part of the Green function (see section (II.1) of the next chapter). Actually, if we want to describe the transition in terms of symmetry breaking it is necessary to introduce an order parameter function: using the formulation of the field theory in terms of supersymmetric fields (see section (II.3)), it has been shown that such a function, introduced in [30], is indeed related to the distribution of one-site Green functions [166, 167]. Due to this non trivial nature of the order parameter, and of the mean field theory of the model, the analysis of the fluctuations around mean field is particularly complicated. The absence of a small parameter and the unusual nature of the order parameter make analytical approaches really challenging, and for this reason numerical techniques are still at the core of the advances in this topic, as explained in section (I.7). Yet, due to the very rapid increase of the running times of the algorithms with the size of the system, only the behavior of systems with quite limited sizes can be simulated, and the sizes for which simulations are possible become smaller and smaller as the dimensionality is increased. As a consequence, the study of the behavior in high dimension results to be challenging also numerically. For all these reasons, some basic questions, as for instance the existence of an upper critical dimension  $d_u$ , remain unanswered. As we will see more in detail in the next Chapters, several observations seem to indicate that  $d_u$  could be infinite [144, 166, 167, 168], while different propositions have been made, corresponding to  $d_u = 4, 6$  and  $8$  [169, 170, 171, 172, 173, 174, 175].

Another issue is the relation with the infinite  $d$  limit. As we have explained in section (I.5) the best way to study the behavior in high dimension is to consider the Anderson model on the Bethe Lattice. On one hand, models on tree-like structures allow for an analytical treatment, such that the transition point and the corresponding critical behavior can be established. The analytical results of Abou-Chacra, Anderson and Thouless [8], who first solved the problem, have been confirmed numerically in Refs. [176] and [177]. Moreover, recently, rigorous results on the mobility edge and the proof of the existence of extended states have been obtained [178, 179]. As already mentioned, the critical behavior has been studied with the supersymmetric method, both in the  $\sigma$  model formulation [34, 35, 36, 37] and in the tight binding version [30]: it has been found that the localization length diverges at the mobility edge as  $\xi \sim$

$|E - E_c|^{-1}$ . An effective method has been developed to study the transition for a lattice in  $d$  dimension [180, 181]: this technique, the effective-medium approximation, consists in calculating exactly the interaction between two fixed sites, and to consider the interaction with the others as the interaction with an effective medium. This gives the same self-consistent equations for the mobility edge as on the Bethe Lattice, but different equations for the density-density correlation functions. This approximation is exact for  $d \rightarrow \infty$ , and gives for the critical exponent describing the behavior of the localization length the value  $\nu = 1/2$ . As we will see in the next Chapter, the supersymmetry method predicts important and non conventional characteristics of the Anderson Transition on the Bethe Lattice, like the exponential singularities of some critical quantities at the transition, as the diffusion coefficient [85, 30], and the behavior of the moments  $\Upsilon_q$  of the normalized measure  $|\psi|^2$ , which show a discontinuous jump at the critical point [30, 182]. On the other hand, several features of the transition on the Bethe Lattice, and in particular some properties of the delocalized phase are still a debated issue, like the statistics of extended wave functions, and the behavior of the level spacing distribution (see section (I.6)): in particular it has been argued that an intermediate mixed phase, delocalized but non-ergodic, could exist. This problem has been the subject of intense discussions in the last years and the question is still open.

The study of the Anderson Transition in high dimension and on tree-like structures has attracted such an interest recently because of its connection with the problem of Many Body Localization (MBL). The next subsection is dedicated to a brief presentation of the problem of Many Body Localization and its connection with the one-particle problem in high dimension and on the Bethe Lattice, while in the paragraph (I.9.2) we present some aspects of the issue of the intermediate phase.

The original part of this thesis deals on one hand with the study, both analytically and numerically, of a random matrix model with long-range hopping, the Lévy Matrices, which presents connections with the infinite  $d$  limit and with tree-like structures: the model and the results are presented in Chapter (III) and are mainly based on Ref. [183]. On the other hand, in Chapter (IV) we present the results of our numerical study of the Anderson Model from dimensions 3 to 6, performed through exact diagonalization (ED) and the transfer matrix method (TM) (see Appendix (A)). The connection and the possible implications of this results on the unusual properties of the delocalized phase observed in tree-like structures and in Lévy Matrices are then discussed.

### 1.9.1 Interactions and Many Body Localization

The problem of localization becomes more complex if we consider interactions among electrons: the fundamental question, which has remained unsolved for years, is if the picture we have so far survives or not once we add interactions. For the one-particle problem, we know that, if the wave function of the electron at the Fermi surface is localized, we can have finite conductance if the electron is thermally activated above the mobility edge. Mott showed that, coupling the electrons with a phonon bath, electrons can hop between the localized states without thermal activation of the mobility edge (“variable range hopping”) [184]. For long time it was discussed if interactions among electrons could play an analogous role as electron-photon interactions, and thus

restore a finite conductivity without thermal activation. The question remained unsolved until the work of Basko, Aleiner and Altshuler [48] in 2006: the authors showed that, if the temperature is finite but small enough, electron-electron interaction alone can not cause finite conductivity. Yet, there exist a critical temperature  $T_c$  such that for  $T > T_c$  the conductivity is finite. For such temperature the system of interacting electrons undergoes thus a phase transition, called Many Body Localization Transition. The analysis in [48] consists in taking into account the interactions in perturbation theory, studying the inelastic quasiparticle relaxation, represented by the imaginary part of the single-particle self-energy. In a pictorial view, MBL can be thought of as localization in the Fock space of Slater determinants, which plays the role of lattice sites in a disordered one-particle Anderson tight-binding model. The problem of  $N \gg 1$  interacting particles in a finite dimensional lattice is thus interpreted as a one-particle localization problem on a very high dimensional lattice, which for spinless electrons consists in an  $N$ -dimensional hyper-cube of  $2^N$  sites. This makes the study of single-particle Anderson Localization in very high dimension (and consequently the problem on the Bethe Lattice) an interesting issue for the comprehension of the problem with interactions. The idea of interpreting a many particle problem as a single-particle one in a very high dimensional space appeared in the context of the study of vibrational degrees of freedom of very big molecules [29], and was then applied in [47] to study the problem of electron-electron lifetime in a quantum dot. The work of Oganesyan and Huse [136], already cited in section (I.6), points out instead the link of MBL with Random Matrix Theory, and offer, at least numerically, a way to study the transition in relation to the level spacing distribution and ergodicity properties. We have to stress indeed that for MBL is particularly significant the description of the transition in terms of breaking of ergodicity (see section (I.6)): it is a transition between a thermal phase, in which we expect all the eigenstates to obey the Eigenstate Thermalization Hypothesis (ETH) [28], according to which each eigenstate is representative of the micro canonical ensemble, and the many body localized phase, in which the ETH stops to hold, and the dynamics conserve some memory of the local initial conditions. The study of the features of this transition has received much attention during the last years, and several questions are open, like the determination of the critical properties, and the presence of an intermediate mixed phase, delocalized but non-ergodic (“bad metal” phase), in analogy with the mixed phase argued for the single-particle problem on the Bethe Lattice (see next paragraph). In the language of MBL the “bad metal” phase is a phase in which thermalization and ergodicity is possible only on certain subregions of the configuration space.

### I.9.2 The problem of the intermediate phase

In the work of 1997 [47] cited above, Altshuler and coworkers studied the problem of electron-electron lifetime in a quantum dot by mapping it into the problem of localization in the Fock space. In this study they found a delocalized and a localized regime, and they identified a broad critical region near the mobility edge on the side of the delocalized phase, in which the states are multifractal. As mentioned in the previous sections, multifractal states, which are extended but non-ergodic, i.e. occupy zero fraction of the lattice in the thermodynamic limit, exist in the problem of single-

particle Anderson Transition in three dimension, but only at the critical point. The authors of [47] suggested instead the presence of non-ergodic extended state in a whole region near the critical point. Following up this suggestion, and the analogy between MBL and the problem of one-particle localization on the Bethe Lattice, in [39] a numerical study of the one-particle problem on the Random Regular Graph (RRG) has been performed. A RRG of connectivity  $k + 1$  is a graph selected at random among all the possible graph of connectivity  $k + 1$  [185]. As we will explain more in detail in section (II.2.1), for a Bethe Lattice of finite size most sites belong to the boundary, and we expect therefore that boundary effects play an important role in numerical simulations, significantly affecting the results. The RRG is one of the possibility to construct a structure which is locally a tree-like graph, but which has no boundary: it essentially corresponds to a finite portion of a Bethe Lattice wrapped into itself<sup>2</sup>. The main result of the analysis of Ref. [39] is that the mobility edge computed from the (numerical) solution of the self-consistent equations [8, 186], and the transition revealed observing the level spacing distribution seem to not coincide. In particular, an intermediate phase which is delocalized but which does not show GOE-like behavior seems to be present. It is however complicated to establish if the observed behavior is the sign of a real intermediate phase transition, or the consequence of very strong finite size effects: in the latter case the data should be interpreted in terms of a finite-size crossover. The answer to this question is non trivial, and the work of Ref. [39] remained unpublished on purpose. More recently, other works on the Anderson Model on the RRG have investigated the problem of the intermediate phase, focusing in particular on the analysis of the statistics of extended wave functions, finding that these statistics may indeed be multifractal [40, 41]. In [44], combining numerical and semi-analytical calculation, has been then found an evidence for a order transition between ergodic and non-ergodic states within the delocalized phase in RRG. The delocalized non-ergodic phase would imply heterogeneous behavior at the level of transport and diffusion: the particle can travel far away from a given site, but only following specific and disorder dependent paths. In the language of MBL, this means that thermalization is possible only on certain subregions of the Hilbert space. As we will see in section (II.3), the presence of such intermediate phase would be in contradiction with the results obtained by the supersymmetric method for the behavior of the moments of the distribution of wavefunction coefficients. The question of the existence of such phase for the single-particle problem on the Bethe Lattice and its implications for MBL is still a subject of research and discussion. We have investigated the problem of the existence of an intermediate phase of this type in Lévy Matrices, which, as we will explain in section (III.1), present connections with the problem of Localization on Bethe Lattice, and could actually be an interesting system to consider in order to understand the mean field properties of Anderson Localization. The possibility of the existence of an intermediate delocalized non-ergodic phase has been advocated for this kind of matrices by [38], and this is one of the reason which motivated us to study this model. Our results support the idea that the delocalized phase of Lévy Matrices is ergodic, both in the sense of the level statistics and the wavefunction statistics.

The analysis performed in Ref. [42] leads to results in contradiction with those of

---

<sup>2</sup>Another possibility is to consider the Sparse Random Matrix model, described in Chapter (II), which is known in mathematical literature as Erdős-Rényi random graph.

Ref. [44] (the two works are almost contemporary): in particular, in [42] a numerical analysis of the Anderson model on RRG has been performed, and the results show that important finite-size effects are present in the delocalized phase. The authors have thus interpreted the data in terms of a crossover, and have studied the non-monotonicity of the spectral and wavefunction statistics, supporting the prediction of the supersymmetric method that eigenstates in the delocalized phase are ergodic. A successive work by two of the same authors [43] shows with analytical and numerical techniques that the intermediate delocalized non-ergodic phase actually emerges when we consider a finite portion of a Bethe Lattice (Cayley tree), in which most sites belong to the boundary: a similar result had been found several years before by Monthus and Garel [187]. At the same time, in Ref. [43] it is also shown that the intermediate non-ergodic phase, which is a property of the delocalized phase of the Cayley tree, seems to be absent when considering locally tree-like structures as the RRG or the Sparse Random Matrix model. During the same period other works have been submitted [44, 45], showing results in contradiction with those presented in Refs. [42, 43], and supporting the violation of ergodicity of the delocalized states on the RRG. Another very recent work [46] studying the Anderson Transition in random graphs through large scale numerical simulations, analyzing systems up to  $N \sim 2 \times 10^6$ , supports instead the idea that there is only a single Anderson transition separating a localized phase from an ergodic delocalized one. However, the authors show that a characteristic non-ergodicity volume emerges in the delocalized phase, such that, for scale below this characteristic volume the system behaves as if it was in an intermediate phase, and the states display a multifractal behavior, while for scale larger than this typical volume the system exhibits ergodicity. The characteristic non-ergodicity volume diverges at the transition, and thus, in the localized phase, the non-ergodic behavior extends to the whole system. Even if this work is a strong hint of the non-existence of the intermediate mixed phase in the RRG, the reason for such strong non-ergodic behavior exhibited up to large system sizes remains unknown. As we will show in Chapter (III), we have found a similar behavior analyzing the localization transition and ergodicity of Lévy Matrices.



# Chapter II

## Overview on analytical techniques and known results

In this Chapter, we describe some of the analytical techniques used to study Anderson Localization Transition and random matrices. We focus in particular on the methods we have used in our works during the theses, in particular for the study of Lévy Matrices, presented in Chapter (III). For simplicity, and for the purposes of this theses, in what follows we refer to real tight binding Hamiltonian  $H$  with some disorder, i.e. to real random matrices of the form (I.6.6). In principle the definitions and techniques presented here can be generalized to all the models showing Anderson Localization Transition: the original classification, corresponding to the symmetries of the three classical Dyson ensembles in RMT, has been discussed in section (I.6). A more general classification and discussion on symmetries and universality classes can be found in [188].

We present first the cavity method, an approximation which is exact in the limit of infinite dimensionality, represented by the Bethe Lattice, and that can be used also for Lévy Matrices leading to an exact equation which is the basis of the computation of the mobility edge. We introduce then the supersymmetric method, a technique largely applied in the study of Anderson Localization which allows for non-perturbative calculations. Finally we present the Dyson Brownian Motion model, a standard technique in the study of random matrices which recently has been used in many works as a tool to extend the results of RMT to larger and more general classes of matrices.

### II.1 Definitions

We consider a real random Hamiltonian  $H$  of the form (I.6.6). Given an eigenstate  $|\alpha\rangle$  of the system, we define the moments of the normalized measure  $|\psi_\alpha|^2$  as

$$\Upsilon_q = \sum_i |\langle \alpha | i \rangle|^{2q} = \sum_i |\psi_{\alpha i}^2|^q, \quad (\text{II.1.1})$$

where  $|\psi_{\alpha i}^2|$  is the weight of the site  $i$  in the eigenstate  $|\alpha\rangle$ , and the sum spreads over all sites  $i$ . For  $q = 1$  we have  $\Upsilon_1 = 1$ , which gives the normalization condition. For  $q = 2$  the expression (II.1.1) gives the definition of the Inverse Participation Ratio

(IPR), the inverse of the number of sites having non-zero weight in the state  $|\alpha\rangle$ . It is easy to see the behavior of  $\Upsilon_2$  in the two following extreme cases: if the state  $|\alpha\rangle$  is completely delocalized, each site  $i$  contributes with a weight  $\psi_{\alpha i}^2 \sim 1/V$ , with  $V$  the volume of the system, therefore, from the definition (II.1.1),  $\Upsilon_2$  goes to zero as  $1/V$  in the thermodynamic limit. In the opposite case, where  $|\alpha\rangle$  is localized on a finite number  $p$  of sites, much smaller than the number of sites of the system, the sum in the expression (II.1.1) has just  $p$  terms different from zero, each one of order  $1/p$ :  $\Upsilon_2$  is thus finite and different from zero in the thermodynamic limit. Studying the behavior of the moments  $\Upsilon_q$  as a function of the system size is therefore a way to inspect the localization transition.

We introduce now the resolvent matrix  $G = ((E - i\eta)\mathbb{1} - H)^{-1}$ . Assuming that  $H$  has a set of eigenvalues  $\{E_\alpha\}_{\alpha=1,\dots,N}$  and a set of eigenvectors  $\{|\alpha\rangle\}$ , for the diagonal elements we have:

$$G_{ii}^{(N)} = \left( \frac{1}{(E - i\eta)\mathbb{1} - H} \right)_{ii} = \sum_{\alpha=1}^N \frac{|\langle i|\alpha\rangle|^2}{(E - E_\alpha) - i\eta}, \quad (\text{II.1.2})$$

where, as in the definition of the IPR,  $|i\rangle$  is the canonical bases of  $H$  and  $N$  is the number of sites of the system. The spectral properties of the Hamiltonian can be expressed in terms of the resolvent. In particular, the eigenvalue density  $E_\alpha$ ,  $\rho(E) = 1/N \sum_{\alpha=1}^N \delta(E - E_\alpha)$ , is expressed in terms of the imaginary part of the trace of  $G$  according to the following expression:

$$\rho(E) = \lim_{\eta \rightarrow 0} \lim_{N \rightarrow \infty} \frac{1}{N\pi} \Im \text{Tr} G(E - i\eta). \quad (\text{II.1.3})$$

However, the density of states (DoS) does not contain information on the localization transition (for the standard symmetry classes), and in order to differentiate between localized and extended states one has to look at the behavior of the distribution of the imaginary part of the resolvent [2, 189, 190, 71, 61], which develops heavy tails in the localized phase due to very large and rare resonances dominating the average: in the delocalized part of the spectrum, the typical value of the imaginary part of  $G$  has a finite limit when  $\eta \rightarrow 0$ , which of the same order as its average value. In the localized region of the spectrum instead, the typical value of  $\Im G$  is zero almost everywhere in the limit  $\eta \rightarrow 0$ , and there is just a discrete set of sites where  $\Im G$  is infinitely large: the typical value of  $\Im G$  is therefore very different from its mean value.

Since the average value of the imaginary part of the resolvent does not distinguish between localized and extended states, we must look at least at the mean square of  $G$  in order to investigate the transition. Indeed, the quantities of interest for studying the localization transition are expressed in terms of products of the retarded and the advanced Green functions  $G_s(E, i, j) = \langle i|(E + i(-1)^{s-1}\eta\mathbb{1} - H)^{-1}|j\rangle$ ,  $s = 1, 2$ . In particular, we have to look at the density-density correlation function  $K_\omega(i, j)$  [191], defined as

$$K_\omega(i, j) = \overline{\left( \frac{1}{(E + \frac{\omega}{2} + i\eta)\mathbb{1} - H} \right)_{ij} \left( \frac{1}{(E - \frac{\omega}{2} - i\eta)\mathbb{1} - H} \right)_{ji}}, \quad \eta \rightarrow 0, \quad (\text{II.1.4})$$

where the average is over the distribution of the random matrix elements of  $H$ .

In the delocalized phase this quantity has the following form in momentum space [71]:

$$K_\omega(q) = \frac{2\pi\rho(E)}{Dq^2 - i\omega}, \quad (\text{II.1.5})$$

where  $D$  is the diffusion coefficient, related to the conductivity by the relation (I.1.4). In the localized phase it takes instead the form

$$K_\omega(i, j) \sim \frac{2\pi\rho(E)}{-i\omega} \exp\left(\frac{|i - j|}{\xi}\right), \quad (\text{II.1.6})$$

decaying exponentially on the scale of the localization length.

If we consider the correlation function  $K_0(i, i)$  for  $i = j$ , which corresponds to  $|G_{ii}|^2$ , we see that for  $\eta$  small but finite this represents the probability for an electron starting at site  $i$  to return to the same site after a time  $\eta$ . Using the spectral representation of the Green function, it is possible to see that the eigenvalue dependent inverse participation ratio, is given in terms of  $K_0(i, i)$  by the expression

$$\frac{1}{N\rho(E)} \sum_{i,\alpha} |\langle i|\alpha\rangle|^4 \delta(E - E_\alpha) = \lim_{\eta \rightarrow 0} \frac{\eta}{\pi N\rho(E)} \sum_i |G_{ii}(E - i\eta)|^2. \quad (\text{II.1.7})$$

The IPR corresponds thus to the probability that the electron returns to the same site after an infinite time interval [192, 193, 93]. It is however important to notice that expression (II.1.7) defines the eigenvalue-dependent IPR, while the IPR introduced at the beginning of this section and defined by expression (II.1.1) for  $q = 2$  is the IPR associated to the state  $\alpha$  (see Appendix (C)).

## II.2 Cavity equations

In this section we describe an approximation used to obtain a self-consistent equation for the resolvent (II.1.2): this result is found to be exact on an infinite Bethe Lattice (see section (II.2.1)), but also for Lévy Matrices (see chapter (III)), where is the basis for the computation of the mobility edge. Historically, the equations we derive here were first obtained by Abou-Chacra, Anderson and Thouless [8] for the Anderson model (I.1.6) with on-site disorder on an infinite Bethe Lattice. In order to make the derivation as general as possible, we consider again a  $N \times N$  random Hamiltonian  $H$ , and we don't make any particular assumption on the probability distribution of the entries. The first step is to write the definition of the resolvent (II.1.2) in terms of a Gaussian integral over real auxiliary fields  $\phi_i$ :

$$G_{ii}^{(N)}(z) = i \frac{\int \prod_{k=1}^N d\phi_k \phi_i^2 \exp\left[-\frac{i}{2} \sum_{k,l=1}^N \phi_k (z\delta_{k,l} - H_{kl})\phi_l\right]}{\int \prod_{k=1}^N d\phi_k \exp\left[-\frac{i}{2} \sum_{k,l=1}^N \phi_k (z\delta_{k,l} - H_{kl})\phi_l\right]}, \quad (\text{II.2.1})$$

where we have defined  $z = E - i\eta$ . We now show how the cavity method yields an exact recursion relation for the elements of the resolvent matrix  $G_{ij}^{(N)}$  of a system of size  $N \times N$  as a function of the elements of the resolvent matrix of a system of size

$(N - 1) \times (N - 1)$ . The cavity method was introduced in the context of the study of disordered spin systems, and it provides a way to compute the local marginals for systems defined on fully-connected [194] and finitely connected random graphs and trees [195]. Given a random matrix  $H$  of size  $N \times N$ , one can always relate it to a random graph of  $N$  nodes, each of which is associated with a variable  $\phi_i$ , ( $i = 1, \dots, N$ ) [196]. The corresponding graph is built in the following way: the pair of nodes  $i$  and  $j$  are connected when  $H_{ij} \neq 0$ , while there is no link between  $i$  and  $j$  when  $H_{ij} = 0$ . In this way the matrix  $H$  contains both the information on the topology of the graph and on the interaction strength between the nodes. By means of this analogy, the cavity method can efficiently be applied to the study of random matrices.

We consider the Gaussian probability measure

$$\mu(\underline{\phi}) = \frac{\exp\left[-\frac{i}{2} \sum_{k,l=1}^N \phi_k (z\delta_{kl} - H_{kl})\phi_l\right]}{\int \prod_{k=1}^N d\phi_k \exp\left[-\frac{i}{2} \sum_{k,l=1}^N \phi_k (z\delta_{kl} - H_{kl})\phi_l\right]}, \quad (\text{II.2.2})$$

defined on the graph associated to the matrix  $H$ , which allows to write the diagonal elements of the resolvent  $G_{ii}^{(N)}(z)$  in the compact form

$$G_{ii}^{(N)}(z) = i \int \prod_{k=1}^N d\phi_k \phi_i^2 \mu(\underline{\phi}). \quad (\text{II.2.3})$$

We also define the marginal at site  $k$  as  $\mu(\phi_k) = \int \prod_{j \in \partial_k} d\phi_j \mu(\underline{\phi})$ , where  $\partial_k$  is the set of neighbors of site  $k$ . If we separate the contribution of site  $k$  from the rest, we have the expression:

$$\mu(\phi_k) \sim \int \prod_{j \in \partial_k} d\phi_j \mu^{(\neq k)}(\underline{\phi}) \exp\left[-\frac{i}{2}(z - H_{kk})\phi_k^2 + i\phi_k \sum_{j \in \partial_k} H_{kj}\phi_j\right], \quad (\text{II.2.4})$$

where  $\mu^{(\neq k)}(\underline{\phi})$  is the measure (II.2.2) defined on the graph obtained from the original one, once the site  $k$  has been removed (cavity graph). If we now consider removing the site  $l$  from the original graph, we have:

$$\mu^{(\neq l)}(\phi_k) \sim \int \prod_{j \in \partial_k \setminus l} d\phi_j \mu^{(\neq k, l)}(\underline{\phi}) \exp\left[-\frac{i}{2}(z - H_{kk})\phi_k^2 + i\phi_k \sum_{j \in \partial_k \setminus l} H_{kj}\phi_j\right]. \quad (\text{II.2.5})$$

In the above eqs. (II.2.4) and (II.2.5) we have omitted the normalization terms corresponding to the integrals over the sites which have been removed in the cavity graphs. The cavity method is based on making two assumptions which allow to close the system of eqs. (II.2.4) and (II.2.5): the first is that the measure  $\mu^{(\neq i)}(\underline{\phi})$ , defined on the original graph after removing the site  $i$ , factorizes over the sites of the cavity graph according to

$$\mu^{(\neq i)}(\underline{\phi}) = \prod_{j \in \partial_i} \mu^{(\neq i)}(\phi_j). \quad (\text{II.2.6})$$

The second assumption is that, when  $N \rightarrow \infty$ , the measure  $\mu^{(\neq i)}(\phi_j)$  is the same as  $\mu^{(\neq i, k)}(\phi_j) \forall j$ . Therefore, eqs. (II.2.4) and (II.2.5) assume the following self-consistent form:

$$\mu(\phi_k) \sim \exp \left[ -\frac{i}{2}(z - H_{kk})\phi_k^2 \right] \prod_{j \in \partial_k} \int d\phi_j \mu^{(\neq k)}(\phi_j) \exp(i \phi_k H_{kj} \phi_j), \quad (\text{II.2.7})$$

$$\mu^{(\neq l)}(\phi_k) \sim \exp \left[ -\frac{i}{2}(z - H_{kk})\phi_k^2 \right] \prod_{j \in \partial_k \setminus l} \int d\phi_j \mu^{(\neq k)}(\phi_j) \exp(i \phi_k H_{kj} \phi_j). \quad (\text{II.2.8})$$

In this way, one can first solve the problem on the cavity graph, and then reconstruct the local marginals on the original graph by means of eq. (II.2.7). In particular, we parametrize the Gaussian measure  $\mu^{(\neq l)}(\phi_k)$  as:

$$\mu^{(\neq l)}(\phi_k) = \sqrt{\frac{i}{2\pi G_{kk}^{(N-1)(\neq l)}(z)}} \exp \left( -\frac{i \phi_k^2}{2G_{kk}^{(N-1)(\neq l)}(z)} \right), \quad (\text{II.2.9})$$

where  $G_{kk}^{(N-1)(\neq l)}(z)$  are the diagonal elements of the resolvent of the matrix  $H$ , in which row  $l$  and column  $l$  have been removed. Substituting this *ansatz* in the eqs. (II.2.7) and (II.2.8) we obtain the following equations:

$$G_{ii}^{(N-1)}(z) = \frac{1}{z - \sum_{j \in \partial_i \setminus k} H_{ij}^2 G_{jj}^{(N-1)}(z)}, \quad (\text{II.2.10})$$

$$G_{ii}^{(N)}(z) = \frac{1}{z - \sum_{j \in \partial_i} H_{ij}^2 G_{jj}^{(N-1)}(z)}. \quad (\text{II.2.11})$$

The diagonal elements of the resolvent  $G_{ii}^{(N)}(z)$  is therefore given by the fixed-point solution of eqs. (II.2.10) and (II.2.11).

As mentioned above, these equations have been derived for the first time by Abou-Chacra, Anderson and Thouless in [8], using a different technique, based on the approach originally used by Anderson in his seminal work [2], where the localization of electron eigenfunctions for strong disorder (or in the tails of the energy spectrum) is shown starting from a perturbative expansion in powers of the hopping term for the self-energy  $\Sigma_i$ , defined as:

$$\Sigma_i = z - H_{ii} - G_{ii}^{-1}. \quad (\text{II.2.12})$$

Indeed, if we consider a tight binding Hamiltonian of the form (I.1.6) with random on-site terms (I.1.7), in the limit of strong disorder  $t \ll W$ , we can write the following expansion for the resolvent  $G$ :

$$G = \frac{1}{z - \epsilon_i - T} = \frac{1}{G_0^{-1} - T} = G_0 (1 + T G_0 + T G_0 T G_0 + \dots), \quad (\text{II.2.13})$$

where  $G_0 = (z - H_0)^{-1}$  is the resolvent defined considering just the diagonal part  $H_0 = \sum_i \epsilon_i c_i^\dagger c_i$  of the Hamiltonian, and  $T = t \sum_{\langle i,j \rangle} c_i^\dagger c_j + h.c.$  is the off-diagonal part of  $H$ . In terms of the matrix elements, this expansion reads for  $G_{ii}$

$$\begin{aligned} G_{ii} &= \frac{1}{z - \epsilon_i} \left( 1 + \sum_{k \neq i} T_{ik} \frac{1}{z - \epsilon_k} T_{ki} + \sum_{k,l \neq i} T_{ik} \frac{1}{z - \epsilon_k} T_{kl} \frac{1}{z - \epsilon_l} T_{li} + \dots \right) = \\ &= \frac{1}{z - \epsilon_i} \left( 1 + \sum_n \sum_{\{j_k\} \in \mathcal{P}} T_{ij_1} \frac{T_{j_1 j_2} \dots T_{j_{n-1} j_n}}{(z - \epsilon_{j_1}) \dots (z - \epsilon_{j_n})} T_{j_n i} \right), \end{aligned} \quad (\text{II.2.14})$$

where  $j_1$  and  $j_n$  are neighbors of the site  $i$ , and we have written the expansion on the right hand side as a sum over all the possible (repeating) paths starting from  $i$  and coming back to  $i$  with intermediate sites  $\mathcal{P} = (j_1, \dots, j_n)$ . It is possible to rearrange the sum in the r.h.s, corresponding to the self-energy, in terms of non-repeating paths, obtaining an equation of this type:

$$\Sigma_i = \sum_n \sum_{(j_1, \dots, j_n) \neq i} T_{ij_1} \frac{T_{j_1 j_2} \dots T_{j_{n-1} j_n}}{(z - \epsilon_{j_1} - \Sigma_{j_1}^{(\neq i)}) \dots (z - \epsilon_{j_n} - \Sigma_{j_n}^{(\neq i)})} T_{j_n i}, \quad (\text{II.2.15})$$

where now the sum is over directed paths  $(j_1, \dots, j_n)$ , the repeating ones having been absorbed in the terms  $\Sigma_{j_1}^{(\neq i)}, \dots, \Sigma_{j_n}^{(\neq i)}$ , corresponding to the self-energies at sites  $i_1, \dots, i_n$ , computed on the graph where the site  $i$  has been removed. The convergence of this series should be studied in order to determine the transition: the region of energies where (II.2.15) is convergent corresponds to localized states, while the extended states correspond to energies where the series is divergent. The expansion (II.2.15) is in general complicated to solve. The approach of Anderson [2] consists in neglecting the self-energies in the denominator, assuming therefore that the terms in the series are statistically independent (*forward approximation*): this approximation is known to overestimate the delocalization mechanism [2, 197]. Abou-Chacra, Anderson and Thouless [8] proposed instead to truncate the series at the second order in the hopping: if we ignore the fact that the self energy on the l.h.s. and on the r.h.s are not the same, we obtain the self consistent equation

$$\Sigma_i = \sum_{j \neq i} T_{ij} \frac{1}{z - \epsilon_j - \Sigma_j} T_{ji}, \quad (\text{II.2.16})$$

where the sum is over the neighbors  $\{j\}$  of the site  $i$ . This equation is exactly the same of (II.2.10) written in terms of the self-energy. As we will see in the next subsection, this equation is exact on an infinite regular tree (Bethe lattice).

### II.2.1 On the Bethe Lattice

The Bethe lattice is an infinite regular tree: a graph without loops in which every vertex has the same degree  $k + 1$ . In the figure (II.1) a portion of a Bethe lattice with connectivity  $k + 1 = 3$  is shown. In order to study the thermodynamical properties of a

model defined on a Bethe lattice, we have to consider finite size versions of the graph, and then take the limit  $N \rightarrow \infty$ . We can construct a finite size Bethe lattice by starting from a root (generation  $n = 0$ ) with  $k + 1$  offsprings and creating  $n - 1$  generations in which each vertex has  $k$  offsprings. The  $n$ -th generation has no descendent. The problem with this definition is that a finite fraction of the sites of the lattice belong to the boundary and have therefore connectivity one. An alternative way to define a finite size Bethe lattice which avoid this boundary effects, as we have explained in section (I.9.2), is to consider a random- $k + 1$  regular graphs (RRG), i.e. a graph selected uniformly from the probability space of all regular graphs of  $N$  vertices with degree  $k + 1$  [185]: this is a way to wrap the lattice into itself, such that the boundary sites are connected each other in a way that preserves the local structure of the tree.

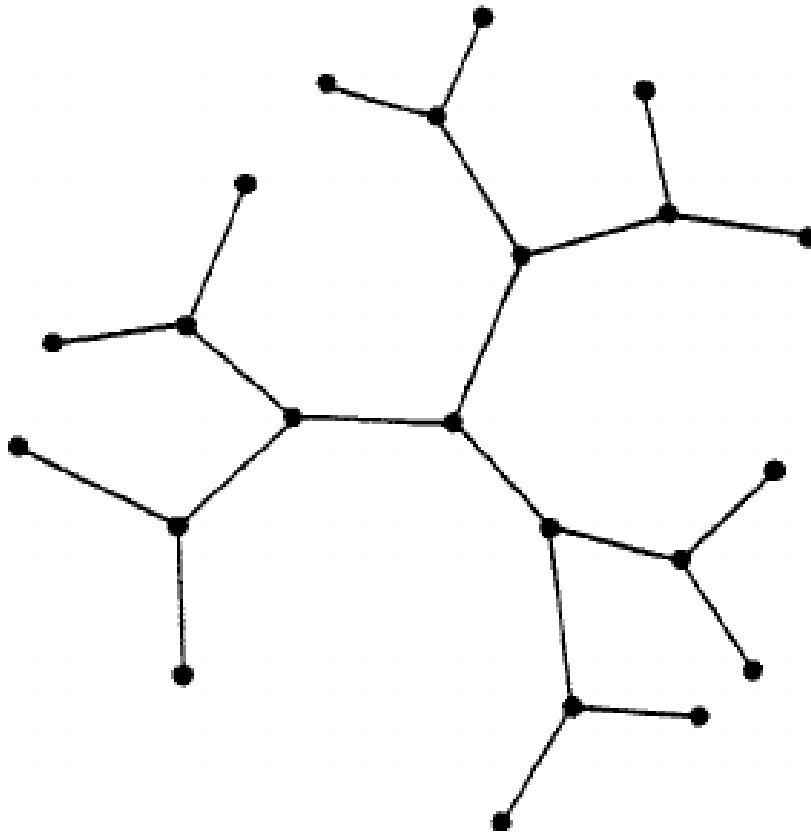


Figure II.1: Bethe lattice with connectivity  $k + 1 = 3$ .

Let's consider the tight-binding Hamiltonian (I.1.6) with on-site disorder (I.1.7) on a Bethe lattice: we can define the gaussian probability measure (II.2.2) for this system and proceed as explained in section (II.2). Due to the particular structure of the graph, where loops are absent, the assumption (II.2.6) that the probability measure factorizes over the cavity graph results verified, and therefore the cavity equations (II.2.10) and (II.2.11) are an exact result. We will show in Chapter (III) that the same is true in the thermodynamic limit for Lévy Matrices. Alternatively, if we follow the approach of Anderson and we construct the expansion (II.2.15), we see that the series reduces to a single term, being the only non-repeating paths starting to  $i$  and coming back to

$i$  those of the form  $i \rightarrow j \rightarrow i$ , with  $j$  neighbor of  $i$ : therefore we obtain exactly the equation (II.2.16).

The cavity equation on the Bethe lattice can be treated as in Ref. [8] by studying the stability of the imaginary part of the self-energy under iteration. First of all we separate explicitly the real and the imaginary part of  $\Sigma_i = S_i + i\Delta_i$ , and we suppose to be in the localized phase, where  $\Im G_i^{typ} \rightarrow 0$  for  $\eta \rightarrow 0$ , and  $\Delta_i$  is thus very small, except for very few resonances, as explained in section (II.1): we can therefore linearize the self-consistent equation (II.2.16) with respect to  $\Delta_i$  obtaining

$$\begin{aligned} S_i &= \sum_{j=1}^k t^2 \frac{1}{E - \epsilon_j - S_j} \\ \Delta_i &= \sum_{j=1}^k t^2 \frac{\eta + \Delta_j}{(E - \epsilon_j - S_j)^2}, \end{aligned} \quad (\text{II.2.17})$$

where we have used  $z = E - i\eta$  and we have substituted the elements  $T_{ij}$  of the hopping matrix with the constant hopping strength  $t$ . The expression for the real part  $S_i$  does not depend on  $\Delta_i$ , and the equation for  $\Delta_i$  is a linear inhomogeneous equation: this can be rewritten as an integral equation which has a finite solution only in the localized phase. The mobility edge is thus found by studying the kernel of such integral equation. As described in Chapter (III), we have followed the same procedure in order to compute the mobility edge of Lévy Matrices.

In the case of the Bethe Lattice a complete analytical solution is not easy to obtain: however, upper and lower bound have been established for the mobility edge  $W_c$  [8, 198], and it has been shown in Ref. [198] that they match in the large connectivity limit, giving the asymptotic behavior

$$W_c/t \sim 4k \log k. \quad (\text{II.2.18})$$

The cavity equations (II.2.10) and (II.2.10), exact on the Bethe lattice, have the same status as the Bethe Peierls approximation for the Ising model. Moreover, since the behavior on the Bethe lattice should be representative of the behavior on high dimensional lattices, the analysis of the Anderson model on the Bethe lattice plays an important role also in the problem of Many Body Localization, as we have explained in section (I.9.1).

### II.3 Supersymmetric method

As pointed out in section (I.4), the first version of the  $\sigma$  model, based on the replica trick, does not allow for non-perturbative calculations, particularly important in the analysis of the level-level correlation functions and the eigenfunctions statistics. This motivated Efetov to develop a novel version of the  $\sigma$  model, based on the combination of fermionic and bosonic degrees of freedom, a technique known as Supersymmetric method [85, 86, 87]. As mentioned in the previous Chapter, this new version of the  $\sigma$  model is equivalent to the previous one on a perturbative level [87], but it indeed succeeds in allowing non perturbative calculations too. In particular,

Efetov applied this method to the calculation of the level-level correlation function in a small metallic particle [199], finding the same expressions as for the three classical Dyson ensembles in RMT, considering the three corresponding possibility for the presence or absence of time reversal symmetry and central symmetry (see section (I.6)). This was an important result, on one hand because it showed that the supersymmetric version of the  $\sigma$  model could provide information on the level statistics, but also because it demonstrated explicitly that RMT could be used to describe properties of real physical systems, since applications of RMT in physics were, up to that moment, mainly based on phenomenological assumption. The method introduced by Efetov was successfully applied to obtain the full solution of the localization problem in long metallic wires [200], and led to important results for the study of the localization transition on the Bethe Lattice and in high dimension. In particular, as already mentioned in section (I.9), the Bethe Lattice version of both the  $\sigma$  model [34, 35, 36, 37] and the tight-binding model [30, 32, 31, 182] were studied with the supersymmetric approach: using this formalism the localization transition emerges as the breaking of a particular symmetry in the supersymmetric space, and can be described by means of an order-parameter function, whose meaning is strictly related to the behavior of the resolvent in the different phases of the system. The properties of the localized and the extended phases have been studied, and the authors obtained results on the level-level correlation functions, as well as on the behavior of the IPR and the diffusion coefficient at the transition point. Here we present the supersymmetric method mainly following the approach of Mirlin and Fyodorov [30, 32, 31, 182]. We focus in particular on the calculation of the level-level correlation functions carried out in [32, 31], since our analysis of such quantity for Lévy Matrices, which we will present in Chapter (III), is based on these works. We also present the main results on the IPR and the anomalous behavior of the diffusion coefficient at the transition, which are important in the characterization of the “mean field” behavior of the Anderson Localization Transition.

In order to introduce the supersymmetric method we consider  $N$  complex numbers  $S_i$  and  $N$  anticommuting Grassmann variables  $\chi_i$ , which obey the anticommutation relations

$$\chi_i \chi_j + \chi_j \chi_i = 0. \quad (\text{II.3.1})$$

The integrals over the Grassmann variables are defined following Berezin [201] as

$$\int d\chi_i = 0, \quad \int \chi_i d\chi_i = 1. \quad (\text{II.3.2})$$

It follows from this definition that the Gaussian integral over the anticommuting variables gives:

$$\int \exp \left( - \sum_{j,k=1}^N \chi_j^* A \chi_k \right) \prod_{i=1}^N d\chi_i^* d\chi_i = \det A, \quad (\text{II.3.3})$$

where  $A$  is an  $N \times N$  matrix of complex numbers. We stress that the corresponding Gaussian integral over complex numbers is instead proportional to  $(\det A)^{-1}$ .

The fermionic and the bosonic degrees of freedom can be combined by defining supervectors  $\Phi$  with components  $\Phi_i$ :

$$\Phi_i = \begin{pmatrix} \chi_i \\ S_i \end{pmatrix}, \quad (\text{II.3.4})$$

and super matrices  $F$  with block elements of the form:

$$F_{ij} = \begin{pmatrix} a_{ij} & \sigma_{ij} \\ \rho_{ij} & b_{ij} \end{pmatrix}, \quad (\text{II.3.5})$$

where  $a_{ij}$  and  $b_{ij}$  are complex numbers and  $\sigma_{ij}$  and  $\rho_{ij}$  are Grassmann variables. The following relation holds for Gaussian integrals over supervectors:

$$\left(\frac{1}{\pi}\right)^N \int \exp(-\Phi^\dagger F \Phi) \prod_{i=1}^N d\chi_i^* d\chi_i dS_i^* dS_i = S\text{Det}F. \quad (\text{II.3.6})$$

In the expression (II.3.6) above, the super determinant  $S\text{Det}F$  is defined as

$$S\text{Det}F = \det(a - \sigma b^{-1} \rho) \det b^{-1}. \quad (\text{II.3.7})$$

We also define the supertrace  $S\text{Tr}$  for supermatrices  $F$  as

$$S\text{Tr}F = \text{Tr}a - \text{Tr}b. \quad (\text{II.3.8})$$

A particular case holds for matrices  $F_0$  such that  $\sigma_{ij} = \rho_{ij} = 0$  and  $a_{ij} = b_{ij}$ :  $F_0$  is thus equal to the unity matrix in the superblocks  $F_{ij}$ , and the Gaussian integral (II.3.6) is equal to one. For such matrices the following relation holds:

$$\left(\frac{1}{\pi}\right)^N \int \Phi_i \Phi_j^\dagger \exp(-\Phi^\dagger F_0 \Phi) \prod_{i=1}^N d\chi_i^* d\chi_i dS_i^* dS_i = F_{0ij}^{-1}, \quad (\text{II.3.9})$$

which is the basis of the use of the supersymmetric method in disordered systems. We notice that in the corresponding Gaussian integral for complex numbers a weight denominator is present on the left hand side of the expression above: the absence of such denominator is due to the cancellation of determinants obtained by the integration over bosonic and fermionic variables, and allows one to average over the disorder at the beginning of the computations.

Given a random matrix  $H_{ij}$ , many quantities of interest can be expressed using integrals over supervectors. In particular, if we are interested in the density of states (DoS), we have to introduce supervectors  $\Phi$  by combining two commutative components  $S_i^{(1)}, S_i^{(2)}$  and two Grassmanian variables  $\chi_i, \chi_i^*$  at each site  $i$ :

$$\Phi_i = \begin{pmatrix} S_i^{(1)} \\ S_i^{(2)} \\ \chi_i \\ \chi_i^* \end{pmatrix}, \quad \Phi_i^\dagger = (S_i^{(1)}, S_i^{(2)}, \chi_i^*, -\chi_i). \quad (\text{II.3.10})$$

The starting point is the field theory  $Z(E, J) = \int \prod_i [d\Phi_i] e^{-[S(\{\Phi_i\}, E, J)]}$  with the action

$$\mathcal{S}(\{\Phi_i\}, E, J) = -\frac{i}{2} \sum_{ij} \Phi_i^\dagger [(E\hat{I} + J\hat{K})\delta_{ij} - H_{ij}] \Phi_j, \quad (\text{II.3.11})$$

where  $\hat{I}$  is the identity matrix,  $\hat{K}$  is defined as

$$\begin{pmatrix} 1 & 0 & 0 & 0 \\ 0 & 1 & 0 & 0 \\ 0 & 0 & -1 & 0 \\ 0 & 0 & 0 & -1 \end{pmatrix} \quad (\text{II.3.12})$$

and  $[d\Phi_i] = dS_i^{(1)} dS_i^{(2)} d\chi_i^* d\chi_i$ .

Combining the definition (II.1.3) and the result (II.3.9) for the Gaussian integral over supervectors we can express the DoS as

$$\rho(E) = \frac{1}{2\pi N} \Im \frac{\partial}{\partial J} \overline{Z(E, J)} \Big|_{J=0}. \quad (\text{II.3.13})$$

The study of the density of states of the Anderson Model on the Bethe Lattice using the supersymmetric method has been performed in [30], while in [31] the analysis regards a random matrix model closely related to that, the ensemble of sparse RMs: the authors study the properties of real, symmetric,  $N \times N$  matrices with identically and independently distributed elements  $H_{ij}$ , with a probability distribution  $f(H_{ij})$  of the form:

$$f(z) = \left(1 - \frac{p}{N}\right) \delta(z) + \frac{p}{N} h(z), \quad p \sim O(1), \quad (\text{II.3.14})$$

where  $h(z)$  has no  $\delta$ -like singularity at  $z = 0$  and  $\int h(z) z^2 dz \sim O(1)$ , such that  $\sum_{ij} H_{ij}^2 = \text{Tr} H^2 \sim N$ , i.e. the eigenvalues of the matrix are of order one. We notice that for this kind of matrices only a finite number  $p$  of elements per row (or column) is different from zero in the thermodynamic limit. This model is generally known in mathematical literature as Erdős-Rényi random graph [202, 203]. The importance of this kind of models had been already remarked in the context of the study of spin systems: indeed, dilute models present characteristics close to short-range models, but have a fully-connected structure which allows for analytical treatment [204, 205]. Before the work of Ref. [31], the density of states of this model had already been studied by Bray and other authors [206, 207]. As the random regular graph, the Erdős-Rényi random graph is another kind of graph which has locally a tree-like structure, and allows to study a finite version of the Bethe Lattice eliminating boundary effects. Even if the connectivity is fixed in the case of the RRG and it is a fluctuating quantity around its average value for the Erdős-Rényi random graph, the two models are very similar tree-like models without boundary, where the typical size of the loops scales as  $\ln N$ .

In Ref. [30, 31] the authors study firstly the DoS of sparse RMs: some details on this analysis are presented in appendix (D). The main result is that it can be expressed in terms of a function  $g_0(\Phi^\dagger \Phi)$ , which depends on supervectors  $\Phi$  only through the norm

$$\Phi^\dagger \Phi = S^2 + 2\chi^* \chi, \quad S^2 = S^{(1)2} + S^{(2)2}. \quad (\text{II.3.15})$$

Using the properties of Grassmanian variables we have  $g_0(\Phi^\dagger\Phi) = g_0(S^2) + 2\chi^*\chi g_0'(S^2)$ , therefore the anticommuting variables can be easily integrated out, and we obtain in the end an expression similar to the one derived with the replica trick in [208] for the Bethe Lattice and in [206] for sparse RM. However, as stated in section (II.1) and in Chapter (I), if we are interested in studying the localization transition, the density of states is not informative.

All the quantities of interest to this end, as the density-density correlation function (II.1.4) or the IPR (II.1.7) are expressed in terms of products of retarded and advanced Green functions. In order to write these observables as supersymmetric Gaussian integrals we have to double the size of the supervectors. In particular, we consider eight-component supervectors

$$\Phi_i = \begin{pmatrix} \Phi_{i,1} \\ \Phi_{i,2} \end{pmatrix}, \quad (\text{II.3.16})$$

where  $\Phi_{i,1}$  and  $\Phi_{i,2}$  have the structure of equation (II.3.10). The advanced and retarded Green functions can be thus expressed as

$$\begin{aligned} G_s(E, i, j) &= (-1)^s i \int \prod_k [d\Phi_{k,s}] \\ &\times \chi_{i,s}^* \chi_{j,s} \exp \left\{ -\frac{i}{2} \sum_{i,j} \Phi_{i,s}^\dagger [(E(-1)^s - i\eta) \delta_{ij} - (-1)^s H_{ij}] \Phi_{j,s} \right\}, \end{aligned} \quad (\text{II.3.17})$$

with  $s = 1, 2$ . In order to write the product of these two functions as Gaussian integrals, we have to choose the action in the form

$$\mathcal{S}(\{\Phi_i\}, E) = -\frac{i}{2} \sum_{i,j} \Phi_i^\dagger \left[ (\hat{L}E + i\eta) \delta_{ij} - \hat{L}H_{ij} \right] \Phi_j, \quad (\text{II.3.18})$$

with  $\hat{L} = \text{diag}\{1, 1, 1, 1, -1 - 1 - 1 - 1\}$ . With this choice we can for example express the density-density correlation function (II.1.4) for  $\omega = 0$  as

$$K_0(i, j) = \int \prod_k [d\Phi_k] \chi_{i,1}^* \chi_{i,2} \chi_{j,1} \chi_{j,2}^* \exp\{-\mathcal{S}\}, \quad (\text{II.3.19})$$

with  $[d\Phi_k] = \prod_{s=1,2} [d\Phi_{k,s}]$ . As mentioned above, we are interested in the computation of the level-level correlation functions, i.e. the correlator between subsequent eigenvalues, defined as

$$R(\omega) = \frac{\overline{\rho(E + \omega/2) \rho(E - \omega/2)}}{\rho^2(E)} - 1. \quad (\text{II.3.20})$$

We define the relative spacing  $\omega = r/N$ , and we have thus to evaluate the correlation function

$$K(E, r) = \frac{1}{N} \overline{\text{Tr} \left( E + \frac{r}{2N} + i\eta \right)^{-1} \text{Tr} \left( E - \frac{r}{2N} - i\eta \right)^{-1}}, \quad \eta \rightarrow 0^+. \quad (\text{II.3.21})$$

If we want to write this quantity as a Gaussian supersymmetric integral we have to modify the action (II.3.18) according to

$$\begin{aligned} \mathcal{S}(\{\Phi_i\}, E, r, J^{(1)}, J^{(2)}) = & -\frac{i}{2} \sum_{i,j} \Phi_i^\dagger \hat{L} (E\delta_{ij} - H_{ij}) \Phi_j + \frac{i}{2} \sum_i \Phi_i^\dagger \Phi_i \left( \frac{r}{2N} + i\eta \right) \\ & + \frac{i}{2} \sum_i \Phi_i^\dagger \hat{L} \hat{J} \hat{M} \Phi_i, \end{aligned} \quad (\text{II.3.22})$$

where  $\hat{J}$  is an  $8 \times 8$  diagonal matrix which contains the sources  $J^{(1)}, J^{(2)}$ , i.e.  $\hat{J} = \text{diag}\{J^{(1)}, J^{(1)}, J^{(1)}, J^{(1)}, J^{(2)}, J^{(2)}, J^{(2)}, J^{(2)}\}$ , and  $\hat{M}$  is also an  $8 \times 8$  diagonal matrix defined as  $\hat{M} = \text{diag}\{1, 1, -1, -1, 1, 1, -1, -1\}$ .

We have thus

$$K(E, r) = \left( \frac{1}{2N} \right)^2 \frac{\partial^2}{\partial J^{(1)} \partial J^{(2)}} \langle Z(E, r, J^{(1)}, J^{(2)}) \rangle |_{J^{(1)}=0, J^{(2)}=0}, \quad (\text{II.3.23})$$

$$Z(E, r, J^{(1)}, J^{(2)}) = \int \prod_i [d\Phi_i] \exp(-\mathcal{S}(\{\Phi_i\}, E, r, J^{(1)}, J^{(2)})). \quad (\text{II.3.24})$$

We present now how this technique has been applied in Refs. [32, 31] to the study of the localization transition of sparse RMs. As already mentioned, the transition appears as the breaking of a symmetry, and a function with a particular physical meaning can be identified as the order parameter. We present here the main steps of the computation, while we refer to the appendix (D) and (E) for further details.

The matrices considered are  $N \times N$  matrices with entries distributed according to the expression (II.3.14), such that only a finite number  $p$  of elements per row (or column) is different from zero in the thermodynamic limit.

By performing the average over the distribution of matrix elements, equations (II.3.24) and (II.3.22) become

$$\begin{aligned} \overline{Z(E, r, J^{(1)}, J^{(2)})} = & \int \prod_i [d\Phi_i] \exp \left\{ \frac{1}{2} \Phi^\dagger \hat{L} (E + \hat{J} \hat{M}) \Phi + \frac{i}{2} \Phi^\dagger \left( \frac{r}{2N} + i\eta \right) \Phi \right. \\ & \left. + \frac{p}{2N} \sum_{ij} [\tilde{h}(\Phi_i^\dagger \hat{L} \Phi_j) - 1] \right\}, \end{aligned} \quad (\text{II.3.25})$$

where

$$\tilde{h}(z) = \int h(t) \exp(-itz) dt. \quad (\text{II.3.26})$$

Since the sum over interacting terms in the partition function (II.3.25) runs over all the couples  $i, j$  of the system, it is useful to use, as explained in Appendix (D), the

functional generalization of the Hubbard-Stratonovich transformation (D.0.4). The interacting term is thus modified according to the following expression:

$$\begin{aligned} & \exp \left\{ \frac{p}{2N} \sum_{ij} \left[ \tilde{h}(\Phi_i^\dagger \hat{L} \Phi_j) - 1 \right] \right\} \\ &= \int Dg \exp \left\{ -\frac{Np}{2} \int [d\Psi][d\Psi'] g(\Psi) C(\Psi, \Psi') g(\Psi') + p \sum_i g(\Psi_i) \right\}, \end{aligned} \quad (\text{II.3.27})$$

where the kernel  $C(\Psi, \Psi')$  verifies

$$\int [d\Psi'] C(\Psi, \Psi') \left[ \tilde{h}(\Psi'^\dagger \hat{L} \Phi) - 1 \right] = \delta(\Psi - \Phi). \quad (\text{II.3.28})$$

Substituting the expression (II.3.27) into (II.3.25), we obtain for the averaged partition function

$$\begin{aligned} \overline{Z(E, r, J^{(1)}, J^{(2)})} &= \int Dg \exp \left\{ -\frac{Np}{2} \int [d\Psi][d\Psi'] g(\Psi) C(\Psi, \Psi') g(\Psi') + N \ln \int [d\Phi] \right. \\ &\quad \left. \times \exp \left[ \frac{i}{2} \Phi^\dagger \left[ \hat{L}(E + \hat{J}\hat{M}) + \frac{r}{2N} + i\eta \right] \Phi + p g(\Phi) \right] \right\}. \end{aligned} \quad (\text{II.3.29})$$

The integration over  $g$  can now be performed with the saddle point method for  $N \rightarrow \infty$ , as for the computation of the DoS in Appendix (D), leading to the following equation

$$g(\Psi) = \frac{\int [d\Phi] \left[ \tilde{h}(\Phi^\dagger \hat{L} \Psi) - 1 \right] \exp \left[ (i/2) E \Phi^\dagger \hat{L} \Phi - (\eta/2) \Phi^\dagger \Phi + p g(\Phi) \right]}{\int [d\Phi] \exp \left[ (i/2) E \Phi^\dagger \hat{L} \Phi - (\eta/2) \Phi^\dagger \Phi + p g(\Phi) \right]}. \quad (\text{II.3.30})$$

In view of the structure of the equation (II.3.30), it is natural to search its solution  $g_0(\Psi)$  as a function of two invariants:  $\Psi^\dagger \Psi$  and  $\Psi^\dagger \hat{L} \Psi$ . Indeed, we can notice that equation (II.3.30) commutes with all rotations  $\hat{S}$  which leave both  $\Psi^\dagger \hat{L} \Psi$  and  $\Psi^\dagger \Psi$  invariant, i.e.

$$\hat{S}^\dagger \hat{S} = \hat{I}, \quad \hat{S}^\dagger \hat{L} \hat{S} = \hat{L}. \quad (\text{II.3.31})$$

We can also observe that, for  $\eta \rightarrow 0$ , the saddle point equation (II.3.30) is invariant for all rotations  $\hat{T}$  for which

$$\hat{T}^\dagger \hat{L} \hat{T} = \hat{L}, \quad (\text{II.3.32})$$

i.e. rotations which leave the norm of the supervector  $\Psi^\dagger \hat{L} \Psi$  invariant. We can thus interpret the parameter  $\eta/2$  as a symmetry breaking parameter, and a spontaneous symmetry breaking might be present from the full symmetry (II.3.32) to the subgroup of rotations (II.3.31). Therefore, two possible forms of the solution  $g_0(\Psi)$  are possible: if, for  $\eta \rightarrow 0$ , the symmetry (II.3.32) is not broken, the function  $g_0(\Psi)|_{\eta \rightarrow 0}$  might

be a function of the variable  $\Psi_1^\dagger \Psi_1 - \Psi_2^\dagger \Psi_2$  only, therefore, once the integration over Grassmanian variable is performed, the solution  $g_0(S_1^2, S_2^2)|_{\eta \rightarrow 0}$  only depends on the variable  $y = S_1^2 - S_2^2$ . If instead the symmetry (II.3.32) is spontaneously broken, the solution  $g_0(\Psi)|_{\eta \rightarrow 0}$  is a function of both the invariants  $\Psi^\dagger \hat{L} \Psi$  and  $\Psi^\dagger \Psi = \Psi_1^\dagger \Psi_1 + \Psi_2^\dagger \Psi_2$ : the function  $g_0(S_1^2, S_2^2)|_{\eta \rightarrow 0}$  depends thus on both  $y = S_1^2 - S_2^2$  and  $x = S_1^2 + S_2^2$ .

The authors of [30, 31, 33] also show that the solution  $g_0(x, y)$  of the saddle point equation (II.3.30) has a clear physical meaning, being related to the joint probability density of real and imaginary parts of the one-site Green function. In particular, the following identity has been proven to hold:

$$g_0(x, y) = \int dz \Gamma_F(z) \int du dv f(u, v) \exp \left\{ \frac{z^2}{2} (vx - iuy) \right\}. \quad (\text{II.3.33})$$

In the expression (II.3.33),  $u$  is the real part of the resolvent and  $v$  is the imaginary part, while  $f(u, v)$  is their joint probability distribution. The function  $\Gamma_F(z)$  depends on the model, and for sparse RMs takes the form  $\Gamma_F(z) = \int d\omega \Gamma(\omega) \exp(i\omega z)/(2\pi)$ ,  $\Gamma(\omega) = p[\tilde{h}(\omega) - 1]$ . As we have seen in section (II.1) the imaginary part of the resolvent has a very different behavior in the localized and in the extended phase: keeping in mind the definition (II.1.2), if we consider an energy lying in the delocalized range of the spectrum, all the weights  $|\langle i|\alpha \rangle|^2$  are of order  $1/N$ , and the typical value of the imaginary part of  $G_{ii}(E)$  is therefore of order one. In contrast, in the localized phase all the weights are exponentially small, except for very few resonances:  $\Im G_{ii}(E)$  is thus of order  $\eta$  almost everywhere, and of order  $\eta^{-1}$  with a small probability going to zero with  $\eta$ . As a consequence, in the localized phase, being  $v$  in equation (II.3.33) of order  $\eta$ ,  $g_0(x, y)$  is independent of  $x$  for  $\eta \rightarrow 0$ , and tends to a function  $g_0(y)$ , which depends on  $y$  only. In the delocalized phase  $v$  is instead of order one, and the solution  $g_0(x, y)$  depends thus on both the invariants  $x$  and  $y$  for  $\eta \rightarrow 0$ . We observe thus that in the localized phase the symmetry of the saddle point equation (II.3.30) and the symmetry of the solution  $g_0(y)$  coincide for  $\eta \rightarrow 0$ , while in the extended phase the solution  $g_0(x, y)$  does not have the full symmetry (II.3.32) for  $\eta \rightarrow 0$ , i.e. the symmetry (II.3.32) is spontaneously broken. The rigorous proof of the identity (II.3.33) is based on the computation of the quantities  $K_{n,m} = \overline{G_1^n(i) G_2^m(i)}$  and can be found in [33]. In Appendix (E) we use a less rigorous procedure in order to show the meaning of the order parameter function  $g_0(x, y)$ .

In the delocalized phase the solution of the equation (II.3.30) is given by a family of functions  $g_T(\Psi)$  of the form

$$g_T(\Psi) = g_0(\Psi^\dagger \hat{T}^\dagger \hat{T} \Psi, \Psi^\dagger \hat{L} \Psi), \quad (\text{II.3.34})$$

where  $\hat{T}$  satisfies the condition (II.3.32). The integration with the saddle point method in the expression (II.3.29) has thus to be performed over a manifold of solution: the computation has been carried out in [31] and the result found for the correlator (II.3.20) is the same as for the GOE case [106]:

$$R(E, r) = 1 - \frac{\sin z^2}{z^2} - \frac{d}{dz} \left( \frac{\sin z}{z} \int_1^\infty \frac{\sin z t}{t} dt \right), \quad z = \pi r \rho(E). \quad (\text{II.3.35})$$

We stress that the use of the Supersymmetric method makes possible the description of the Localization Transition in terms of the breaking of a symmetry, and shows how a function strictly connected to the behavior of the imaginary part of the resolvent plays the role of the order parameter. As explained in Chapter (I), previous attempts to describe the two phases with a single order parameter in a field-theoretical approach had failed: the quantity which naturally emerged as order parameter is proportional to the average density of states, which is non-zero both in the localized and in the extended phase and is therefore not informative. The supersymmetric method makes clear the origin of this difficulty, showing that, in order to properly describe the phenomenon, a whole function  $g_0(x, y)$  has to be considered as order parameter.

As mentioned in Chapter (I) and again at the beginning of this paragraph, the supersymmetric method allows for non-perturbative calculations, and is up to now the only method which allows analytically a connection between the Localization Transition and the behavior of quantity as the level-level correlation function, and thus to the properties of ergodicity of the system. In the case of sparse RMs we have seen that the integration over the manifold of solutions in the delocalized phase leads to GOE statistics: we will follow the same steps in the following Chapter in order to study the behavior of the level-level correlation function in the delocalized phase for Lévy Matrices.

We conclude observing that the analysis presented in this paragraph and the results obtained lay on the possibility to perform the integral in the equation (II.3.30) with the saddle point method. Indeed, the Hubbard-Stratonovich transformation, used to obtain the equation (II.3.27), allows one to decouple variables in an interacting problem, transforming it into an integral of non-interacting problems. Yet, once this transformation performed, what makes the problem analytically tractable is the possibility to compute the integral with the saddle point method: this typically happens when the interactions are long-range, or when we consider short-range interaction problems but in the limit of infinite dimensionality. In the case analyzed the interactions present a percolative long-range structure which makes the problem solvable with the saddle point integration. The study of this kind of model let thus the characterization of some mean field properties of the Localization Transition: as explained at the beginning of this Chapter, such analysis is particularly important, since the mean field behavior can not be studied with the conventional approach. The study performed in [182] explores the features of both the localized and the extended phase and determines the critical behavior of the IPR and the diffusion constant. In particular, as mentioned in section (I.9), these quantities appear to be non-power like at criticality: their behavior is controlled by a scale  $A$  which is the scale on which the imaginary part of the resolvent is finite, and which presents a critical behavior of the form

$$A = \exp(\text{const}/|E - E_c|^{1/2}), \quad (\text{II.3.36})$$

with  $E_c$  the mobility edge. This determine an “exponential” critical behavior for the diffusion constant  $D$ , defined in the expression (II.1.5), of the type

$$D \propto (E_c - E)^{-3/2} \exp[-\text{const}/(E_c - E)^{-1/2}]. \quad (\text{II.3.37})$$

An expression of this type has been also found in [30] studying the Anderson Model

on the Bethe Lattice with the supersymmetric approach.

Analogously, a non-power like critical behavior has been shown to hold for the eigenvalue-dependent IPR, studied by looking at the correlation function at coinciding points, as explained in section (II.1). The analysis shows that  $\Upsilon_2(E)$  presents a jump at the critical point  $E = E_c$ , and its behavior near  $E_c$ , starting from the delocalized phase, is described by

$$\Upsilon_2(E) \propto \frac{1}{N} \exp[\text{const}(E_c - E)^{-1/2}]. \quad (\text{II.3.38})$$

This anomalous critical behavior had been found also studying the supersymmetric version of the  $\sigma$ -model on the Bethe Lattice [35, 36] and has been recovered in the framework of the effective medium approximation (EMA) developed by Efetov [180, 181], which is exact in the limit  $d \rightarrow \infty$ . In successive works of Mirlin and Fyodorov [166, 167] the supersymmetric method has been used to investigate the statistical properties of the resolvent for the Anderson Model in a  $d$ -dimensional system: the analysis shows that for  $d \rightarrow \infty$  a conventional power-law critical behavior occurs for the quantities above, and the “exponential” atypical behavior seems therefore to be a feature of the infinite dimensional model. The authors also proposed an interpretation of this result: as we have explained above, there is a characteristic symmetry breaking scale  $A$  which is responsible for the non-power like feature, and which shows the exponential behavior (II.3.36) near the critical point. This scale should be proportional to the “correlation volume”, i.e. the number of sites which are at a distance not larger than the correlation length  $\xi$  from a given site: on the Bethe Lattice, which is representative of the infinite dimensional limit, this volume scales as  $V_{\text{BL}} \propto \exp(\text{const } \xi)$ , and the behavior (II.3.36) is thus reproduced. On a lattice in dimension  $d$  the “correlation volume” scales instead as  $\xi^d$ , giving a power-like behavior of  $A$  of the type  $A \propto |E - E_c|^{-d/2}$ . The predictions of the EMA for a  $d$ -dimensional space appears therefore to be wrong for any  $d < \infty$ : this picture suggests thus that  $d = \infty$  plays the role of an upper critical dimension.

## II.4 Dyson Brownian motion model

As we have seen in section (I.6), thanks to the invariance under rotations, RMT provides an explicit expression for the joint probability distribution  $P(x_1, \dots, x_N)$  of the eigenvalues of  $N \times N$  matrices belonging to the three classical Gaussian ensembles [106]:

$$P(x_1, \dots, x_N) = C_{N\beta} e^{-\beta W}, \quad (\text{II.4.1})$$

$$W = \frac{1}{2} \sum_{j=1}^N x_j^2 - \sum_{i < j} \log |x_i - x_j|, \quad (\text{II.4.2})$$

where  $\beta = 1, 2$  or  $4$  respectively for the GOE, GUE and GSE case (see section (I.6)). This expression is identical to the probability density of the position of  $N$  unit charges on an infinite straight line  $-\infty < x < \infty$  subjected to the potential energy (I.6.2). If

the parameter  $\beta$  is identified with the inverse temperature  $\beta = (K_B T)^{-1}$ , the computation of averages over the distribution (II.4.1) is equivalent to the computation of thermodynamic quantities. With this picture, referred to as the Coulomb gas model, the problem of averaging over Gaussian ensembles is mapped into a statistical mechanics model. Dyson extended this idea, in such a way that the Coulomb gas model acquires meaning not only on a thermodynamic point of view, but also as a dynamical system out of equilibrium: to do that, the variables  $x_j$  must be interpreted as positions of particles in Brownian motion [209, 210, 211]. Each particle has therefore no inertia and is subjected to a fluctuating force  $f_j$  and to a frictional force proportional to the velocity: the motion of the particles is thus described by the following system of Langevin equations:

$$\gamma \frac{dx_j}{dt} = -\frac{dW}{dx_j} + f_j, \quad j = 1, \dots, N, \quad (\text{II.4.3})$$

where the fluctuating force  $f_j$  is a Gaussian white noise of zero mean  $\overline{f_j(t)} = 0$  and covariance

$$\overline{f_i(t)f_j(t')} = \frac{2\gamma}{\beta} \delta_{ij} \delta(t-t'). \quad (\text{II.4.4})$$

If  $x_1, \dots, x_N$  are the positions of the particles at time  $t$ , at a later time  $t + \delta t$  this positions change to  $x_1 + \delta x_1, \dots, x_N + \delta x_N$ . The  $\delta x_j$  are random variables, and from the relations (II.4.3) and (II.4.4) we have, to the first order in the small quantities:

$$\gamma \overline{\delta x_j} = -\frac{\partial W}{\partial x_j} \delta t, \quad (\text{II.4.5})$$

$$\gamma \overline{\delta x_j^2} = \frac{2}{\beta} \delta t. \quad (\text{II.4.6})$$

The Brownian motion can be alternative described by deriving the Fokker-Plank equation, which determines the evolution of the time dependent joint probability distribution of the positions of the particles  $P(x_1, \dots, x_N; t)$  [210]:

$$\gamma \frac{\partial P}{\partial t} = \sum_{j=1}^N \frac{\partial}{\partial x_j} \left( P \frac{\partial W}{\partial x_j} + \beta^{-1} \frac{\partial P}{\partial x_j} \right). \quad (\text{II.4.7})$$

It can be shown that the description of the motion in terms of equation (II.4.7) is equivalent to the one in terms of equations (II.4.5) and (II.4.6). If we start from an initial probability density  $P$  at time  $t = t_0$ , the solution of the Fokker-Plank equation (II.4.7) is unique for all  $t \geq t_0$ , and for  $t \rightarrow \infty$  the equilibrium solution coincides with the distribution (II.4.1), (II.4.2). We stress that the time variable introduced in this description is a fictitious time which has to be actually related to a parameter characterizing the original Hamiltonian, and it is thus a property of the mathematical model.

It is also possible to construct a Brownian motion model for the matrix elements of  $H$ , of which the variables  $x_j$  are the eigenvalues. The Brownian motion is defined for the  $p = N + N(N-1)\beta/2$  independent matrix elements separately. If at time  $t$  they

have values  $H_1, \dots, H_p$  and at time  $t + \delta t$  they change in  $H_1 + \delta H_1, \dots, H_p + \delta H_p$ , the Brownian motion is defined by the ensemble averages

$$\gamma \overline{\delta H_\mu} = -H_\mu \delta t, \quad (\text{II.4.8})$$

$$\gamma \overline{(\delta H_\mu)^2} = g_\mu \beta^{-1} \delta t, \quad (\text{II.4.9})$$

where  $g_\mu = g_{ij} = 1 + \delta_{ij}$ . The corresponding Fokker-Plank equation for the distribution  $P(H_1, \dots, H_p; t)$  of the matrix elements is

$$\gamma \frac{\partial P}{\partial t} = \sum_\mu \left( \frac{1}{2} g_\mu \beta^{-1} \frac{\partial^2 P}{\partial H_\mu^2} + \frac{\partial}{\partial H_\mu} (H_\mu P) \right). \quad (\text{II.4.10})$$

The solution of the equation (II.4.10) with the initial condition  $H = H^{(0)}$  at  $t = 0$  is known explicitly [210, 62, 86] and is given by

$$P(H, t) = C (1 - q^2)^{-p/2} \exp \left( -\frac{\beta \text{Tr}(H - q H^{(0)})^2}{2(1 - q^2)} \right), \quad (\text{II.4.11})$$

where  $q = \exp(-t/\gamma)$ . The distribution  $P(H, t)$  is invariant under simultaneous unitary transformation of the matrices  $H$  and  $H^{(0)}$ . In the limit  $t \rightarrow \infty$  we have  $q \rightarrow 0$ , and the solution tends to the stationary distribution

$$P(H_1, \dots, H_p) = C \exp \left( -\frac{1}{2} \beta \text{Tr} H^2 \right), \quad (\text{II.4.12})$$

which is the expression of the distribution of matrix elements in the three Gaussian ensembles. Equations (II.4.8) and (II.4.9) construct a GOE (in the real symmetric case) matrix for  $t \rightarrow \infty$ : they provide thus a way to obtain the GOE ensemble as the limit  $t \rightarrow \infty$  of a stochastic dynamical process.

It is possible to prove that the two approaches based on the Fokker-Plank equations (II.4.7) and (II.4.10) are equivalent, and in particular that when the matrix  $H$  executes a Brownian motion described by equations (II.4.8) and (II.4.9), starting from any initial conditions, its eigenvalues  $x_1, \dots, x_N$  execute a Brownian motion according to the equations (II.4.5) and (II.4.6) of the time dependent Coulomb gas. The proof is based on the fact that equations (II.4.8) and (II.4.9) are independent of the representation of  $H$ , and it is thus possible to choose  $H$  diagonal at time  $t = 0$ :

$$H_{jj}^{(0)} = x_j, \quad j = 1, \dots, N, \quad (\text{II.4.13})$$

and  $H_{i,j} = 0$  for  $i \neq j$ . At time  $t + \delta t$ ,  $H + \delta H$  is no longer diagonal, and its eigenvalues  $x_j + \delta x_j$  can be computed in perturbation theory: up to the second order in  $\delta H$  we have

$$\delta x_j = \delta H_{jj}^{(0)} + \sum_{i \neq j} \sum_{\lambda=0}^{\beta-1} \frac{(\delta H_{ij}^{(\lambda)})^2}{x_j - x_i}. \quad (\text{II.4.14})$$

Higher terms in the perturbation series do not contribute to the first order in  $\delta t$ , which is necessary to write the Fokker-Plank equation. Taking the ensemble average

of both sides in the equation above, and using equations (II.4.8) and (II.4.9) we obtain equation (II.4.5). When we take the ensemble average of  $\delta x_j^2$ , only the first term on the right side of (II.4.14) contributes to the order  $\delta t$ , and using the equation (II.4.9) we arrive to equation (II.4.6).

We notice from expression (II.4.14) how perturbations split levels: in the picture of Dyson Brownian motion this is at the origin of the potential (I.6.2) of the Coulomb gas model responsive for level repulsion in the Gaussian ensembles.

The technique of introducing a fictitious time related to some property of the model and to construct a Brownian motion for the matrix elements (or equivalently for the eigenvalues) has been largely use in order to extend the results of RMT, classically established for the Gaussian Ensembles, to larger universality classes. In section (I.6) we have seen how a central question about random matrices is the universality conjecture: it is commonly believed that local statistics of eigenvalues are determined by the symmetries of the ensembles but are independent from the details of the distributions. In particular, the bulk universality, e.g. the universality concerning the interior of the spectrum, has been proven for general classes of unitary invariant ensembles using techniques based on the analysis of orthogonal polynomials [212, 213, 214, 106, 215]. The local behavior of eigenvalues is known to follow the so called Dyson sine-kernel [106]. For non-unitary matrices, the most natural class is the ensemble of the Wigner matrices [116], e.g.  $N \times N$  random matrices with i.i.d. entries following a general distribution with finite second moment.

The first step in order to generalize the results on the local statistics of eigenvalues for unitary invariant matrices to non-unitary matrices was made by Johansson [117], who proved the bulk universality for matrices of the form

$$H = W + aV, \quad (\text{II.4.15})$$

where  $W$  is a Wigner matrix,  $V$  is an independent standard GUE matrix, and  $a$  is a positive constant independent of  $N$  (of order one). The bulk universality for the matrix (II.4.15), belonging to the so called *Gaussian divisible ensemble*, has been shown by using an exact expression for the correlation function of its eigenvalues [216, 217]. We can notice now that such matrix can be generated by the following stochastic flow:

$$s \rightarrow W + \sqrt{s}V, \quad s > 0, \quad (\text{II.4.16})$$

and the evolution of the eigenvalues is given by the Dyson Brownian motion as explained above. From the result of Ref. [117] we know that the asymptotic distribution of the Dyson Brownian motion, e.g. the eigenvalue distribution of GUE, is reached for time of order one. However, local equilibrium (i.e. equilibrium in an energy window containing a certain fraction of the eigenvalues), can be reached on shorter time scale. In Ref. [118] it has been proven local equilibrium in a window of size  $N^{-1+\epsilon}$  (with  $\epsilon > 0$ ), and it has been shown that this result, combined to other techniques, leads to the Dyson sine kernel.

In a further work [119] the bulk universality has been proved for Wigner matrices by developing a technique which allows to approach the comparison between the eigenvalues of  $W$  and  $W + \sqrt{s}V$ . We consider an Hermitian matrix  $W$ , and we define

the following Ornstein-Uhlenbeck (OU) process for the real and imaginary parts of the off-diagonal matrix elements

$$\partial_t u_t = L u_t, \quad L = \frac{1}{4} \frac{\partial^2}{\partial x^2} - \frac{x}{2} \frac{\partial}{\partial x}, \quad (\text{II.4.17})$$

with the measure  $\mu(dx) = e^{-x^2} dx$  and initial distribution  $u_0 = u$ . The matrix elements evolve thus according to

$$t \rightarrow e^{-t/2} W + (1 - e^{-t})^{1/2} V. \quad (\text{II.4.18})$$

If  $F$  is the initial joint probability distribution of entries, the distribution  $F_t$  at time  $t$  is found by applying the dynamic  $e^{tL}$  of the OU process to all the matrix elements.

What one would like to do, in order to prove the bulk universality for the Wigner matrix  $W$ , is to approximate the initial local correlation function  $F$  with  $F_t$  at some small time of the order  $N^{-1}$ , the time scale for which bulk universality has been proven in [118]. The approximation is defined in a weak sense by the integral

$$\text{Var}(F, F_t) = \int |F - F_t| \{du_i\}, \quad (\text{II.4.19})$$

where the integral runs over  $N^2$  variables. Heuristically we have  $\text{Var}(F, F_t) \sim t N^2$ , and it would imply convergence of the DBM for  $t \ll N^{-2}$ , which is far from  $t \geq N^{-1}$ . The argument used in [119] is that, while it is not possible to compare  $F$  to  $F_t$ , it is sufficient to find a function  $G$  such that the correlation functions for  $G_t = e^{\mathcal{L}t} G$  at time  $t$  can be computed and such that  $\text{Var}(F, e^{\mathcal{L}t} G) = o(N^{-2})$  (here we indicate with  $e^{\mathcal{L}t} := (e^{Lt})^{\otimes N^2}$  the operator which represents the dynamic of the OU process for all the matrix elements). Since  $F = e^{t\mathcal{L}}(e^{-t\mathcal{L}}F)$ , we could, in principle, choose  $G = e^{-t\mathcal{L}}F$ , but the diffusive dynamics can not be reversed besides few special cases. We can however approximately reverse it and choose the function  $G_t = \left[1 - tL + \frac{1}{2}t^2 L^2\right]^{\otimes N^2} F$ . We have thus  $e^{t\mathcal{L}}G_t - F = O(N^2 t^3)$  and it can be shown [119] that  $|\text{Var}(e^{t\mathcal{L}}G_t, F)|^2$  is upper bounded by a quantity of order  $t^6 N^2$ . This argument, called *reverse heat flow*, has been first used to prove bulk universality for Wigner matrices with smooth distribution in Ref. [119], where exponential decay of the off-diagonal matrix elements is required. The argument has been then used to extend universality to more general ensembles of Wigner matrices. In Chapter (III) we will use an argument based on the DBM technique and on the reverse heat flow method, to study the behavior of local eigenvalue statistics of Lévy matrices.

For completeness we mention that the reverse heat flow argument is one of the two recently most used techniques to study bulk universality. Another method, developed by T. Tao and V. Vu is known as *swapping method* and lays on the observation that spectral statistics of Wigner matrices tend to be stable if just one or two entries of the matrix are replaced with another distribution: the stability of the swapping process is stronger if one assumes that there are some matching moments between the new and old distribution [120, 218, 219]. The method of Dyson Brownian motion combined with the reverse heat flow argument, and the moment comparison method seem to be in general complementary to each other and both necessary in the study of bulk universality. We report the recent work of Ref. [121], in which bulk universality has been proven for

generalized Wigner matrices, whose distribution of the entries shows a subexponential decay. The matrix elements  $H_{ij}$  are not required to be identically distributed, provided that the variances of the matrix entries  $\sigma_{ij}$  are of comparable size, e.g.  $\frac{c}{N} \leq \sigma_{ij} \leq \frac{C}{N}$ , with  $c$  and  $C$  positive constants. We can notice that with this hypothesis, even if the matrix element are not required to be identically distributed, they retain however the main-field character of Wigner matrices. In the more recent work of Ref. [220], analysis of Dyson Brownian motion and the Green function comparison method have been combined to prove bulk universality for a more general class of matrices whose entries are not identically distributed and they do not have comparable variances, including random band matrices with  $W \gg N^{1-\epsilon_n}$ , with  $\epsilon_n > 0$  [99, 100, 101, 102]. As explained in section (I.6) it is still an open mathematical problem to extend universality to the delocalized phase of random Schrödinger operator.

# Chapter III

## Localization Transitions of Lévy Matrices

### III.1 Introduction and motivations

This Chapter is dedicated to the study of Lévy Matrices, a model of Random Matrices which constitutes a more general universality class than the one usually dealt with in RMT. We consider matrices with i.i.d. entries extracted from a heavy tail distribution, such that the second moment of such probability density is not finite. The study of the properties of such kind of matrices is interesting on a purely mathematical point of view, but is also related to the problem of Anderson Localization, and in particular to the characterization of the mean field properties of this phenomenon.

As we have explained in section (I.6) and (II.4), in the field of Random Matrices, much effort has been devoted in the attempt to extend the results of RMT to larger and larger ensembles of matrices. Indeed, the conjecture of universality states that eigenvalue statistics don't depend on the particular distribution of the entries, provided that their second moment is finite, but behave asymptotically as if the matrix elements were Gaussian. In particular, this has been proven for matrices with i.i.d. entries under the assumption of finiteness of the fourth moment [120, 218, 219]. It is however interesting to explore the properties of larger ensembles of matrices eliminating some constraints, and considering new and larger universality classes. One possibility, as we have mentioned in the previous Chapters, is for example to consider Wigner matrices with non-identically distributed entries, as in Refs. [121] and [220]. Another way is to remove some constraints on the momenta of the distribution of matrix elements, by considering heavy-tailed i.i.d. random entries. In particular, we consider  $N \times N$  real symmetric matrices  $H$  with entries  $H_{ij} = H_{ji}$  distributed independently according to a law,  $P(H_{ij}) = N^{1/\mu} f(N^{1/\mu} H_{ij})$ , characterized by heavy tails:

$$P(H_{ij}) \simeq \frac{\mu}{2N|H_{ij}|^{1+\mu}}, \quad |H_{ij}| \rightarrow \infty; \quad 0 < \mu < 2, \quad (\text{III.1.1})$$

For  $\mu > 2$  the distribution has a finite variance, and we fall in the GOE universality class [38]. The specific form of the function  $f$  doesn't matter. For concreteness, in this work, for numerical applications we will use a distribution  $P(H_{ij})$  proportional

to  $|H_{ij}|^{-1-\mu}$  for  $|H_{ij}| > N^{-1/\mu}$ , and zero for  $|H_{ij}| < N^{-1/\mu}$ . The scaling we have chosen is such that the typical order of magnitude of the entries  $H_{ij}$  is  $(1/N)^{1/\mu}$  and the largest element of a row is typically of order 1: this guarantees that almost all eigenvalues are  $O(1)$  with  $N \rightarrow \infty$ , and so the distribution of eigenvalues reaches a stable form in the thermodynamic limit, as shown in [38]. The reference case for this new universality class corresponds to entries that are Lévy distributed. Indeed, for probability distributions that have infinite variance a generalized version of the CLT holds [221, 222] (see Appendix (F)): the limiting distribution of the sum of a large number of heavy-tailed i.i.d. random variables is the Lévy stable distribution, which plays the role of the Gaussian distribution for non heavy tailed i.i.d. variables.

The Lévy distribution lacks of an explicit representation, and it is known by means of its Fourier transform  $\hat{L}_\mu^{C,\beta}$  [221, 223]

$$\begin{aligned} L_\mu^{C,\beta}(x) &= \frac{1}{2\pi} \int dk \hat{L}_\mu^{C,\beta}(k) e^{ikx}, \\ \log \hat{L}_\mu^{C,\beta}(k) &= -\frac{1}{N} |k|^\mu \gamma_\mu \left[ 1 + i\beta \tan\left(\frac{\pi\mu}{2}\right) \text{sgn}(k) \right], \end{aligned} \quad (\text{III.1.2})$$

where  $\mu, C$  and  $\beta$  are three parameter which characterize respectively the power-law behavior of the tails, the typical value and the asymmetry of the distribution, and  $\gamma_\mu$  is defined by expression (F.0.2) of Appendix (F).

This kind of matrices has been introduced in the pioneering work of Cizeau and Bouchad [38] and has then received attention both in physical and mathematical literature [224, 225, 226, 227, 228, 229, 230]. Actually, since a huge variety of distributions in physics and in other disciplines exhibits power-law tails, Lévy Matrices appear in different contexts, spreading from models of spin glasses with RKKY interactions [231] and disordered electronic systems [232], to portfolio optimization [233] and study of correlations in big data sets [234]. Contrary to the case of Gaussian matrices, few rigorous results are available for Lévy Matrices. The density of states has been well studied and understood: a pioneering analysis had been already carried out in Ref. [38], and successively in Refs. [224] and [225]. Finally, rigorous results have been obtained by G. Ben Arous and A. Guionnet [227]. Much less understood is the behavior of local observables, like the level statistics or the eigenvalue statistics. Actually, one of the most interesting properties of Lévy Matrices, which was studied since the first analysis of Ref. [38], is the presence of a mobility edge in the spectrum, separating low-energy delocalized states from high energy localized eigenvectors. The presence of such localization transition is a really interesting property which relates this kind of matrices to the study of Anderson Localization. On a mathematical point of view, even if the existence of a sharp localization transition has not been rigorously proven, the very recent work of Ref. [235] proves delocalization at sufficiently small energy in the spectrum and localization of the eigenstates for high energies for  $0 < \mu < 1$ .

In Chapter (I) and (II) we have seen how the study of the mean field theory for the Anderson Localization transition is a difficult task because of the unusual nature of the order parameter, which is a function related to the distribution of the local density of states. The mean field approximation is generally exact in the limit of infinite range interactions, i.e. for fully-connected models. Nevertheless, If we consider the fully

connected version of the Anderson model, we have a Hamiltonian which falls in the universality class of RMT and which exhibits therefore no localization transition. This problem is solved by considering, as we have seen in detail, the Anderson model on the Bethe Lattice, whose finite version without boundary can be defined both as a Random Regular Graph or as an Erdős-Renyi random graph. The latter version has been analyzed in section (II.3) with the supersymmetric method following the works of Refs. [31, 32, 182], and we have seen how the sparse tree-like structure of the model allows for an analytical treatment. Similar features are also typical of Lévy Matrices, which are a fully connected model with a sparse-like character: indeed, as a consequence of the form of the distribution (II.1), each row or column of the matrix  $H$  contains  $O(N)$  elements vanishing in the thermodynamic limit and  $O(1)$  elements of  $O(1)$ . The strong matrix elements can be explicitly distinguished from the small ones by introducing a cutoff  $\gamma$ . This technique, introduced to study spin systems [236, 226], has been already used in [225] for Lévy matrices, and it allows one to treat the backbone of strong matrix elements  $|H_{ij}| > \gamma$  as a sparse random matrix: in particular, as we will see in section (III.5) it constitutes the adjacency matrix of an Erdős-Rényi random graph with an average connectivity  $c_\gamma$  depending on the cutoff  $\gamma$ . The weak matrix elements have finite variance, since we have introduced the cutoff  $\gamma$  in their distribution, and play the role of a Gaussian bath. Using this strategy, and considering the limit  $\gamma \rightarrow 0$ , i.e. the limit  $c_\gamma \rightarrow \infty$ , Lévy matrices can be viewed as the limit of infinite connectivity of the adjacency matrix of an Erdős-Renyi random graph, and they can therefore be considered a useful model to investigate the mean field properties of the localization transition. As we have explained in section (I.9.1), the study of Localization on the Bethe Lattice in the limit of large connectivity is also important in relation to the problem of Many Body Localization if we relate, in a pictorial view, the problem of localization of  $N$  interacting particles to localization of one particle in a space of very high dimension [47]. As we will see in the next paragraph, for Lévy Matrices, in the thermodynamic limit, the cavity equations (II.2.10) and (II.2.11) are exact, and the model is thus described by equations very similar to those obtained by Abou-Chacra, Anderson and Thouless for the Bethe Lattice [8]: the difference is that the sum in the cavity equations runs, in the case of Lévy, over all the  $N$  sites of the system, while for the Bethe Lattice the sum is over the  $k$  neighbors that each site has on the tree. As we will see in this Chapter, in the case of Lévy Matrices the cavity equations result to be more easily treatable on a purely analytical point of view than the cavity equations on the Bethe Lattice.

We have seen in section (I.9.2) that on the Bethe Lattice and in systems exhibiting Many Body Localization transition, the existence of a mixed phase, delocalized but non-ergodic, has been advocated. This has been at the origin of a long debate, which is still open. A similar behavior seems to occur also in Lévy Matrices, where the question of the presence of such a phase was opened since the early work of Cizeau and Bouchaud [38]: as we will explain much in detail in section (III.6), using different criteria for localization two different transition lines are found numerically in the  $\mu - E$  plane. Some of the results of Ref. [38] are in contradiction with the recent rigorous results of Bordernave and Guionnet [230], showing that for  $1 < \mu < 2$  all the moments  $\Upsilon_q$  vanish in the thermodynamic limit for  $q > 2$ , and goes to infinity for  $q < 2$ . The question of the existence of an intermediate phase for Lévy matrices remained open

for years, and has recently received renewed attention due to the similarity with the problem of Anderson transition on the Bethe Lattice and with MBL.

In this Chapter we present the analysis we have performed on Lévy matrices using both analytical and numerical techniques and the results we have obtained and which have been published in Ref. [183]. First we show how the cavity equations presented in section (II.2) are exact in the case of Lévy in the thermodynamic limit, and how they are a starting point for the study of the density of state and for the computation of the mobility edge. The transition line obtained in the  $\mu - E$  plane is checked using a semi-analytical method, in which the cavity equation are solved by means of a population dynamics algorithm. In analogy with the analysis performed for sparse RMs in Refs. [38] with the supersymmetric method, presented in Chapter (II), we show how information on the behavior of the level statistics can be obtained. To study the level statistics we also use an argument based on the Dyson Brownian Motion method, presented in section (II.4). Finally, we present our numerical results obtained performing exact diagonalization of Lévy matrices of sizes from  $2^8$  to  $2^{15}$  and analyzing the scaling behavior with the system size of various observables. As we have anticipated in Chapter (I.9), our results are compatible with the existence of only one transition, between a delocalized ergodic and a localized non-ergodic phase. However, in the region  $0 < \mu < 1$ , the system is characterized by the presence of a large crossover region, in which it behaves as if it was in a mixed phase: this is due to the behavior of the characteristic size governing the finite size effects, which diverges much faster than a power law at the transition and is very large already far from it.

## III.2 The recursion equation for the resolvent

In section (II.2) we have presented the cavity approximation, which is based on the assumption that the Gaussian probability measure (II.2.2), used to write the resolvent in the form of a Gaussian integral over auxiliary fields  $\phi_i$ , factorizes over the sites of cavity graph: this assumption is exact on the Bethe Lattice (see section (II.2.1)), thanks to the particular tree-like structure in which loops are absent. We can show that such assumption is justified also in the case of Lévy Matrices, using the fully-connected structure of the model and the generalized central limit theorem.

The starting point is the expression of the resolvent (II.2.1) of a system of size  $N$  in terms of a Gaussian integral over auxiliary fields  $\phi_i$ . Following the authors of Ref. [38] we can imagine to add a row  $k$  and its symmetric columns to the matrix  $H$ : this, in terms of the tight binding representation of the matrix is equivalent to add a site to the system. For the resolvent of the system with  $(N + 1)$  sites, if we integrate over all fields except  $\phi_k$ , we obtain

$$G_{kk}^{(N+1)} = i \frac{\int d\phi_k \phi_k^2 \exp \left[ -\frac{i}{2} \sum_{i,j=1}^N H_{ki} G_{ij}^{(N)} H_{jk} \phi_k^2 - \frac{i}{2} (z - H_{kk}) \phi_k^2 \right]}{\int d\phi_k \exp \left[ -\frac{i}{2} \sum_{i,j=1}^N H_{ki} G_{ij}^{(N)} H_{jk} \phi_k^2 - \frac{i}{2} (z - H_{kk}) \phi_k^2 \right]}. \quad (\text{III.2.1})$$

Integrating now over  $\phi_k$  we find

$$\frac{1}{G_{kk}^{(N+1)}(z)} = z - \sum_j H_{kj}^2 G_{jj}^{(N)}(z) - \sum_{j \neq l} H_{kj} G_{jl}^{(N)}(z) H_{lk}, \quad (\text{III.2.2})$$

where we have neglected a term  $H_{kk}$  in the right hand side, which is of order  $N^{-1/\mu}$  and tends to zero for  $N \rightarrow \infty$ . The expression above corresponds to the cavity equation (II.2.11), with an additional term in the right hand side which takes into account the contribution of the off-diagonal terms of the resolvent. One argument which shows that for large  $N$  these off-diagonal terms can be neglected with respect to the diagonal one, was proposed by [224]: it is based on the fact that, since we are only interested in the behavior of the diagonal elements, the off-diagonal ones can be replaced by their typical values: as a result, the contributions of positive and negative elements lead to the cancellation of the off-diagonal term (the elements of  $H_{ij}$  and the ones of  $G_{ij}$  are suppose to be uncorrelated). Another possibility to estimate the contribute of the off-diagonal term is to use the generalized central limit theorem, as suggested in Ref. [38]: the off-diagonal term is therefore of order  $\left[1/N^2 \sum_{i \neq j} |G_{ij}|^\mu\right]^{1/\mu}$ . We have now to estimate the off-diagonal term of the resolvent  $G_{ij}$ . If we expand  $G = (z\mathbb{1} - H)^{-1}$  in perturbation theory, up to the first order in  $H$ , we have  $G_{ij} = H_{ij}/z + O(H_{ij}^2)$ , and we can therefore consider that  $G_{ij}$  is of the same order of  $H_{ij}$ , e.g.  $O(N^{-1/\mu})$ . The quantity  $\left[1/N^2 \sum_{i \neq j} |G_{ij}|^\mu\right]^{1/\mu}$  is thus of order  $N^{-1/\mu}$ , and vanishes for  $N \rightarrow \infty$ . We obtain thus the following recursive equation for the elements  $G_{ii}$ :

$$\frac{1}{G_{kk}^{(N+1)}(z)} = z - \sum_j H_{kj}^2 G_{jj}^{(N)}(z). \quad (\text{III.2.3})$$

In the limit  $N \rightarrow \infty$  we can then assume that the distribution of the resolvent for the system of size  $N + 1$  is the same as for the system of size  $N$ , at we obtain exactly the cavity equation (II.2.11), where we can drop the index labeling the size of the system.

If we use the analogy between random matrices and random graph, we can read the sums in equation (III.2.3) as sums over all the paths we can build on the graph associated to the matrix  $H$ , starting from a site  $k$  and coming back to  $k$ : getting rid of the off-diagonal term  $\sum_{j \neq l} H_{ij} G_{jl}^{(N)}(z) H_{li}$  corresponds therefore to neglect the loop on the graph. We notice thus again the relation with the Bethe Lattice, in which the cavity approximation is exact thanks to the lack of loops. The cavity equation obtained for Lévy Matrices are the same as equations (II.2.10) and (II.2.11) for the Bethe Lattice: the only difference is that in the latter case the sum spreads over  $k$  terms instead of over all the  $N$  sites of the system.

The recursive equation (III.2.3) had been already derived in Ref. [38], and has been rigorously proved in Ref. [227], where is the starting point for the derivation of the density of states, as we will see in the next section.

### III.3 The density of states

The recursion equation derived above for the diagonal elements of the resolvent allows one to obtain the density of states and the mobility edge of the model. We can

introduce the self-energy  $\Sigma_i(z) = z - 1/G_{ii}(z)$ , and separate the real and imaginary part of  $\Sigma_i$  and  $G_{ii}$  according to  $\Sigma_i = S_i + i\Delta_i$  and  $G_{ii} = \Re G_{ii} + i\Im G_{ii}$ . The cavity equation for  $S_i$  and  $\Delta_i$  will then read as follows:

$$S_i = \sum_{j=1}^{N-1} H_{ij}^2 \Re G_{jj}, \quad \Delta_i = \sum_{j=1}^{N-1} H_{ij}^2 \Im G_{jj}. \quad (\text{III.3.1})$$

Hereafter we will use the following simplified notation: we will omit the double indices and we define the random variable  $x_j = H_{ij}^2$ , distributed according to

$$P(x_j) \simeq \frac{\mu}{4Nx_j^{1+\mu/2}}, \quad x_j \rightarrow \infty. \quad (\text{III.3.2})$$

Then, we have  $S = \sum_{i=1}^N x_i \Re G_i$  and  $\Delta = \sum_{i=1}^N x_i \Im G_i$ , where we have replaced the sum over  $N-1$  terms with a sum over  $N$  terms, since in thermodynamic limit we can assume that the distribution of  $\{G_i^{(N-1)}\}$  is the same as the distribution of  $\{G_i^{(N)}\}$ . We can also notice that the matrix elements  $H_{ij}$  and the elements of the self-energy  $\Sigma_i$  are by construction uncorrelated.

It is now possible to determine, at least formally, the joint probability distribution  $Q(S, \Delta)$  of the real and imaginary part of the self-energy, which is given by

$$\begin{aligned} Q(S, \Delta) &= \int \prod_{i=1}^N \left[ \frac{dx_i dk_i}{2\pi} e^{ik_i x_i} \hat{P}(k_i) \right] \delta \left( S - \sum_{i=1}^N x_i G_i^R \right) \delta \left( \Delta - \sum_{i=1}^N x_i G_i^I \right) \\ &= \int \frac{dk_1 dk_2}{(2\pi)^2} e^{i(k_1 S + k_2 \Delta)} \prod_{i=1}^N \left[ \frac{dx_i dk_i}{2\pi} e^{i(k_i - k_1 G_i^R - k_2 G_i^I) x_i} \hat{P}(k_i) \right], \end{aligned} \quad (\text{III.3.3})$$

where  $\hat{P}(k_i)$  is the Fourier transform of the distribution (III.3.2). We use now the expansion of  $\hat{P}(k_i)$  up to the lowest order in  $k_i$ :

$$\hat{P}(k_i) = 1 - \frac{1}{N} |k|^{1-\mu/2} \gamma_{\mu/2} \left[ 1 + i \tan \left( \frac{\pi\mu}{4} \right) \text{sign}(k) \right], \quad (\text{III.3.4})$$

with  $\gamma_{\mu/2}$  defined as in eq. (F.0.3). Performing the integrals in  $dx_i$  and using the expression (III.3.4), we find that for  $N \rightarrow \infty$  the Fourier transform  $Q(S, \Delta)$  coincides with the characteristic function of a complex Lévy stable distribution:

$$\begin{aligned} \hat{Q}(k_1, k_2) &= \prod_{i=1}^N \hat{P}(k_1 G_i^R + k_2 G_i^I) \\ &= \exp \left[ -\gamma_{\mu/2} \int d\nu(G) \left| k_1 G^R + k_2 G^I \right|^{\frac{\mu}{2}} \left( 1 + i \tan \left( \frac{\pi\mu}{4} \right) \text{sign} \left( k_1 G^R + k_2 G^I \right) \right) \right]. \end{aligned} \quad (\text{III.3.5})$$

This result could have been derived also by applying the generalized central limit theorem (F.0.4) to the real random variable  $k_1 S + k_2 \Delta$ . Since  $\Sigma_i = E - i\eta - G_{ii}^{-1}$  we have that:

$$\int f(G) d\nu(G) = \int f \left( \frac{1}{E - i\eta - \Sigma} \right) dQ(\Sigma), \quad (\text{III.3.6})$$

where  $\nu(G)$  is the probability distribution of the diagonal elements of the resolvent  $G$ . As a result, Eq. (III.3.5) can be seen as a very complicated self-consistent integral equation for the probability distribution of the self-energy.

The result (III.3.5) has been rigorously derived in ref. [227], relying on a result about the convergence of sums of triangular arrays to complex stable law. Also the equation (III.3.6) is proved for every bounded continuous function  $f$ .

In order to determine the density of states we now need some preliminary results. First of all the average value of  $e^{-sx}$  over the Student distribution  $P(x)$  of eq. (III.3.2), with  $s$  being a complex number with positive real part, is for large  $N$ :

$$\langle e^{-sx} \rangle \simeq \exp \left[ -\frac{\Gamma(1 - \frac{\mu}{2})}{N} s^{\frac{\mu}{2}} \right]. \quad (\text{III.3.7})$$

Since the self-energy  $\Sigma$  is defined as  $\Sigma = \sum_{i=1}^N x_i G_i$  we have that (for  $t > 0$ ):

$$\begin{aligned} \langle e^{it\Sigma} \rangle &= \langle e^{it \sum_{i=1}^N x_i G_i} \rangle = \prod_{i=1}^N \langle e^{it G_i x_i} \rangle = \prod_{i=1}^N \exp \left[ -\frac{\Gamma(1 - \frac{\mu}{2}) (-it)^{\frac{\mu}{2}} G_i^{\frac{\mu}{2}}}{N} \right] \\ &= \exp \left[ -\Gamma \left( 1 - \frac{\mu}{2} \right) (-it)^{\frac{\mu}{2}} \int d\nu(G) G^{\frac{\mu}{2}} \right], \end{aligned} \quad (\text{III.3.8})$$

where in the last step we have replaced the sum over the diagonal elements of the resolvent by an integral over the probability distribution  $\nu(G)$ , the elements  $G_i$  becoming independent and identically distributed in the limit  $N \rightarrow \infty$ . The relation (III.3.8) can be also found by direct integration in the complex plane of  $\int e^{it\Sigma} dQ(\Sigma)$ , where  $Q(\Sigma)$  is the complex Lévy stable distribution given by equation (III.3.5).

Another relation that we will need to use is the following integral identity, which holds for every complex number  $z$  with negative imaginary part:

$$\left( \frac{1}{z} \right)^{\frac{\mu}{2}} = -i \frac{e^{-i \frac{\pi\mu}{2}}}{\Gamma(\frac{\mu}{2})} \int_0^\infty (-it)^{\frac{\mu}{2}-1} e^{-itz} dt. \quad (\text{III.3.9})$$

The relation (III.3.9) can be proved by contour integration. Let us now compute the  $\mu/2$ -th moment of  $G$ . Using equation (III.3.6) we find:

$$\langle G^{\frac{\mu}{2}} \rangle = \int d\nu(G) G^{\frac{\mu}{2}} = \int \left( \frac{1}{E - i\eta - \Sigma} \right)^{\frac{\mu}{2}} dQ(\Sigma). \quad (\text{III.3.10})$$

We now apply the integral identity, equation (III.3.9), to  $(E - i\eta - \Sigma)^{\frac{\mu}{2}}$  and obtain:

$$\langle G^{\frac{\mu}{2}} \rangle = -i \frac{e^{-i \frac{\pi\mu}{2}}}{\Gamma(\frac{\mu}{2})} \int_0^\infty dt (-it)^{\frac{\mu}{2}-1} e^{-it(E-i\eta)} \int e^{it\Sigma} dQ(\Sigma). \quad (\text{III.3.11})$$

From equation (III.3.8) we have that:

$$\int e^{it\Sigma} dQ(\Sigma) = \exp \left[ -\Gamma \left( 1 - \frac{\mu}{2} \right) (-it)^{\frac{\mu}{2}} \langle G^{\frac{\mu}{2}} \rangle \right]. \quad (\text{III.3.12})$$

Thus we get the following self consistent equation for the complex number  $\langle G^{\frac{\mu}{2}} \rangle$ :

$$\langle G^{\frac{\mu}{2}} \rangle = -i \frac{e^{-i \frac{\pi\mu}{2}}}{\Gamma\left(\frac{\mu}{2}\right)} \int_0^\infty dt (-it)^{\frac{\mu}{2}-1} e^{-it(E-i\eta)} \exp \left[ -\Gamma\left(1 - \frac{\mu}{2}\right) (-it)^{\frac{\mu}{2}} \langle G^{\frac{\mu}{2}} \rangle \right]. \quad (\text{III.3.13})$$

We can now introduce the function  $g(y)$ :

$$g(y) = \frac{2}{\mu} \int_0^\infty e^{-v^{\frac{2}{\mu}}} e^{-vy} dv = \int_0^\infty w^{\frac{\mu}{2}-1} e^{-w} e^{-w^{\frac{\mu}{2}} y} dw, \quad (\text{III.3.14})$$

and we can define  $Y = (-1/z)^{\mu/2} \langle G^{\frac{\mu}{2}} \rangle$ . Using this definition of  $Y$  and  $g(y)$ , the self consistent equation (III.3.13) can be recast in the form:

$$(-z)^\mu Y = \frac{e^{-i \frac{\pi\mu}{2}}}{\Gamma\left(\frac{\mu}{2}\right)} g\left(\Gamma\left(1 - \frac{\mu}{2}\right) Y\right). \quad (\text{III.3.15})$$

As shown in [227], it is possible to prove that there exist a unique analytic solution  $\langle G^{\frac{\mu}{2}} \rangle$  of the equation (III.3.13) such that  $\langle G^{\frac{\mu}{2}} \rangle = O(|E - i\eta|^{-\frac{\mu}{2}})$  at infinity. Moreover, it is possible to show that  $Y = (-1/z)^{\mu/2} \langle G^{\frac{\mu}{2}} \rangle$  is the unique analytic solution of the equation (III.3.15) tending to zero at infinity. In fact,  $Y = O(|E - i\eta|^{-\mu})$ .

Once  $\langle G^{\frac{\mu}{2}} \rangle$  is determined, one can compute all moments of the resolvent using the relations (III.3.6) and (III.3.12). In particular, for  $\langle G \rangle$  we have:

$$\begin{aligned} \langle G \rangle &= \int d\nu(G) G = \int \left( \frac{1}{E - i\eta - \Sigma} \right) dQ(\Sigma) \\ &= i \int_0^\infty dt e^{-it(E-i\eta)} \int e^{it\Sigma} dQ(\Sigma) \\ &= i \int_0^\infty dt e^{-it(E-i\eta)} \exp \left[ -\Gamma\left(1 - \frac{\mu}{2}\right) (-it)^{\frac{\mu}{2}} \mu \langle G^{\frac{\mu}{2}} \rangle \right]. \end{aligned} \quad (\text{III.3.16})$$

Taking the imaginary part of the above expression in the limit  $\eta \rightarrow 0$  yields  $\pi \rho_\mu(E)$ . In ref. [227] some properties of  $\rho_\mu(E)$  are proved: it is possible to show that the density of states is symmetric, unbounded, and it has heavy tails. In particular, the asymptotic behavior of  $\rho_\mu(E)$  is given by

$$\rho_\mu(E) \sim \pi^{-1} \Gamma(\mu) \frac{\Im Y(E)}{E}, \quad (\text{III.3.17})$$

where we have defined  $Y(E) = \lim_{\eta \rightarrow 0} Y(E - i\eta)$ . Since we know that  $Y(E - i\eta) = O(|E - i\eta|^{-\mu})$ , as a result  $\rho_\mu(E)$  has heavy tails in  $1 + \mu$ . This scaling behavior was first predicted by Cizeau and Bouchaud in their seminal paper [38] using a different method (see also Ref. [224]).

In fig. (III.1) the density of states for Lévy matrices with  $\mu = 0.5, 1$  and  $1.5$  is represented. The DoS has been computed numerically by exact diagonalization. We see as the power-law behavior of the tails with exponent  $1 + \mu$  predicted analytically is correctly reproduced. As expected, the distribution becomes less broad with increasing  $\mu$ , approaching the semi-circle law (I.6.3) for  $\mu \rightarrow 2$ .

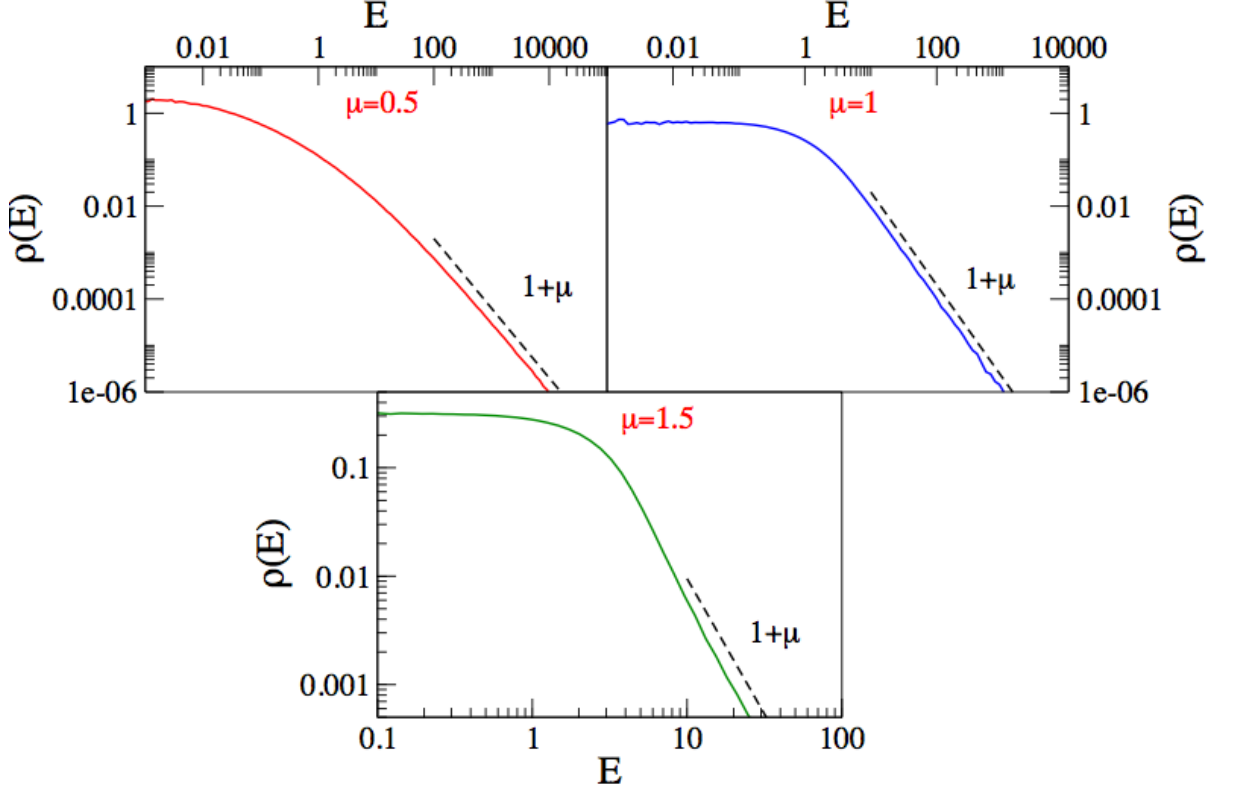


Figure III.1: The plot shows the distribution of the eigenvalues for Lévy matrices with  $\mu = 0.5, 1$  and  $1.5$  computed numerically by exact diagonalization. The size of the matrices considered is  $2^{11} \times 2^{11}$  and we performed averages over 500 samples. We notice the power-law behavior of the tails of the distributions, characterized by an exponent  $1 + \mu$ . As  $\mu$  is increased the width of the distribution becomes smaller, approaching the semicircle law in the limit  $\mu \rightarrow 2$ .

### III.4 Computation of the mobility edge

As explained above, one of the most interesting features of Lévy matrices is the presence of a mobility edge in the spectrum, separating the extended states from the localized ones. We present here a procedure to obtain the transition point in the spectrum, based on studying the stability of the localized phase under a perturbation obtained adding a small imaginary part to the resolvent. This is the approach used by Abou Chacra, Anderson and Thouless to study the localization transition for the Anderson Model on the Bethe Lattice [8]. The criterion is based on the different behavior of the distribution of the imaginary part of the diagonal elements of the resolvent  $G(E)$  in the two phases: if the energy  $E$  corresponds to a delocalized states,  $\Im G(E - i\eta)$  has a finite typical value when  $\eta \rightarrow 0$ , which is of order one. On the contrary, if  $E$  belongs to the portion of the spectrum which is localized, the typical value of  $\Im G(E)$  tends to zero when  $\eta \rightarrow 0$ . Since in the localized phase there is a discrete set

of sites where  $\Im G(E)$  is infinitely large, therefore the mean value of  $\Im G(E)$  is however finite. The stability of the localized phase is governed by an eigenvalue equation for the same integral operator found in Ref. [38]: here we show how the analysis of such equation can be simplified, and we identify the mobility edge. We start from the equations (III.3.1) for the real and imaginary part of the self-energy, which we can rewrite in the form:

$$S_i + i\Delta_i = \sum_{j=1}^N x_{ij} \frac{E - S_j + i(\eta + \Delta_j)}{(E - S_j)^2 + (\eta + \Delta_j)^2}. \quad (\text{III.4.1})$$

As explained above, the quantity of interest in the study of the localization transition is the distribution of the self-energy  $Q(S, \Delta)$ : we want to analyze its behavior in the thermodynamic limit near the mobility edge. First of all, since in the localized phase  $\Delta$  is of order  $\eta$  with probability one, we can linearize the equation (III.4.1) with respect to the imaginary part, obtaining the following expressions:

$$\begin{aligned} S_i &= \sum_{j=1}^N x_j \frac{1}{E - S_j} \\ \Delta_i &= \sum_{j=1}^N x_j \frac{\eta + \Delta_j}{(E - S_j)^2}. \end{aligned} \quad (\text{III.4.2})$$

We can notice that the expression above for the real part  $S$  does not depend on the imaginary part  $\Delta$ . The probability distribution  $Q_R(S)$  is given by:

$$\begin{aligned} Q_R(S) &= \int \prod_{i=1}^N \left[ \frac{dx_i dk_i}{2\pi} e^{ik_i x_i} \hat{P}(k_i) \right] \delta \left( S - \sum_{i=1}^N x_i G_i \right) \\ &= \int \frac{dk}{2\pi} e^{ikS} \prod_{i=1}^N \left[ \frac{dx_i dk_i}{2\pi} e^{i(k_i - kG_i)x_i} \hat{P}(k_i) \right]. \end{aligned} \quad (\text{III.4.3})$$

Using the expansion (III.3.4) we have that for  $N \rightarrow \infty$  the Fourier transform of  $Q_R(S)$  coincides with the characteristic function of a Lévy stable distribution with exponent  $\mu/2$ :

$$\hat{Q}_R(k) = \prod_{i=1}^N \hat{P}(kG_i) \simeq \exp \left[ -C|k|^{\frac{\mu}{2}} \left( 1 + i\beta \tan \left( \frac{\pi\mu}{4} \right) \text{sign}(k) \right) \right]. \quad (\text{III.4.4})$$

Therefore,  $Q_R(S) = L_{\mu/2}^{C(E), \beta(E)}$ , with the effective parameters  $C(E)$  and  $\beta(E)$  given by

$$\begin{aligned} C(E) &= \gamma_{\mu/2} \frac{1}{N} \sum_{i=1}^N |G_i^R|^{\frac{\mu}{2}} = \gamma_{\mu/2} \int d\nu_R(G^R) |G^R|^{\frac{\mu}{2}}, \\ \beta(E) &= \frac{\frac{1}{N} \sum_{i=1}^N |G_i^R|^{\frac{\mu}{2}} \text{sign}(G_i^R)}{\frac{1}{N} \sum_{i=1}^N |G_i^R|^{\frac{\mu}{2}}} = \frac{\int d\nu_R(G^R) |G^R|^{\frac{\mu}{2}} \text{sign}(G^R)}{\int d\nu_R(G^R) |G^R|^{\frac{\mu}{2}}}, \end{aligned} \quad (\text{III.4.5})$$

where  $\nu(G)$  is the probability distribution of the diagonal elements of the real part of the resolvent matrix and  $\gamma_{\mu/2}$  is defined by the expression (F.0.3) in Appendix (F). The sums over  $N$  have been replaced by integrals over such distribution because the diagonal elements of the resolvent become independent and identically distributed in the limit  $N \rightarrow \infty$ .

Although the resolvent matrix (II.1.2) can only be defined in the complex plane in presence of a small imaginary regulator  $\eta$ , in order to compute the mobility edge we have to consider the recursion equation for the self energy (III.4.1) in the limit  $\eta = 0$ , thus in absence of the imaginary part. Since in this limit  $S = E - 1/G^R$ , we have:

$$\nu_R(G^R) dG^R = Q_R\left(E - \frac{1}{G^R}\right) \frac{dG^R}{|G^R|^2}, \quad (\text{III.4.6})$$

and the expressions (III.4.5) can be rewritten in terms of the distribution of the self-energy:

$$\begin{aligned} C(E) &= \gamma_{\mu/2} \int_{-\infty}^{+\infty} dG^R L_{\mu/2}^{C(E),\beta(E)}\left(E - \frac{1}{G^R}\right) |G^R|^{\frac{\mu}{2}-2} \\ &= \gamma_{\mu/2} \int_{-\infty}^{+\infty} dx L_{\mu/2}^{C(E),\beta(E)}(E-x) |x|^{-\frac{\mu}{2}}, \end{aligned} \quad (\text{III.4.7})$$

$$\begin{aligned} \beta(E) &= \frac{\int_{-\infty}^{+\infty} dG^R L_{\mu/2}^{C(E),\beta(E)}\left(E - \frac{1}{G^R}\right) |G^R|^{\frac{\mu}{2}-2} \text{sign}(G)}{\int_{-\infty}^{+\infty} dG^R L_{\mu/2}^{C(E),\beta(E)}\left(E - \frac{1}{G^R}\right) |G^R|^{\frac{\mu}{2}-2}} \\ &= \frac{\int_{-\infty}^{+\infty} dx L_{\mu/2}^{C(E),\beta(E)}(E-x) \text{sign}(x) |x|^{-\frac{\mu}{2}}}{\int_{-\infty}^{+\infty} dx L_{\mu/2}^{C(E),\beta(E)}(E-x) |x|^{-\frac{\mu}{2}}}, \end{aligned}$$

where we have defined  $x = 1/G^R$ . We have therefore a set of two self-consistent equations for the parameters  $C(E)$  and  $\beta(E)$ .

If we come back now to equations (III.4.2), since the expression for the real part  $S$  does not depend on the imaginary part  $\Delta$ , we can consider the equation for the imaginary part and study the stability over iteration. Following the steps explained in Appendix (G) we obtain the integral equation that corresponds to (III.4.2):

$$\hat{Q}(k_1, k_2) = \left[ \int dx dS P(x) \hat{Q}_2\left(S, \frac{k_2 x}{(E-S)^2}\right) e^{-ik_1 x/(E-S)} e^{-ik_2 \eta x/(E-S)^2} \right]^N, \quad (\text{III.4.8})$$

where  $\hat{Q}(k_1, k_2)$  is the standard double Fourier transform of  $Q(S, \Delta)$ , and  $\hat{Q}_2(S_i, k_i)$  is the Fourier transform of  $Q(S, \Delta)$ , defined as

$$\hat{Q}_2(S_i, k_i) = \int_{-\infty}^{+\infty} d\Delta_i e^{-ik_i \Delta_i} Q(S_i, \Delta_i). \quad (\text{III.4.9})$$

We can now make an assumption for the asymptotic behavior of  $Q(S, \Delta)$  in the localized phase. We have seen above, considering the recursion equation for the self-energy in the limit  $\eta = 0$ , that the real part of the self-energy is a Lévy stable law

$L_{\mu/2}^{C(E),\beta(E)}$  with effective parameters  $C(E)$  and  $\beta(E)$  given by the set of equations (III.4.5). A very similar result holds for the probability distribution of the imaginary part  $Q(\Delta)$ : the only difference with the expressions (III.4.5) is that in this case the parameter  $\beta$  is equal to 1 since all the  $\Im G_i$  are positive. We also know that the joint probability distribution  $Q(S, \Delta)$  is a complex Lévy stable law given by the equation (III.3.5). Since the marginal  $Q(\Delta)$  is obtained integrating over  $S$  the joint probability  $Q(S, \Delta)$ , a reasonable *ansatz* for the behavior of the tails of  $Q(S, \Delta)$  in the localized phase is

$$Q(S, \Delta) \sim \frac{A(S)}{\Delta^{1+m}}. \quad (\text{III.4.10})$$

As observed in [38], the exponent  $m$  is constrained to be larger or equal than  $\mu/2$ , since integrating over  $S$  can only make the decaying of the tails of  $\Delta$  slower. This expression in the Fourier space gives:

$$\hat{Q}_2(S, k) \sim \hat{Q}_2(S, 0) + c|k|^m A(S). \quad (\text{III.4.11})$$

$Q_2(S, 0)$  is the marginal of  $Q(S, \Delta)$  once we integrate over  $\Delta$ : therefore, as we have seen above, it is a Lévy stable law  $L_{\mu/2}^{C(E),\beta(E)}(S)$  with exponent  $\mu/2$  and effective parameters  $C(E)$  and  $\beta(E)$  given by the self-consistent equations (III.4.7).

As shown in details in the appendix (G), using this result for  $Q_2(S, 0)$ , Eq. (III.4.11), and expanding the right hand side of Eq. (III.4.11) in powers of  $k_2$  up to the order  $|k_2|^m$ , one obtains the following integral equation:

$$\hat{A}(k_1) = N \hat{L}_{\mu/2}^{C(E),\beta(E)}(k_1) \int dx dS P(x) \left| \frac{x}{(E-S)^2} \right|^m A(S) e^{-ik_1 x/(E-S)}. \quad (\text{III.4.12})$$

We have to study now the behavior of the kernel of this equation, which has well defined solutions only in the localized phase. In the appendix (G) we explain how it can be simplified, yielding the following equation for the mobility edge:

$$K_{m,\mu}^2 \ell_+ \ell_- \left[ s_\mu^2 - s_m^2 \right] - K_{m,\mu} (\ell_+ + \ell_-) s_\mu + 1 = 0, \quad (\text{III.4.13})$$

where we have used the following definitions:

$$\begin{aligned} K_{m,\mu} &= \frac{\mu}{2} \Gamma\left(m - \frac{\mu}{2}\right) \Gamma\left(1 - m - \frac{\mu}{2}\right), \\ s_\mu &= \sin\left(\frac{\pi\mu}{2}\right), \\ s_m &= \sin(\pi m). \end{aligned}$$

and

$$\begin{aligned} \ell_+ &= \int_0^{+\infty} \frac{dk_1}{\pi} e^{ik_1 E} |k_1|^{\mu-1} \hat{L}_{\mu/2}^{C(E),\beta(E)}(k_1), \\ \ell_- &= \int_{-\infty}^0 \frac{dk_1}{\pi} e^{ik_1 E} |k_1|^{\mu-1} \hat{L}_{\mu/2}^{C(E),\beta(E)}(k_1). \end{aligned} \quad (\text{III.4.14})$$

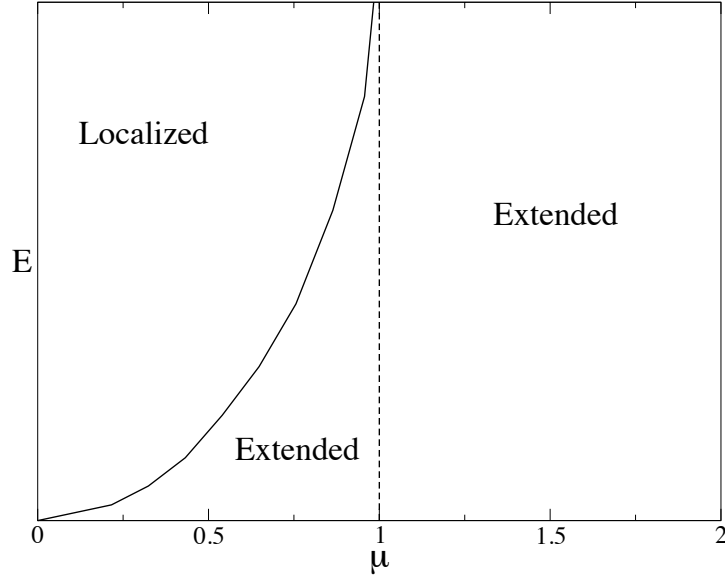


Figure III.2: Phase diagram of Lévy Matrices in the  $\mu - E$  plane. The result is obtained solving the equation (III.4.15) for different values of  $\mu$ .

The equation (III.4.13) expresses the condition to have a non-trivial solution compatible with our *ansatz* of the asymptotic behavior of  $Q(S, \Delta)$ .

Given a value of  $\mu$ , the equation (III.4.13) can be solved for different values of  $m \in [1/2, 1]$ , and we obtain a critical energy  $E(\mu, m)$ . The value of the mobility edge  $E^*(\mu)$  for each value of  $\mu$  is given by the stationary point of the eigenvalue of the equation (III.4.12) with respect to  $m$ : the reason will be more clear in the next section. We can notice that, as in the case of the Anderson model on the Bethe lattice, the equation (III.4.13) is symmetric around  $m = 1/2$ , therefore, if a solution of this equation exists, the eigenvalue of the equation (III.4.12) can have a stationary point only for  $m = 1/2$ . For the Bethe lattice, this result has been rigorously proven in [178] and [198], and indirectly found in [8]. Hence, the equation (III.4.13) finally becomes

$$K_\mu^2 (s_\mu^2 - s_{1/2}^2) |\ell(E^*)|^2 - 2s_\mu K_\mu \Re \ell(E^*) + 1 = 0. \quad (\text{III.4.15})$$

We have solved the equation above for different values of  $\mu \in (0, 1)$ . The mobility edge  $E^*(\mu)$  is plotted in the  $\mu - E$  plane in the figure (III.2). The result we find is in agreement with the sketch of [38] and with the numerical results of [225] for  $\mu < 1$  (for larger value of  $\mu$  the numerics of [225] were very inaccurate due to the large value of  $E$  which had to be explored).

### III.4.1 The mapping to directed polymers in random media

The result we have found for the mobility edge can be obtained, always starting from the recursion equation (III.4.2), in another way, making an analogy with the problem of directed polymers in random media [237, 238]. In particular, we can notice that the equation (III.4.2) for the imaginary part of the self energy can be rearranged

in a form which coincides with the expression of the partition function of directed polymers in random media. We proceed replacing the  $\Delta_j$ s appearing in the sum of the right hand side of the equation (III.4.2) by their expression in terms of their “neighbors”: if we do that one time we obtain the expression

$$\Delta_{i_1} = \sum_{i_2 \neq i_1} \frac{x_{i_1 i_2}}{(E - S_{i_2})^2} \Delta_{i_2}. \quad (\text{III.4.16})$$

Proceeding iteratively, say  $R$  times, we obtain:

$$\Delta_{i_1} = \sum_{i_2 \neq i_1} \frac{x_{i_1 i_2}}{(E - S_{i_2})^2} \sum_{i_3 \neq i_2} \frac{x_{i_2 i_3}}{(E - S_{i_3})^2} \cdots \sum_{i_R \neq i_{R-1}} \frac{x_{i_{R-1} i_R}}{(E - S_{i_R})^2} \Delta_{i_R}.$$

This expression can be read as a sum over directed paths  $\mathcal{P} = (i_1, \dots, i_R)$  of length  $R$  originating from the site  $i_1$ . For each edge  $(i_{n+1}, i_n)$  belonging to a given path, the contribution to  $\Delta_i$  coming from the path picks the random factor  $x_{i_n i_{n+1}} / (E - S_{i_{n+1}}^2)$ . Therefore, we can rewrite the equation above as

$$\Delta_{i_1} = \sum_{\mathcal{P}} \left( \prod_{(i_{n+1}, i_n) \in \mathcal{P}} \frac{x_{i_n, i_{n+1}}}{(E - S_{i_{n+1}})^2} \right) \Delta_{i_R}. \quad (\text{III.4.17})$$

As mentioned above, this equation has the same form of the recursion equation for the partition function of directed polymers in random media in presence of quenched disorder  $e^{-\epsilon_{ij}} = x_{ij} / (E - S_j)^2$ . We can therefore use the results known in this context in order to analyze the behavior of the distribution of the imaginary part of the self-energy and to study the localization transition.

Directed polymers in random media present a freezing transition which has been studied making an analogy with the freezing transition of the Random Energy Model (REM) [238, 237, 239, 240, 107]. The sum in the expression (III.4.17) runs over an exponential number of paths,  $(N - 1)! / (N - R - 1)! \sim N^R$ . In the case of large  $R$ , two cases are possible, corresponding to the two phases of the Random Energy Model: if the sum is dominated by few paths giving a contribute of order 1, we are in the frozen (glassy) phase. If, on the contrary, there is an exponential number of paths giving a small contribution such that their sum is of order 1, we are in the ergodic phase. It is easy now to understand the analogy with the Localization Transition, if we think about the behavior of the distribution of the imaginary part of the self-energy in the localized and in the extended phase. Indeed, as we have explained in the section (III.4), in the localized phase  $\Im \Sigma$  has a typical value which tends to zero when  $\eta \rightarrow 0$ , therefore, just large and rare resonances give a contribution of order 1 to the main value of  $\Im \Sigma$ : this situation corresponds to the glassy phase of the REM. In the extended phase instead, all sites contribute to the main value of  $\Im \Sigma$  with a small but non negligible term, and we can make the analogy with the ergodic phase of the REM. The transition is thus related to an ergodicity breaking. One of the possibility to determine the critical point is using the replica method [241]. In particular, we introduce  $n$  replicas of the system with the same realization of the disorder: the partition function of the system is thus given by

$$Z^n = \left[ \sum_{\mathcal{P}} \prod_{(i_{n+1}, i_n)} e^{-\epsilon_{ij}} \right]^n$$

and minus the quenched free energy per site is  $\phi = \overline{\log Z^n} / Rn$ . Using the one-step Replica Symmetry Breaking *ansatz* we divide the  $n$  replicas in  $n/m$  groups of  $m$  replicas all freezed in the same specific path. Therefore, we have:

$$Z^n = \left[ \sum_{\mathcal{P}} \prod_{(i_{n+1}, i_n)} e^{-m\epsilon_{ij}} \right]^{\frac{n}{m}},$$

and the expression for the free energy is

$$\phi(m, E) = \frac{1}{Rm} \log \left( \sum_{\mathcal{P}} \prod_{(i_{n+1}, i_n)} \left| \frac{H_{i_n, i_{n+1}}}{E - S_{i_{n+1}}} \right|^{2m} \right). \quad (\text{III.4.18})$$

We compute the annealed free energy per site  $\phi = \log \overline{Z^n} / Rn$  instead of the quenched one, since the result for the transition point is the same [238]. The expression (III.4.18) gives the typical value of the imaginary part of the self-energy: in the localized phase it decays exponentially to zero under iteration, while in the delocalized phase it blows up, and the linearization done in the equation (III.4.2) is not justified. In the terminology of directed polymers, the free energy needs to be extremized with respect to the parameter  $m$ :  $\partial\phi/\partial m|_{m=m^*} = 0$ . In the localized phase  $\phi(m^*, E) < 0$ , therefore the partition function is exponentially small and tends to zero over iterations. Conversely, in the delocalized phase  $\phi(m^*, E) > 0$ , and the partition function grows exponentially under iteration. The condition for the localization transition is thus given by

$$\begin{cases} \left. \frac{\partial\phi(m, E)}{\partial m} \right|_{m=m^*} = 0, \\ \phi(m^*, E) = 0. \end{cases}$$

As we will show below, the parameter  $m$  corresponds to the exponent of the tail of the distribution  $Q(S, \Delta)$  of the imaginary part of the self-energy which appears in the equation (III.4.10): so, as anticipated in the previous paragraph, the localization transition takes place for  $m = 1/2$ .

More in details, in order to determine the mobility edge, using the equation (III.4.18), we have to analyze the behavior of

$$N \frac{|x_{i_1}|^m}{|E - S_{i_1}|^{2m}} N \frac{|x_{i_2}|^m}{|E - S_{i_2}|^{2m}} N \frac{|x_{i_3}|^m}{|E - S_{i_3}|^{2m}} \dots \quad (\text{III.4.19})$$

Using the recursion equation (III.4.2), the real part of the self-energy can be rewritten as

$$S_{i_n} = \frac{H_{i_n, i_{n+1}}^2}{E - S_{i_{n+1}}} + \sum_{i'_n=1}^{N-2} \frac{H_{i_n, i'_n}^2}{E - S'_{i'_n}},$$

where the sum over  $i'_n$  runs over all the  $N - 2$  neighbors of  $i_n$  except the sites  $i_n$  and  $i_{n+1}$  which belong to the path. As a result, we have to analyze the following integral operator:

$$\begin{aligned} Z_{i_n}(S_{i_n}) &= (N - 2) \int dS_{i_{n+1}} Z_{i_{n+1}}(S_{i_{n+1}}) dH_{i_n, i_{n+1}} P(H_{i_n, i_{n+1}}) \\ &\times \prod_{i'_n}^{N-2} \left[ dH_{i_n, i'_n} P(h_{i_n, i'_n}) dS_{i'_n} L_{\mu/2}^{C(E), \beta(E)}(S_{i'_n}) \right] \\ &\times \left| \frac{H_{i_n, i_{n+1}}}{E - S_{i_{n+1}}} \right|^{2m} \delta \left( S_{i_n} - \frac{H_{i_n, i_{n+1}}^2}{E - S_{i_{n+1}}} - \sum_{i'_n}^{N-2} \frac{H_{i'_n}^2}{E - S_{i'_n}} \right). \end{aligned} \quad (\text{III.4.20})$$

The factor  $(N - 2)$  in the expression above takes account for the number of possibility we can choose the neighbors  $i_{n+1}$  of the site  $i_n$ , once we have excluded the site  $i_{n-1}$ . Studying the stability of the imaginary part of the self-energy, is therefore equivalent to study the behavior of the largest eigenvalue of the equation (III.4.20), in the same way we did in the previous paragraph analyzing the integral equation (III.4.12). In particular, if  $\lambda(E, m)$  is the largest eigenvalue of the equation (III.4.20), for large  $R$  we have:

$$\phi(m, E) \simeq \frac{1}{m} \log \lambda(m, E). \quad (\text{III.4.21})$$

The mobility edge thus is found for the value  $E^*$  such that:

$$\begin{cases} \frac{1}{m} \log \lambda(m, E^*) = 0, \\ \frac{\partial}{\partial m} \left[ \frac{1}{m} \log \lambda(m, E^*) \right] = 0, \end{cases}$$

which corresponds to:

$$\begin{cases} \lambda(m, E^*) = 1, \\ \frac{\partial}{\partial m} \lambda(m, E^*) = 0. \end{cases} \quad (\text{III.4.22})$$

We will show now how it is possible to recover exactly the equation (III.4.12) found in the previous section starting from the equation (III.4.20): we can see in this way that  $\lambda(m, E)$  corresponds to the Lyapunov exponent of the imaginary part of the self-energy, and  $m$  to the exponent of the tails of its probability distribution. For this purpose, we introduce the variable  $S$  via the integral

$$\int dS \delta \left( S - \sum_{i'_n=1}^{N-2} \frac{H_{i_n, i'_n}^2}{E - S_{i'_n}} \right) = 1.$$

According to the generalized central limit theorem, in the thermodynamic limit  $S$  has the same distribution of the real part of the self-energy,  $L_{\mu/2}^{C(E), \beta(E)}(S)$ :

$$\int \prod_{i'_n}^{N-2} \left[ dH_{i_n, i'_n} P(H_{i_n, i'_n}) dS_{i'_n} L_{\mu/2}^{C(E), \beta(E)}(S_{i'_n}) \right] \delta \left( S - \sum_{i'_n=1}^{N-2} \frac{H_{i_n, i'_n}^2}{E - S_{i'_n}} \right) \underset{N \rightarrow \infty}{\simeq} L_{\mu/2}^{C(E), \beta(E)}(S).$$

We can therefore rewrite the equation (III.4.20) as:

$$Z(X) = N \int dH P(H) dS L_{\mu/2}^{C(E),\beta(E)}(S) dX' Z(X') \delta \left( X - S - \frac{H^2}{E - X'} \right) \left| \frac{H}{E - X'} \right|^{2m}. \quad (\text{III.4.23})$$

Taking the Fourier transform of both sides of the expression above we finally obtain:

$$\hat{Z}(k) = N \hat{L}_{\mu/2}^{C(E),\beta(E)}(k) \int dH dX' P(H) \left| \frac{H}{E - X'} \right|^{2m} Z(X') e^{-ikH^2/(E-X')}, \quad (\text{III.4.24})$$

where  $\hat{L}_{\mu/2}^{C(E),\beta(E)}(k)$  is the Fourier transform of the Lévy stable distribution:

$$\hat{L}_{\mu/2}^{C(E),\beta(E)}(k) = \exp \left[ -C(E)|k|^{\mu/2} \left( 1 + i\beta(E) \tan \left( \frac{\pi\mu}{4} \right) \text{sign}(k) \right) \right]. \quad (\text{III.4.25})$$

This is exactly the same equation as (III.4.12) found in the previous paragraph: so, as announced, studying the freezing transition of directed polymers in random media corresponds to find the localization transition in Lévy matrices analyzing the behavior of the Lyapunov exponent of the imaginary part of the self-energy under iteration.

### III.5 Numerical check of the phase diagram

The phase diagram of the figure (III.2) has been found by solving the equation for the mobility edge (III.4.13) for different values of  $\mu$ . We have checked this result with a semi-analytical approach: the cavity equation (III.2.2) (where we neglect the off-diagonal terms) found in the paragraph (III.2) is a recursion equation for the probability distribution of the diagonal elements  $G_{ii}$  of the resolvent, which can be rewritten as

$$Q(G) = \int \prod_{i=1}^N [dG_i Q(G_i) dH_i P(H_i)] \delta \left( G^{-1} - E + i\eta + \sum_{i=1}^N H_i^2 G_i \right). \quad (\text{III.5.1})$$

As in the previous paragraph, for simplicity we drop the double-index notation and we assume that in the thermodynamic limit the distribution of the resolvent of a system with  $N$  sites is the same as the distribution of  $G$  for a system of  $N - 1$  sites. Using a particular property of Lévy matrices it is now possible to put this equation in a form which makes it easily solvable numerically. As explained in section (III.1), Lévy matrices present a “sparse-like” character [225]: as a consequence of the power-law tails of the distribution (F.0.1), each row or column of the matrix  $H$  contains  $O(N)$  elements vanishing in the thermodynamic limit and  $O(1)$  elements of  $O(1)$ . In order to distinguish explicitly the strong matrix elements from the small ones, we introduce a small but finite cutoff  $\gamma$ . This technique, introduced to study spin systems [236, 226], has been already used in [225] for Lévy matrices, and allows one to treat the backbone of strong matrix elements  $H_{ij} > \gamma$  as a sparse random matrix: in

particular, it constitutes a Erdős-Rényi random matrix with an average connectivity which can be computed from the Lévy distribution  $P(H)$  and which depends on the cutoff  $\gamma$ . In particular, separating the backbone of strong matrix elements from the weak one, the self-consistent equation (III.2) for the resolvent reads:

$$G_i = \frac{1}{E - i\eta - \sum_{\{j_+\}} H_j^2 G_j - \sum_{\{j_-\}} H_j^2 G_j}, \quad (\text{III.5.2})$$

where  $\{j_+\}$  includes the indices  $j$  such that  $H_j > \gamma$ , and  $\{j_-\}$  the  $js$  such that  $H_j < \gamma$ .

By definition, the joint distribution of the real and imaginary part of the diagonal elements of the resolvent  $Q(G)$  is given by:

$$Q(G) = \lim_{N \rightarrow \infty} \frac{1}{N} \sum_{i=1}^N \delta(G - G_i), \quad (\text{III.5.3})$$

$$\delta(G - G_i) = \delta(\Im G - \Im G_i) \delta(\Re G - \Re G_i).$$

The sum in the term containing the small matrix elements in the equation (III.5.2) runs over a number of term of order  $N$ , so, using the definition (III.5.3), we can apply the central limit theorem for random variables with finite variance, obtaining

$$\lim_{N \rightarrow \infty} \sum_{j=1}^N H_j^2 G_j = \sigma_\gamma^2 \int dG Q(G) G = \sigma_\gamma^2 \langle G \rangle. \quad (\text{III.5.4})$$

In the expression (III.5.4),  $\sigma_\gamma^2$  is the variance of the distribution of the weak matrix elements, defined by

$$\sigma_\gamma^2 = 2 \int_{(N)^{-1/\mu}}^\gamma H^2 P(H) dH = \frac{\mu \gamma^{2-\mu}}{N(2-\mu)}. \quad (\text{III.5.5})$$

Using this result, and substituting the relation (III.5.2) in the definition (III.5.3), we can obtain a self-consistent equation for  $Q(G)$ . The procedure is the same used in the context of the study of Lévy spin glasses [236, 226], and leads to the following result for the probability distribution  $Q(G)$ :

$$Q_\gamma(G) = \sum_{k=0}^{\infty} p_\gamma(k) \int \prod_{i=1}^k [dG_i Q_\gamma(G_i) dH_i P(H_i)] \delta \left( G^{-1} - E + i\eta + \sigma_\gamma^2 \langle G \rangle + \sum_{i=0}^k H_i^2 G_i \right), \quad (\text{III.5.6})$$

where  $p_\gamma(k) = e^{-c_\gamma} c_\gamma^k / k!$  is the Poisson distribution of the connectivity  $k$  of the random graph generated by the strong matrix elements. We can notice that in the expression above we have a Gaussian term coming from an infinite (in the thermodynamic limit) number of small matrix elements, and a Poissonian term coming from a finite number of strong matrix elements. In particular, the backbone of strong bonds constitutes a Erdős-Rényi random graph: every two nodes in the graph have a probability to be connected which is independent from every other couple of nodes. In particular, if  $N$  is the number of nodes of the graph, and  $c$  is the average value of the connectivity, the probability  $P(k)$  of two nodes to be connected by an edge is given by

$$P(k) = \binom{N-1}{k} k^{\frac{c}{N}} (N-1-k)^{1-\frac{c}{N}}. \quad (\text{III.5.7})$$

For  $N \rightarrow \infty$ , the expression (III.5.7) tends to the Poisson distribution  $P(k) \propto e^{-c} c^k / k!$ . In the case of the Erdős-Rényi random graph obtained from the strong elements of the Lévy matrices, the average connectivity  $c_\gamma$ , as mentioned above, depends on the cutoff  $\gamma$  we have introduced to separate the backbone from the Gaussian terms, and is given by

$$c_\gamma = 2N \int_\gamma^\infty P(H) dH = \gamma^{-\mu}. \quad (\text{III.5.8})$$

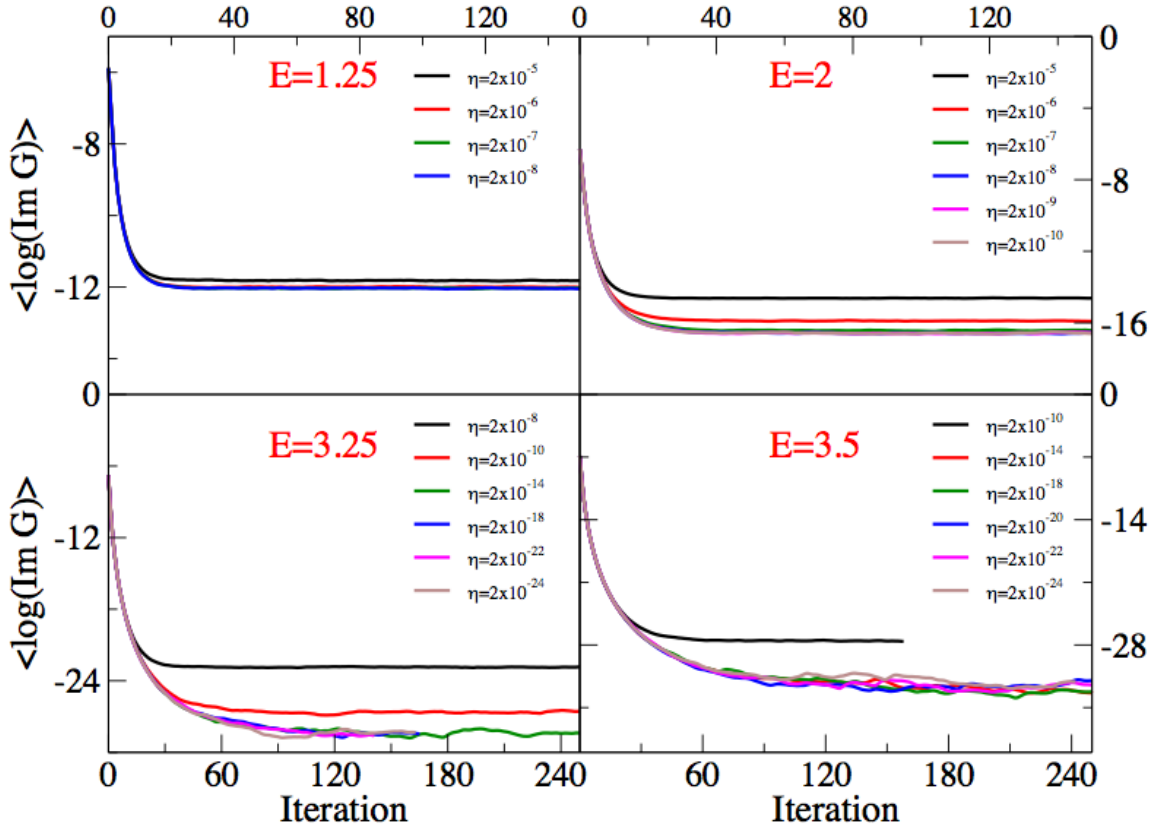


Figure III.3: Typical value of the imaginary part of the diagonal elements of the resolvent for  $\mu = 0.5$ , and different energies  $E$  in the delocalized phase as a function of the iteration in the population dynamics algorithm. We see that, as the mobility edge  $E_C \simeq 3.85$  is reached, the stationary value of  $\log(\Im G)$  is reached for smaller and smaller values of  $\eta$ .

In order to find the mobility edge, we solved the equation (III.5.6) with a population dynamics algorithm [195]. The technique consists in representing the distribution  $Q(G)$  as a sum of delta function, according to the definition (III.5.3). At each step of the algorithm the population is updated according to the recursion equation (III.5.6)

until a stationary distribution is reached. With this procedure, we have obtained the distribution of the real and the imaginary part of  $G$  for different values of  $\mu$  as a function of  $\eta$  and we have computed the typical value of the imaginary part: for the value of the energy  $E$  lying in the delocalized part of the spectrum, the typical value of  $\Im G$  becomes smaller as  $\eta$  is reduced and it reached a finite stationary value for a certain value of  $\eta = \eta_c$ . The value of  $\eta_c$  becomes smaller and smaller as the mobility edge is approached. If  $E$  belongs to the localized part of the spectrum, the typical value of  $\Im G$  becomes smaller and smaller as  $\eta$  is reduced and tends to zero for  $\eta \rightarrow 0$ . We have solved the equation (III.5.6) with this method with a population of  $2^{26}$  elements. We computed  $Q_\gamma(G)$  for  $\gamma = 10^{-3}, 10^{-4}, 5 \times 10^{-5}$  and extrapolated the results for  $\gamma \rightarrow 0$ . In the figure (III.3) we show the results for the typical value of  $\Im G$  for  $\mu = 0.5$  for different energies  $E$  in the delocalized phase. The numerical results in presence of the cutoff  $\gamma$  are in good agreement with the exact equation for the mobility edge found in the previous section.

### III.6 The problem of the intermediate phase: previous results

The work of Cizeau and Bouchaud [38] cited several times in the previous sections constitutes the pioneering work on Lévy Matrices. The results the authors obtained on the recursion equation for the resolvent, as discussed in section (III.2), have been rigorously proven by Ben Arous and Guionnet [227]. The authors also found results for the density of states: even if the method they used has not been rigorously justified, it actually gives the correct behavior of the tails of the spectrum of Lévy Matrices shown in figure (III.1) and confirmed in Ref. [227] and by numeric successive works [225, 224]. In the same work the authors combine analytical and numerical techniques in order to determine the phase-diagram of the model in the  $\mu - E$  plane. The key result of the work is that, looking at the behavior of different quantities, each one related to a different definition of the Localization Transition, two different transition lines are found, as shown in the plot of figure (III.4). In section (II.1) we have defined the moments  $\Upsilon_q$  of the normalized measure  $|\psi_\alpha|^2$ , and we have seen that  $\Upsilon_2$ , the IPR, represents the inverse of the number of sites having non-zero weight in the state  $|\alpha\rangle$ : if  $|\alpha\rangle$  is completely delocalized, each site  $i$  has the same weight  $\psi_{\alpha i}^2 = 1/N$ , therefore,  $\Upsilon_2$  goes to zero as  $1/N$  in the thermodynamic limit. In the opposite case, where  $|\alpha\rangle$  is localized on  $p \ll N$  sites,  $\Upsilon_2$  is finite and different from zero when  $N \rightarrow \infty$ . The authors in [38] computed  $\Upsilon_2$  numerically by performing exact diagonalization of Lévy Matrices for different values of  $\mu$  and averaging over several realizations of the disorder. The sizes of the matrices considered spread from  $N = 200$  to  $N = 1500$ . The results for  $\Upsilon_2$  are shown in the phase diagram of figure (III.4): studying the behavior of the IPR as a function of the system size, it appears finite and different from zero for  $N \rightarrow \infty$  in the whole region  $\mu < 1$ . For  $\mu > 1$ , the analysis of the scaling of  $\Upsilon_2$  with  $N$  gives the transition line represented in blue in figure (III.4).

The localization transition has also been investigated analytically in Ref. [38] by means of another criterion: using the recursion equation for the resolvent (III.2.2), the localization condition is expressed in terms of the distribution of the weight  $\psi_{\alpha i}^2$  over the sites. In particular, the behavior of the quantity  $\Upsilon_{1/2}$  is used in order to

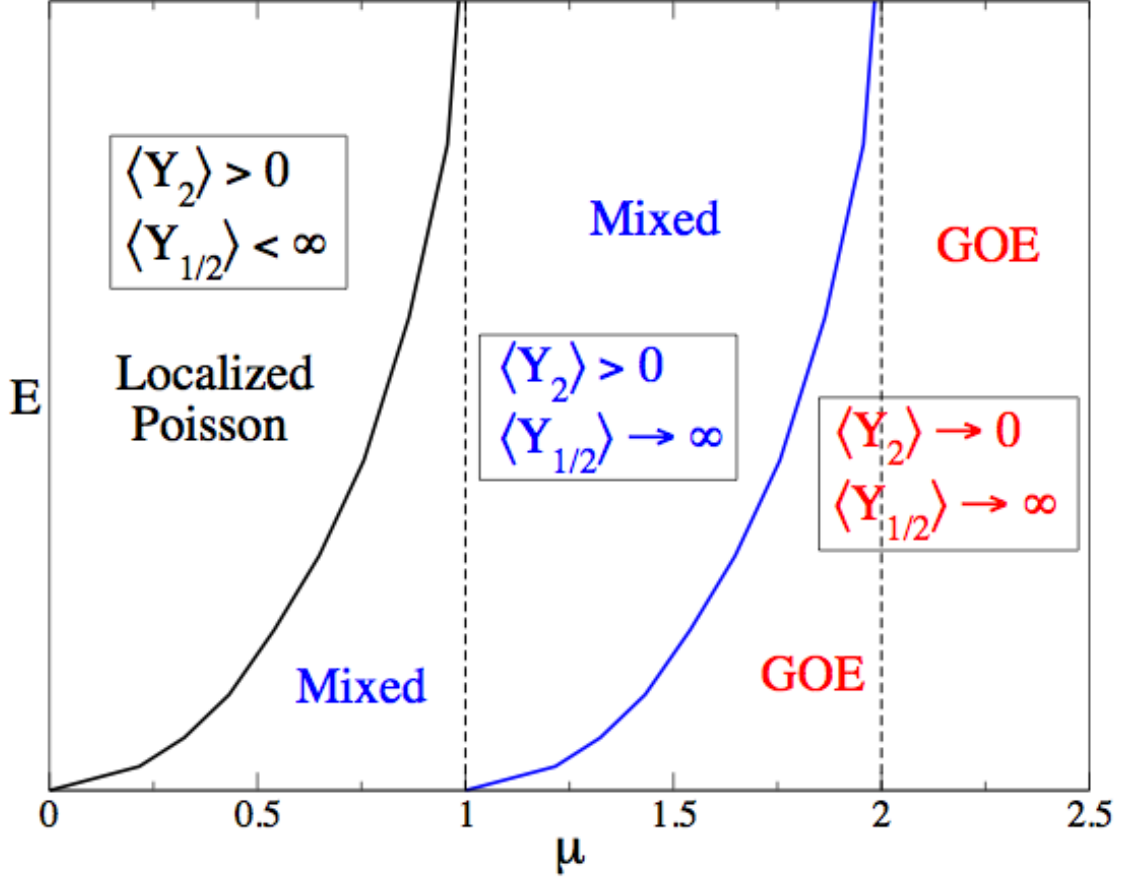


Figure III.4: Phase diagram obtained in Ref. [38] combining analytical and numerical techniques: for  $0 < \mu < 1$  the black curve delimits a region on the left of the  $\mu - E$  plane in which eigenstates are localized both following the analytical criterion based on the analysis of the recursion equation for the resolvent, i.e.  $\langle \Upsilon_{1/2} \rangle < \infty$  in the thermodynamic limit, and looking numerically at the behavior of the IPR, which stays finite for  $N \rightarrow \infty$ . The central region of the phase diagram, delimited by the black curve on the left and by the blue one on the right, is characterized by a mixed behavior: the states are delocalized from the analysis of  $\langle \Upsilon_{1/2} \rangle$ , which tends to infinity in the thermodynamic limit, but the numerical study of the IPR shows that  $\langle \Upsilon_2 \rangle$  remains finite for  $N \rightarrow \infty$ . On the right of the blue curve the states are delocalized both from the numerical observation of the IPR ( $\langle \Upsilon_2 \rangle \rightarrow 0$  for  $N \rightarrow \infty$ ) and from the analysis of  $\langle \Upsilon_{1/2} \rangle$ , which is infinite in the thermodynamical limit. The numerical study of the distribution of the level spacing  $P(s)$  suggests that in the mixed phase a non-universal behavior, intermediate between the GOE-like and the Poisson-like limits emerges. The Poisson-like and the GOE-like behavior characterize instead the localized phase (in black) and the delocalized one (in red) respectively.

discriminate between the two phases: if the state  $\alpha$  is completely delocalized, each projection  $\psi_{\alpha i}^2$  of  $\alpha$  over the site  $i$  is  $1/N$ , therefore  $\Upsilon_{1/2}$  diverges as  $\sqrt{N}$  as  $N \rightarrow$

$\infty$ . In the case of  $\alpha$  localized on  $p \ll N$ , as the IPR,  $\Upsilon_{1/2}$  remains finite in the thermodynamic limit. With this criterion, for  $\mu > 1$  all eigenstates appear delocalized, while for  $0 < \mu < 1$  the transition line represented by the black curve in figure (III.4) is found. The study of the localization transition in [38] is completed with the numerical analysis of other “observables”. In particular, the level spacing distribution  $P(s)$ , introduced in section (I.6), is computed for different values of  $\mu$  and for several regions of energies. As a result, in the localized phase delimited by the black curve in figure (III.4), the distribution  $P(s)$  found by exact diagonalization is well fitted by the Poisson distribution. In the delocalized phase (the region of the phase diagram on the right of the blue curve), the behavior of the distribution of  $s$  is well represented by the Wigner surmise (I.6.5). In the “mixed” region of the phase diagram, delimited by the two transition line in figure (III.4), the authors find that the behavior of  $P(s)$  is compatible with the existence of a non universal distribution, intermediate between the Poisson distribution and the GOE-like behavior. The phase diagram in figure (III.4) is the summary of all these results.

As we have stressed in section (III.1), Lévy Matrices are an interesting subject in its own, with many applications in physics and other disciplines: the connection with the study of disordered electronic system is just one of the possible field of application, and the work of Ref. [38] was published almost ten years before the works on the intermediate phase in MBL and for the Anderson Model on the Bethe Lattice discussed in section (I.9). As pointed out in section (III.1) the interest in the comprehension of Lévy Matrices is strong also on the mathematical point of view, since they belong to a larger and new universality class than the one constituted by standard Wigner matrices: this motivated the efforts in mathematical literature to prove rigorous results. In particular, after the work of Ref. [227] on the DoS, it has been proven by Bordenave and Guionnet [230] that for  $1 < \mu < 2$  all the moments  $\Upsilon_q$  vanish in the thermodynamic limit for  $q > 2$ , and goes to infinity for  $q < 2$ : this invalidates the conjecture of Ref. [38]. The presence of contradictory results in literature and the emerging of a similar behavior in the context of the study of Anderson Transition and Many Body Localization motivated us to perform a careful analysis in the attempt to understand if an intermediate mixed phase actually exist in the phase diagram of Lévy Matrices. In particular, motivated by the analogy with the Bethe Lattice explained in the previous sections, and by the analysis which had been performed in Ref. [39], we have tried to understand if there is a transition from an ergodic regime to a non-ergodic one which takes place inside the delocalized phase in the diagram of figure (III.2), determined analytically in section (III.4) and confirmed numerically (see section (III.5)). Since we have found that for  $1 < \mu < 2$  all states are delocalized, in this region the question is just if, for a fixed  $\mu$ , an ergodicity-nonergodicity transition takes place for a certain energy. In the region  $0 < \mu < 1$ , where for any fixed  $\mu$  a mobility edge appears in the spectrum, as shown in figure (III.2), we ask if the ergodicity transition takes place before the localization transition, i.e. for an energy  $E_T$  smaller than the mobility edge  $E^*$ . The definition of “ergodicity” here refers mainly to level statistics and is synonymous of GOE-like behavior (see section (I.6)). Nonetheless, in various recent works on the intermediate phase of the Anderson transition on the Bethe Lattice, the word refers to the statistics of wavefunctions (see section (I.9)): in particular it has been suggested that in the delocalized phase of the Anderson model on the Bethe

Lattice all the eigenstates exhibit multifractal behavior (see Appendix (B)), which is a feature of the critical point of the Anderson transition. Some of these works were published [40, 41] while we were working on this analysis on Lévy Matrices, and this motivated us to study numerically also the multifractal spectrum.

In the following two sections we present two analytical arguments based on the techniques explained in Chapter (II), the supersymmetric method and the Dyson Brownian Motion method, which support the idea that the delocalized phase of the diagram in figure (III.2) is ergodic. We present later our numerical results obtained by exact diagonalization and by solving with a population dynamics algorithm the cavity equation (III.5.6).

### III.7 The Supersymmetric method applied to Lévy Matrices

In section (II.3) we have shown, following Refs. [32, 31, 182], how the supersymmetric method applied to the model of sparse RMs allows to find GOE level statistics in the delocalized phase. We have seen in particular that the dilute fully connected structure of the model allows for an analytical treatment: after using the Hubbard-Stratonovich transformation (D.0.4), the integral (II.3.29) can be performed with the saddle point method, giving the expression (II.3.30). Equation (II.3.29), for  $\eta \rightarrow 0$ , is invariant for rotations  $\hat{T}$  such that  $\hat{T}^\dagger \hat{L} \hat{T} = \hat{L}$ . The term proportional to  $\eta/2$  is responsible for the breaking of this symmetry: if, for  $\eta \rightarrow 0$ , the symmetry is not broken, the solution is invariant under the full symmetry (II.3.32) and the solution of the saddle point equation only depends on  $\Psi_1^\dagger \Psi_1 - \Psi_2^\dagger \Psi_2$ ; if instead the symmetry is broken for  $\eta \rightarrow 0$ , the solution will depend on the two invariants  $\Psi^\dagger \hat{L} \Psi$  and  $\Psi^\dagger \Psi = \Psi_1^\dagger \Psi_1 + \Psi_2^\dagger \Psi_2$ . We have also seen that this symmetry breaking is responsible for the localization transition: indeed, the solution of the saddle point equation has a particular physical meaning, being related to the probability distribution of the real and imaginary part of the resolvent (see equation (II.3.33) and the Appendix (E)).

We show now that in the case of Lévy Matrices it is possible to follow exactly the same steps: we find in this way that the mechanism responsible for the localization transition is the same as in the Erdős-Rényi graph.

Using the formalism introduced in section (II.3) we consider the action

$$\begin{aligned} \mathcal{S}(\{\Phi_i\}, E, r, J^{(1)}, J^{(2)}) = & -\frac{i}{2} \sum_{i,j} \Phi_i^\dagger \hat{L} (E\delta_{ij} - H_{ij}) \Phi_j + \frac{i}{2} \sum_i \Phi_i^\dagger \Phi_i \left( \frac{r}{2N} + i\eta \right) \\ & + \frac{i}{2} \sum_i \Phi_i^\dagger \hat{L} \hat{J} \hat{M} \Phi_i, \end{aligned} \tag{III.7.1}$$

which has the same form of equation (II.3.22), but now  $H_{ij}$  are distributed according to the heavy-tail law (II.1). The fields in equation (III.7.1) are 8-components supervectors and the matrices are  $8 \times 8$  matrices defined as in equation (II.3.22). Averaging over matrix elements we obtain

$$\begin{aligned} \overline{Z(E, r, J^{(1)}, J^{(2)})} &= \int \prod_i [d\Phi_i] \exp \left\{ \frac{1}{2} \Phi^\dagger \hat{L}(E + \hat{J}\hat{M}) \Phi + \frac{i}{2} \Phi^\dagger \left( \frac{r}{2N} + i\eta \right) \Phi \right. \\ &\quad \left. + \frac{\mu}{2N} \sum_{ij} \int \frac{dx}{|x|^{1+\mu}} [\exp(-ix \Phi_i^\dagger \hat{L} \Phi_j) - 1] \right\}. \end{aligned} \quad (\text{III.7.2})$$

We proceed now as in the case of sparse RMs and we modify the interacting term using the Hubbard-Stratonovich transformation (D.0.4), obtaining

$$\begin{aligned} &\exp \left\{ \frac{\mu}{2N} \sum_{ij} \int \frac{dx}{|x|^{1+\mu}} [\exp(-ix \Phi_i^\dagger \hat{L} \Phi_j) - 1] \right\} \\ &= \int Dg \exp \left\{ -\frac{N\mu}{2} \int [d\Psi][d\Psi'] g(\Psi) C(\Psi, \Psi') g(\Psi') + \mu \sum_i g(\Psi_i) \right\}, \end{aligned} \quad (\text{III.7.3})$$

where the kernel  $C(\Psi, \Psi')$  is defined by

$$\int [d\Psi'] C(\Psi, \Psi') \int \frac{dx}{|x|^{1+\mu}} [\exp(-ix\Psi' \hat{L} \Phi) - 1] = \delta(\Psi - \Phi). \quad (\text{III.7.4})$$

With this substitution we obtain for the averaged partition function

$$\begin{aligned} \overline{Z(E, r, J^{(1)}, J^{(2)})} &= \int Dg \exp \left\{ -\frac{N\mu}{2} \int [d\Psi][d\Psi'] g(\Psi) C(\Psi, \Psi') g(\Psi') + N \ln \int [d\Phi] \right. \\ &\quad \left. \times \exp \left[ \frac{i}{2} \Phi^\dagger \left[ \hat{L}(E + \hat{J}\hat{M}) + \frac{r}{2N} + i\eta \right] \Phi + \mu g(\Phi) \right] \right\}. \end{aligned} \quad (\text{III.7.5})$$

As in the case of the Erdős-Rényi graph, the fully connected structure of the model allows to perform the integration over  $g$  with the saddle point method for  $N \rightarrow \infty$ , yielding

$$g(\Psi) = \frac{\int [d\Phi] \int \frac{dx}{|x|^{1+\mu}} [\exp(-ix\Psi^\dagger \hat{L} \Phi) - 1] \exp[(i/2)E \Phi^\dagger \hat{L} \Phi - (\eta/2) \Phi^\dagger \Phi + \mu g(\Phi)]}{\int [d\Phi] \exp[(i/2)E \Phi^\dagger \hat{L} \Phi - (\eta/2) \Phi^\dagger \Phi + \mu g(\Phi)]}. \quad (\text{III.7.6})$$

We can notice now that the structure of the solution (III.7.6) is exactly the same as the one obtained in the case of the Erdős-Rényi graph (II.3.30): the only difference derives from the specific form of the distribution of matrix elements over which we have averaged, and does not affect the symmetry structure of the solution. Exactly as in the case of the Erdős-Rényi graph, for  $\eta \rightarrow 0$  equation (III.7.6) has the full symmetry (II.3.32), which is broken for  $\eta \neq 0$  by the term proportional to  $\eta/2$ . The same discussion as for the case of sparse RMs thus applies: the localization transition corresponds to the breaking of the full symmetry (II.3.32), and since the solution of equation (III.7.6) is related to the real and imaginary part of the resolvent, in the way

explained in section (II.3) and in Appendix (E), the symmetric solution corresponds to the localized phase, while in the delocalized phase the symmetry (II.3.32) is broken and we have a manifold of solution: the integration over this manifold leads to GOE statistics as for sparse RMs. The supersymmetry method thus predicts GOE statistics in the whole delocalized region of the phase diagram (III.2).

*Caveat:* We have to observe that the presence of the fermionic fields makes the definition of the averaged partition function (III.7.2) very subtle: indeed the expansion of the exponential in the Grassmanian variables reduces only to the terms in  $\bar{\theta}\theta + \theta\bar{\theta}$ , and as a consequence the first and the second moment of the Lévy distribution appear in expression (III.7.2).

One possibility to define the integral (III.7.2) avoiding this problem is to regularize somehow the problem, for instance introducing an upper cutoff  $\Gamma$ , sufficiently large such that the structure of the matrix will still be similar to an Erdős Rényi graph (given by the term of the same order of the cutoff) plus a GOE background. The mechanism of the transition should thus be the same as in tree-like structures. Even if we are not able to directly show that the limit  $\Gamma \rightarrow \infty$  is well-defined in general, it is possible to see that, even without regularization (putting  $\Gamma \rightarrow \infty$  from the beginning), with the supersymmetric method the recursion equation for the probability distribution of the diagonal elements of the self-energy already found in section (III.7.2) is recovered. This equation is the basis for the computation of the mobility edge: it is therefore reasonable to think that in the limit  $\Gamma \rightarrow \infty$  the properties of the transition are correctly described.

### III.7.1 Equation on $R(\Sigma)$ with the supersymmetric method

As we have seen in section (III.2), for the local self energy,  $R(\Sigma)$  the following recursion equation holds:

$$\Sigma_{ii} \stackrel{d}{=} \sum_{j=1}^N H_{ij}^2 G_{jj} = \sum_{j=1}^N \frac{H_{ij}^2}{E - \Sigma_{jj}}, \quad (\text{III.7.7})$$

where  $\stackrel{d}{=}$  denotes the equality in distribution between random variables and  $E$  contains an infinitesimally small imaginary part  $i0^+$ . Since the correlations between the terms on the right hand side can be neglected, as shown rigorously in [227],  $\Sigma_{ii}$  is a sum of a large number or heavy tailed i.i.d. variables and, hence, it's a complex Lévy random variable. We consider its generating function:

$$\int d\Sigma R(\Sigma) e^{-iX_1 \Sigma + iX_2 \Sigma^*} = \prod_j \overline{e^{-iH_{ij}^2 (X_1 G_{ij} - X_2 G_{ij}^*)}},$$

where  $X_1$  and  $X_2$  are two real variables. The right hand side can be computed in the following way:

$$\prod_j \overline{e^{-iH_{ij}^2 (X_1 G_{ij} - X_2 G_{ij}^*)}} = \left( 1 + \frac{\mu}{N} \int d\Sigma R(\Sigma) \int \frac{dH}{2|H|^{1+\mu}} \left[ e^{-ih^2 \left( \frac{X_1}{E-\Sigma} - \frac{X_2}{E-\Sigma^*} \right)} - 1 \right] \right)^N.$$

Henceforth we neglect all the subleading (vanishing) terms in  $1/N$ . This allows one to derive the identity:

$$\int d\Sigma R(\Sigma) e^{-iX_1\Sigma + iX_2\Sigma^*} = \exp\left(\mu \int d\Sigma R(\Sigma) \int \frac{dH}{2|H|^{1+\mu}} \left[ e^{-iH^2\left(\frac{X_1}{E-\Sigma} - \frac{X_2}{E-\Sigma^*}\right)} - 1 \right]\right). \quad (\text{III.7.8})$$

This is an implicit version of the self-consistent equation satisfied by  $R(\Sigma)$ , or equivalently by the resolvent  $G$ , as seen in Chapter (III).

We show in the following that this same result also follows directly from the super-symmetric method. We consider for simplicity the action (E.0.4) defined in Appendix (E), with

$$\mathcal{F}(y) = \mu \int \frac{dx}{2|x|^{1+\mu}} \left[ e^{-ixy} - 1 \right]. \quad (\text{III.7.9})$$

By extremizing the action (E.0.4) on  $\rho(\Phi)$  and taking into account the normalization condition on  $\rho(\Phi)$ , at leading order in  $N$  one finds:

$$\rho(\Phi) = \exp\left(\frac{i}{2}E\Phi^\dagger\mathcal{L}\Phi + \int d\Psi\mathcal{F}(\Phi^\dagger\mathcal{L}\Psi)\rho(\Psi)\right).$$

By plugging the expression (E.0.7) into the previous equation, one can perform the integral over  $\Psi$ :

$$\int d\Sigma R(\Sigma) \exp\left(\frac{i}{2}\Phi^{(1)\dagger}\Phi^{(1)}(E-\Sigma) - \frac{i}{2}\Phi^{(2)\dagger}\Phi^{(2)}(E-\Sigma^*)\right) = \exp\left(\frac{i}{2}E\left(\Phi^{(1)\dagger}\Phi^{(1)} - \Phi^{(2)\dagger}\Phi^{(2)}\right) + \mu \int d\Sigma R(\Sigma) \int \frac{dx}{2|x|^{1+\mu}} \left[ e^{-ix^2\left(\frac{\Phi^{(1)\dagger}\Phi^{(1)}}{E-\Sigma} - \frac{\Phi^{(2)\dagger}\Phi^{(2)}}{E-\Sigma^*}\right)} - 1 \right]\right).$$

This expression has to be valid for any  $\Phi^{(1)\dagger}\Phi^{(1)}$  and  $\Phi^{(2)\dagger}\Phi^{(2)}$ , hence it defines a self-consistent on  $R(\Sigma)$  which actually coincides with Eq. (III.7.8) established previously. This result shows that our super-symmetric formalism is in agreement with previous exact results:  $R(\Sigma)$  is the complex Lévy stable distribution obtained rigorously in [227].

### III.8 The Dyson Brownian motion argument

In section (II.4) we have introduced the Dyson Brownian motion model: for matrices belonging to Gaussian ensembles this technique allows to recover the expression for the joint probability distribution of the eigenvalue (I.6.1), (I.6.2) as the equilibrium distribution of a dynamical process, constructed by introducing a fictitious time.

The technique of constructing a Brownian motion for matrix elements has been used to prove the universality of the results of RMT, and to extend them to Wigner matrices with less and less constraints. Recently, the Dyson Brownian motion combined with the reverse heat flow argument and with other techniques based on the comparison of some moments of the distribution, has been used to prove universality for general class of Wigner RMs [220]. The results of Ref. [220] apply to matrices with entries that are not necessarily identically distributed, and some previous upper and lower bounds on the second moment of the distribution of matrix elements are relaxed. Taking

inspiration by these recent mathematical progresses, we use a strategy based on the same type of argument to show that in the region  $1 < \mu < 2$  the eigenvalue statistics is GOE-like.

Our strategy consists in modifying the distribution of matrix elements  $P(H_{ij})$  (II.1) into  $(1 - \epsilon)P(H_{ij}) + \epsilon N^{1/\mu}W(N^{1/\mu}H_{ij})$ , where  $W(x)$  is a Gaussian distribution with unit variance. This does not alter the fat tails of the matrix elements, and thus our modified matrix belongs to the same universality class as the original matrix. This is equivalent to modify the matrix  $H$  into  $H_\epsilon = (1 - \epsilon)H + \epsilon W$ , where  $H$  is a Lévy matrix and  $W$  a very small GOE matrix whose elements have exactly the same scaling with  $N$  than the ones of  $H$ . The level statistics of  $H_\epsilon$  can be obtained using the Dyson Brownian Motion, and in the spirit of the reverse heat flow argument, the result can be extended to  $H$ .

Let's denote  $E_i(t)$  the eigenvalues of the matrix  $H_t = (1-t)H + tW$ . For  $t = 0$  these coincides with the eigenvalues of  $H$  and for  $t = \epsilon$  with the ones of  $H_\epsilon$ . Using the Dyson Brownian Motion technique we can construct a stochastic process for the eigenvalue which describes the interpolation  $t = 0 \rightarrow \epsilon$ : using the property that a Gaussian variable can be considered as the sum of two independent Gaussian variables, the dynamic from  $H_t$  to  $H_{t+dt}$  can be interpreted as the addition of a GOE matrix and a rescaling. Taking an infinitesimal  $dt$  allows one to use perturbation theory. The eigenvalues of  $H$  are the initial conditions for the stochastic process for the eigenvalues that we obtain, while the ones of  $H_\epsilon$  are the eigenvalues obtained after a "time"  $t = \epsilon$ .

The stationary distribution for this stochastic process, as explained in section (II.4), is the GOE distribution. The question is if the  $E_i(t)$  have enough "time" to equilibrate to their equilibrium (GOE) probability measure. If we use the results of Ref. [220] we have that, with our scaling, the DBM has enough "time" to reach the GOE distribution if  $N^{-1/\mu} \gg N^{-1}$  and the typical level spacing of  $H$  is  $O(1/N)$ . This last assumption is very reasonable and agrees well with the numerics. This implies that for  $\mu > 1$  the level statistics of the modified Lévy matrix, is indeed GOE-like in the bulk of the spectrum. Using the assumption that all matrices with the same heavy tails are characterized by the same level statistics, we find GOE level statistics for all matrices  $H_\epsilon$ , and in particular for  $H = H_{\epsilon=0}$ .

We stress however to conclude this section that the results of Ref. [220] were derived under more strict hypothesis on the probability distribution than the ones satisfied by Lévy Matrices, the argument shown here has thus not to be intended as a rigorous proof. We hope anyway that it may be a hint for further mathematical advances.

We conclude this section showing the phase diagram of figure (III.5), which summarizes the analytical results obtained for Lévy Matrices: the transition line shows the mobility edge computed in section (III.4) as a function of  $\mu$ . Combining this result with the ones obtained using the supersymmetric method and the Dyson Brownian motion argument, we have that, for  $1 < \mu < 2$  all states are delocalized for any value of the energy in the spectrum, and the system has GOE statistics. For  $0 < \mu < 1$ , there is a critical energy  $E^*(\mu)$  for any value of  $\mu$  separating localized and extended energy in the spectrum. The level statistics is Poisson-like in the localized phase and GOE-like in all the extended phase.

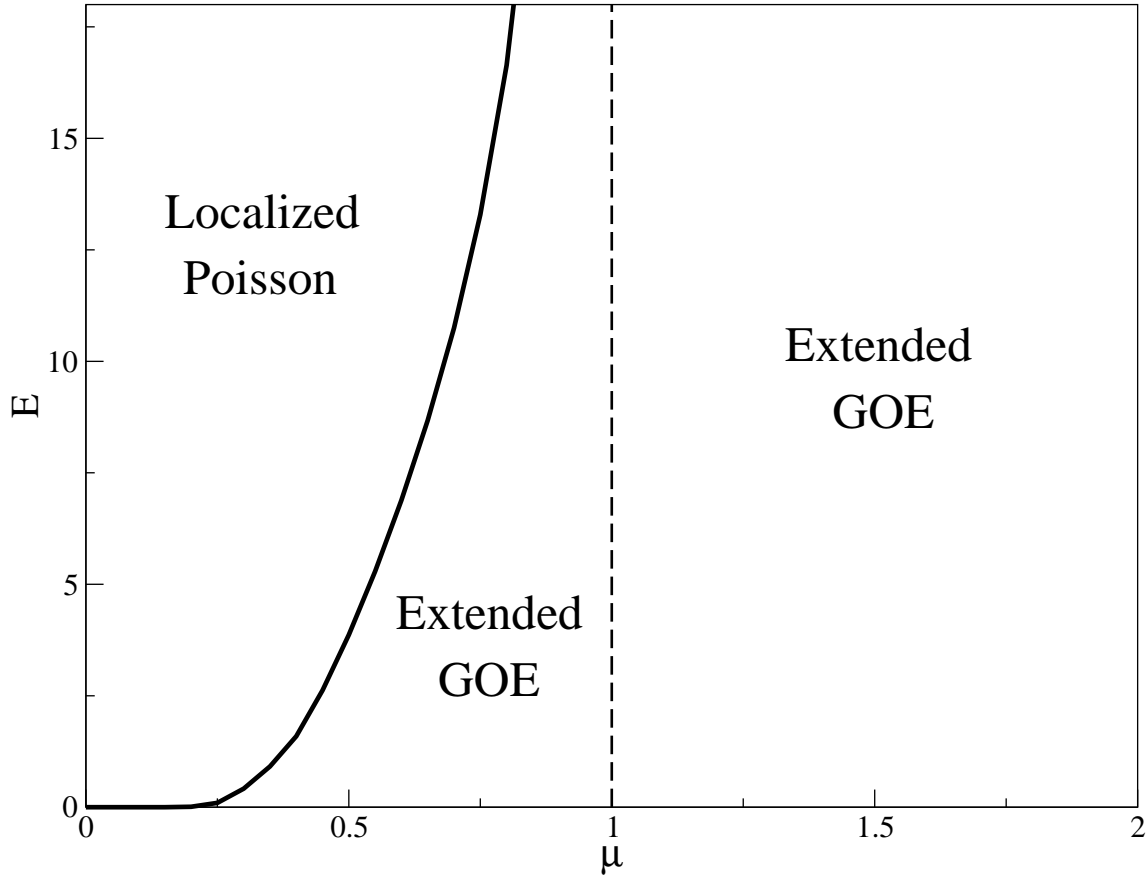


Figure III.5: Summary of the analytical results obtained through the computation of the mobility edge, the supersymmetric method and the Dyson Brownian motion argument: for  $1 < \mu < 2$  all states are delocalized for any value of energy in the spectrum, and the system has GOE statistics. For  $0 < \mu < 1$ , there is a critical energy  $E^*(\mu)$  for any value of  $\mu$  separating localized and extended energy in the spectrum. The level statistics is Poisson-like in the localized phase and GOE-like in all the extended phase.

### III.9 Numerical results for $\mu \in (1, 2)$

We have performed exact diagonalizations of Lévy Matrices in the range  $1 < \mu < 2$  for several system sizes  $N = 2^m$ , with  $m$  from 8 to 14. The data are averaged over at least  $2^{22-m}$  realization of the disorder. We have resolved the energy spectrum in 64 small intervals  $\nu$ , centered around the energies  $E_\nu = \langle \lambda_n \rangle_\nu$ , where we indicate with  $\lambda_n$  the  $n$ -th eigenvalue.

The behavior of several observables has been studied, in order to characterize numerically the transition and to analyze the ergodicity properties of the system.

First of all we have focused on the gap ratio  $r_n = \min\{\delta_\alpha, \delta_{\alpha+1}\} / \max\{\delta_\alpha, \delta_{\alpha+1}\}$ , introduced in section (I.6). The quantity  $\delta_n = \lambda_{n+1} - \lambda_n \geq 0$  indicates the level spacing between subsequent levels. This gap ratio  $r_n$  has been introduced in Ref. [136] and

contains the same information as the level statistics  $p(s)$ : the distributions of  $r_n$  in the GOE and Poisson cases are known, and the mean value of this quantity can be used to discriminate between the two behaviors. In particular, given a value of  $\mu \in (1, 2)$ , we have computed for each interval of energy  $\nu$  the mean value of  $r$  averaged over the disorder and over the energy window considered, and we have studied how the behavior of this quantity changes with the system size.

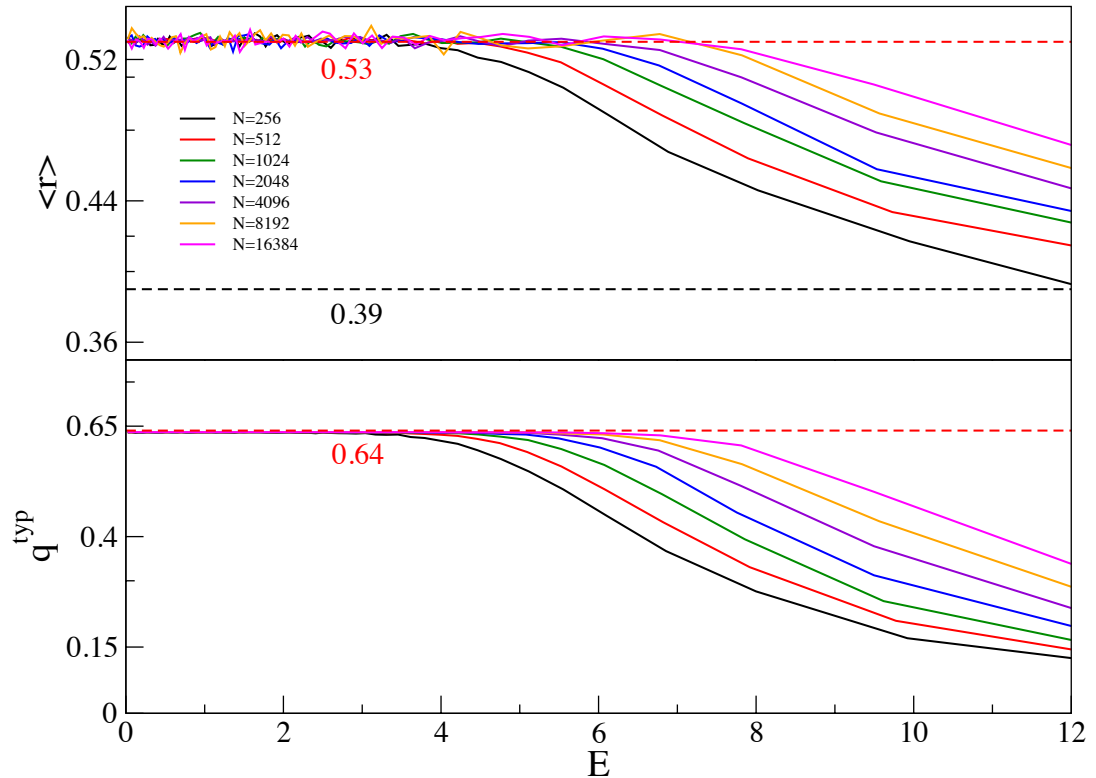


Figure III.6: Gap ratio  $\langle r \rangle$  (top panel) and typical value of the overlap  $q^{\text{typ}}$  (bottom panel) for different system sizes for  $\mu = 1.5$ : the system tends towards the GOE limit, represented by the red dashed curve, even if we cannot observe full convergence for high value of energy with the system sizes considered.

In the top panel of figure (III.6)  $\langle r \rangle$  is plotted as a function of the energy for different sizes for  $\mu = 1.5$ : even if at high energies for the system sizes considered the data are still far from full convergence, it is clear that  $\langle r \rangle$  evolves towards its GOE limit represented by the horizontal dashed red line, corresponding to  $\langle r \rangle_{\text{GOE}} = 0.53$ .

The full probability distribution of  $r$  corresponding to four different value of energy is plotted in figure (III.7): the GOE limit, which has been computed exactly in Ref. [242], corresponds to the dashed red curves, represented in the four panels. We see that, as for the main value of  $r$ , the distribution of  $\Pi(r)$  tends to the GOE limit when the system size is increased, even if with our data we manage to observe full

convergence only for small values of energy.

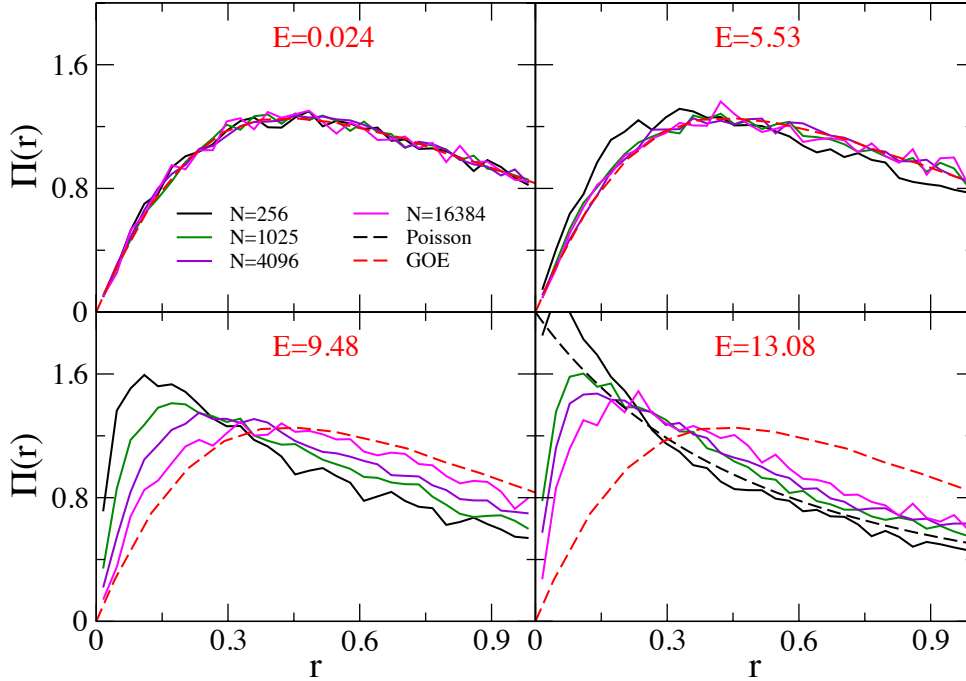


Figure III.7: Probability distribution of the gap ratio  $r$  for different values of energy for  $\mu = 1.5$ : the full convergence towards the GOE limit is observed only for small energies, but it is clear that the system evolves towards this limit for increasing size.

Another interesting quantity to study is the overlap  $q_n$  between eigenvectors corresponding to subsequent eigenvalues, defined as

$$q_n = \sum_{i=1}^N |\langle i|n\rangle| |\langle i|n+1\rangle|. \quad (\text{III.9.1})$$

In the GOE limit, the eigenvector components  $|\langle i|n\rangle|$  are independent Gaussian random variables of variance  $1/N$ : computing the average of  $q$  over the GOE ensemble we find thus  $\langle q \rangle_{\text{GOE}} = 2/\pi$ , and we expect that this coincides with the typical value  $q^{\text{typ}} = e^{\langle \log q \rangle}$ . In the Poisson case, on the contrary, the eigenvectors are exactly localized on the site wave functions and we have  $q^{\text{typ}} = 0$ . As shown in the bottom panel of figure (III.6), where  $q^{\text{typ}}$  is plotted as a function of the energy for the case  $\mu = 1.5$  for different system sizes, the behavior of this observable is the same as the one of  $\langle r \rangle$ : for increasing system sizes  $q^{\text{typ}}$  tends to its GOE limit, represented by the dashed horizontal line. The behavior of  $q^{\text{typ}}$  we have found numerically is interesting

and quite surprising: in the case of Lévy Matrices there is no reason to assume that the eigenvector components are independent random variables distributed as in the GOE case. Actually, in figure (III.8) the distribution of the wave vector components  $\Xi_N(|\psi^2|) = \Xi_N(w)$  is considered for  $\mu = 1.5$  and  $E = 0.24$ : plotting the distribution  $\Xi_N(Nw)/N$ , the curves corresponding to different sizes all collapse on a single curve  $P(Nw)$ , as we expect in the delocalized regime, being the weights all of the order  $1/N$ . Such distribution is compared with the Porter-Thomas distribution represented by the black dashed line and given by [243]

$$P_{\text{PT}}(x) = \frac{1}{\Gamma(1/2)} \left(\frac{1}{x}\right)^{1/2} \exp(-x), \quad (\text{III.9.2})$$

which characterizes the wavefunction statistics in the GOE case. We observe in the plot of figure (III.8) that for values of  $Nw$  of order one the behavior of  $P(Nw)$  differs from the one of expression (III.9.2) and the distribution appears broader than in the GOE case: nonetheless the limiting value of  $q^{\text{typ}}$  is  $2/\pi$  exactly as for GOE. As we will see in the next sections, this happens also for  $0 < \mu < 1$ , and we are not able at present to justify this numerical result.

We also studied numerically the behavior of the IPR  $\Upsilon_2$  defined by expression (II.1.1). In particular we have considered its typical value  $\exp\langle \ln \Upsilon_2 \rangle$ : the scaling of this quantity with the system size is described by the exponent  $\beta = \langle \ln \Upsilon_2 \rangle_\nu / \ln N$ . In figure (III.9) we plot the energy dependence of  $\beta$  for various  $N$ . At small enough energies we find  $\beta \simeq 1$ , corresponding to the standard scaling of the IPR for fully delocalized states. For high energy finite size effects are stronger, and we observe that  $\beta$  decreases as the energy grows for a fixed system size  $N$ . However, for fixed energy we observe that  $\beta$  increases monotonously with  $N$ , and seems to approach the asymptotic value  $\beta \rightarrow 1$  in the thermodynamic limit in all energy windows, even if it seems that really large sizes are needed (much larger than those we have) in order to observe this convergence for all energies.

While we were working on this project on Lévy Matrices, an interesting observable has been introduced by A. De Luca and other authors in Ref. [40], the support set: for an eigenvector  $n$  with sites ordered according to  $|\langle i|n \rangle| > |\langle i+1|n \rangle|$ , it is defined as the sets of sites  $i < S_\epsilon^{(n)}$  such that  $\sum_{i=1}^{S_\epsilon^{(n)}} |\langle i|n \rangle|^2 \leq 1 - \epsilon < \sum_{i=1}^{S_\epsilon^{(n)}+1} |\langle i|n \rangle|^2$ . The scaling of  $\langle S_\epsilon^{(n)} \rangle$  for  $N \rightarrow \infty$  and  $\epsilon$  arbitrary small but finite allows to discriminate between the extended and the localized regimes, as  $S_\epsilon^{(n)}$  is  $N$ -independent for localized wave-functions while it diverges for  $N \rightarrow \infty$  for delocalized states. This observable has been introduced in the context of the study of ergodicity of extended states on the Bethe Lattice, as a measure of wavefunctions multifractality. In figure (III.9) we plot the exponent  $\beta' = \ln \langle S_\epsilon^{(n)} \rangle_\nu / \ln N$ , describing the scaling of the support set at large  $N$ : its behavior is very similar to the one of  $\beta$  described above for the IPR. However, as it was noticed in Ref. [40], the support set is apparently a sharper measure of wavefunctions ergodicity compared to the IPR, as the values of  $\beta'$  are much closer to 1 in all energy windows.

Similar results are obtained for  $\mu = 1.1$ , confirming that for  $\mu \in (1, 2)$  all eigenstates of Lévy Matrices are extended and the level statistics is described by GOE in the whole spectrum. Finite size effects can however be strong: in particular, the results we have

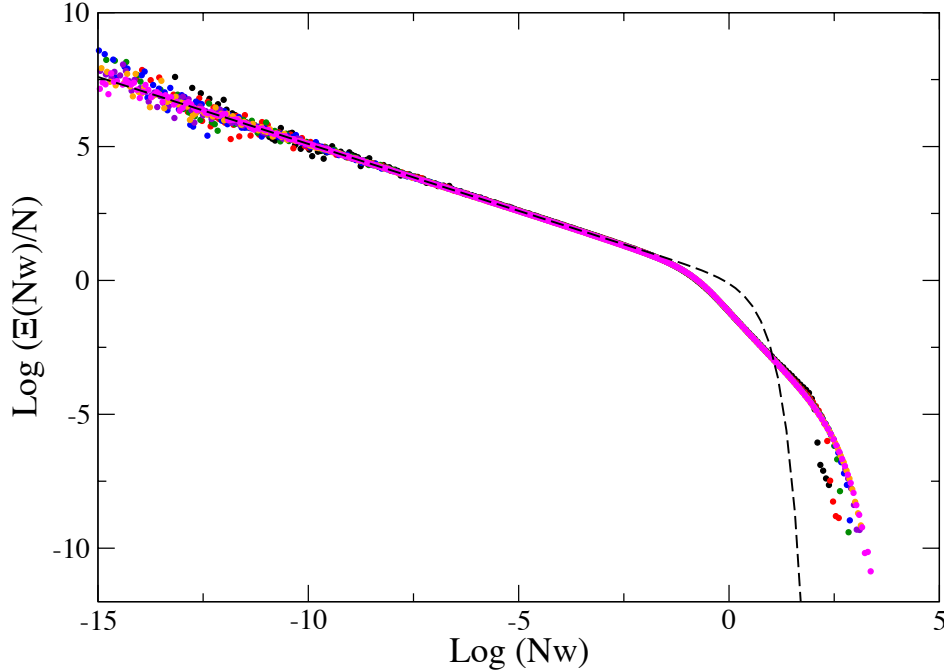


Figure III.8: Wavefunction statistics for  $\mu = 1.5$  for different system sizes and  $E = 0.024$ . The distribution has the stretched exponential behavior (III.9.2), represented by the black dashed curve up to value of  $Nw$  of order one: for larger value of  $Nw$  the distribution is broader than in the GOE case.

for the IPR, where these effects are particularly evident, explain why originally the numerical analysis of this observable had suggested the existence of a nonergodic phase in the region  $\mu \in (1, 2)$ . These finite size effects become stronger as  $\mu$  is lowered and can be extremely important at high energies, where one needs to consider relatively large  $N$  to observe full converge towards the asymptotic values.

### III.10 Numerical results for $\mu \in (0, 1)$

We also explored numerically the region  $0 < \mu < 1$  and analyzed the behavior of various observables with varying system sizes.

The numerical study of the range  $0 < \mu < 1$  may be slightly more complicated than that in the region  $1 < \mu < 2$ . As explained in section (III.5), each row (or column) of the Lévy Matrix  $H$  has  $O(N)$  elements of  $O(N^{-1/\mu})$  and  $O(1)$  elements of  $O(1)$ , ensuring a well-defined thermodynamic limit. However, the largest element of the whole matrix (which contains  $N^2$  terms) is of order  $N^{1/\mu}$ . As a consequence, the range of variability of the matrix elements goes from  $O(N^{-1/\mu})$  to  $O(N^{1/\mu})$ , which

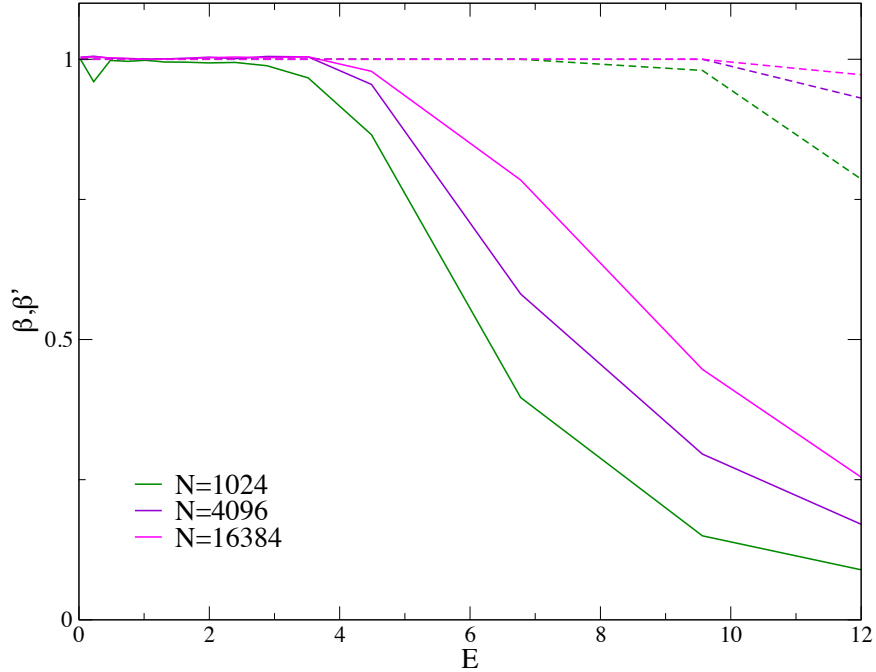


Figure III.9: Exponents  $\beta$  (continuous lines) and  $\beta'$  (dashed lines) describing the scaling with  $N$  of the typical value of the Inverse Participation Ratio and of the support set as a function of the energy for  $\mu = 1.5$ .

is, for large enough system sizes and for  $\mu < 1$ , extremely broad. This could affect the numerical precision of our results. In order to overcome this problem, we have introduced a cut-off on large matrix elements scaling as  $\Lambda N^{1/\mu}$ , where  $\Lambda$  is a constant much larger than 1. Since we are only interested in the properties of Lévy Matrices for energies of  $O(1)$ , i.e. we want to study the bulk properties of the ensemble, the presence of such cut-off does not have any influence on our numerical results (provided that  $\Lambda$  is large enough). The analysis of edge properties of Lévy Matrices is a quite disconnected problem, which has been studied for example in Refs. [228, 244].

Furthermore, as explained in section (III.1) and (III.5), Lévy Matrices have a “sparse-like” character which allows one to describe them in terms of a sparse Erdős-Rényi random matrix constituted by the backbone of large entries and a Wigner matrix (with finite variance) constituted by an infinite (in the thermodynamic limit) number of very small terms. As we have seen in section (III.5), in order to exploit this property in numerical simulations, we introduce a cut-off  $\gamma$  (very small but finite) on small matrix elements which eliminates the contribution of small “Gaussian” terms. This allows to simplify and speed-up the numerical calculations, since numerical routines for exact diagonalization are faster for sparse matrices. The probability distributions of the entry thus becomes:

$$P_N^{(\gamma, \Lambda)}(H_{ij}) = p_N^{(\gamma)} \delta(H_{ij}) + \left(1 - p_N^{(\gamma)}\right) \theta\left(\gamma < |H_{ij}| < N^{1/\mu} \Lambda\right) \frac{C_N^{(\gamma, \Lambda)}}{2|H_{ij}|^{1+\mu}},$$

where  $p_N^{(\gamma)} = 1 - 1/(N\gamma^\mu)$  and  $C_N^{(\gamma, \Lambda)} = \mu/[\gamma^{-\mu} - N^{-1}\Lambda^{-\mu}]$ .

We have performed exact diagonalizations of such random matrices for several system sizes  $N = 2^m$ , with  $m$  from 8 to 15, and for  $\Lambda = 2^{15}$  and we have averaged the data over (at least)  $2^{22-m}$  realization of the disorder. The energy spectrum is resolved in 64 small intervals  $\nu$ , centered around the energies  $E_\nu = \langle \lambda_n \rangle_\nu$ . In order to make sure that the cut-off on small entries is small enough to reproduce the  $\gamma \rightarrow 0$  limit, we have considered different values of  $\gamma$  ( $\gamma = 10^{-3}$ ,  $10^{-4}$ , and  $5 \times 10^{-5}$ ) and checked that the data become independent of it (within our numerical accuracy).

In the following we report our data for  $\mu = 0.5$ . Similar results are found for  $\mu = 0.8$  and  $\mu = 0.3$ , although finite size effects become bigger as  $\mu$  is decreased and the crossover region gets broader.

In figure (III.10) we plot  $q_\nu^{typ}$  as a function of  $E_\nu$  for  $\mu = 0.5$  and for different system sizes, averaged over samples and eigenstates within each energy window. For small energies we recover the universal values  $q_P^{typ} = 2/\pi$  corresponding to GOE statistics, and for high energies the value  $q_P^{typ} \rightarrow 0$  corresponding to Poisson statistics. We notice however that the curves corresponding to different values of  $N$  seem to cross much before the localization transition, which can be computed analytically solving equation (III.4.15) for  $\mu = 0.5$  and should occur at  $E^* \simeq 3.85$ : we can ask thus if this is the sign of a different phase transition, which takes place before the localization transition and within the delocalized region, delimiting delocalized ergodic states from delocalized non-ergodic states with a mixed behavior. However, since our numerical data on  $q^{typ}$  are extremely clean, they allow us to observe that the crossing point is actually slowly drifting towards higher values of the energy (and most probably converging to  $E^*$  in the thermodynamic limit): there is a large region of energy in which the value of  $q^{typ}$  as a function of  $N$  has a non-monotonic behavior, as shown in figure (III.12): this defines a characteristic length  $N_m$  governing finite size effects such that, if we consider sizes  $N < N_m$ , the system seems to approach the Poisson limit, but if we go over this characteristic size, we see actually that the system evolves towards the GOE limit for  $N \rightarrow \infty$ .

In figure (III.13), we show the probability distribution of the gap ratio,  $\Pi(r)$ , for  $\mu = 0.5$ , for different system sizes, and for four different values of the energy. As expected, for small enough energies (e.g.,  $E \simeq 0.016$ , represented in the top-left panel) the entire probability distribution is described by GOE statistics, given by the red dashed curve. Conversely, for high enough energies (e.g.,  $E \simeq 7.68$ , in the bottom-right panel), in the localized regime, the data nicely approach the Poisson distribution  $\Pi(r) = 2/(1+r)^2$ , corresponding to the black dashed curve, except for very small values of  $r$  where convergence is exponentially slow due to finite size effects. For moderately high energies (e.g.,  $E = 1.25$  in the top-right panel),  $\Pi(r)$  evolves towards the GOE distribution as  $N$  is increased, although we are not able to observe full convergence for the largest system size. Finally, for energies in the crossover region (e.g.,  $E = 2.28$ , bottom-left panel), one seems to observe that  $\Pi(r)$  is described by a stationary (i.e.,  $N$ -independent) and non-universal (neither GOE nor Poisson) distribution, as observed in Ref. [38]. Nevertheless, if one analyzes carefully the numerical data, focusing, for instance, on the behavior of  $\Pi(r)$  at small  $r$ , one realizes that  $\Pi(r)$  evolves in a non-monotonic way: for system sizes smaller than the crossover size,  $N < N_m \simeq 1200$  for  $E \simeq 2.28$  (see figure (III.12)), it evolves towards the Poisson distribution, while for large system sizes,  $N > N_m$ , it commences to approach the GOE distribution.

However, it is evident that we were able to make this kind of remark because the analysis of the data for  $q^{\text{typ}}$  in figure (III.10) allowed us to recognize the existence of the crossover scale. It is clear that, based on the bottom-left panel of figure (III.13) solely, one would certainly conclude that for intermediate energies a new and non-universal “mixed” level statistics is found.

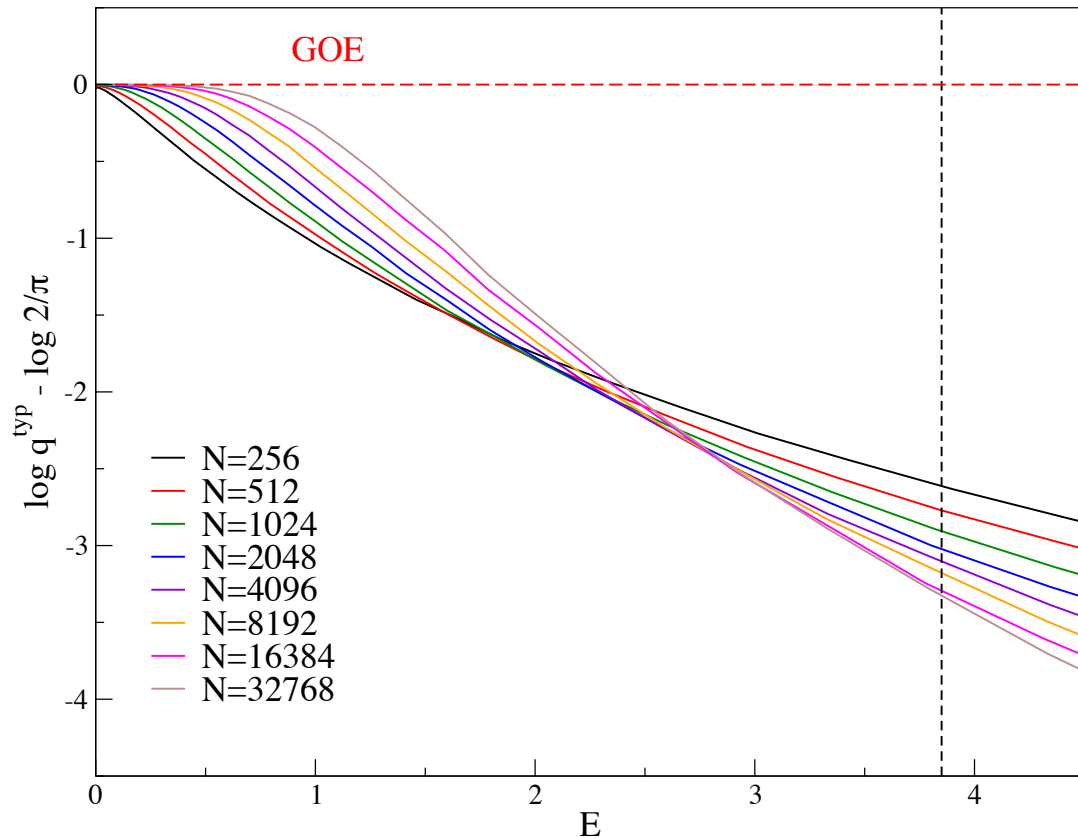


Figure III.10:  $\ln(q^{\text{typ}}/q_{\text{GOE}}^{\text{typ}})$  as a function of the energy  $E$  for different system sizes for  $\mu = 0.5$ .

As for the region  $1 < \mu < 2$ , we have studied the dependence of the exponents  $\beta = \langle \ln \Upsilon_2 \rangle_\nu / \ln N$  and  $\beta' = \ln \langle S_\epsilon^{(n)} \rangle_\nu / \ln N$  describing the scaling with the system size of the typical value of the IPR and of the average support set respectively. In figure (III.11) we show the data for  $\mu = 0.5$ . The behavior of  $\beta$  and  $\beta'$  is coherent with previous results, at least for sufficiently small and sufficiently large energies. More precisely, one observes that, at fixed  $N$ ,  $\beta$  and  $\beta'$  decrease as the energy is increased. Nevertheless, at fixed and small enough energy, they both grow with  $N$  and seem to approach the standard value 1 for  $N \rightarrow \infty$ . Conversely, at fixed and large enough energy, in the localized regime,  $\beta$  and  $\beta'$  decrease to zero as the system size is increased, implying that  $\langle \Upsilon_2 \rangle_\nu, \langle S_\epsilon^{(n)} \rangle_\nu \rightarrow \text{cst}$ . As mentioned above, the support set provides a more precise measure of wave-function ergodicity compared to the IPR. In particular, the exponent  $\beta$  is much smaller than one already very far from the localization transition. In the crossover region one should expect that  $\beta$  and  $\beta'$  show

a non-monotonic behavior as a function of  $N$  on the crossover scale  $N_m(E)$ . However, our numerical data are too noisy to capture this behavior. As already remarked, in fact, numerics based solely on the IPRs are inconclusive and could be undoubtedly misinterpreted, especially for intermediate energies within the crossover regime, since they are affected by strong finite size effects.

### III.10.1 Numerical results for $Q(G)$

In section (III.5) we have explained how the “sparse-like” character of Lévy Matrices can be exploited in order to simplify the recursion equation for the probability distribution of the resolvent  $Q(G)$ , leading to equation (III.5.1): in the expression, the terms corresponding to the large matrix elements ( $|H_{ij}| > \gamma$ ) are splitted from small ones ( $|H_{ij}| < \gamma$ ), and for the latter the central limit theorem for variables with finite variance has been used.

We have solved equation (III.5.1) using a population dynamics algorithm, which, as explained in section (III.5) has allowed us to check numerically the mobility edge computed in section (III.4). In particular, we have used a population of  $2^{26}$  elements, and computed  $Q_\gamma(G)$  for  $\gamma = 10^{-3}, 10^{-4}, 5 \times 10^{-5}$ , and extrapolated the results for  $\gamma \rightarrow 0$ .

We present now an argument which shows how the properties of the distribution  $Q(G)$  can be used to explain the existence of a crossover size. As we have pointed out many times, what characterizes the delocalized phase is that, at any site  $i$ , the imaginary part of  $G_{ii}$  receives an infinitesimal contribution from an infinite number of eigenfunctions. This leads to a typical value of  $G_{ii}$  which is finite for  $N \rightarrow \infty$  and  $\eta \rightarrow 0$ . Instead,  $\Im G_{ii}^{\text{typ}} = 0$  in the localized phase. Approaching the transition from the delocalized side,  $\Im G_{ii}^{\text{typ}}$  becomes extremely small. Thus, one needs to take large enough systems in order to realize that it is different from zero, and hence that the system is in the delocalized and GOE-like phase. The argument, which is based on the interpretation of  $\Im G_{ii}$  as the local density of states, is as follows. The number of states per unit of energy close to  $E$  is  $N\rho(E)$ . This number, multiplied by the typical value of the local density of states, has to be larger than one in order to be in a regime representative of the large- $N$  limit. This defines the crossover scale  $N'_m(E) \propto 1/(\Im G_{ii}^{\text{typ}} \rho(E))$ . In order to extract this crossover scale from our numerical data we have computed the typical value of  $\Im G_{ii}$ ,  $\Im G_{ii}^{\text{typ}} = e^{\langle \ln \Im G_{ii} \rangle}$ , over the stationary distribution on the delocalized phase for different values of the energy  $E$ : the characteristic crossover length corresponding to a certain energy is  $N'_m(E) = 1/(\Im G_{ii}^{\text{typ}} \rho(E))$ .

We have compared numerically  $\ln N'_m(E)$  and  $\ln N_m(E)$  and found that they are indeed proportional, as we can see from the plot in figure (III.15), showing that our argument correctly captures the origin of the finite size effects.

We plot the crossover scale  $N'_m(E)$  as a function of  $E$  in figure (III.14) for  $\mu = 0.5$ : it diverges very fast approaching  $E^*(\mu)$ , and we see that it is already really large quite before the mobility edge. A good fit is provided by an essential singularity. These results therefore unveil what is the mechanism responsible for the non-GOE statistics observed for finite Lévy Matrices in a wide regime before the localization transition, as predicted by the supersymmetric method on the Bethe Lattice for the characteristic volume  $V_{BL}$  (see section (II.3)).

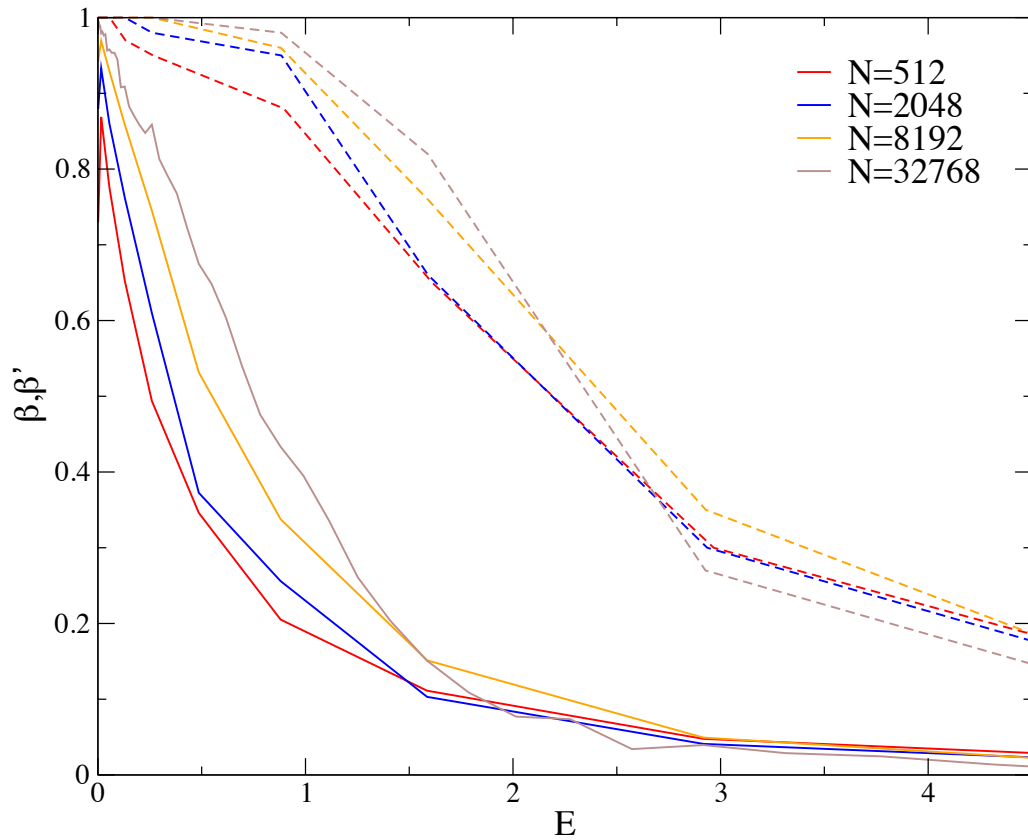


Figure III.11: Exponents  $\beta$  (continuous lines) and  $\beta'$  (dashed lines) describing the scaling with  $N$  of the typical value of the Inverse Participation Ratio and of the support set as a function of the energy for  $\mu = 0.5$ .

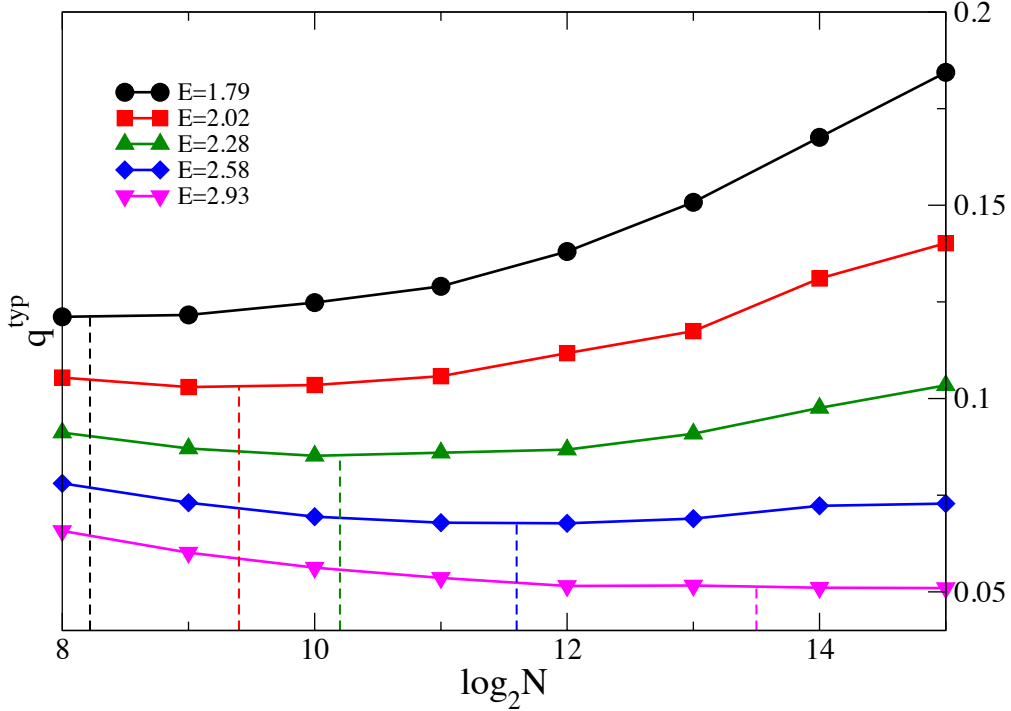


Figure III.12: The typical value of the overlap  $q$  is plotted for different energies belonging to the crossover region as a function of the characteristic size: this defines a characteristic length  $N_m$  which governs finite size scaling effects.

In figure (III.16) we show the marginal probability distribution of  $\ln \Im G_{ii}$  for several values of the imaginary regulator  $\eta$  and for  $E = 5$ , deep in the GOE ergodic phase. Since the system is delocalized and the spectrum is absolutely continuous,  $\tilde{Q}_I(\ln \Im G)$  must have a non-singular limit as  $\eta \rightarrow 0^+$ . We indeed observe a stationary  $\eta$ -independent distribution for  $\eta$  sufficiently small ( $\eta \lesssim 10^{-6}$ ). As a consequence, from equation (II.1.7) we have  $\langle \Upsilon_2 \rangle \rightarrow 0$  for  $\eta \rightarrow 0^+$ .

Conversely, in the localized phase the marginal probability distribution of the imaginary part of  $G_{ii}$  has a singular behavior as  $\eta \rightarrow 0^+$ , as illustrated in figure (III.17). Almost all values of  $\Im G_{ii}$  are of order  $\eta$ , except extremely rare events, whose fraction vanishes as  $\eta$ , described by heavy power-law tails with an exponent  $1+m$  and  $m = 1/2$ . More precisely,  $\tilde{Q}_I(\Im G)$  has a scaling form  $f(x/\eta)\eta$  for  $x \sim \eta$ , with  $\int f(y) dy = 1$ , and fat tails

$$\tilde{Q}_I(\Im G) \simeq \frac{c\eta^{1-m}}{(\Im G)^{1+m}}, \quad (\text{III.10.1})$$

with  $c$  being a constant of  $O(1)$ , and a cut-off for  $\Im G_{ii} \simeq 1/\eta$ . The main contribution (of order one) to the density of states comes from these tails, whereas the bulk part

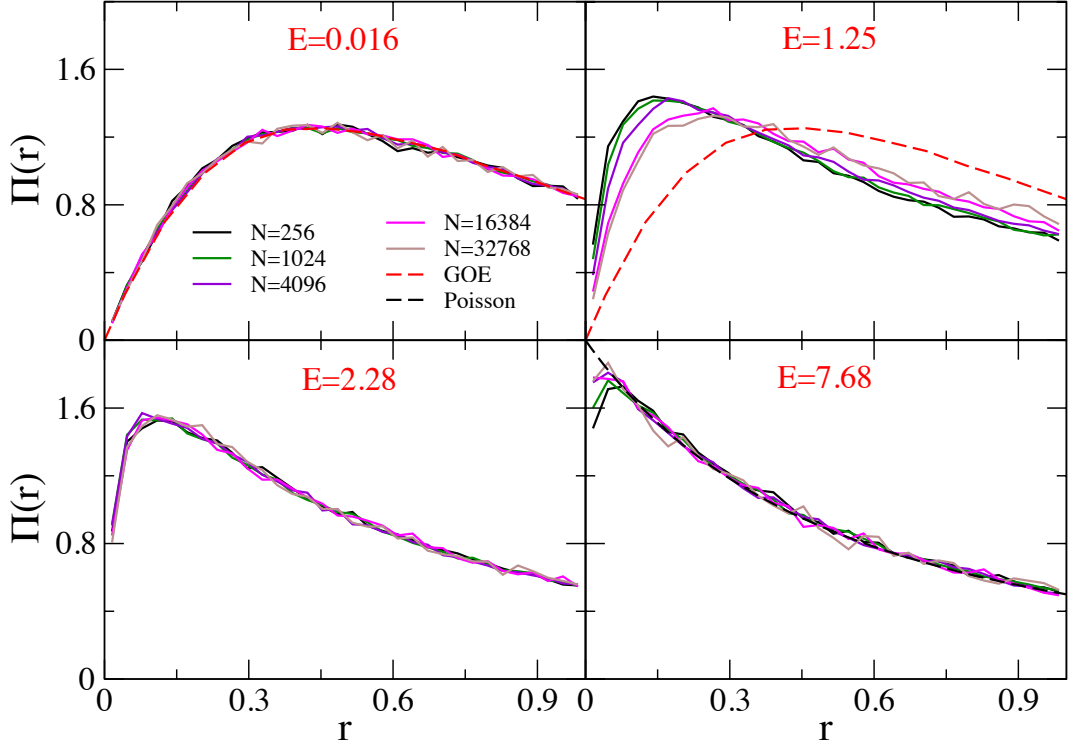


Figure III.13: Probability distribution of the gap ratio for  $\mu = 0.5$ , for different system sizes, and for four different values of the energy. The Poisson and GOE counterparts of  $\Pi(r)$  are also shown. Top-left panel:  $E = 0.016$ ; The entire probability distribution is described by the GOE. Top-right panel:  $E = 1.25$ ;  $\Pi(r)$  evolves towards the GOE distribution as  $N$  is increased, although we are not able to observe full convergence. Bottom-left panel:  $E = 2.28$ ;  $\Pi(r)$  seems to be described by a  $N$ -independent non-universal distribution. Bottom-right panel:  $E = 7.68$ ;  $\Pi(r)$  converges to the Poisson distribution for large  $N$ .

only yields a vanishing contribution.

In figure (III.18) we show the behavior of  $\tilde{Q}_I(\ln \Im G)$  in the crossover region. Since the system is delocalized, we know that the  $\eta \rightarrow 0^+$  limit exists and is non-singular. However, convergence to a stationary distribution is observed only for extremely small values of the imaginary regulator,  $\eta \lesssim 10^{-13}$  in this case. For  $\eta$  small enough but still larger than  $10^{-13}$ , one observes that, similarly to the localized regime, the marginal distribution of  $\Im G_{ii}$  displays “singular” power-law tails described by  $\tilde{Q}_I(\Im G) \sim \eta^{1-m}/(\Im G)^{1+m}$  with an exponent  $1/2 \lesssim m < 1$ , and a cut-off for  $\Im G_{ii} \simeq 1/\eta$  (the exponent is instead  $m \simeq 1$  for the marginal distribution of  $\text{Re} G_{ii}$ ).

This implies that for large enough  $\eta$  the tails of  $\tilde{Q}_I(\ln \Im G)$  give a  $O(1)$  contribution to the density of states, whereas the bulk part gives a contribution of  $O(\eta)$ , as if the system was non-ergodic.

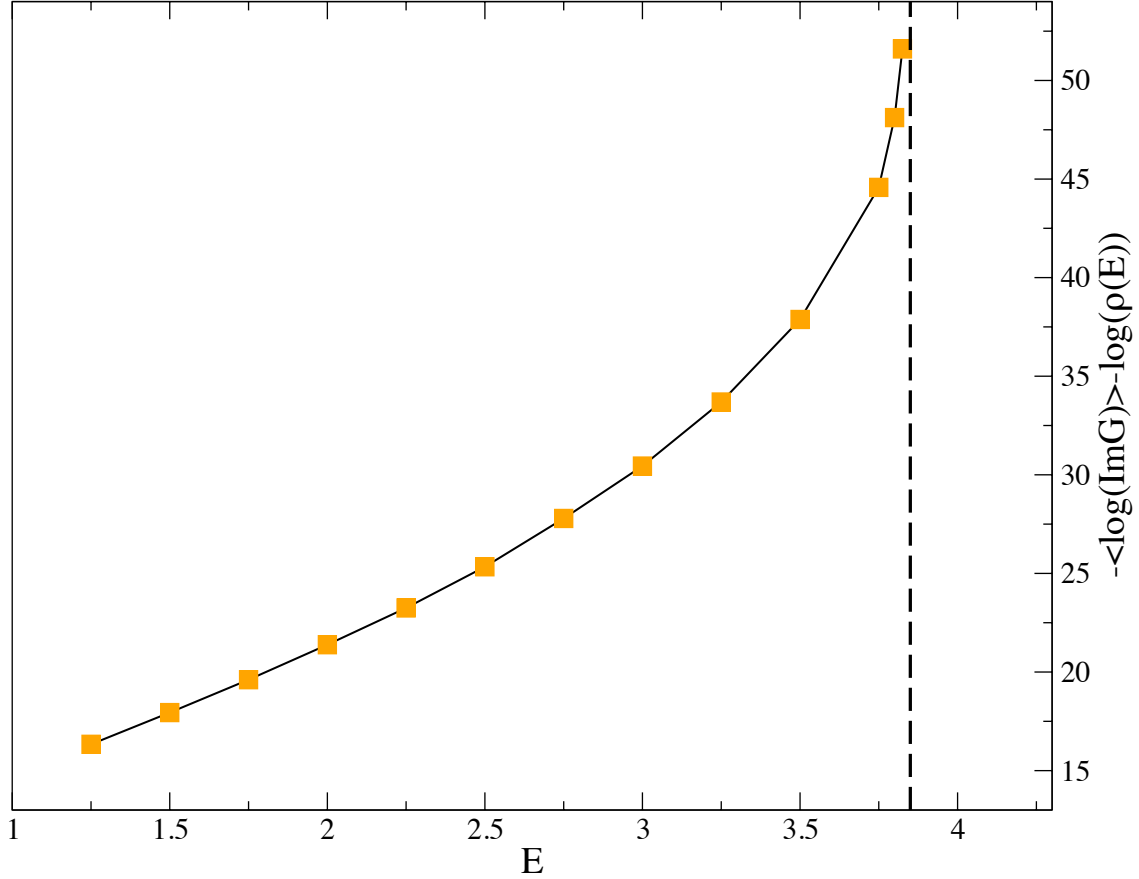


Figure III.14:  $\log N'_m(E) = -\log(\Im G_{ii}^{\text{typ}} \rho(E)) = -\langle \log \Im G_{ii} \rangle - \log(\langle \Im G \rangle / \pi)$  as a function of  $E$  for  $\mu = 0.5$ .

### III.10.2 Wavefunction statistics and multifractal spectrum

We show in this section the results for the probability distribution of the eigenfunction components for  $\mu \in (0, 1)$ . In figure (III.19) the scaled distribution  $\Xi(Nw)/N$  is plotted for different system sizes and  $\mu = 0.5$ , for the energy  $E = 0.016$ , in the delocalized phase. Except for very small values of the weights  $w$ , the curves scaled as  $\Xi(Nw)/N$  collapse to a unique curve. From the data we can clearly distinguish two regimes: for small values of  $Nw$  we have a power-like behavior which corresponds to the limit  $x \rightarrow 0$  of the Porter-Thomas distribution (III.9.2). For values of  $Nw$  larger but still smaller than one, the behavior of the distribution appears instead to be still power-like, but with an exponent different from  $1/2$ , and whose estimation with a fit is compatible with the value  $(1 + \mu)/2$ . We see therefore that the wavefunction statistics in the deeply delocalized phase is significantly different from that in the GOE

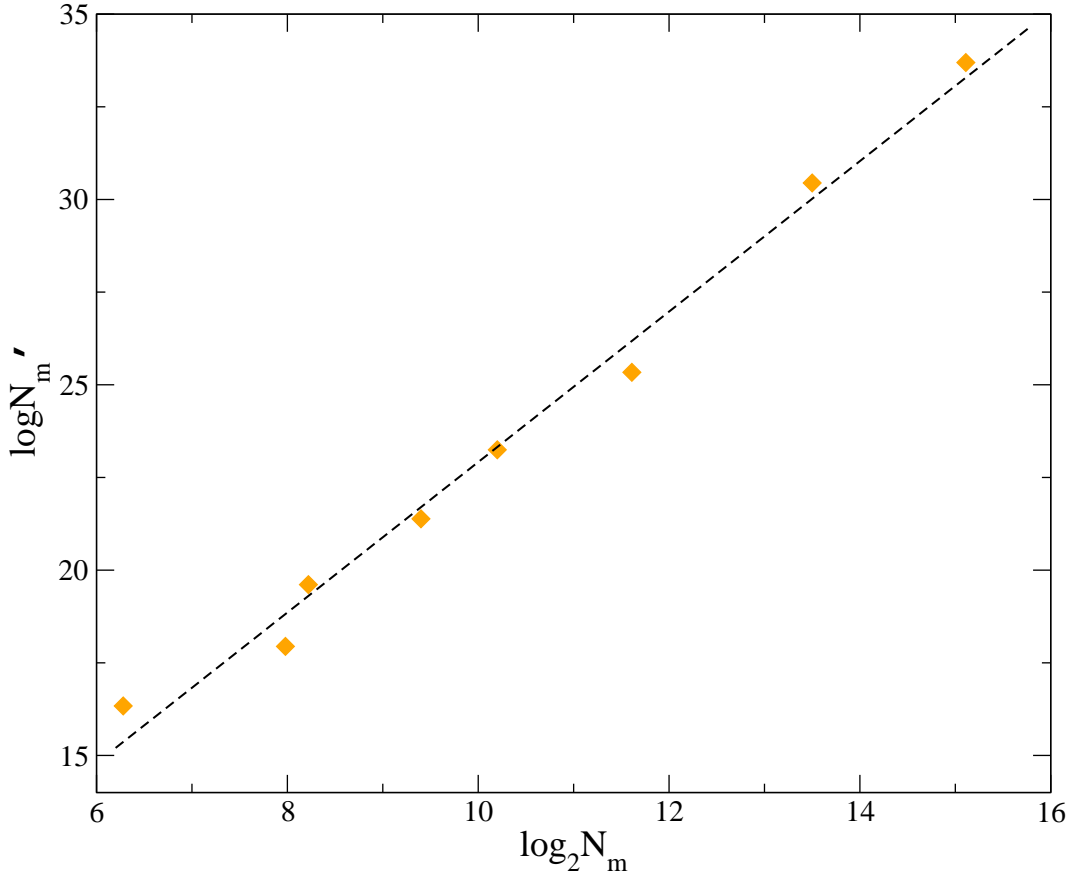


Figure III.15:  $\ln N'_m(E)$  as a function of  $\ln N_m(E)$ .

case: nonetheless, as we have seen in section (III.10) and shown in figure (III.10), the typical value of the overlap  $q^{typ}$  (III.9.1) in the delocalized phase converges for  $N$  sufficiently large to the GOE value  $2/\pi$ . As we have already remarked analyzing the case  $\mu \in (1, 2)$  this is quite surprising and we are still not able to justify this behavior. In figure (III.21) the distribution  $\Xi(Nw)/N$  is plotted for the energy  $E = 7.68$ , deeply in the localized phase. As we expect, the curves do not collapse to a unique curve, since the typical value of the weights deviate significantly from  $1/N$ . The curves exhibit power-law behaviors with three different exponents corresponding to three regime: for extremely small values of  $Nw$  we have the Porter-Thomas exponent  $1/2$ , for intermediate values of  $Nw$  we have the exponent  $(1+\mu)/2$ , and while the tails of the distribution are characterized by an exponent compatible with the value  $1 + (\mu/2)$ , the same as the exponent of the tails of the distribution  $Q(\Im G)$  in the localized phase showed in section (III.10.1). In the crossover region the distribution  $\Xi(Nw)/N$  presents the behavior shown in figure (III.20), corresponding to the energy  $E = 1.25$ : the curves present the GOE behavior corresponding to the Porter Thomas coefficient  $1/2$  in the region of very small weights, and the exponent  $(1+\mu)/2$  for intermediate values of  $Nw$ . The tails of distribution seem to exhibit a power-law behavior as in the localized phase for small sizes, but as  $N$  is increased we are not able any more to fit the curve with

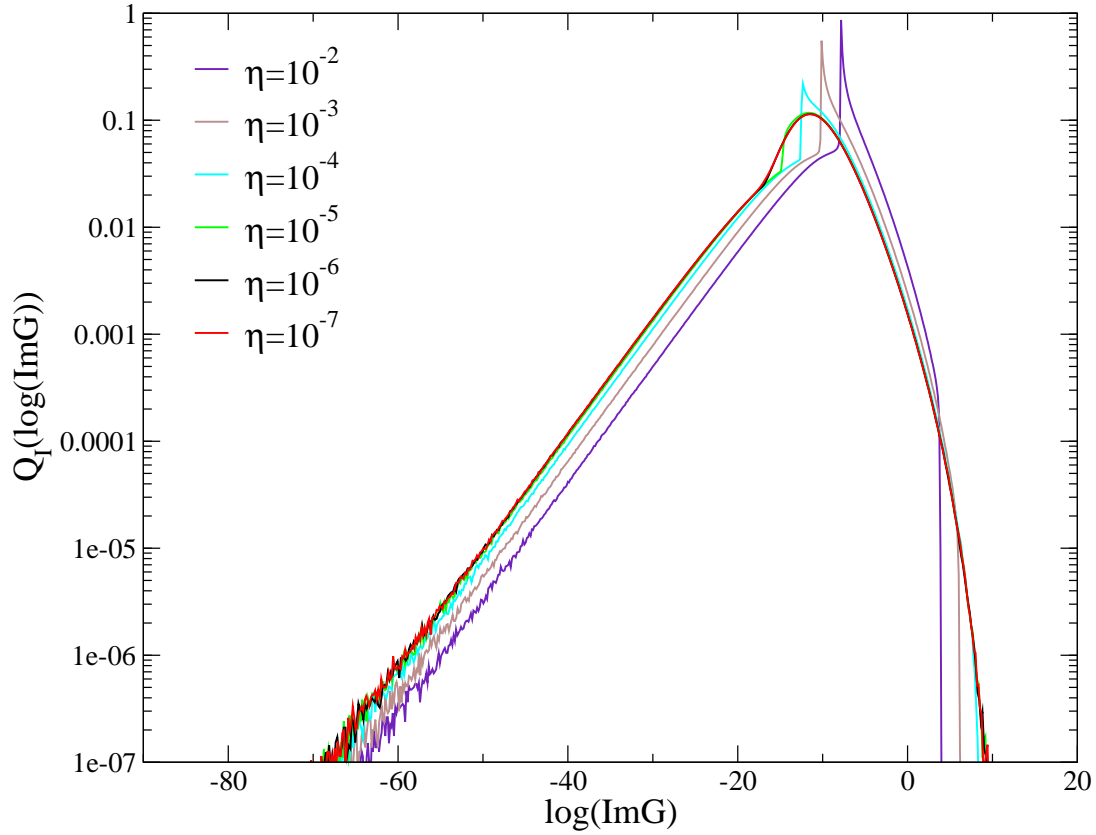


Figure III.16: Marginal probability distribution of  $\ln \Im G$  for different values of the imaginary regulator  $\eta$  and for  $E = 1.25$ , showing convergence to a stationary  $\eta$ -independent distribution for small enough  $\eta$ .

a power-law, indicating that the behavior is evolving towards the one characteristic of the delocalized phase, and we expect thus that for sufficiently large system sizes the curve collapse to an unique curve, even if with our data we do not see the full convergence.

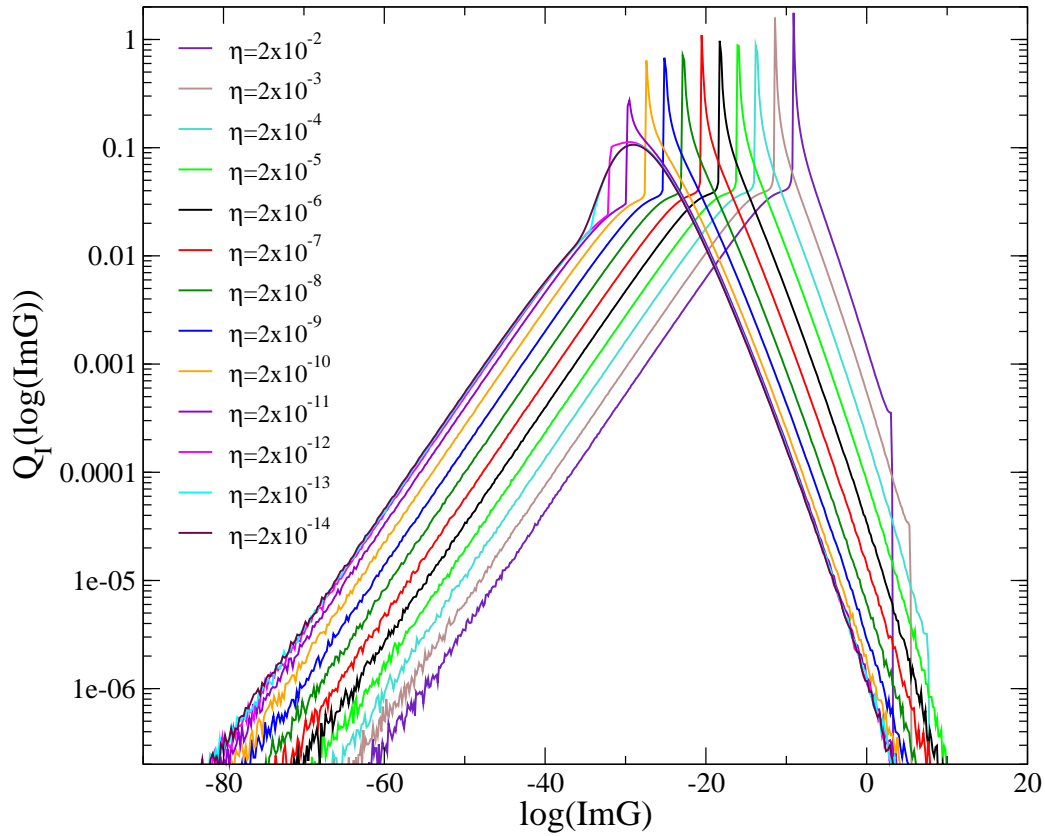


Figure III.17: Marginal probability distribution of  $\ln \Xi G$  for different values of the imaginary regulator  $\eta$  and for  $E = 5.5$ . In the localized phase the limit  $\eta \rightarrow 0^+$  is singular: almost all values of  $\Xi G_{ii}$  are of order  $\eta$ , except extremely rare events described by heavy power-law tails with an exponent  $1 + m = 3/2$  whose coefficient vanishes as  $\sqrt{\eta}$ .

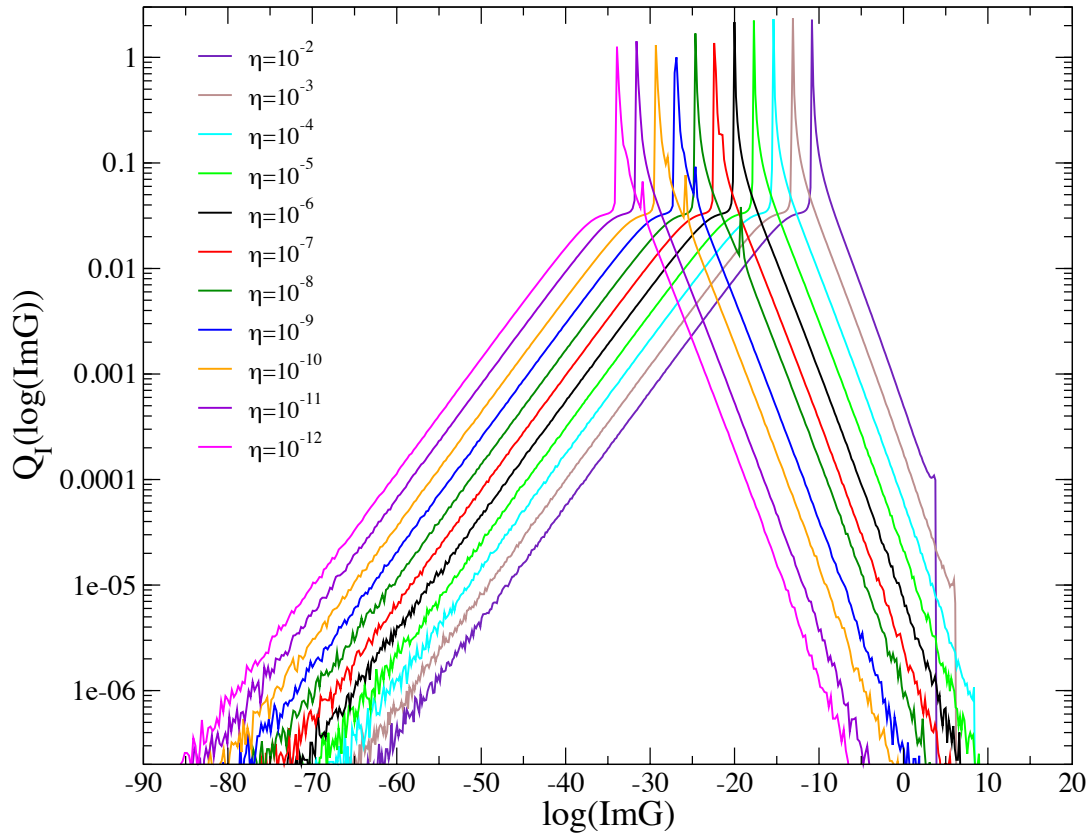


Figure III.18: Marginal probability distribution of  $\ln \Im G$  for different values of the imaginary regulator  $\eta$  and for  $E = 3.25$ , in the crossover phase. For  $\eta > 10^{-13}$  the system behaves as it was localized and non ergodic, showing “singular” power-law tails with an exponent  $1 + m$  with  $1/2 \lesssim m < 1$  and a cut-off in  $\Im G = 1/\eta$ . Convergence to a stationary non-singular distribution is achieved for  $\eta < 10^{-13}$ .

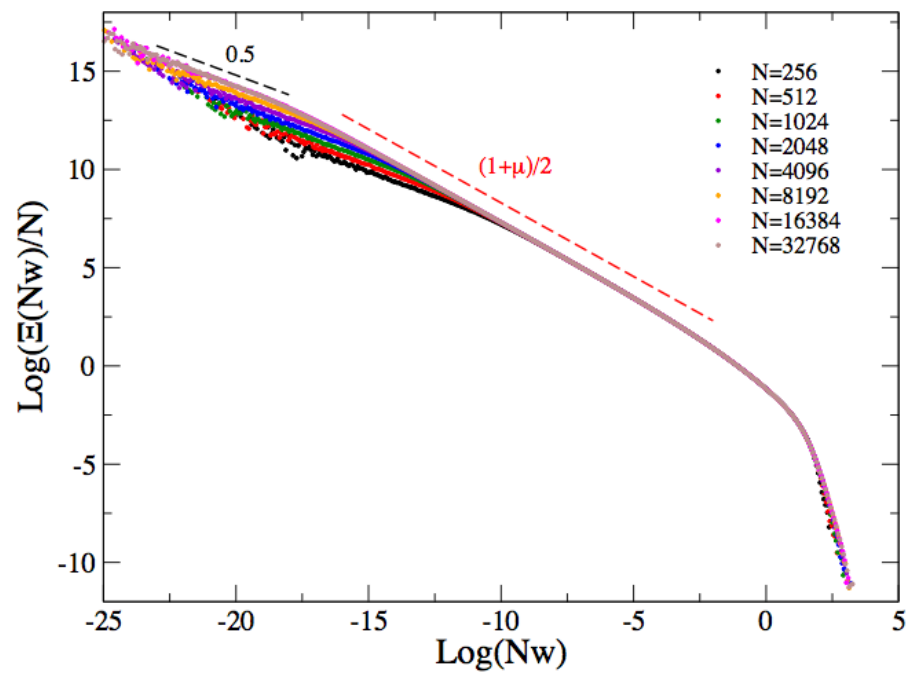


Figure III.19: Wavefunction statistics for  $\mu = 0.5$  for different system sizes and  $E = 0.016$ . For very small values of  $Nw$  the distribution has the power-law behavior with exponent  $1/2$  corresponding to the limit of small weights of the Porter-Thomas distribution. For larger  $Nw$ , until values of  $O(1)$ , the distribution still exhibits power-law behavior but with an exponent  $(1 + \mu)/2$ .

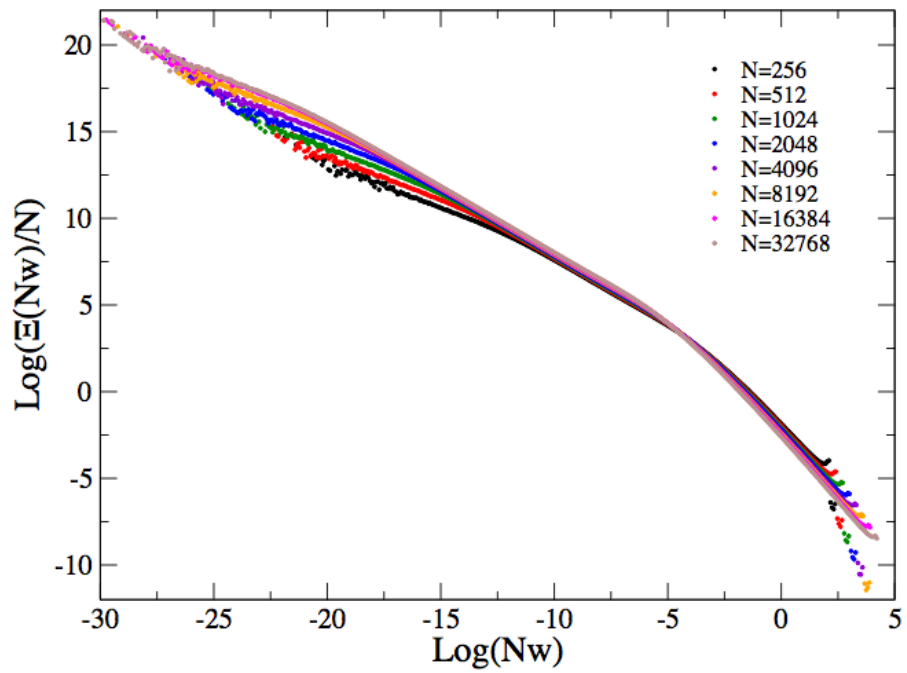


Figure III.20: Wavefunction statistics for  $\mu = 0.5$  in the crossover region ( $E = 1.25$ ) for different system sizes: the limit of small weights coincides with the one of the Porter-Thomas distribution. For intermediate value of  $Nw$  we have a power-law behavior with exponent  $(1 + \mu)/2$ , while the tails of the distribution seem to have a power-law shape as in the localized phase, but the fit get worse increasing the system size.

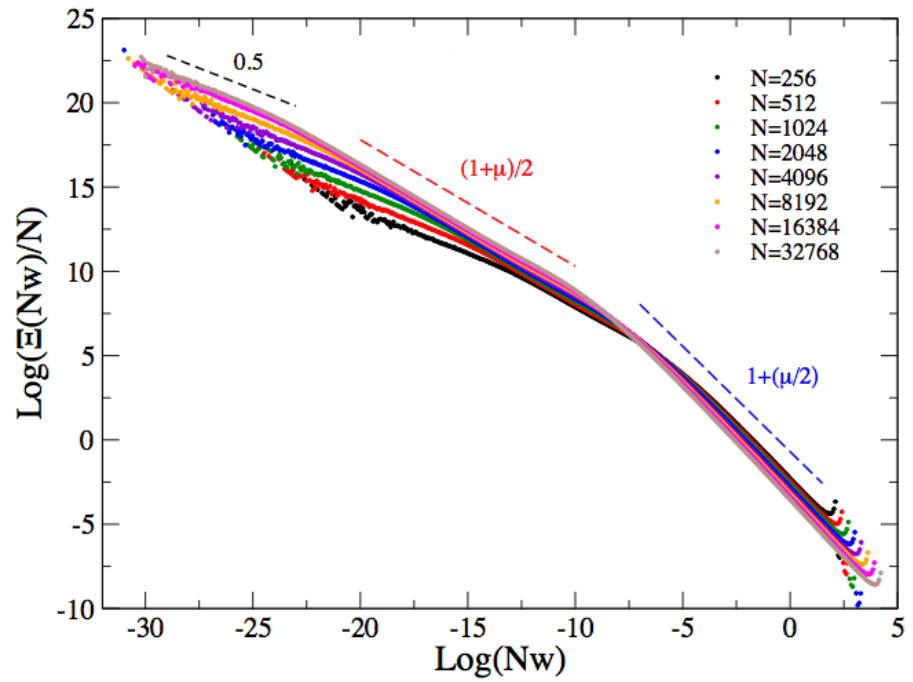


Figure III.21: Wavefunction statistics for different system sizes for  $\mu = 0.5$  in the deeply localized phase ( $E = 7.68$ ): the limit of extremely small weights is the same as that of the Porter Thomas distribution, with an exponent  $1/2$ . The regime of intermediate value of  $Nw$  is characterized by a power-law tail with an exponent  $(1 + \mu)/2$ , while the tails of the distribution also exhibit a power-like behavior with an exponent  $1 + (\mu/2)$ .

To conclude the numerical study in the range  $\mu \in (0, 1)$  we have computed the multifractal spectrum  $f(\alpha)$  (see Appendix (B)) for different energy windows in the delocalized regime, in the crossover region and in the localized phase. The results are shown in figure (III.22): we see that in the delocalized phase  $f(\alpha)$  becomes sharper increasing  $N$ , approaching for  $N \rightarrow \infty$  the behavior  $f(1) = 1$  and  $f(\alpha) = -\infty$ ,  $\alpha \neq 1$ . The top-right panel and the bottom left one of figure (III.22) show the behavior in the crossover region: apparently the curves seem to cross at a certain point  $\alpha_c < 1$ , which could be interpreted as a fixed point: the existence of such fixed point would exclude the possibility for the spectrum  $f(\alpha)$  to evolve towards a sharp function concentrated in  $\alpha = 1$  for increasing  $N$ , and thus to approach the ergodic behavior. However, analyzing carefully the data we see that the crossing point actually drifts with the system size. To characterize this drift we have considered for each size the point  $\alpha_1$  such that  $f(\alpha_1) = \alpha_1$ , and we have studied its behavior as a function of  $N$  for different energies in the crossover region. In the main panel of figure (III.23) we have plotted  $\alpha_1$  as a function of the (log of) the system size for  $E = 2.28$  (red curve), and we show in the same panel the behavior of  $q^{typ}$  (black curve). We see that, analogously to the overlap,  $\alpha_1$  is non monotonic with  $N$ , and in the same way as for the overlap, we see that the characteristic size  $N_m$  which can be found by looking at the minima of  $\alpha_1$  for the different energies, grows with  $E$  in the crossover region. In the inset of figure (III.23) we show the behavior of this characteristic length extracted by the analysis of  $\alpha_1$  as function of the energy, (red curve): the behavior is very similar to the one shown by the black curve, representing the characteristic length extracted from the analysis of  $q^{typ}$  (black curve), and we expect that the two curves diverge at the transition point  $E^* \simeq 3.85$ . These results on the fractal spectrum complete the numerical analysis of the model, and confirm the presence of a large crossover region characterized by strong finite size effects which affect the results already far from the critical point and for large system sizes.

### III.11 Summary of the results

We conclude this Chapter summarizing the main results we have obtained from the study of Lévy Matrices. The analysis of the stability of the imaginary part, starting from the cavity equations, yields the equation (III.4.15) for the mobility edge, the solution of which allows to trace the phase diagram of figure (III.2) in the  $\mu - E$  plane. Arguments based on the supersymmetric method (section (III.7)) and on the Dyson Brownian motion model (section (III.8)) support the idea that for  $1 < \mu < 2$  there is only one regime, in which eigenstates are delocalized and the system is ergodic, e.g. exhibits GOE statistics. For  $0 < \mu < 1$  there is only one transition line, separating delocalized ergodic states from localized non-ergodic ones. This picture, summarized by the phase diagram of figure (III.5), is confirmed by the numerical results of section (III.9) and (III.10). In the region  $0 < \mu < 1$  the system reveals however an interesting and non-conventional behavior: the data in a large region in the delocalized phase, even far from the critical point, are affected by dramatic finite size effect. Indeed, the characteristic length scale governing this finite size effects results to diverge faster than a power law, leading to a large crossover region in which the system behaves as if it

was in a mixed phase, delocalized but non-ergodic.

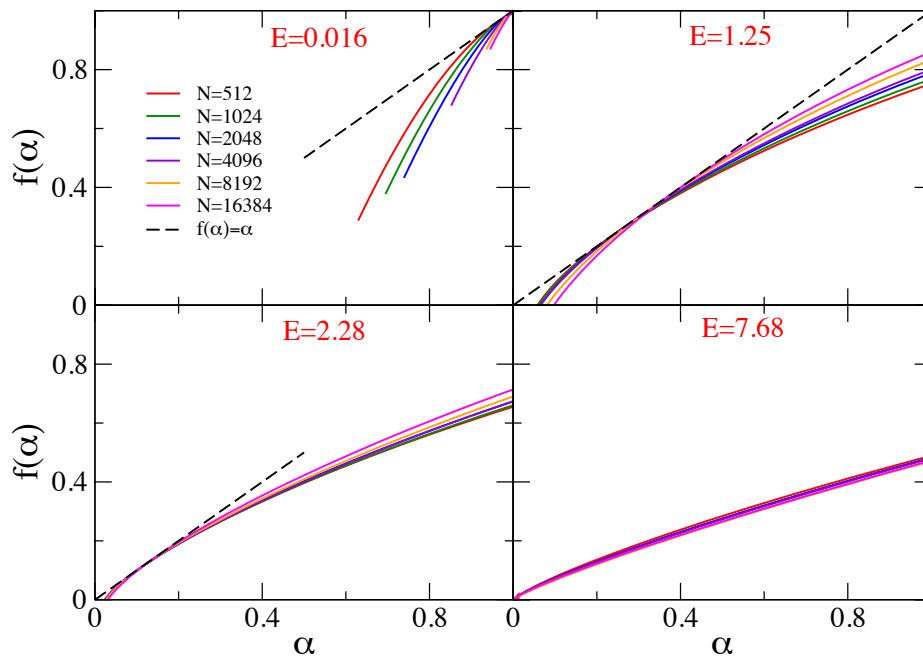


Figure III.22: Analysis of multifractal spectrum  $f(\alpha)$  for different energy and different system sizes. For small energies (top-left panel)  $f(\alpha)$  evolves towards a  $\delta$ -function concentrated in  $\alpha = 1$ . In the crossover region (top-right panel and bottom-left panel) the curves corresponding to different sizes cross at a point  $\alpha < 1$ , which however drifts with increasing  $N$ : this effect can be studied in a similar way as we have analyzed the behavior of  $q^{typ}$  and  $\langle r \rangle$ . In the deeply localized phase (bottom-right panel),  $f(\alpha)$  becomes broader and seems to converge to a  $N$ -independent distribution.

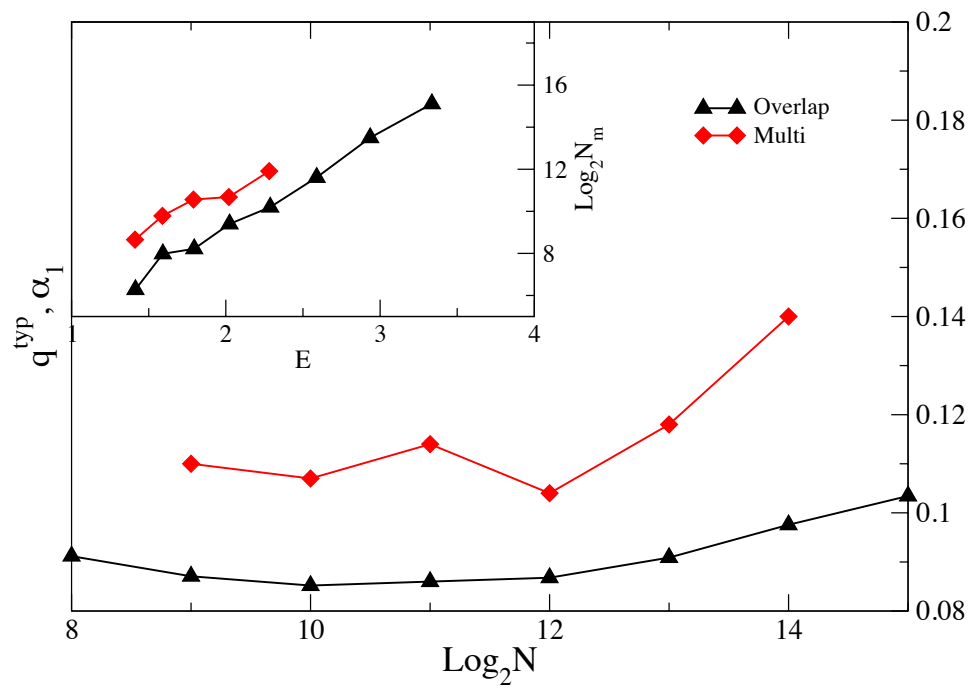


Figure III.23: Characteristic length extracted from the analysis of the multifractal spectrum  $f(\alpha)$  and compared with the characteristic length  $N_m$  obtained by the analysis of the overlap  $q^{typ}$ .



## Chapter IV

# Critical properties of the Anderson model in high dimension

As we have explained in the introductory Chapter (I) of this thesis, the properties of Anderson Localization in low dimensional systems are, by now, very well established and understood. Nonetheless, despite about 60 years of intense research, there is still (almost) no available analytical approach for Anderson Localization away from the low-dimensional limit and much less is known in higher dimensions.

One of the reasons for that is, as we have seen in section (I.9), the absence of a small parameter, since the critical disorder is of the same order than the bandwidth already in three dimensional systems. We have also seen that another reason for the difficulty in studying the properties of the transition in high dimension is the unconventional nature of the order parameter, which, as the supersymmetry method has clarified (see Chapter (II)), is a function related to the distribution of the local density of states, whose typical value is singular at the critical point.

Because of these unconventional properties, the analytical study of the problem is possible only perturbatively in a small region near the lower critical dimension  $d = 2$ , whereas analytical approaches in higher dimensions are challenging. Numerical techniques are thus still very important for advances in the field.

As we have explained in section (I.7), the majority of the numerical results has been provided for the Anderson model in three dimensions, which has been analyzed by many authors by studying the scaling of various observables for increasing system sizes. These quantity are related to transport properties, to the statistics of energy levels and to wave-functions statistics.

The summary of the main works has been presented in section (I.7): here we recall that for the Anderson Model (I.1.6) in three dimension, with box-distributed disorder (I.1.7), for  $E = 0$  (in the middle of the band) a localization transition is found at a critical value of the disorder  $W_c \simeq 16.5$ .

At present, the most precise numerical estimate of the critical exponent  $\nu$  describing the divergence of the localization length (I.2.3) for systems with orthogonal symmetry is  $\nu = 1.58 \pm 0.01$  [91, 92, 14, 15, 16, 17, 18, 19, 20, 21].

About the level statistics, the numerical results of Ref. [142], show that it is GOE-like in the delocalized phase and Poisson-like in the localized one. The critical point is

instead characterized by a universal distribution which depends on the dimensionality and which is neither GOE-like nor Poisson. The critical wave-functions amplitudes show a multifractal spectrum (see Appendix (B)), the critical eigenstates being neither extended nor localized at the transition: large fluctuations of wave-function amplitude are present at all length scales.

In  $4d$  and  $5d$  few recent accurate results have been provided [143], based on the study of transport properties only. There are however no results on transport properties above dimension five, and very few results on level statistics for  $d > 3$  [144].

As explained in section (I.7), the reason for that is that running times of numerical algorithms increase very rapidly with the size of the system, increasing as  $L^{3d}$  for exact diagonalization algorithms, and as  $L^{3d-2}$  for algorithms based on transfer matrix method. This sets a very severe limitation on the system sizes which can be simulated as dimensionality is increased.

For these reasons, some basic questions of Anderson Localization remain unanswered or debated, as discussed in section (I.9). For instance, the existence of an upper critical dimension  $d_u$  is still an issue. As we have seen in the end of section (II.3), the analysis based on the supersymmetric method suggests that  $d_u$  might be infinite [166, 167], and the same proposition has been done in Refs. [245, 144]. Different possibility corresponding to  $d_u = 4, 6,$  and  $8$  have instead been put forward in Refs. [169, 170, 171, 172, 173].

As we have seen in Chapter (I), another important and highly debated aspect is the relation with the infinite  $d$  limit, corresponding to Anderson Localization on tree-like structures [8] and to other random matrix models with long-range hopping, as Lévy matrices [183], studied in detail in Chapter (III). We have seen that on one hand, these models allow for an exact solution, making it possible to establish the transition point and the corresponding critical behavior. On the other hand, however, the properties of the delocalized phase are very unusual, since they are affected by dramatic finite-size effects even very far from the critical point, which produce a strong non-ergodic behavior in a crossover region where the correlation volume is larger than the accessible system sizes. We have seen the emergence of this behavior in the study of Lévy Random Matrices, but the same effect has been observed in the numerical study of localization on tree-like models [39, 41, 44, 43, 42, 46], and as we have seen, it has been interpreted by some authors [41, 44] in terms of the existence of a new intermediate delocalized but non-ergodic phase. This possibility would be very intriguing, although it appears to be in conflict with the predictions of the supersymmetric method formalism we have presented in section (II.3), and may have interesting consequences for the phenomenon of Many Body Localization, as explained in section (I.9.1).

This Chapter is dedicated to a detailed study of the critical properties of the Anderson model in dimensions from 3 to 6 based on “exact” numerical methods (exact diagonalizations and transfer matrix method) and on an approximate Strong Disorder Renormalization Group (SDRG) approach [246, 247]. We focus on both the statistics of energy levels and wave-functions coefficients and on transport properties.

We anticipate that our results support the idea that the upper critical dimension of Anderson Localization is infinite. In fact, the critical exponent  $\nu$  we find from our analysis smoothly evolves from  $\nu \rightarrow \infty$  in  $d = 2$  to the value  $\nu = 1/2$  in  $d \rightarrow \infty$  predicted by the supersymmetric method (see section (II.3)), showing no sign of

saturation. Moreover, the critical values of all observables smoothly approach the ones of the localized phase as the dimensionality is increased: Anderson Localization in high dimension seems to be governed by a strong disorder limit, as signaled by the fact that the critical values of all observables smoothly approach the ones of the localized phase as the dimensionality is increased: in  $d \rightarrow \infty$  the critical states correspond to an insulator, the statistics of energy levels is of Poisson type, and the multifractal spectrum of wave-functions amplitudes takes its strongest possible form. In support of this picture, as we have explained in section (I.4), the weak coupling limit seems to control only a very narrow region close to  $d = 2$  (even up to five-loops), contrary to the SDRG approach which gives much more accurate results in estimating the critical parameters in all dimensions  $d \geq 3$ .

We also show that finite size effects become larger and larger as the dimensionality of the system is increased. As a matter of fact, analyzing corrections to scaling, we find that they are proportional to  $L^y$ , with an exponent  $y$  which stays roughly constant as dimensionality is increased ( $y \simeq -1$ ). This implies that finite-size corrections decrease as the inverse linear system size (and not as the inverse of the volume, as in conventional phase transitions) yielding possibly logarithmic corrections in  $d \rightarrow \infty$ .

In this Chapter, we present our numerical results based on exact diagonalization and transfer matrix method for dimensions from 3 to 6. We discuss then the SDRG approach, focusing especially on the properties of the flow close to criticality, and we conclude with a brief summary of the results found and a discussion on the possible implications on the unusual properties of the delocalized phase observed in the Anderson model on tree-like structures.

## IV.1 Numerical results in $d = 3, \dots, 6$

The model we focus is the Anderson model (I.1.6), consisting in non-interacting spinless electrons in a disordered potential given by expression (I.1.7).

As observed in section (I.6), in terms of Random Matrix Theory, the model (I.1.6) can be thought as a sum of two matrices,  $H = H_0 + T^{(d)}$ :  $T^{(d)}$  is the deterministic off-diagonal part, proportional to the connectivity matrix  $C^{(d)}$  of the  $d$ -dimensional hyper-cube,  $C_{ij} = -1$  if sites  $i$  and  $j$  are connected and zero otherwise.  $H_0$  is a diagonal random matrix corresponding to the on-site energies,  $H_{0ij} = \epsilon_i \delta_{ij}$ .

In the following we will focus only on the middle of the spectrum,  $E = 0$ .

We present our numerical results in dimensions from 3 to 6 obtained from exact diagonalization and from a Transfer Matrix approach, focusing first on transport properties and then on the statistics of energy gaps and wave-functions amplitudes.

### IV.1.1 Transport properties

As mentioned in section (I.3), transport properties can be determined in one and quasi-one dimensional systems with the technique of Transfer Matrix, explained in Appendix (A). The approach we use here is very similar. We consider a very long (length  $L_x$ ) quasi-one dimensional bar of cross-section  $L^{d-1}$ , as sketched in figure (A.2) of Appendix (A). The system is open along the  $x$ -direction, while periodic boundary condition are enforced along the transverse directions. Such quasi-1d system is always

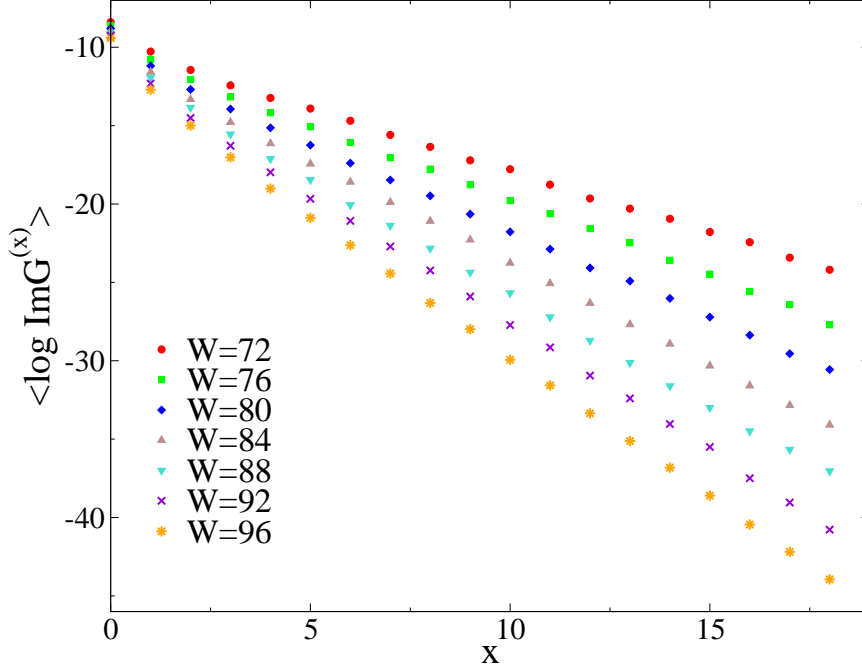


Figure IV.1:  $\langle \ln \text{Im} G(x) \rangle$  as a function of  $x$  in 6 dimensions, for  $L = 6$  and for several values of the disorder, showing that  $\xi_{1d}$  can be measured from Eq. (IV.1.4) by linear fitting of the data at large enough  $x$ .

localized at any arbitrarily weak value of the disorder. We consider now the resolvent matrix  $G$  defined by (II.1.2): we have seen that its matrix elements can be expressed in terms of a Gaussian integral over real auxiliary fields as in equation (II.2.1), which we rewrite in a more compact way as

$$G_{lm} = -\frac{i}{Z} \int \prod_{i=1}^N d\phi_i \phi_l \phi_m e^{S[\phi_i]}, \quad (\text{IV.1.1})$$

where the action  $S[\phi_i]$  is given by:

$$\begin{aligned} S[\phi_i] &= \frac{i}{2} \sum_{i,j=1}^N \phi_i (z\delta_{ij} - H_{ij}) \phi_j \\ &= \frac{i}{2} \sum_i (E + i\eta + \epsilon_i) \phi_i^2 + i \sum_{\langle i,j \rangle} t_{ij} \phi_i \phi_j, \end{aligned} \quad (\text{IV.1.2})$$

and the “partition function” reads:

$$Z = \int \prod_{i=1}^N d\phi_i e^{S[\phi_i]}. \quad (\text{IV.1.3})$$

We set  $E = 0$  throughout, which corresponds to the band center. We use now a slightly different approach than the classical Transfer Matrix technique: we put just the left

boundary of the quasi-1d bar of figure (A.2) in contact with a bath of electrons, and study how these electrons propagate through the sample. This corresponds to putting a finite positive value of  $\eta$  at  $x = 0$ , and setting  $\eta = 0$  elsewhere inside the bar,  $x > 0$ . Then, we can measure the quasi-1d localization length,  $\xi_{1d}$ , from the exponential decay of the typical value of the imaginary part of the Green's function,  $\exp\langle \ln \text{Im}G(x) \rangle$ , as a function of  $x$ , averaged over all the sites of the  $x$ -th layer and over several realizations of the disorder:

$$\langle \ln \text{Im}G(x) \rangle \simeq \text{cst} - \frac{x}{\xi_{1d}}. \quad (\text{IV.1.4})$$

Since equation (IV.1.2) is a Gaussian action, in order to compute the l.h.s. of equation (IV.1.4) we can proceed formally in the same way as in the derivation of the cavity equations in section (II.2), and we can integrate over all the sites on a given layer  $x$  in equation (IV.1.1), yielding an exact recursive relation expressing Green's function on the subsequent layer,  $x + 1$ , in terms of the Green's function on the layer  $x$ :

$$[G(x+1)]_{ij}^{-1} = \epsilon_{x,i} \delta_{ij} + t C_{ij}^{(d-1)} - t^2 G_{ij}(x), \quad (\text{IV.1.5})$$

where the index  $i$  runs over all the sites of layer  $x$ ,  $\epsilon_{x,i}$  is the random on-site energy on site  $i$  belonging to layer  $x$ , and  $C^{(d-1)}$  is the connectivity matrix of the transverse layers, i.e., the  $(d-1)$ -dimensional hyper-cube. This equation can be solved numerically by iteration, starting from the following initial condition at  $x = 0$ :

$$[G(0)]_{ij}^{-1} = (\epsilon_{0,i} + i\eta) \delta_{ij} + t C_{ij}^{(d-1)}. \quad (\text{IV.1.6})$$

In order to do this we need to invert the matrix  $G(x)$  layer by layer, which can be done by LU decomposition. Since the computer time required to perform this operation is proportional to the third power of the total number of sites of the matrix,  $L^{3(d-1)}$ , the running time of the TM algorithm scales as  $L^{3d-2}$ .

In order to measure  $\xi_{1d}$  we performed a linear fit of the data we have obtained for  $\langle \ln \text{Im}G(x) \rangle$  at large enough  $x$  using equation (IV.1.4). In figure (IV.1) we show the data obtained for  $\langle \ln \text{Im}G(x) \rangle$  as a function of  $x$  in 6 dimensions, for  $L = 6$  and for several values of the disorder  $W$ . In the localized regime, the quasi-1d localization length grows as the transverse system size is increased at a fixed value of the disorder, and saturates to the actual value of the localization length  $\xi$  for large enough  $L$ . Conversely, in the metallic phase  $\xi_{1d}$  diverges as  $L^{d-1}$  at fixed  $W$  for  $L \rightarrow \infty$ . Hence, the good scaling variable is the dimensionless quasi-1d localization length, defined as  $\lambda_{1d} = \xi_{1d}/L$ . This quantity is the inverse of the smallest positive Lyapunov exponent  $\gamma$ , and behaves as:

$$\lambda_{1d} = \begin{cases} (L/\xi)^{d-2} & \text{for } W < W_c \\ \lambda_c & \text{for } W = W_c \\ (\xi/L) & \text{for } W > W_c \end{cases}$$

The upper-left panels of figures (IV.2), (IV.3), and (IV.4) show the behavior of the log of the dimensionless quasi-1d localization length  $\lambda_{1d}$  as a function of  $W$  for several system sizes in dimensions 4, 5 and 6 respectively. As expected, for small values of the disorder  $\lambda_{1d}$  grows as  $L$  is increased, and decreases with  $L$  for large  $W$ . The curves corresponding to different  $L$  cross at the critical point for large enough system sizes. However, systematic finite size effects are present due to practical limitations

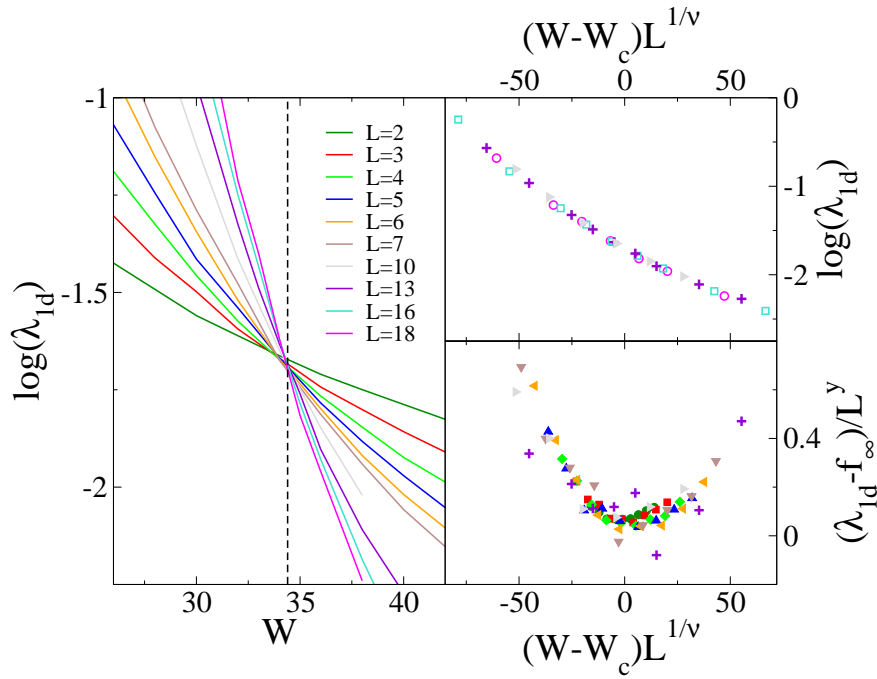


Figure IV.2: Left panel:  $\lambda_{1d}$  as a function of the disorder  $W$  for several system sizes  $L$  from 2 to 18 for  $d = 4$ . The vertical dashed line spots the position of the critical point,  $W_c \simeq 34.5$ . Top-right panel: Finite size scaling of the same data for  $L$  from 10 to 18, showing data collapse for  $\nu \simeq 1.11$ . Bottom-right panel:  $\psi f_1 = (\lambda_{1d} - f_\infty)/L^y$  as a function of the scaling variable  $(W - W_c)L^{1/\nu}$  for different sizes  $L$  from 2 to 7, showing data collapse for the same value as before of  $W_c$  and  $\nu$  and for  $y \simeq -1$ .

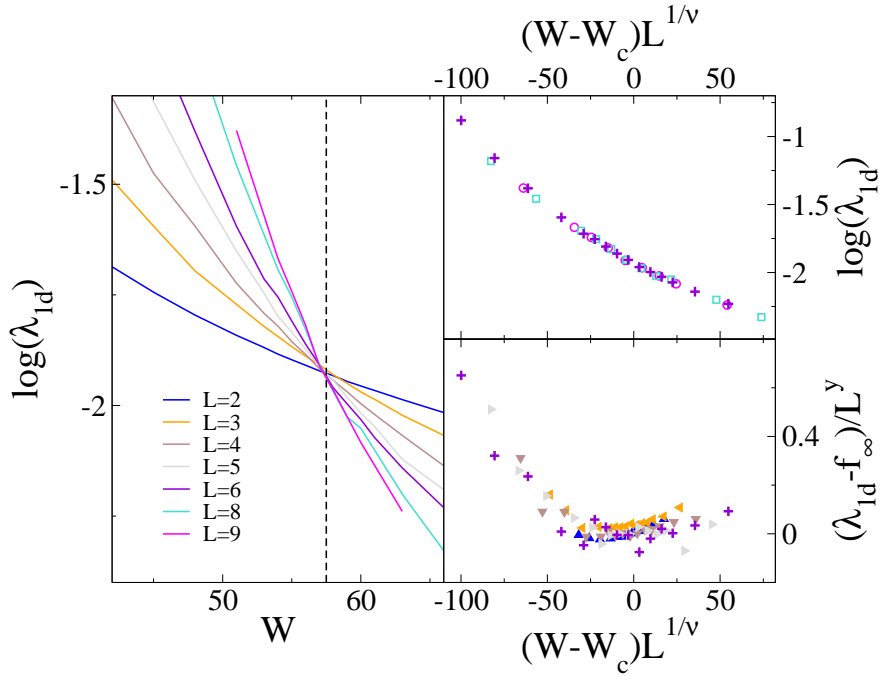


Figure IV.3: Left panel:  $\lambda_{1d}$  as a function of the disorder  $W$  for several system sizes  $L$  from 2 to 9 for  $d = 5$ . The vertical dashed line spots the position of the critical point,  $W_c \simeq 57.5$ . Top-right panel: Finite size scaling of the same data for  $L$  from 6 to 9, showing data collapse for  $\nu \simeq 0.96$ . Bottom-right panel:  $\psi f_1 = (\lambda_{1d} - f_\infty)/L^y$  as a function of the scaling variable  $(W - W_c)L^{1/\nu}$  for different sizes  $L$  from 2 to 6, showing data collapse for the same value as before of  $W_c$  and  $\nu$  and for  $y \simeq -1.2$ .

on the system sizes, and it is evident from the plots that the crossing point exhibits a shift as the size of the system is increased. In particular, in  $4d$  we observe a shift towards higher values of  $W$  of about 2.5% as  $L$  is increased from 2 to 18, while in  $5d$  it moves towards lower values of the disorder (again by about 2.5%) when  $L$  goes from 2 to 9. Finite size effects become very strong in  $6d$ , where the crossing point shifts systematically to lower values of  $W$  by about 10% when  $L$  varies from 2 to 6. We have thus a first indication of the fact that, differently from conventional phase transitions, for Anderson Localization finite size effects get more and more important as the dimensionality is increased.

If we want to accurately estimate the critical values of the disorder strength and of the critical exponent we have thus to take into account such finite size corrections. In order to do that we can introduce irrelevant scaling variables, and suppose that the observables become independent of such variables for sufficiently large system sizes. More precisely, we follow [92, 91, 143] and suppose that the dependence of  $\lambda_{1d}$  on  $W$  and  $L$  can be described in terms of a scaling function:

$$\lambda_{1d}(W, L) = F(wL^{1/\nu}, \psi L^y), \quad (\text{IV.1.7})$$

where  $w = (W - W_c)/W_c$  is the dimensionless distance from the critical point,  $\nu$  is the critical exponent,  $\psi$  is the leading irrelevant scaling variable, and  $y$  is the smallest (in absolute value) irrelevant critical exponent: consistently, we expect to find  $y < 0$  if  $\psi$  is irrelevant. For finite  $L$  there is no phase transition and  $F$  has not singularities. Hence, assuming that the irrelevant scaling variable is not dangerous, for  $L$  large enough we can expand Eq. (IV.1.7) up to first order in  $\psi L^y$ :

$$\lambda_{1d}(W, L) = f_\infty(wL^{1/\nu}) + \psi L^y f_1(wL^{1/\nu}), \quad (\text{IV.1.8})$$

where  $f_\infty$  is the asymptotic scaling function depending only on the relevant scaling variable. In order to estimate  $W_c$ ,  $\nu$  and  $y$  we then proceed in the following way: the first step is to approximately evaluate the function  $f_\infty$ , by performing a cubic fit of the numerical data for the largest available system sizes (in practice we use  $L = 18$  and 16 in  $d = 4$ ,  $L = 9$  and 8 in  $d = 5$ , and  $L = 6$  in  $d = 6$ ). The validity of this assumption must be verified *a posteriori*, once an estimation of the value the irrelevant exponent  $y$  and of the scaling function  $f_1$  are available. Plotting the difference between the numerical data for  $L < L_{\max}$  and the function  $f_\infty$ , divided by  $L^y$ ,  $(\lambda_{1d} - f_\infty)/L^y$ , as a function of the scaling variable  $(W - W_c)L^{1/\nu}$ , we can look for the values of  $W_c$ ,  $\nu$  and  $y$  that give the best data collapse of the curves corresponding to different values of  $L$  (see bottom-right panels of figures (IV.2), (IV.3), and (IV.4)). In this way we have an approximate estimation of  $(\psi \text{ times})$  the scaling function  $f_1$  (which can also be estimated performing a cubic fit). We then plot  $\lambda_{1d}$  as a function of  $(W - W_c)L^{1/\nu}$  for the largest sizes only, checking that our estimation of the critical parameters give a good data collapse (see top-right panels of figures (IV.2), (IV.3), and (IV.4)). Now we have an estimation for the scaling function  $\psi f_1$  and for the critical parameters  $W_c$ ,  $\nu$ , and  $y$ , and we can use it to iteratively improve the estimation of  $f_\infty$  originally obtained, by performing a cubic fit of  $\lambda_{1d}(W, L_{\max}) - \psi L_{\max}^y f_1(W, L_{\max})$ , which takes into account finite-size corrections also for the largest system sizes in a self-consistent way. The whole process can be repeated until it converges.

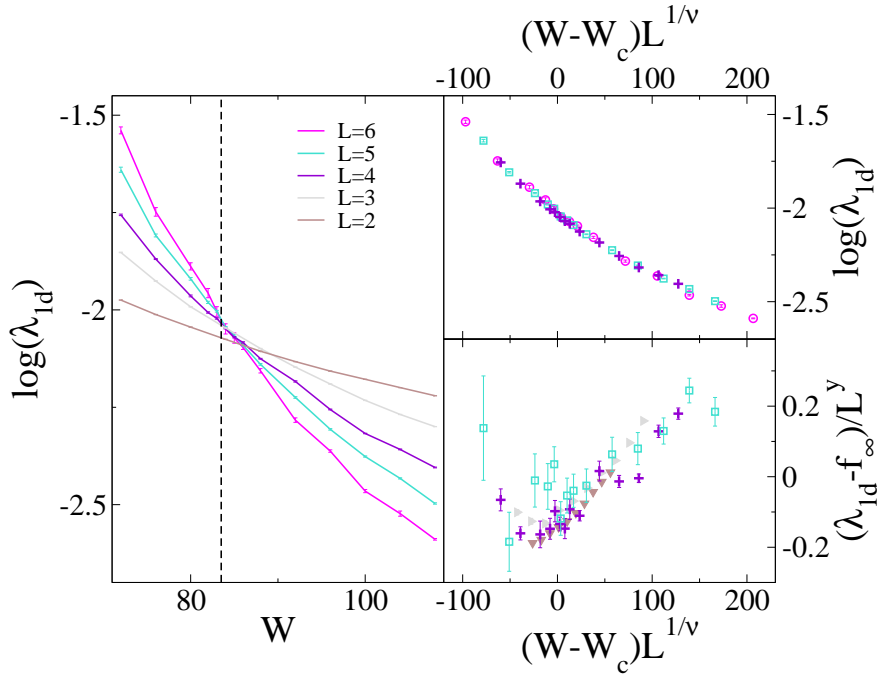


Figure IV.4: Left panel:  $\lambda_{1d}$  as a function of the disorder  $W$  for several system sizes  $L$  from 2 to 6 for  $d = 6$ . The vertical dashed line spots the position of the critical point,  $W_c \simeq 83.5$ . Top-right panel: Finite size scaling of the same data for  $L$  from 4, 5 and 6, showing data collapse for  $\nu \simeq 0.84$ . Bottom-right panel:  $\psi f_1 = (\lambda_{1d} - f_\infty)/L^y$  as a function of the scaling variable  $(W - W_c)L^{1/\nu}$  for different sizes  $L$  from 2 to 5, showing data collapse for the same value as before of  $W_c$  and  $\nu$  and for  $y \simeq -1.4$ .

This analysis yields the following values for the critical parameters:

$d = 4$	$d = 5$	$d = 6$	
$W_c = 34.5 \pm 0.2$	$W_c = 57.5 \pm 0.2$	$W_c = 83.5 \pm 0.4$	(IV.1.9)
$\nu = 1.11 \pm 0.05$	$\nu = 0.96 \pm 0.06$	$\nu = 0.84 \pm 0.07$	
$y = -1 \pm 0.1$	$y = -1.2 \pm 0.1$	$y = -1.4 \pm 0.2$	

The agreement of our results in  $4d$  and  $5d$  with the recent accurate estimations of [143] is excellent. Moreover, our analysis provides the first direct calculation of the critical parameters for Anderson Localization in six dimensions. We also applied this method in  $3d$  (not shown), yielding  $W_c = 16.35 \pm 0.1$ ,  $\nu = 1.57 \pm 0.02$ , and  $y = -1 \pm 0.1$ , in excellent agreement with [92, 91, 20, 21].<sup>1</sup>

As we have anticipated at the beginning of this Chapter, the leading irrelevant exponent  $y$  seems to be almost independent of the dimension of the system, at least up to 6 dimensions. Accordingly, finite size corrections for Anderson Localization should be proportional to the inverse of the linear size of the system, whereas in conventional phase transition they are proportional to the inverse of the volume  $N$  to some power dependent on the upper critical dimension. If this result which we observe for Anderson Localization up to dimension 6 holds also in higher dimension, it would mean that for a fixed value of  $N$ , finite size effects get worse with increasing  $d$ : the numerical study of Anderson Localization in dimension higher than 6 is then complicated not only by the limited system sizes accessible by the algorithms, but also by huge finite size effects. Moreover, if finite size corrections are proportional to  $L^{-1} = N^{-1/d}$ , in the limit  $d \rightarrow \infty$  they should become of order  $1/\log(N)$ : this may explain the anomalous behavior of the delocalized phase of the Anderson model on tree-like structures (or other related  $d \rightarrow \infty$  models like the Lévy model analyzed in Chapter (III)) in terms of huge finite size effects which would affect the data even for large system sizes.

#### IV.1.2 Statistics of level spacings and of wave-functions coefficients

In this section we present the result we have obtained through exact diagonalization of the Hamiltonian (I.1.6) for dimensions from 3 to 6, for several system sizes  $L$  (with periodic boundary conditions), and for several values of the disorder strength  $W$ . In particular we have analyzed the statistics of energy gaps and of wave-functions amplitudes. For each  $L$  and  $W$ , we have averaged over several realizations of the on-site quenched disorder. Since we are interested in  $E = 0$ , we only focused on 1/16 of the eigenstates centered around the middle of the band (we have checked that taking 1/32 or 1/64 of the states does not affect the results, but yields a poorer statistics). Since the running time required for exact diagonalization algorithms grows as the third power of the total number of sites of the matrix,  $L^{3d}$ , slightly smaller system sizes with respect to the Transfer Matrix method are accessible. For low enough dimensions, systems of large sizes can still be analyzed (e.g.,  $L_{\max} = 30$  for  $d = 3$  and  $L_{\max} = 13$  for  $d = 4$ ), whereas one is instead limited to very small sizes as dimensionality is increased

<sup>1</sup>Note, however, that in order for the assumption in (1) to be correct, one has to check self-consistently that  $\psi L_{\max}^y f_1(0) \ll f_\infty(0)$ . While this seems fully justified in  $d = 4$  and  $d = 5$ , it might be slightly less well grounded in  $d = 6$ . Hence, the critical disorder  $W_c$  and the absolute value of the exponent  $y$  might be overestimated in six dimensions.

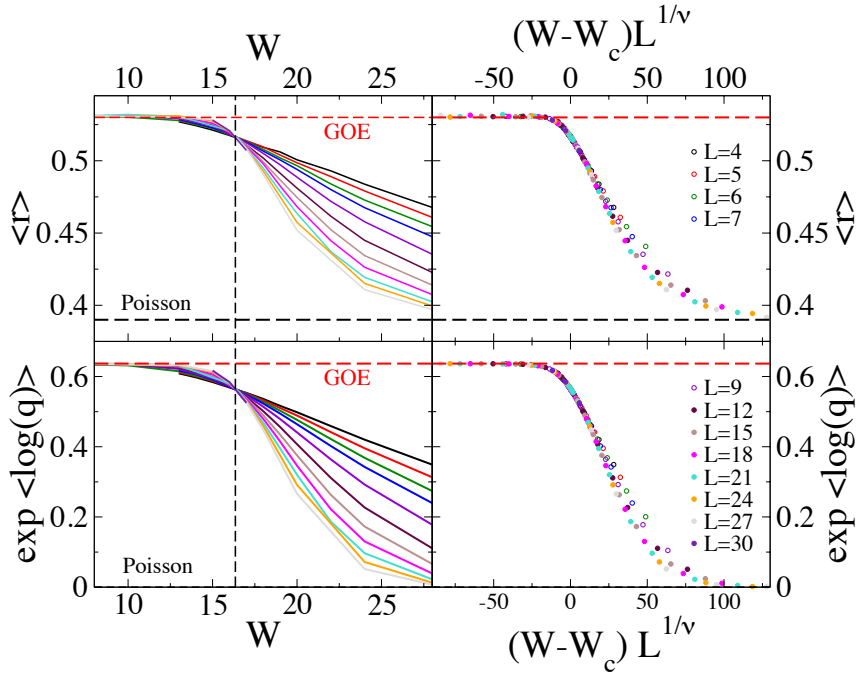


Figure IV.5:  $\langle r \rangle$  (top-left) and  $q^{typ}$  (bottom-left) as a function of the disorder  $W$  for several system sizes  $L$  from 4 to 30 for  $d = 3$ . The horizontal dashed lines correspond to the reference GOE and Poisson asymptotic values. The vertical dashed line spots the position of the Anderson Localization transition,  $W_c \simeq 16.35$ . Finite size scaling of the same data (top and bottom-right panels) showing data collapse obtained for  $\nu \simeq 1.57$ . Finite-size corrections to Eq. (IV.1.10) are observed at small sizes (open symbols), and can be described by Eq. (IV.1.8) with  $y \simeq -1$ .

( $L_{\max} = 8$  for  $d = 5$  and  $L_{\max} = 5$  for  $d = 6$ ). Exact diagonalization algorithms are however faster if one only computes the eigenvalues and *not* eigenvectors. For this reason, in  $d = 6$  we have been able to obtain some data for the statistics of energy gaps, for which the knowledge of the eigenfunctions is not necessary, also for  $L_{\max} = 6$ .

As in Chapter (III), in order to study the statistics of the spacings of neighboring eigenvalues we focused on the gap ratio  $\langle r \rangle$  (see definition (I.6.7)) and on the typical value of the overlap  $q^{\text{typ}}$  (III.9.1).

In the plots of figures (IV.5), (IV.6), and (IV.7) we show the behavior of these observables as a function of the disorder  $W$ , for several system sizes  $L$ , and for  $d = 3, 4, \text{ and } 5$  respectively. As expected, for small enough disorder we recover the universal GOE values  $\langle r_{\text{GOE}} \rangle \simeq 0.53$ , and  $q_{\text{GOE}}^{\text{typ}} = 2/\pi$ , while for large value of  $W$  we have the Poisson limit  $\langle r_{\text{P}} \rangle \simeq 0.39$  and  $q_{\text{P}}^{\text{typ}} \rightarrow 0$ . Data for different system sizes exhibit a crossing point around the critical points  $W_c$ , within our numerical accuracy, are in agreement with the ones obtained in the previous subsection from the analysis of the Lyapunov exponent, and with the ones reported in the literature [92, 91, 21, 20, 143]. One also finds that for large enough  $L$  the whole probability distribution  $\Pi(r)$  converges to its GOE and Poisson counterparts for  $W < W_c$  and  $W > W_c$  respectively. As shown in the right panels of figures (IV.5), (IV.6), and (IV.7), we see that for the largest accessible system sizes the dependence of  $\langle r \rangle$  and  $q^{\text{typ}}$  on  $W$  and  $L$  can be described in terms of the scaling functions:

$$\begin{aligned} \langle r(W, L) \rangle &= g_{\infty}(wL^{1/\nu}) , \\ q^{\text{typ}}(W, L) &= h_{\infty}(wL^{1/\nu}) , \end{aligned} \tag{IV.1.10}$$

with  $w = (W - W_c)/W_c$ . The values of  $\nu$  are consistent, within our numerical accuracy, with the ones estimated using the transfer matrix method in the previous subsection, and are in perfect agreement with [92, 91, 21, 20, 143]. For small system sizes there are evident finite size effects responsible for deviations from equation (IV.1.10): these effects can be described in terms of systematic corrections to the one-parameter scaling due to the presence of irrelevant scaling variables as explained above (see equation (IV.1.8)). It is possible to estimate the exponent  $y$  describing finite-size corrections to scaling for  $\langle r \rangle$  and  $q^{\text{typ}}$  in the same way as explained in the previous section for corrections to the dimensionless localization length  $\lambda_{1d}$ : the values of  $y$  found in this way are compatible, within our numerical precision, with the ones reported in table (IV.1.9), confirming that critical properties of level statistics and transport properties are described by the same sets of critical parameters.

As we have already seen in the previous subsection considering transport properties, finite size effects get stronger as dimensionality is increased, and this effect is even more visible when level statistics is considered. As it is clear from the left panel of figure (IV.8), where we show the behavior of  $\langle r \rangle$  as a function of the disorder strength  $W$ , for  $L$  from 2 to 6 in six dimensions, finite size effects are dramatic: the crossing point shifts towards smaller values of  $W$  from about  $W \sim 130$  to  $W \sim 86$  as  $L$  is increased from 2 to 6, and it has not converged yet to  $W_c$  even for the largest available system size. Considering this finite size effects and using the critical parameters estimated in section (IV.1.1) from the analysis of the Lyapunov exponent ( $W_c \simeq 83.5$ ,  $\nu \simeq 1.19$ , and  $y \simeq -1.5$ ), we are however able to obtain a reasonably good finite-size scaling. This

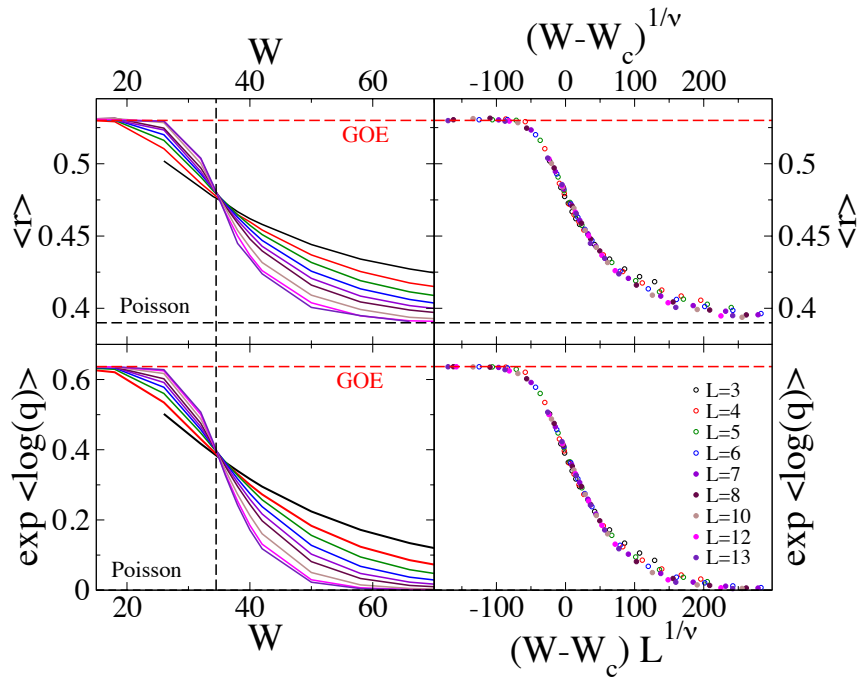


Figure IV.6:  $\langle r \rangle$  (top-left) and  $q^{typ}$  (bottom-left) as a function of the disorder  $W$  for several system sizes  $L$  from 3 to 13 for  $d = 4$ . The horizontal dashed lines correspond to the reference GOE and Poisson asymptotic values. The vertical dashed line spots the position of the Anderson Localization transition,  $W_c \simeq 34.5$ . Finite size scaling of the same data (top and bottom-right panels) showing data collapse obtained for  $\nu \simeq 1.11$ . Finite-size corrections to Eq. (IV.1.10) are observed at small sizes (open symbols), and can be described by Eq. (IV.1.8) with  $y \simeq -1$ .

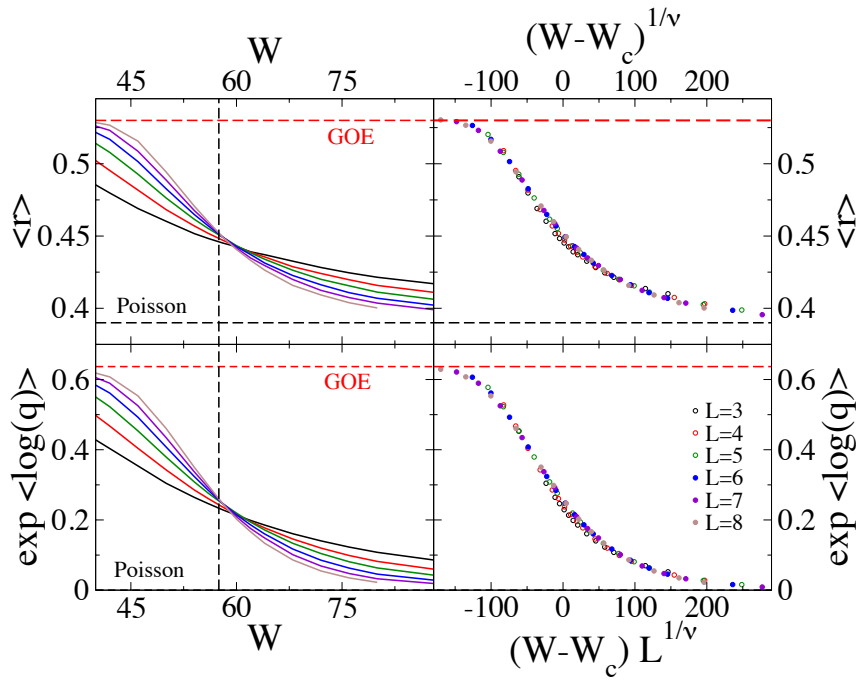


Figure IV.7:  $\langle r \rangle$  (top-left) and  $q^{typ}$  (bottom-left) as a function of the disorder  $W$  for several system sizes  $L$  from 3 to 8. The horizontal dashed lines correspond to the reference GOE and Poisson asymptotic values. The vertical dashed line spots the position of the Anderson Localization transition,  $W_c \simeq 57.5$  for  $d = 5$ . Finite size scaling of the same data (top and bottom-right panels) showing data collapse obtained for  $\nu \simeq 0.96$ . Finite-size corrections to Eq. (IV.1.10) are observed at small sizes (open symbols), and can be described by Eq. (IV.1.8) with  $y \simeq -1.2$ .

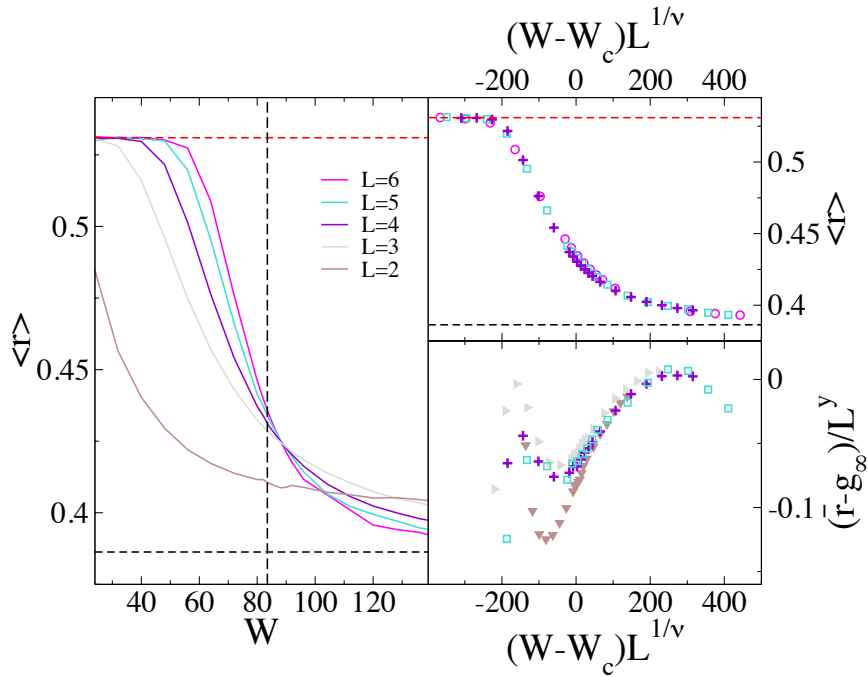


Figure IV.8: Left panel:  $\langle r \rangle$  as a function of the disorder  $W$  for several system sizes  $L$  from 2 to 6 for  $d = 6$ . The horizontal dashed lines correspond to the reference GOE and Poisson asymptotic values. The vertical dashed line spots the position of the Anderson Localization transition,  $W_c \simeq 83.5$ . Top-right panel: Finite size scaling of the same data for the largest system sizes only, showing data collapse for  $\nu \simeq 1.19$ . Bottom-right panel:  $\psi g_1 = (\langle r \rangle - g_\infty)/L^y$  as a function of the scaling variable  $(W - W_c)L^{1/\nu}$  for different sizes  $L$  from 2 to 5, showing a reasonably good data collapse for the same value as before of  $W_c$  and  $\nu$ , and for  $y \simeq -1.4$ .

is shown in the top-right and bottom-right panels of figure (IV.8), where the scaling functions  $g_\infty$  and ( $\psi$  times)  $g_1$  are found from the data collapse of the numerical data in terms of the scaling variables  $(W - W_c)L^{1/\nu}$ . Since analysis of  $q^{typ}$  requires the computation of the eigenvectors component of the Hamiltonian, for  $q^{typ}$  data are available up to  $L = 5$ , and we were therefore not able to repeat the same analysis for the overlap.

As we did in the study of Lévy Matrices in Chapter (III), we have considered the typical value of the IPR, defined as  $\exp\langle \ln \Upsilon_2 \rangle$ , for several values of the disorder strength and of the system size  $L$ , and for dimensions from 3 to 5 and we have analyzed the exponent  $\beta$ , approximated as

$$\beta = -\frac{(\ln \Upsilon_2^{typ}(W, L) - \ln \Upsilon_2^{typ}(W, L - 1))}{(\ln L - \ln(L - 1))}. \quad (\text{IV.1.11})$$

The numerical results for the exponent  $\beta$  as a function of  $W$  for several system sizes in four dimensions are shown in figure (IV.9): even if there are large statistical fluctuations, the behavior is similar to the one found for the statistics of energy gaps. For  $W < W_c$   $\beta$  grows with  $L$  and approaches 1 for  $L$  large enough, as we expect for fully delocalized wave-functions. Conversely, for  $W > W_c$  the exponent  $\beta$  decreases as the system size is increased, and tends towards 0 for large  $L$ , implying that  $\Upsilon_2^{typ} \rightarrow \text{const}$ , as expected for localized eigenstates. For the largest available sizes, the curves corresponding to different values of  $L$  cross approximately around  $W_c \simeq 34.5$ . Moreover, as remarked in Chapter (III), the IPR, and thus  $\beta$ , is affected by large finite size effects, and the numerical study of localization based on the analysis of this parameter solely could lead to wrong conclusions. However, if we use the same set of critical parameters found before ( $W_c \simeq 34.5$ ,  $\nu \simeq 1.11$ , and  $y \simeq -1$ ), and we use the data for the IPR as a check of our previous results, we find that the finite size scaling yields a reasonably good data collapse of numerical data, as shown in the right panel of figure (IV.9). Similar results are also found in dimensions 3 and 5. However, this analysis can not be performed in six dimensions, due to the fact that the IPR can be measured only up to  $L_{\text{max}} = 5$ , which is not sufficiently large to take care in an accurate way of the strong finite size effects.

## IV.2 Strong Disorder RG

In this section we present our results based on the Strong Disorder Renormalization Group (SDRG) approach for Anderson Localization recently introduced in [246, 247]. The SDRG is a real-space decimation procedure in which, iteratively, the strong energy scale in the Hamiltonian is individuated and integrated out.

The ideas behind this method reside in the seminal work of [248], and have been successfully applied to describe the critical and near-critical behavior of the Random Transverse-Field Ising model and other random magnetic transitions [249, 250, 251], and have also been recently used in electronic systems [252].

In the case in which the strongest energy scale happens to be the on-site energy  $|\epsilon_a|$  on site  $a$ , then site  $a$  is eliminated from the system, as sketched in the top panel of figure (IV.10): this means that one performs the Gaussian integral over  $\phi_a$  in equation

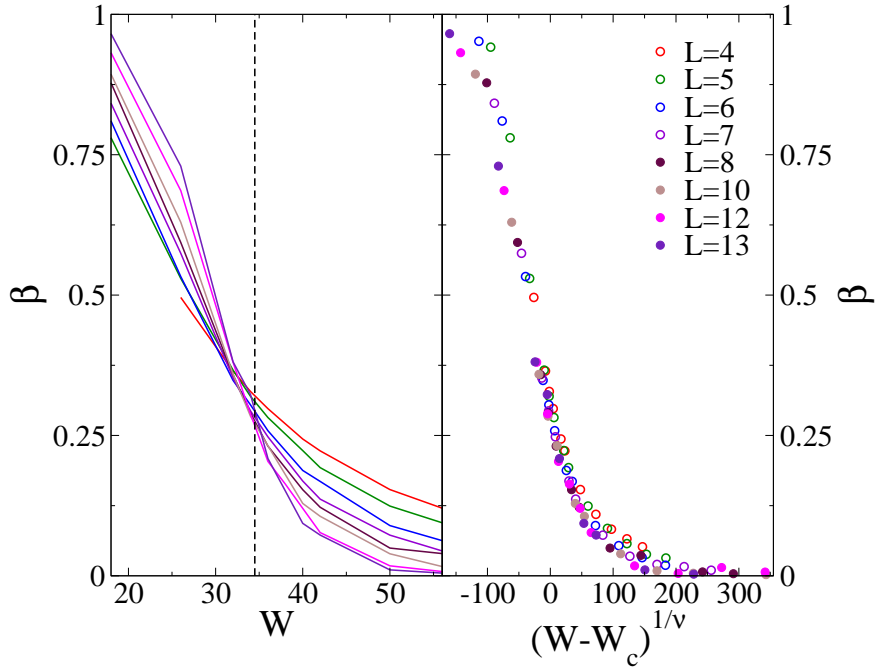


Figure IV.9: Left panel: Flowing fractal exponent  $\beta$  describing the scaling of the typical value of the IPR with the system size for  $d = 4$ . The vertical dashed black line corresponds to the critical disorder  $W_c \simeq 34.5$ . Right panel: Finite size scaling of the same data showing a reasonably good data collapse obtained for  $\nu \simeq 1.11$ . Strong finite-size corrections to the one-parameter scaling are observed at small sizes (open symbols), and can be described by Eq. (IV.1.8) with  $y \simeq -1$ .

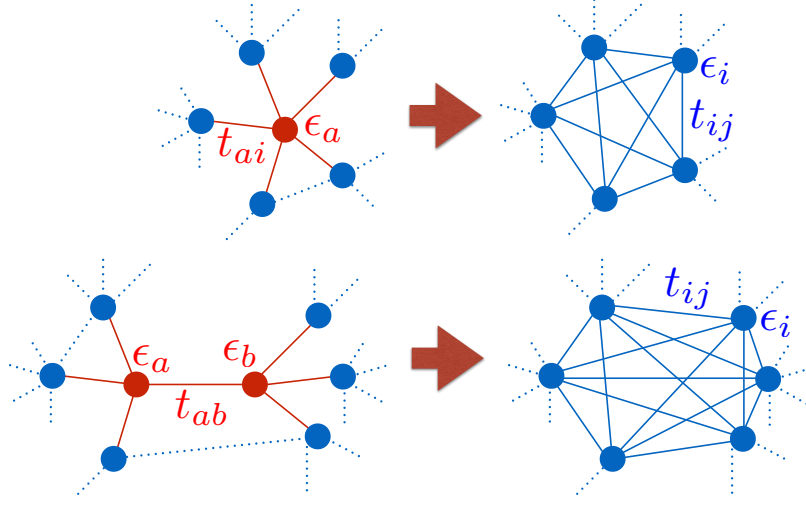


Figure IV.10: Sketch of the SDRG decimation procedure for a site (top), and a bond (bottom) transformation. Dotted blue lines represent pre-existing hopping amplitudes before decimation. Solid blue lines represent new or renormalized bonds. The on site energies of all the neighbors of the decimated sites (blue circles) are renormalized as well.

(IV.1.3), obtaining a RG transformation for the on-site energies on all the neighbors  $i$  of  $a$  and for the hopping amplitudes between all possible pairs of neighbors ( $ij$ ) of  $a$ :

$$\begin{aligned} \epsilon_i &\rightarrow \epsilon_i - \frac{t_{ai}^2}{\epsilon_a}, \\ t_{ij} &\rightarrow t_{ij} - \frac{t_{ai}t_{aj}}{\epsilon_a}. \end{aligned} \quad (\text{IV.2.1})$$

Similarly, if the strongest energy scale is the hopping amplitude  $|t_{ab}|$  between sites  $a$  and  $b$ , then sites  $a$  and  $b$  are eliminated, as sketched in the bottom panel of figure (IV.10), performing the Gaussian integrals over  $\phi_a$  and  $\phi_b$  in equation (IV.1.3) this yields the following RG transformation for the on-site energies on all the neighbors  $i$  of  $a$  and  $b$  and for the hopping amplitudes between all possible pairs of neighbors ( $ij$ ) of  $a$  and/or  $b$ :

$$\begin{aligned} \epsilon_i &\rightarrow \epsilon_i - \frac{\epsilon_a t_{bi}^2 - 2t_{ab}t_{ai}t_{bi} + \epsilon_b t_{ai}^2}{\epsilon_a \epsilon_b - t_{ab}^2}, \\ t_{ij} &\rightarrow t_{ij} - \frac{\epsilon_a t_{bi}t_{bj} - t_{ab}(t_{ai}t_{bj} + t_{aj}t_{bi}) + \epsilon_b t_{ai}t_{aj}}{\epsilon_a \epsilon_b - t_{ab}^2}. \end{aligned} \quad (\text{IV.2.2})$$

We note that equations. (IV.2.2) can be obtained using equation (IV.2.1) twice to eliminate first site  $a$  and then site  $b$ .

Equations. (IV.2.1) and (IV.2.2) are in fact exact RG transformations, as it was first shown in Ref. [253]. In  $d > 1$  however, since the procedure explained above

introduces new bounds, the number of non-zero matrix elements grows very rapidly under RG, making the numerical analysis unpractical. Several procedures have been proposed to solve this problem, which are also encountered in similar SDRG schemes for electronic systems [252] as well as for other disordered models such as random transverse-field Ising model [249, 250, 251]. Following Ref. [247] we set a maximum coordination number  $k_{\max}$  per site, throwing away most of the weak couplings. This procedure is justified if we think that, at least in high enough dimension, the critical properties of Anderson Localization are controlled by a strong disorder limit, as we have mentioned in section at the beginning of this Chapter, and the weak coupling constants generated under RG are in fact “irrelevant”.

In order to check whether or not this assumption is correct, it is important to analyze the accuracy of the results obtained with the SDRG and study their convergence with  $k_{\max}$ . In order to do this, we first focus on the average DOS, which can be written in terms of Gaussian integrals over auxiliary fields  $\phi_i$  as:

$$\begin{aligned} \rho &= -\frac{1}{\pi L^d} \text{Tr Im} G \\ &= \frac{1}{\pi L^d} \text{Im} \left[ i \int \prod_{i=1}^N d\phi_i \left( \sum_{l=1}^N \phi_l^2 \right) e^{S[\phi_i]} / Z \right], \end{aligned} \quad (\text{IV.2.3})$$

where  $Z$  is defined in Eq. (IV.1.3). The object  $\sum_{l=1}^N \phi_l^2$  is a function of all fields  $\phi_1, \dots, \phi_N$ . When a given site, say site  $a$ , is integrated out under RG, this object will become independent of  $\phi_a$ , but new terms dependent on products of fields of the form  $\phi_i \phi_j$  corresponding to all possible couple of neighbors  $(i, j)$  of  $a$  will appear, in addition to a constant. In order to compute the density of states by successive integrations under RG, we define thus the quadratic form  $\Gamma[\phi_i]$ , which is a function of all fields  $[\phi_i]$ :

$$\Gamma[\phi_i] = \sum_i \omega_i \phi_i^2 + \sum_{i<j} \sigma_{ij} \phi_i \phi_j + i\kappa. \quad (\text{IV.2.4})$$

At the level of the initial conditions one has that  $\omega_i = 1$  for all  $i$ ,  $\sigma_{ij} = 0$  for all  $(ij)$ , and  $\kappa = 0$ . Each time a site is integrated out, one has to renormalize the coefficients  $\omega_i$ ,  $\sigma_{ij}$  and  $\kappa$ . The renormalized values are found by Gaussian integration as follows:

$$\begin{aligned} \omega_i &\rightarrow \omega_i + \frac{\omega_a t_{ai}^2}{\epsilon_a^2} + \frac{t_{ai} \sigma_{ai}}{\epsilon_a}, \\ \sigma_{ij} &\rightarrow \sigma_{ij} + \frac{2\omega_a t_{ai} t_{aj}}{\epsilon_a^2} + \frac{t_{ai} \sigma_{aj} + t_{aj} \sigma_{ai}}{\epsilon_a}, \\ \kappa &\rightarrow \kappa + \frac{\omega_a}{\epsilon_a}. \end{aligned} \quad (\text{IV.2.5})$$

Similarly, when the hopping amplitude between sites  $a$  and  $b$  is eliminated, one can determine analogous RG relations for the coefficients of Eq. (IV.2.4). At the end of the RG, when all sites have been integrated out,  $\rho$  can be then obtained from Eq. (IV.2.3) as (minus) the imaginary part of the final value of  $\kappa$  divided by  $\pi L^d$ .

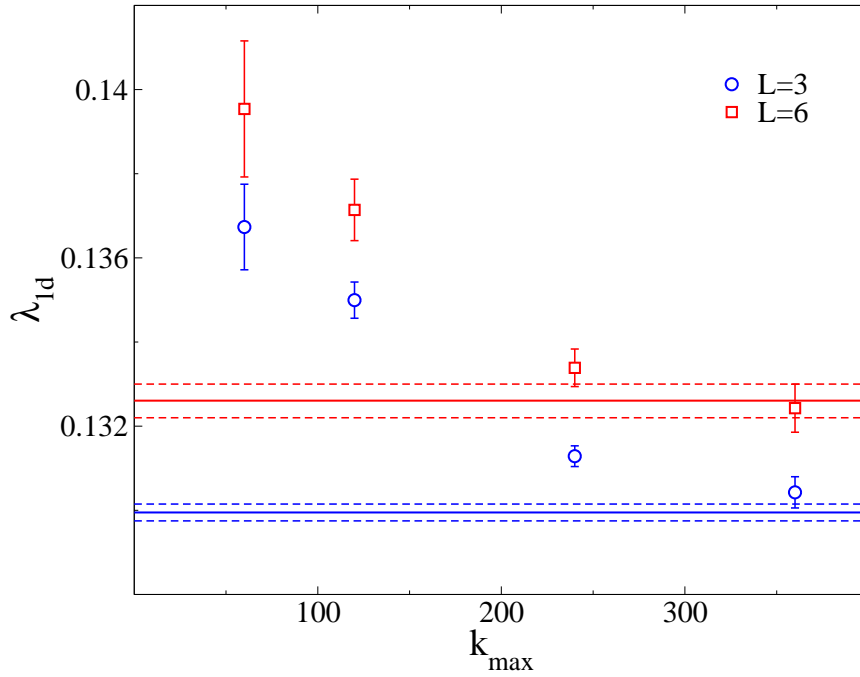


Figure IV.11: Quasi-1d dimensionless localization length,  $\lambda_{1d}$ , obtained using the SDRG procedure for different values of  $k_{\max}$ , at the Anderson Localization critical point,  $W_c \simeq 83.5$ , in 6 dimensions, and for  $L = 3$  (blue circles) and  $L = 6$  (red squares). The horizontal blue (resp., red) solid and dashed lines corresponds to the average value of  $\lambda_{1d}$  and its fluctuations computed using the transfer matrix method for  $L = 3$  (resp.,  $L = 6$ ), showing that for  $k_{\max} \gtrsim 240$  the approximate SDRG results converge, within our numerical accuracy, to the exact values.

We have computed the average DOS around the Anderson Localization critical points for dimensions from 3 to 6 using this method for several values of  $k_{\max}$ , and compared its numerical value with the one obtained from exact diagonalization, finding an excellent agreement even at small values of  $k_{\max}$ . In practice, already for  $k_{\max} \gtrsim 60$  the average DOS obtained via the SDRG coincides within error-bars and sample-by-sample with the one computed from exact diagonalization for all the accessible system sizes and in all dimensions.

We turn now to transport properties. In particular, in the following we compare the results for the dimensionless quasi-1d localization length computed from the Transfer Matrix approach as described in section (IV.1.1), with the ones obtained using the SDRG with different values of  $k_{\max}$ . More precisely, instead of solving equation (IV.1.5) exactly via LU decomposition, we apply the SDRG to invert the matrix  $[G(x)]^{-1}$  in an approximate way, starting from  $x = 0$ . In order to do this, on each layer  $x$  we integrate-out progressively all the sites using equations (IV.2.1) and (IV.2.2), eliminating iteratively the strongest energy scale, until no sites are left on that layer. In figure (IV.11) we plot the results for  $\lambda_{1d}$  at the Anderson Localization critical point in dimension 6 ( $W_c \simeq 83.5$ ) for different values of  $k_{\max}$  and for  $L = 3$  and 6, showing that for  $k_{\max} \gtrsim 240$  the numerical values of  $\lambda_{1d}$  obtained via the SDRG approach converge, within our numerical precision, with the ones obtained from exact techniques. Similar results are found in all dimensions down to  $d = 3$  (not shown).

This analysis shows that the results obtained using the SDRG approach both for the average DOS and the Lyapunov exponent converge already for reasonably small values of  $k_{\max}$  to the exact ones in all spatial dimensions, at least close enough to the Anderson Localization critical point.<sup>2</sup> Hence, the critical parameters found using the SDRG approach (for sufficiently large  $k_{\max}$ ) coincide, within error-bars, with the ones given in equation (IV.1.9). Since the computer time required for an efficient algorithmic implementation of the SDRG procedure scales as  $dL^d(\log L)k_{\max}^2(\log k_{\max})$ , one can in principle apply this method to obtain very accurate results for much larger system sizes compared with the exact numerical techniques such as exact diagonalization or Transfer Matrix. The SDRG can then also be applied to study Anderson Localization in dimensions larger than 6. Preliminary results in this direction have already been obtained in [247] up to  $d = 10$ .

In the last part of this section, we focus instead on the properties of the flow of the SDRG close to the Anderson Localization critical point. More precisely, we study the evolution under RG of the probability distributions of the diagonal and off-diagonal matrix elements,  $Q_\tau(\epsilon)$  and  $R_\tau(t)$  respectively (the index  $\tau$  corresponds to the RG “time”). Of course, these probability distributions do not contain all the important physical information on the system. For instance, they are insensitive to correlations between on-site energies and hopping amplitudes and/or spatial correlations between matrix elements which may be possibly generated during the flow. However, as we will discuss below, they can be still used to gather some important qualitative insights on the critical properties of Anderson Localization in high dimension.

In the following, for simplicity, we will restrict ourselves to the case of real matrix elements (i.e., we set  $\eta = 0$  on all the sites of the system). Similar results are obtained

<sup>2</sup>It is natural to expect that the accuracy of the SDRG gets worse at small disorder strength, deep into the metallic phase.

if one considers a finite (but small, e.g.  $\eta \sim 10/L^d$ ) imaginary regulator and study, for instance, the flow of the probability distributions of the modulus of diagonal and off-diagonal matrix elements. At the Anderson Localization critical point, the initial conditions for the probability distributions of on-site energies and hopping amplitudes are:

$$\begin{aligned} Q_{\tau=0}(\epsilon) &= \frac{1}{W_c} \theta\left(\frac{W_c}{2} - |\epsilon|\right), \\ R_{\tau=0}(t) &= \frac{2d}{N-1} \delta(t-1) + \frac{N-1-2d}{N-1} \delta(t). \end{aligned} \tag{IV.2.6}$$

The critical disorder  $W_c$  is much larger than 1 already in three dimensions—and it grows very fast as  $d$  is increased. As a consequence, at the beginning of the RG, the strongest energy scales are provided by the sites with on-site energies close to the edges of the support of  $Q_{\tau=0}(\epsilon)$ . As these sites are integrated out, new hopping amplitudes are generated, and the two  $\delta$ -peaks of  $R_{\tau=0}(t)$  acquire a finite support. Hence, as the RG time  $\tau$  grows,  $Q_{\tau}(\epsilon)$  shrinks and  $R_{\tau}(t)$  broadens. When the support of the two distributions become approximately the same, we observe a stationary state.<sup>3</sup> As  $\tau$  is further increased, the number of matrix elements left in the systems becomes very small and the stationary distribution is wiped out. However, this is a finite-size effect which could in principle be avoided taking larger and larger systems.

The stationary distributions  $Q_{\tau_*}(\epsilon)$  and  $R_{\tau_*}(t)$  at the AL critical points in dimensions from 3 to 6 are plotted in figure (IV.12). Despite the fact that the initial conditions are very different, we observe that  $Q_{\tau_*}(\epsilon)$  and  $R_{\tau_*}(t)$  are similar in all spatial dimensions. This suggests that the RG flow, and thus the critical properties of Anderson Localization are controlled by a fixed point which is very similar for all  $d \geq 3$ . As shown in the inset of figure (IV.12), the tails of  $R_{\tau_*}(t)$  seems to be described by a power law,  $R_{\tau_*}(t) \sim t^{-\gamma}$ , with an exponent  $\gamma \simeq 2$  which is also independent on  $d$ , and a cut-off for hopping amplitudes of  $O(1)$ . Note that as  $d$  is increased, the initial conditions (IV.2.6) get further and further from the quasi-stationary distributions. One needs then more and more RG steps to approach the quasi-stationary regime of the flow, i.e.,  $\tau_*$  increases as  $d$  grows. For this reason, finite size effects on  $Q_{\tau_*}(\epsilon)$  and  $R_{\tau_*}(t)$  also increase as  $d$  is increased since for  $\tau = \tau_*$  we are left with smaller systems and fewer matrix elements (see the caption of figure (IV.12) for more details).

These observations, together with the fact that the SDRG procedure gives very accurate results in all dimensions  $d \geq 3$  for reasonably small values of  $k_{\max}$ , provide a convincing indication of the fact that the properties of Anderson Localization in high dimensions are governed by a “strong disorder” fixed point, as already suggested in [42, 247]. This idea is also supported by the results of the supersymmetry approach for the critical properties of Anderson Localization on tree-like structures and infinite dimensional models [167, 166, 33]. It is natural to conjecture that for  $d \rightarrow \infty$  ( $W_c \rightarrow \infty$ ), and in the thermodynamic limit, the power law tails of  $R_{\tau_*}(t)$  might extend to infinitely large values of the hopping amplitudes.

---

<sup>3</sup>In practice, we observe that in all dimensions from 3 to 6 this happens when the support of the probability distributions of the diagonal and off-diagonal elements become of  $O(1)$ .

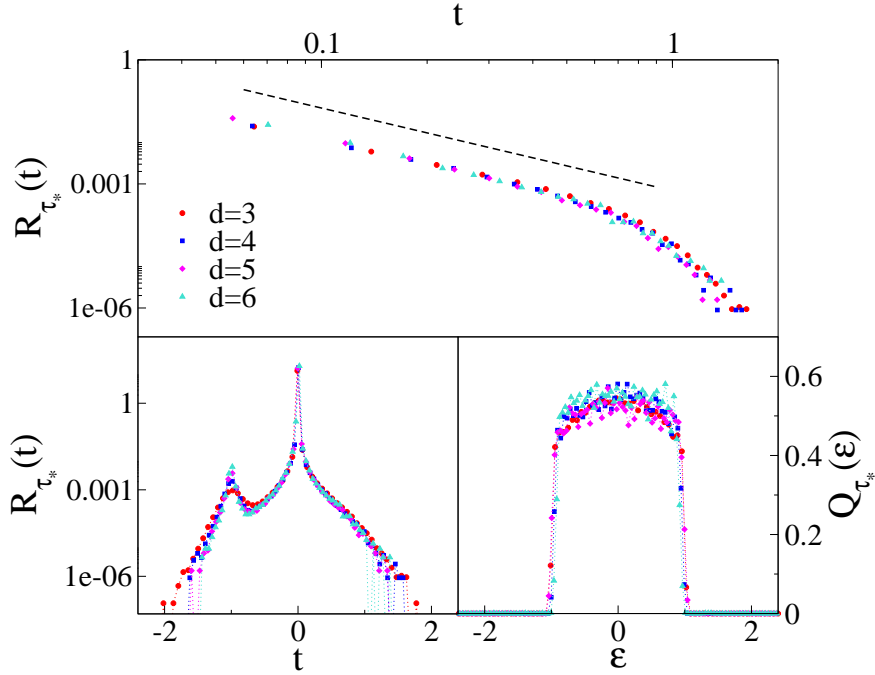


Figure IV.12: Bottom-left and bottom-right panels: The quasi-stationary distributions  $R_{\tau_*}(t)$  and  $Q_{\tau_*}(\epsilon)$  at the Anderson Localization critical points in dimensions from 3 to 6. The system size is  $L = 33$  in  $3d$ ,  $L = 14$  in  $4d$ ,  $L = 8$  in  $5d$ , and  $L = 6$  in  $6d$ , in such a way that the total number of sites is approximately the same,  $N \sim 4 \cdot 10^4$ , in all dimensions. The quasi-stationary state is reached for a RG time  $\tau_*$  such that the number of sites left in the system are approximately  $1/8$  of the initial ones in  $3d$ ,  $1/16$  in  $4d$ ,  $1/26$  in  $5d$ , and  $1/40$  in  $6d$ . The value of  $k_{\max}$  is set to 360 in all dimensions. Top-panel: The same data of the bottom-left panel plotted in a log-log scale, showing the power law behavior of  $R_{\tau_*}(t) \sim t^{-\gamma}$  with  $\gamma \simeq 2$  (black dashed line), for  $t$  smaller than a cut-off of  $O(1)$ .

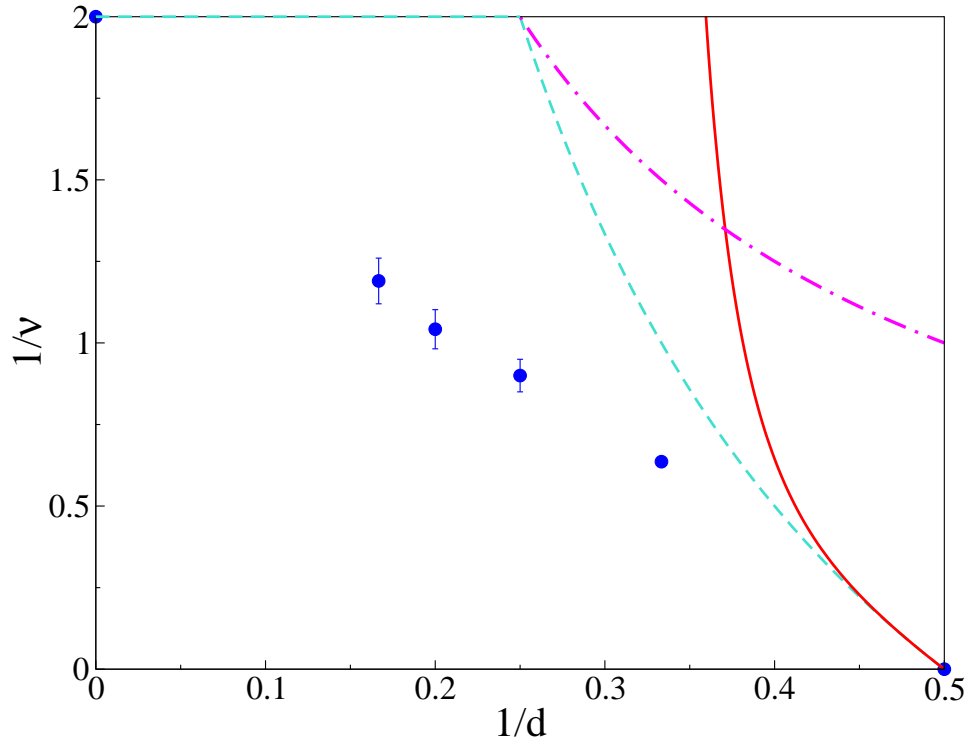


Figure IV.13: Numerical values of the inverse of the critical exponent  $\nu$  as a function of  $1/d$  in dimensions from 3 to 6 (blue circles), showing a smooth behavior interpolating from  $\nu \rightarrow \infty$  in  $d = 2$  to  $\nu = 1/2$  in  $d \rightarrow \infty$  [166]. The turquoise dashed line shows the predictions of the self-consistent theory of [174], with  $d_u = 4$ . The dashed-dotted magenta line corresponds to the lower bound  $\nu \geq 2/d$  provided by the Harris criterion [171]. The red solid line shows the dimensional dependence of  $\nu$  obtained from a perturbative analysis of the NL $\sigma$ M to five-loops in  $\epsilon = d - 2$  [88, 89], given by equation. (IV.3.1).

### IV.3 Summary of the results

In this section we summarize all the results we have obtained from the study of the Anderson model in  $d = 3, \dots, 6$  through both “exact” numerical techniques (exact diagonalization and transfer matrix method) and the SDRG approach. We start by focusing on the critical exponent  $\nu$ , whose behavior as a function of  $1/d$  is plotted in figure (IV.13). One clearly observes that  $\nu$  continuously decreases from  $\nu \rightarrow \infty$  in  $d = 2$  to the value  $\nu = 1/2$  in  $d \rightarrow \infty$  predicted by the supersymmetric method (see section (II.3)), showing no sign of saturation. This strongly indicates that the upper critical dimension of Anderson Localization is infinite, as already suggested in [166, 167, 144], in contrast with other propositions, as for instance, the one of the self-consistent theory [174], which predicts  $d_u = 4$  (turquoise dashed line). As explained in section (I.4), the perturbative analysis of the effective field theory based on the replicated NL $\sigma$ M has been carried to five-loops order in  $\epsilon = d - 2$  [88, 89], yielding for  $\nu$  the estimation:

$$\nu = \frac{1}{\epsilon} - \frac{9}{4}\zeta(3)\epsilon^2 + \frac{27}{16}\zeta(4)\epsilon^3 + O(\epsilon^4). \quad (\text{IV.3.1})$$

As already pointed out, the evaluations of critical properties based on the  $2 + \epsilon$  expansion yield a very poor agreement with the numerical results even in low dimensions, as shown in figure (IV.13), where the dimensional dependence of the critical exponent of equation (IV.3.1) corresponds to the solid red line. In fact, equation (IV.3.1) violates the lower bound  $\nu \geq 2/d$  based on the Harris criterion [171], represented by the dashed-dotted magenta curve already in  $3d$ . This implies that the weak disorder regime controls only a very narrow region in the vicinity of dimension 2, in contrast with the strong disorder approach based on the SDRG, which, as we have seen in the previous section, gives much more accurate results in estimating the critical properties of Anderson Localization in all dimensions  $d \geq 3$ .

As mentioned above, these observations suggest that the critical properties of Anderson Localization away from the lower critical dimension become closer to a strong disorder regime. This idea is fully confirmed by the analysis of the critical values and their dimensional dependence: in figure (IV.14) we plot  $\langle r_c \rangle$  (top-left panel),  $q_c^{typ}$  (bottom-left panel),  $(\lambda_{1d})_c$  (top-right panel), and  $\beta_c$  (bottom-right panel) as a function of  $1/d$ . In  $d = 2 + \epsilon$  dimensions the critical point corresponds to weak disorder (or, equivalently, weak coupling in terms of the NL $\sigma$ M), which means that the critical level statistics is close to the GOE one. With increasing  $d$  the critical point moves continuously towards strong disorder (strong coupling), and  $\langle r_c \rangle$  and  $q_c^{typ}$  approach the Poisson reference values, suggesting that the critical level statistics in the infinite dimensional limit is Poisson-like as in the localized phase. Similarly,  $\beta_c$  decreases as  $d$  is increased and seems to vanish in the  $d \rightarrow \infty$  limit, implying that the IPR has a finite limit at the Anderson Localization critical point in infinite dimensions, as predicted by the supersymmetric approach [182, 167] (see section (II.3)). Finally,  $(\lambda_{1d})_c$  is also a decreasing function of  $d$ , and smoothly approaches 0 for  $d \rightarrow \infty$ , showing that this picture of strongly localized critical point in infinite dimensions is supported also by the analysis of transport properties.

This extreme form of Anderson Localization criticality also manifests itself in the supersymmetric solution of tree-like models [182, 166], which reproduce properly the

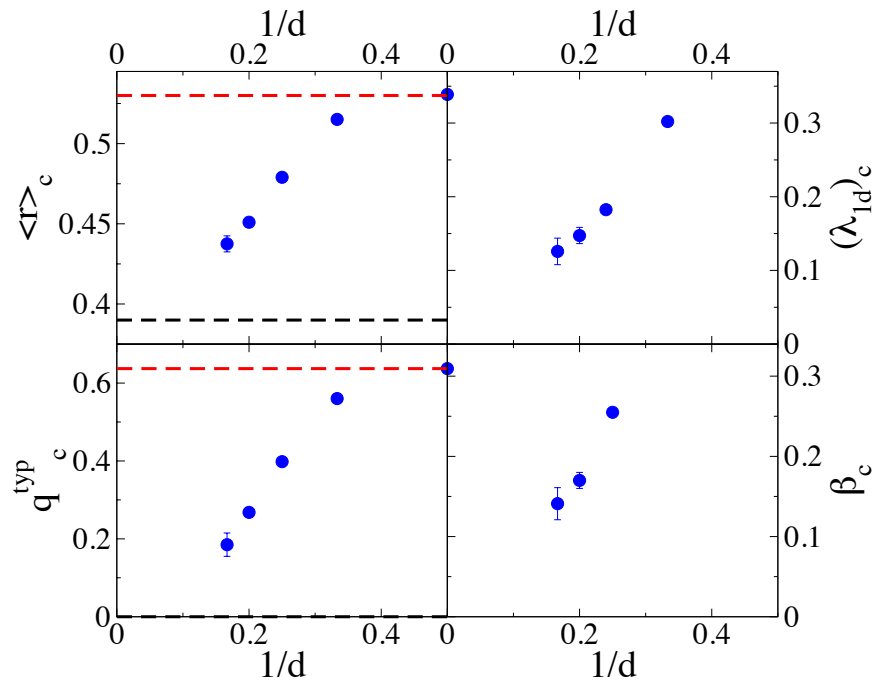


Figure IV.14: Dimensional dependence of  $\langle r_c \rangle$  (top-left panel),  $q_c^{typ}$  (bottom-left panel),  $(\lambda_{1d})_c$  (top-right panel), and  $\beta_c$  at the Anderson Localization critical point as a function of  $1/d$ . The dashed horizontal red lines correspond to the reference GOE value, while the dashed black one to the Poisson value.

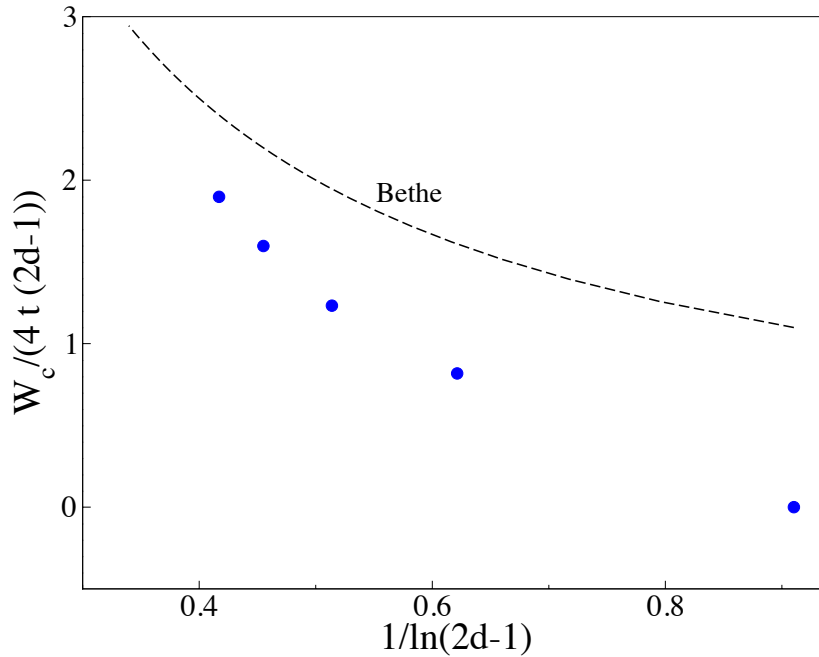


Figure IV.15: Critical value of the disorder strength,  $W_c$  divided by  $4(2d - 1)$ , as a function of  $1/\log(2d - 1)$ . The dashed black lines corresponds to the asymptotic exact behavior on tree-like structures in the large connectivity limit.

critical properties of infinite dimensional systems. In this respect, it is interesting to study the dimensional dependence of the critical value of the disorder strength  $W_c$ , plotted in figure (IV.15).  $W_c$  grows faster than  $d$  (which would be the natural scale set by the coordination number for conventional phase transitions) as the dimensionality is increased and seems to approach the behavior  $W_c/t \sim 4(2d - 1) \log(2d - 1)$  for large  $d$ , corresponding to equation (II.2.18) with  $k = 2d$ : this is the exact asymptotic behavior on tree-like structures in the large connectivity limit [8, 198].

We conclude this Chapter with the analysis of the dimensional dependence of the critical multifractal spectra of wave-function amplitudes (see Appendix (B)). From the exact diagonalization data we have evaluated the typical value of the exponent  $\tau(q)$  at the Anderson Localization critical point as [22, 24, 25]:

$$\tau_q^{typ} = -\frac{d \langle \log \Upsilon_q \rangle}{dL},$$

from which the spectrum of fractal dimensions  $f(\alpha)$  can be determined applying the Legendre transformation (B.0.5). Our numerical results in dimensions from 3 to 5 are plotted in figure (IV.16), showing that the (re-scaled) singularity spectrum of critical wave-functions broadens as  $d$  is increased and seems to approach the one correspondent to tree-like structures in the large  $d$  limit. These observations support once again the extreme form of Anderson Localization criticality in the  $d \rightarrow \infty$  limit, where the critical states correspond to an insulator, are described by Poisson statistics, and their multifractal spectrum takes its strongest possible form. Due to the limitations in

running times and memory of the algorithm of exact diagonalization, we didn't manage to obtain with sufficient accuracy the eigenfunctions statistics in  $d = 6$ .

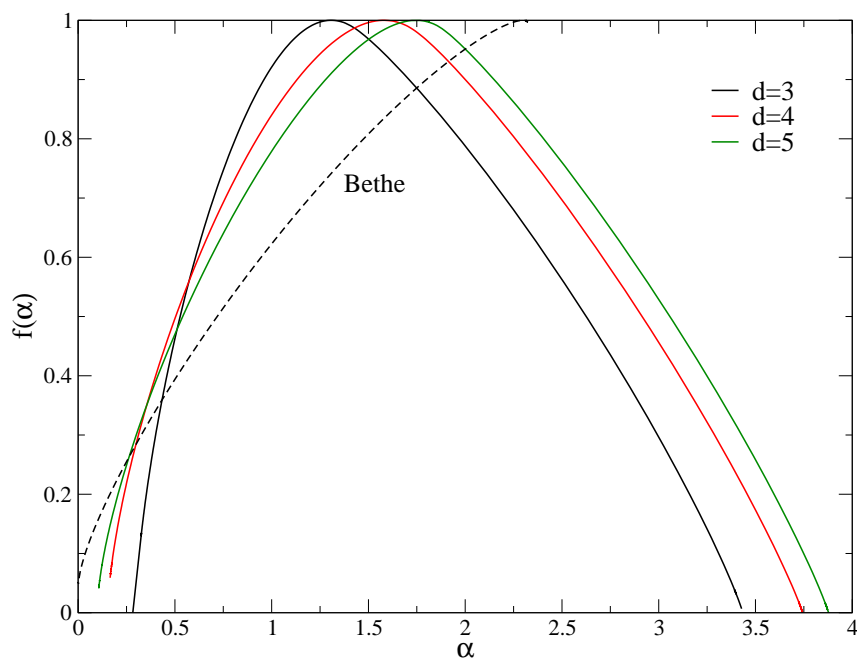


Figure IV.16: Re-scaled singularity spectrum  $f(\alpha)/d$  as a function of  $\alpha/d$  at the AL critical point in dimensions from 3 to 5. The dashed black line shows  $f(\alpha)$  obtained at the Anderson transition of the Anderson model on random regular graphs of connectivity 3.



# Conclusion and perspectives

In the first part of this thesis we have studied a random matrix model, the Lévy Matrices, early introduced in Ref. [38], which is known to present a localization-delocalization transition in the spectrum. The ensemble is constituted by random matrices with independently and identically distributed entries, characterized by a probability distribution with heavy-tails in  $1 + \mu$ , with  $\mu < 2$ . On one hand we have presented the interest of this model in the field of RMs, on a mathematical point of view, since the ensemble belongs to a more general universality class than the one usually considered by RMT. The properties and the rich behavior of this kind of matrices make it an interesting model in the study of Anderson Localization. It is indeed a fully connected analytically treatable model which exhibits a localization transition, and at the same time, due to the heavy-tail law of the distribution of the entries, presents a sparse-like character which relates it to Anderson Localization on tree-like structure, and thus to the limit of infinite dimensionality of the Anderson model.

First, starting from an exact recursion equation for the imaginary part of the resolvent already derived in [38] and rigorously proven in [227], we have obtained an exact equation for the mobility edge. The phase diagram found in the  $\mu - E$  plane presents a localization-delocalization transition in the region  $0 < \mu < 1$ , whereas for  $1 < \mu < 2$  all states in the spectrum are delocalized. This phase diagram has been checked with a semi-analytical method by solving the recursion equation for the probability distribution of the resolvent via a population dynamics algorithm. We have then investigated the problem of the existence of an intermediate delocalized non-ergodic phase in Lévy Matrices, already suggested in [38] and advocated for the Anderson model on tree-like structure. The application of the supersymmetric method to this ensemble of matrices, exactly in the same way as it was shown for sparse random matrices [31, 32, 33], allows to conclude that the delocalized phase is characterized by GOE statistics. In the region  $1 < \mu < 2$  we have also shown that the level statistics is GOE-like using an argument based on the Dyson Brownian motion approach: this result has not to be taken as a mathematical proof, but as a hint which can be useful for future more rigorous investigation.

We have then analyzed in detail, by exact diagonalization, the behavior of the system both in the region  $\mu \in (1, 2)$  and  $\mu \in (0, 1)$ . For  $1 < \mu < 2$  our numerical analysis of the level statistics, the Inverse Participation Ratio and the Support Set confirms the analytical result that the system is delocalized and ergodic. In particular, the analysis of the numerical data shows that the IPR is an observable affected by large finite size effects: this observation explains why in the early work of Ref. [38] the authors were led to interpret the behavior of their data as the sign of an intermediate

mixed phase, being the numerical analysis based mainly on the computation of the IPR. In the region  $\mu \in (0, 1)$  the system exhibits a richer behavior: through a careful analysis of the data we conclude that the localization and the level statistics transition coincide, but strong finite size effects characterize the delocalized phase even very far from the mobility edge. From the analysis of the properties of the distribution of the imaginary part of the resolvent we have interpreted these results by identifying a crossover scale which diverges at the mobility edge but is very large even far from the transition: the system behaves thus for practical purposes as if it was in an intermediate mixed phase, delocalized but non-ergodic. The analysis of the wave-function statistics and the multifractal spectrum are in agreement with the existence of a unique transition in the thermodynamic limit, and with the presence of a large crossover region in the delocalized phase.

In the second part of this work we have performed a detailed numerical study of the critical properties of the Anderson model in dimensions from 3 to 6, through exact diagonalization and transfer matrix techniques, and through a strong disorder renormalization group analysis, focusing both on the statistics of energy levels and wave-functions coefficients and on transport properties. Our results strongly support the hypothesis that the upper critical dimension of Anderson Localization is infinite. Indeed, the estimated values of the critical exponent  $\nu$  continuously decrease from  $\nu \rightarrow \infty$  in  $d = 2$  to the value  $\nu = 1/2$  in  $d \rightarrow \infty$  predicted by the supersymmetric approach [180] without showing any sign of saturation. The comparison with the values of  $\nu$  predicted by the perturbative renormalization group analysis of the NL $\sigma$ M in  $d = 2 + \epsilon$  shows that the weak disorder regime controls only a very small region near the lower critical dimension  $d_c = 2$ . From our analysis based on the strong disordered renormalization group approach we see instead that this approximation gives much more accurate results in estimating the critical properties of Anderson Localization for  $d \geq 3$ . This suggests that the critical behavior of Anderson Localization, except for a narrow region near  $d = 2$ , is governed by a strong disorder regime: this idea is supported by the analysis of the critical values of different observables, which move continuously towards strong disorder with increasing  $d$ : in particular, observables related to the level statistics move towards their Poisson limit, the exponent controlling the scaling of the IPR decreases and seems to approach 0 in the limit  $d \rightarrow \infty$ , and the quasi-one dimensional localization length obtained with the transfer matrix technique also decreases and smoothly approaches 0 for  $d \rightarrow \infty$ . We have also studied the behavior of finite size corrections in the scaling of the observables with the system size, finding that the leading irrelevant exponent describing this corrections is almost independent from the dimensionality, at least up to  $d = 6$ .

This results can have interesting implications on the unusual delocalized phase observed in models related to the  $d \rightarrow \infty$  limit, as the Anderson model on tree-like structures [39, 40, 41, 42, 43, 44, 45, 46] or, as we have seen in detail, Lévy Matrices [183], where the system manifests a strongly non-ergodic behavior on the delocalized phase when we look it on a scale lower than a characteristic crossover scale which is very large even far from the critical point. First of all we observe that, if the upper critical dimension of Anderson Localization is infinite, in the limit  $d \rightarrow \infty$  the system will have a finite-size scaling in terms of the variable  $w(\log N)^{1/2}$ , with  $\nu = 1/2$  (the value of the critical exponent predicted by the supersymmetric method

for Anderson model on tree-like structures). This implies that in order to explore system sizes larger than the correlation volume, exponentially large values of  $N$  would be required. Another important consequence of our results is that, since the critical point of Anderson Localization seems to be governed by a strong disorder regime, the critical values of the various observables correspond to the values they assume in the localized phase: therefore, the curves corresponding to different system sizes do not cross at a well-defined point. Increasing  $N$  the crossing point drifts instead towards the limiting value of the observable in the localized phase, justifying the non-monotonic behavior observed in the delocalized phase of Lévy Matrices and Anderson model on tree-like structures. Finally, since the leading irrelevant exponent governing finite size corrections seems to be almost independent of  $d$ , at least up to  $d = 6$ , finite size effects should depend on the system size as  $1/L$ , becoming more and more important with increasing dimensionality for fixed  $N$ . In the limit of infinite dimension they should be very large, depending on the size as  $1/\log N$ .

It would be interesting to apply the SDRG to higher dimensions (preliminary results are already available [247]), but also to implement an alternative strong disorder real space renormalization approach introduced for the family of the power-law random banded matrix ensembles [265], which may also be appropriate in the strong disorder limit.



# Appendix A

## Transfer Matrix, conductance and localization length

### A.1 Transfer Matrix and conductance

An important part of localization theory concentrates on the electron propagation, and interesting quantities as the conductance can be expressed in terms of the transmission and reflection amplitudes of the electron. Considering the scattering experiment in figure (A.1), where the sample is connected to semi-infinite ideal leads on both sides, we want to study the probability that an electron, coming from the left or the right side of the sample transfers to the opposite side. We define thus the scattering matrix  $\mathbf{S}$  as

$$\mathbf{S} = \begin{pmatrix} t^+ & r^- \\ r^+ & t^- \end{pmatrix}, \quad (\text{A.1.1})$$

where  $t^+$  and  $t^-$  are transmission coefficients of the wave from the left to the right and from the right to the left respectively, and  $r^+$  and  $r^-$  are the reflection coefficients from the right to the right and from the left to the left respectively.



Figure A.1: Definition of amplitudes  $A_1$ ,  $A_2$ ,  $B_1$ ,  $B_2$ .

This matrix, considering the figure (A.1), expresses the outgoing wave functions amplitudes  $B_1$  and  $A_2$  in terms of the incoming amplitudes  $A_1$  and  $B_2$ :

$$\begin{pmatrix} A_2 \\ B_1 \end{pmatrix} = \mathbf{S} \begin{pmatrix} A_1 \\ B_2 \end{pmatrix} \quad (\text{A.1.2})$$

The expression (A.1.2) can be rewritten in terms of the transfer matrix  $\mathbf{T}$  as

$$\begin{pmatrix} A_2 \\ B_2 \end{pmatrix} = \mathbf{T} \begin{pmatrix} A_1 \\ B_1 \end{pmatrix} \quad (\text{A.1.3})$$

where the matrix  $\mathbf{T}$  [61] is given by

$$\mathbf{T} = \begin{pmatrix} t^+ - r^-(t^-)^{-1}r^+ & r^-(t^-)^{-1} \\ -(t^-)^{-1}r^+ & (t^-)^{-1} \end{pmatrix}. \quad (\text{A.1.4})$$

In the case of a one dimensional system there is only one possible channel, therefore  $\mathbf{T}$  is a  $2 \times 2$  matrix and we have  $t^+ = t^- = t$ . The probability for the electron to be transmitted from one side to the other is given by  $T = |t|^2$ . If we consider instead a quasi-one dimensional system propagating along the  $x$  direction with a cross-section  $L^{(d-1)}$ , like the one in figure (A.2), the electron can propagate also in directions perpendicular to the propagation direction  $x$ : being the cross section of the leads finite, the wave vector in directions perpendicular to  $x$  is quantized and can have only discrete values, defining one channel for each possible value.  $t^+$  and  $t^-$  are therefore matrices, whose size is determined by the number of possible channels.

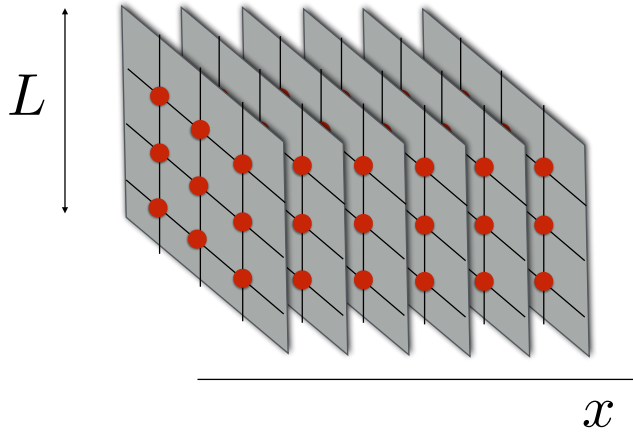


Figure A.2: Sketch of a quasi-one dimensional system with cross section  $L^{(d-1)}$  propagating along the  $x$  direction.

An important quantity in the study of electron propagation is the conductance, which has been defined by Landauer [254] and Economou and Soukoulis [255]. If we consider a sample connected to two semi-infinite ideal leads and which transmits electrons from two reservoirs, the conductance  $g$  is defined by the relation

$$j = g \Delta V, \quad (\text{A.1.5})$$

where  $j$  is the current through the sample and  $\Delta V$  is the voltage difference: if we measure the voltage difference between the leads, as proposed by Landauer [254], we obtained the conductance

$$g_L = \frac{e^2}{h} \frac{T}{1-T}. \quad (\text{A.1.6})$$

If we consider instead the voltage difference between the reservoirs we obtained the definition of Economou and Soukoulis [255]

$$g_{ES} = \frac{e^2}{h} T. \quad (\text{A.1.7})$$

While in the limit of small transmission,  $T \rightarrow 0$ , the two definitions are equivalent, they lead to different limit when  $T \rightarrow 1$ : the conductance  $g_L$  (A.1.6) diverges in this case, while the expression (A.1.7) converges to  $e^2/h$ , this difference being originated by the presence of a contact resistance between leads and reservoirs.

In the case of a quasi-one dimensional system discussed above, where we have different possible channels, the conductance  $g_{ES}$  is generalized by the relation

$$g_{ES} = \frac{e^2}{h} \text{Tr } t^\dagger t, \quad (\text{A.1.8})$$

[256, 257, 258, 259]. It was proved in [257, 258] that the conductance  $g_{ES}$  defined by relation (A.1.8), in the metallic regime is related to the conductivity  $\sigma$  by

$$g_{ES} = \sigma L^{d-2}. \quad (\text{A.1.9})$$

This behavior indicates that  $g_{ES}$  is closely related to the Thouless conductance  $g_T$  defined by expression (I.4.1), and thus that  $g_{ES}$  not only measures the transmission properties of the sample but also the sensitivity of the wave functions to the change of the boundary conditions.

## A.2 Transfer Matrix and localization length

The transfer matrix  $\mathbf{T}$  connects the propagating waves on the left and right hand side of the sample. We can also define the transfer matrix  $\mathbf{M}$  relating the wave functions in the site representation. In particular, if we consider the Anderson model in one dimension, with a system of size  $L_x$ , the Schrödinger equation reads

$$(\epsilon_i - E) \psi_i + t \psi_{i-1} + t \psi_{i+1} = 0, \quad (\text{A.2.1})$$

which can be rewritten as

$$\begin{pmatrix} \psi_{i+1} \\ \psi_i \end{pmatrix} = \mathbf{M}_i \begin{pmatrix} \psi_i \\ \psi_{i-1} \end{pmatrix} = \begin{pmatrix} E - \epsilon_i & -t \\ t & 0 \end{pmatrix} \begin{pmatrix} \psi_i \\ \psi_{i-1} \end{pmatrix}. \quad (\text{A.2.2})$$

The evolution of the state is described by the matrix product

$$\mathbf{Q}_{L_x} = \prod_{i=1}^{L_x} \mathbf{M}_i, \quad (\text{A.2.3})$$

and then we can write

$$\begin{pmatrix} \psi_{i+1} \\ \psi_i \end{pmatrix} = \mathbf{Q}_{L_x} \begin{pmatrix} \psi_1 \\ \psi_0 \end{pmatrix}. \quad (\text{A.2.4})$$

The matrix product (A.2.3) satisfies the theorem of Oseledec [260], which assures that there exists a limiting matrix

$$\Gamma = \lim_{L_x \rightarrow \infty} (\mathbf{Q}_{L_x}^\dagger \mathbf{Q}_{L_x})^{\frac{1}{2L_x}} \quad (\text{A.2.5})$$

with eigenvalues  $\exp \gamma_i$ , where  $\gamma_i$  are the Lyapunov exponents of  $\mathbf{Q}_{L_x}$ . The smallest of these exponents determines the slowest possible exponential increase of the wave function for  $L_x \rightarrow \infty$ , and it can thus be identified with the inverse of the localization length of the system  $\xi = \gamma^{-1}$ . Indeed, the Lyapunov exponent  $\gamma(E)$  of the one dimensional system is defined by the relation

$$\gamma(E) = \lim_{L_x \rightarrow \infty} \frac{1}{2L_x} \log(\psi_{L_x}^2 + \psi_{L_x+1}^2). \quad (\text{A.2.6})$$

Using the definition of the matrices  $\mathbf{M}_i$  and  $\mathbf{Q}_{L_x}$  (A.2.2) and (A.2.3) we can write

$$\psi_{L_x+1}^2 + \psi_{L_x}^2 = \begin{pmatrix} \psi_{L_x+1} & \psi_{L_x} \end{pmatrix} \begin{pmatrix} \psi_{L_x+1} \\ \psi_{L_x} \end{pmatrix} = \begin{pmatrix} \psi_1 & \psi_0 \end{pmatrix} \mathbf{Q}_{L_x}^\dagger \mathbf{Q}_{L_x} \begin{pmatrix} \psi_1 \\ \psi_0 \end{pmatrix}, \quad (\text{A.2.7})$$

thus, in the limit  $L_x \rightarrow \infty$ , the Lyapunov exponent  $\gamma$  (A.2.6) is related to the eigenvalues of the limiting matrix  $\mathbf{Q}_{L_x}$ : we have to notice that, since  $\mathbf{Q}_{L_x}$  depends on the random energies  $\epsilon_i$ , the Lyapunov exponent  $\gamma$  is a random variable too. It was shown by Oseledec [260] that  $\gamma$  is a self-averaging quantity. Intuitively, this can be understood by looking at expression (A.2.7):  $\gamma$  is the logarithm of the eigenvalue of a product of random matrices, and it can be considered as the sum of logarithm of the eigenvalues of matrices  $\mathbf{M}_i$ ,  $i = 1, 2, \dots, L_x$ . Thus we can expect applying the central limit theorem that both the mean value and variance of  $\gamma$  are proportional to  $L_x$ . The identification of the localization length of the system with a limiting property of a product of random matrices generated great interest in the search of precise conditions for the existence and positivity of the Lyapunov exponent: the results of Furstenberg [261], Oseledec [260], and others [262, 63, 68, 69, 70] provide the proof that in one dimension all states are localized no matter the strength of the disorder ( $W \neq 0$ ).

The concepts explained above can be generalized to the quasi-one dimensional system of size  $L^{(d-1)} \times L_x$  sketched in figure (A.2). The Schrödinger equation in this case takes the form

$$\psi_{i+1} = \mathbf{t}^{-1}(E - \mathbf{H}_i)\psi_i - \psi_{i-1}, \quad (\text{A.2.8})$$

where  $\mathbf{t}$  and  $\mathbf{H}_i$  are  $L^{(d-1)} \times L^{(d-1)}$  matrices, representing the coupling between successive layers and the Hamiltonian of the  $i$ -th layer respectively.  $\psi_i$  is a  $L^{(d-1)}$  dimensional vector containing the amplitudes of the states. As in the one dimensional case, equation (A.2.8) can be written in terms of the transfer matrix  $\mathbf{M}_i$ , which is now a  $2L^{(d-1)} \times 2L^{(d-1)}$  matrix, giving

$$\begin{pmatrix} \psi_{i+1} \\ \psi_i \end{pmatrix} = \mathbf{M}_i \begin{pmatrix} \psi_i \\ \psi_{i-1} \end{pmatrix}, \quad \mathbf{M}_i = \begin{pmatrix} E - \mathbf{H}_i & -\mathbf{t} \\ \mathbf{t} & 0 \end{pmatrix}. \quad (\text{A.2.9})$$

Analogously to the one dimensional case, the behavior of the system in the limit  $L_x \rightarrow \infty$  is determined by the following matrix product

$$\mathbf{Q}_{L_x} = \prod_{i=1}^{L_x} \mathbf{M}_i. \quad (\text{A.2.10})$$

Since the system is effectively one-dimensional, the wave function must decrease exponentially when  $L_x$  increases: this exponential decrease is given by the eigenvalues of  $\mathbf{Q}_{L_x}$ ,  $\exp(-\gamma_\alpha)$ , the smallest  $\gamma_\alpha$  determining the localization length. As above, since the matrix  $\mathbf{Q}_{L_x}$  contains the random energies  $\epsilon_i$ , the Lyapunov exponents  $\gamma_\alpha$  will also be a random variable. The theorem of Oseledec [260] assures again that in the limit  $L_x \rightarrow \infty$  all the eigenvalues of the matrix product

$$\left[ \mathbf{Q}_{L_x}^\dagger \mathbf{Q}_{L_x} \right]^{L/L_x} \quad (\text{A.2.11})$$

converges to  $e^{\zeta_\alpha}$  and  $e^{-\zeta_\alpha}$  in pairs, with

$$\zeta_\alpha = \frac{2L}{L_x} \gamma_\alpha. \quad (\text{A.2.12})$$

The main value of  $\zeta_\alpha$  does not depends on  $L_x$  and the variance is proportional to  $L/L_x$ : the parameters  $\zeta_\alpha$  are thus self-averaging quantities in the limit  $L_x \rightarrow \infty$ .



## Appendix B

# Critical wave functions: multifractality

Given an Hamiltonian of the type (I.6.6), we consider an eigenstate  $|\alpha\rangle$  of the system: the moments of the normalized measure  $|\psi_\alpha|^2$  are defined as

$$\Upsilon_q = \sum_i \langle \alpha | i \rangle^{2q} = \sum_i |\psi_{\alpha i}^2|^q, \quad (\text{B.0.1})$$

where  $\psi_{\alpha i}^2$  is the weight of the site  $i$  in the eigenstate  $|\alpha\rangle$ , and the sum spreads over all sites  $i$ .

In the Anderson Model for  $d \geq 3$ , at the critical point, the moments  $\Upsilon_q$  (B.0.1) shows an anomalous scaling with the system size  $L$ . This feature is described by introducing a continuous set of critical exponents  $\tau_q$ , defined as:

$$\langle \Upsilon_q \rangle = L^d \langle |\psi_i|^{2q} \rangle \sim L^{-\tau_q}, \quad (\text{B.0.2})$$

For a metal we have  $\tau_q = d(q - 1)$ , while in the localized phase  $\tau_q = 0$ , and the moments  $\Upsilon_q$  are finite in the thermodynamic limit. The anomalous behavior at the critical point is described by introducing the fractal dimension  $D_q$  defined as  $\tau_q = D_q(q - 1)$ . The expression (B.0.2) can be obtained integrating over a distribution of  $|\psi|^2$  of the form

$$P(|\psi|^2) \sim \frac{1}{|\psi|^2} L^{-d+f(-\frac{\log |\psi|^2}{\log L})}. \quad (\text{B.0.3})$$

In this way we obtain

$$\langle \Upsilon_q \rangle = L^d \langle |\psi|^{2q} \rangle \sim \int d\alpha L^{-q\alpha+f(\alpha)}, \quad (\text{B.0.4})$$

where we have defined  $\alpha = -\log |\psi|^2 / \log L$ . The integral in the expression (B.0.4) can be evaluated for large  $L$  with the saddle point method, giving the result (B.0.2): the exponent  $\tau_q$  is related to  $\alpha$  through the Legendre transformation:

$$\tau_q = q\alpha - f(\alpha) \quad q = \frac{df(\alpha)}{d\alpha} \quad \alpha = \frac{d\tau_q}{dq}. \quad (\text{B.0.5})$$

The expressions (B.0.3) and (B.0.4) define the multifractal spectrum  $f(\alpha)$ , which represents the fractal dimension of the set of points in the lattice where the measure  $|\psi|^2$  scales as  $|\psi|^2 \sim L^{-\alpha}$ , i.e. the number of such points scales as  $L^{f(\alpha)}$  with the system size [263].

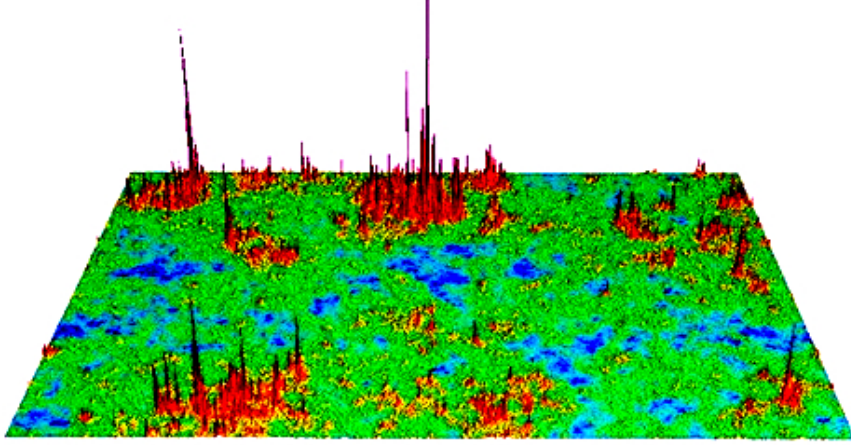


Figure B.1: Multifractal electron wave-function. The figure is from <https://www.int.kit.edu/918.php>.

From the definitions of  $\tau_q$  and  $f(\alpha)$  general properties of these functions follow [188]:  $\tau_q$  is non-decreasing and convex ( $\tau'_q \geq 0$ ,  $\tau''_q \leq 0$ ), with  $\tau_0 = -d$ ,  $\tau_1 = 0$ .  $f(\alpha)$  is also a convex function ( $f''(\alpha) \leq 0$ ) defined on the semiaxis  $\alpha \geq 0$  with a maximum for  $\alpha_{\max} = \alpha_0$  (corresponding to  $q = 0$  under Legendre transformation) and  $f(\alpha_0) = d$ . Moreover, for the point  $\alpha_1$  corresponding to  $q = 1$  we have  $f(\alpha_1) = \alpha_1$  and  $f'(\alpha_1) = 1$ .

For a metal  $f(\alpha)$  is concentrated at  $\alpha = d$ , with  $f(d) = d$  and  $f(\alpha) = -\infty$  otherwise. At the critical point  $f(\alpha)$  acquires finite width and the maximum shifts to a point  $\alpha > d$ , as shown in figure (B.2).

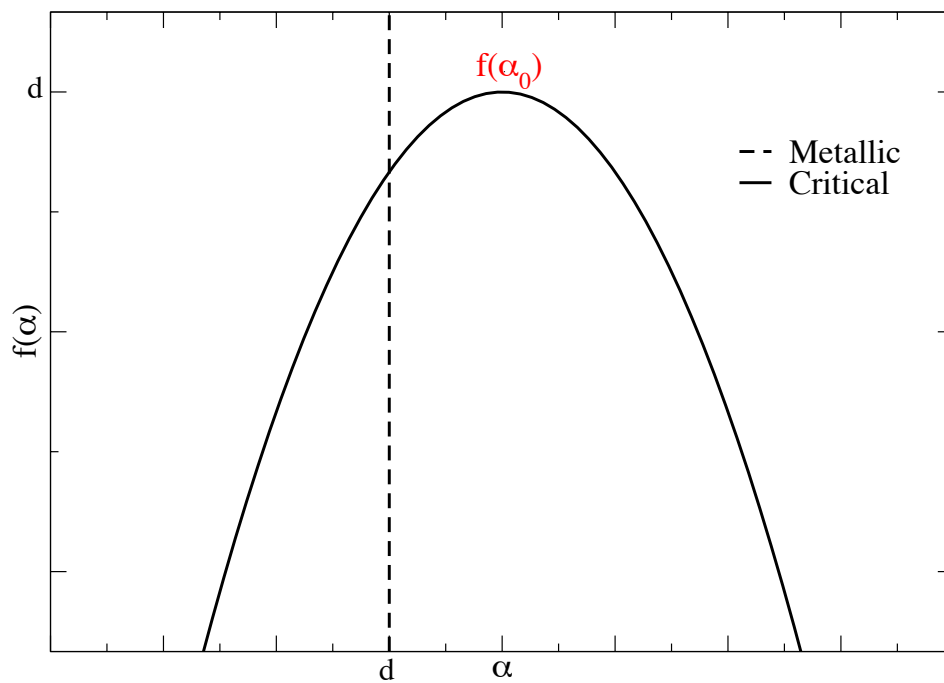


Figure B.2: Plot of the multifractal spectrum  $f(\alpha)$ . In the metallic phase  $f(\alpha)$  is concentrated at  $\alpha = d$ . At the critical point it acquires a finite width, with a maximum which shift to  $\alpha > d$ .



# Appendix C

## The IPR in terms of the Green function

By substituting the definition (II.1.2) of the resolvent in the quantity

$$A_i^N(E) = \lim_{\eta \rightarrow 0} \eta |G_{ii}^N(E - i\eta)|^2 \quad (\text{C.0.1})$$

we obtain

$$A_i^N(E) = \lim_{\eta \rightarrow 0} \eta \sum_{\alpha=1}^N \frac{\psi_{\alpha i}^4}{(E - E_\alpha)^2 + \eta^2} + \lim_{\eta \rightarrow 0} D_i^N(\eta, E), \quad (\text{C.0.2})$$

where the non-diagonal contribution  $D_i^N(\eta, E)$  is defined as

$$D_i^N(\eta, E) = \eta \sum_{\alpha=1}^N \frac{\psi_{\alpha i}^2}{E - E_\alpha + i\eta} \sum_{\beta \neq \alpha} \frac{\psi_{\beta i}^2}{E - E_\beta - i\eta}. \quad (\text{C.0.3})$$

If there are no degenerate eigenvalues in the spectrum, the off-diagonal term  $D_i^N(\eta, E)$  vanishes for  $\eta \rightarrow 0$ .

We can thus write from equation (C.0.2) in the limit  $\eta \rightarrow 0$ :

$$A_i^N(E) = \pi \sum_{\alpha=1}^N |\psi_{\alpha i}|^4 \delta(E - E_\alpha). \quad (\text{C.0.4})$$

If we sum over all sites and we divide by  $N\rho(E)$ , we obtain for  $N \rightarrow \infty$

$$\lim_{\eta \rightarrow 0} \frac{\eta}{N\rho(E)} \sum_i |G_{ii}^N(E - i\eta)|^2 = \frac{\pi}{N\rho} \sum_i \sum_{\alpha=1}^N |\psi_{\alpha i}|^4 \delta(E - E_\alpha), \quad (\text{C.0.5})$$

which coincide with equation (II.1.7).

We stress that this expression gives the eigenvalue-dependent IPR, while equation (II.1.1) defines the IPR associated to the state  $\alpha$ :  $\Upsilon_2 = \sum_i |\psi_{\alpha i}^4|$ . In the expression (C.0.5), before taking the sum over the sites, the average of the weight  $|\psi_{\alpha i}|^4$  over a small energy window around  $E$  is performed.



## Appendix D

# The DoS of Sparse RM model with the supersymmetric method

We consider  $N \times N$  matrix  $H_{ij}$  with independent and identically distributed entries with a probability distribution  $f(H_{ij})$  of the form:

$$f(z) = \left(1 - \frac{p}{N}\right) \delta(z) + \frac{p}{N} h(z), \quad p \sim O(1), \quad (\text{D.0.1})$$

where  $h(z)$  has no  $\delta$ -like singularity at  $z = 0$  and  $\int h(z) z^2 dz \sim O(1)$ .

Introducing supervectors  $\Phi_i$  of the form (II.3.10), we consider the action (II.3.11) with the definition (II.3.12) of the matrix  $\hat{K}$ . By averaging over the disorder we get

$$\overline{Z(E, J)} = \int \prod_i [d\Phi_i] \exp \left\{ \frac{i}{2} \sum_i \Phi_i^\dagger (E\hat{I} + J\hat{K}) \Phi_i + \frac{p}{2N} \sum_{ij} [\tilde{h}(\Phi_i^\dagger \Phi_j) - 1] \right\}, \quad (\text{D.0.2})$$

$$\tilde{h}(z) = \int h(t) \exp(-itz) dt. \quad (\text{D.0.3})$$

We can use now a the following functional generalization of the Hubbard-Stratonovich transformation

$$\begin{aligned} \int Dg \exp \left\{ -\frac{Np}{2} \int [d\Psi] [d\Psi'] g(\Psi) C(\Psi, \Psi') g(\Psi') + p \int [d\Psi] g(\Psi) v(\Psi) \right\} \\ = \exp \left\{ \frac{p}{2N} \int [d\Psi] [d\Psi'] v(\Psi) C^{-1}(\Psi, \Psi') v(\Psi') \right\}, \end{aligned} \quad (\text{D.0.4})$$

where  $C^{-1}(\Psi, \Psi')$  is an integral operator inverse to that with kernel  $C(\Psi, \Psi')$ . If we choose  $v(\Psi) = \sum_{i=1}^N \delta(\Psi - \Phi_i)$  and the kernel  $C^{-1}(\Theta, \Phi)$  equal to a function  $\tilde{h}(\Theta^\dagger \Phi) - 1$ , we obtain the following expression

$$\begin{aligned} \exp \left\{ \frac{p}{2N} \sum_{ij} [\tilde{h}(\Phi_i^\dagger \Phi_j) - 1] \right\} \\ = \int Dg \exp \left\{ -\frac{Np}{2} \int [d\Psi] [d\Psi'] g(\Psi) C(\Psi, \Psi') g(\Psi') + p \sum_i g(\Psi_i) \right\}, \end{aligned} \quad (\text{D.0.5})$$

where

$$\int [d\chi] C(\Phi, \chi) [\hat{h}(\chi^\dagger \eta) - 1] = \delta(\Phi, \eta), \quad (\text{D.0.6})$$

where  $\delta(\Phi, \eta)$  is the  $\delta$ -function in the space of supervectors. Using the expression (D.0.5) we obtain for the averaged partition function

$$\begin{aligned} \overline{Z(E, J)} = \int Dg \exp \left\{ -\frac{Np}{2} \int [d\Psi] [d\Psi'] g(\Psi) C(\Psi, \Psi') g(\Psi') \right. \\ \left. + N \log \int [d\Phi] \exp \left[ \frac{i}{2} \Phi^\dagger (E\hat{I} + J\hat{K}) \Phi + p g(\Phi) \right] \right\}. \end{aligned} \quad (\text{D.0.7})$$

Due to the fully-connected structure of the model, we can now perform the integration in the limit  $N \rightarrow \infty$  with the saddle-point method, obtaining for  $J = 0$

$$g(\Psi) = \frac{\int [d\Phi] \{\hat{h}(\Psi^\dagger \Phi) - 1\} \exp((i/2)\Phi^\dagger E \Phi + p g'(\Phi))}{\int [d\Phi] \exp((i/2)\Phi^\dagger E \Phi + p g(\Phi))}. \quad (\text{D.0.8})$$

Equation (D.0.8) is invariant with respect to transformations of the type  $g(\Phi) \rightarrow g(\hat{T}\Phi)$ , with  $\hat{T}$  such that

$$\hat{T}^\dagger T = \hat{I}. \quad (\text{D.0.9})$$

The solution of (D.0.8) will be therefore a function of the invariant  $\Phi^\dagger \Phi = S^2 + 2\chi^* \chi$  only, with  $S^2 = (S^{(1)})^2 + (S^{(2)})^2$ . Thanks to the properties of the integration of an invariant function over supervectors [264, 37], the denominator in equation (D.0.8) is one. Using the properties (II.3.1), (II.3.2) of Grassmanian variables, the solution  $\tilde{g}$  is reduced to the form  $\tilde{g}(\Phi^\dagger \Phi) = \tilde{g}(S^2) + 2\chi^* \chi \tilde{g}'(S^2)$ . If we integrate over Grassmanian variables we obtain for the solution  $\tilde{g}(S^2)$  the expression

$$\tilde{g}(S^2) = -S \int_0^\infty dR \exp \left[ \frac{i}{2} ER^2 + p \tilde{g}(R^2) \right] \int dz z h(z) J_1(zRS), \quad (\text{D.0.10})$$

where  $J_1(zRS)$  is the Bessel function of order one. The density of states can be found from  $\tilde{g}(S^2)$  through the relations

$$\rho(E) = -\frac{2}{\pi B} \Re \tilde{g}'(0), \quad B = \int dz h(z) z^2. \quad (\text{D.0.11})$$

# Appendix E

## Meaning of the order parameter function

The identity (II.3.33) used in Chapter (II.3) in order to explain the meaning of the order parameter function  $g_0(x, y)$  has been rigorously proven in Ref. [33]. The proof lays on the computation of the correlation functions  $K_{n,m} = G_1^n(i) G_2^m(i)$ . We present here a less rigorous argument in order to establish a relation between the order parameter which emerges in the supersymmetric formulation and the real and imaginary part of the self energy.

As stated in the main text, the starting point is the field theory  $Z(E) = \int \prod_i [d\Phi_i] e^{-[S(\{\Phi_i\}, E)]}$  with the action

$$S(\{\Phi_i\}, E, r) = -\frac{i}{2} \sum_{i,j} \Phi_i^\dagger \hat{L} (E\delta_{ij} - H_{ij}) \Phi_j + \sum_i \Phi_i^\dagger \Phi_i \left( \frac{r}{2N} + i\eta \right), \quad (\text{E.0.1})$$

which we have written here without sources. Averaging over the disorder we obtain

$$\overline{Z(E, r)} = \int \prod_i [d\Phi_i] \exp \left\{ \frac{i}{2} \Phi^\dagger \hat{L} E \Phi + \frac{i}{2} \Phi^\dagger \left( \frac{r}{2N} + i\eta \right) \Phi + \frac{p}{2N} \sum_{ij} [\tilde{h}(\Phi_i^\dagger \hat{L} \Phi_j) - 1] \right\}, \quad (\text{E.0.2})$$

where

$$\tilde{h}(z) = \int h(t) \exp(-itz) dt. \quad (\text{E.0.3})$$

We can now introduce the function  $\rho(\Phi) = \frac{1}{N} \sum_i \delta(\Phi - \Phi_i)$  and rewrite  $S$  as

$$S = \frac{i}{2} NE \int d\Phi \rho(\Phi) \Phi^\dagger \hat{L} \Phi + \frac{i}{2} (r + i\eta) \int d\Phi \rho(\Phi) \Phi^\dagger \Phi + \frac{i}{2} N \int d\Phi d\Psi \rho(\Phi) \mathcal{F}(\Phi^\dagger \hat{L} \Phi) \rho(\Psi), \quad (\text{E.0.4})$$

with

$$\mathcal{F}(y) = p \int dx [h(x) e^{-ixy} - 1]. \quad (\text{E.0.5})$$

The further integration over all  $\Phi_i$ s leads to an additional entropic-like term in the action  $-N \int d\Phi \rho(\Phi) \log(\rho(\Phi))$ : in the main text we have seen how it emerges if the Hubbard-Stratonovich transformation is performed in a more rigorous way. The field theory has thus been transformed in a new one:  $Z = \int \mathcal{D}\rho(\Phi) e^{S[\rho]}$ . We can thus perform the integral with the saddle-point method thanks to the fully-connected structure of the model, which allows one to factorize out the  $N$  in the action, and we recover the result of the main about the symmetries of the solution and the breaking of the symmetry leading to the phase transition.

We can notice that, before averaging over the disorder, the field theory is Gaussian, therefore, integrating over all fields but  $\Phi_i$  we still have a Gaussian integral to handle. Moreover, the field theory is constructed in such a way that  $\langle \Phi_i^{(1)\dagger} \Phi_j^{(1)} \rangle = 4iG_{ij}$  and  $\langle \Phi_i^{(2)\dagger} \Phi_j^{(2)} \rangle = 4iG_{ij}^*$ . The average  $\langle \delta(\Phi - \Phi_i) \rangle$  is the gaussian measure on  $\Phi_i$ , and collecting all terms we obtain

$$\overline{\langle \rho(\Phi) \rangle} = \frac{1}{N} \sum_i \overline{\exp \left( \frac{i}{2} \Phi^\dagger \hat{L} \Phi (E - \Re \Sigma_{ii}) + \frac{1}{2} \Phi^\dagger \Phi \Im \Sigma_{ii} \right)} \quad (\text{E.0.6})$$

By introducing the distribution of the local self-energy  $R(\Sigma)$  we obtain

$$\overline{\langle \rho(\Phi) \rangle} = \int d\Sigma R(\Sigma) \left( \exp \frac{i}{2} \Phi^\dagger \hat{L} \Phi (E - \Re \Sigma) + \frac{1}{2} \Phi^\dagger \Phi \Im \Sigma \right). \quad (\text{E.0.7})$$

The above expression (E.0.7) has the same meaning as expression (II.3.33): in the localized phase, where the typical value of the imaginary part of the resolvent is zero, the parameter order function, e.g. the saddle-point solution of equation (E.0.4), is invariant under the symmetry  $\Phi \rightarrow \hat{T}\Phi$ , with  $\hat{T}^\dagger \hat{L} \hat{T} = \hat{T}$ , thus, given a solution  $\rho(\Phi)$ ,  $\rho(\hat{T}\Phi)$  is also a solution. The localization transition corresponds to the breaking of this symmetry: in delocalized phase the typical value of  $\Im \Sigma$  is non-zero and the solution depends thus also on the invariant  $\Phi^\dagger \Phi$ .

# Appendix F

## The generalized central limit theorem

As is generally known, the Central Limit Theorem (CLT) states that the Gaussian distribution is an attractive fixed point for all distributions with a finite variance. If, instead, the variance of the distribution is infinite, as in the case of eq. (II.1), a generalized version of the CLT holds [221, 222]. In particular, given a set of i.i.d. random variables  $\{x_i\}$ ,  $i = 1, \dots, N$ , distributed according to

$$P(x_i) \simeq \frac{C_{\pm}}{N|x_i|^{1+\mu}}, \quad x_i \rightarrow \pm\infty, \quad (\text{F.0.1})$$

with  $\mu < 2$ , the distribution of the sum  $S = \sum_{i=1}^N x_i$ , when  $N \rightarrow \infty$ , is a Lévy stable law  $L_{\mu}^{C,\beta}$ , a distribution entirely defined by three parameters: the exponent  $\mu$  describing the power-law behavior of the tails, the coefficient  $C$  such that the typical value of the distribution is  $C^{1/\mu}$ , and  $\beta$  characterizing the asymmetry of the law. The two parameters  $C$  and  $\beta$  are given by the relations:

$$\begin{aligned} \beta &= \frac{C_+ - C_-}{C_+ + C_-}, & C &= \gamma_{\mu}(C_+ + C_-), \\ \gamma_{\mu} &= \Gamma(1 - \mu) \cos\left(\frac{\pi\mu}{2}\right). \end{aligned} \quad (\text{F.0.2})$$

The Lévy distribution lacks of an explicit representation, and it is known by means of its Fourier transform  $\hat{L}_{\mu}^{C,\beta}$  [221, 223]

$$\begin{aligned} L_{\mu}^{C,\beta}(x) &= \frac{1}{2\pi} \int dk \hat{L}_{\mu}^{C,\beta}(k) e^{ikx}, \\ \log \hat{L}_{\mu}^{C,\beta}(k) &= -\frac{1}{N} |k|^{\mu} \gamma_{\mu} \left[ 1 + i\beta \tan\left(\frac{\pi\mu}{2}\right) \text{sgn}(k) \right], \end{aligned} \quad (\text{F.0.3})$$

where  $\mu$ ,  $C$  and  $\beta$  are three parameter which characterize respectively the power-law behavior of the tails, the typical value and the asymmetry of the distribution.

If  $\mu < 1$ , the distribution of the sum  $S$  is  $P(S) = L_{\mu}^{C,\beta}(S)$ ; if  $1 < \mu < 2$ , the mean value  $\bar{x}_i$  of the distribution (F.0.1) is defined, and it holds  $P(S) = L_{\mu}^{C,\beta}(S - N\bar{x}_i)$ .

A generalization of this theorem is the following: if  $\{x_i\}$ ,  $i = 1, \dots, N$  is a set of variables distributed according to eq. (F.0.1), and  $\{c_i\}$  is a set of regular variables, the sum  $S = \sum_{i=1}^N c_i x_i$ , in the limit  $N \rightarrow \infty$ , is distributed according to a Lévy stable law  $L_\mu^{C,\beta}$ , with

$$\beta = \frac{C_+ - C_-}{C_+ + C_-} \left[ \frac{1}{N} \sum_{i=1}^N \text{sgn}(c_i) \right], \quad C = \gamma_\mu (C_+ + C_-) \left[ \frac{1}{N} \sum_{i=1}^N |c_i|^\mu \right]. \quad (\text{F.0.4})$$

This can be viewed using the Fourier representation of the Lévy distribution. The probability density for the variable  $S$  can be written as:

$$\begin{aligned} Q(S) &= \int \prod_{i=1}^N \left[ \frac{dx_i dk_i}{2\pi} e^{ik_i x_i} \hat{P}(k_i) \delta \left( S - \sum_{i=1}^N c_i x_i \right) \right] \\ &= \int \frac{dk}{2\pi} e^{ikS} \prod_{i=1}^N \left[ \frac{dx_i dk_i}{2\pi} e^{i(k_i - k c_i) x_i} \hat{P}(k_i) \right]. \end{aligned} \quad (\text{F.0.5})$$

If we use now the expansion (III.3.4) of  $\hat{P}(k_i)$  up to the lowest order in  $k_i$ , we find that for  $N \rightarrow \infty$  the Fourier transform  $Q(S)$  coincides with the characteristic function of a complex Lévy stable distribution  $L_\mu^{C,\beta}$ , with parameters  $\beta$  and  $C$  given by the expression (F.0.4).

## Appendix G

# Computation of the mobility edge of Lévy Matrices

The self consistent equation derived in the section (III.2) for the real and imaginary part of the self-energy reads:

$$S_i + i\Delta_i = \sum_{j=1}^N x_{ij} \frac{E - S_j + i(\eta + \Delta_j)}{(E - S_j)^2 + (\eta + \Delta_j)^2}. \quad (\text{G.0.1})$$

As explained in the section (III.4) of the main text, we want to analyze the behavior of the distribution of the self-energy  $Q(S, \Delta)$  in the thermodynamic limit near the mobility edge. Since in the localized phase  $\Delta$  is of order  $\eta$  with probability one, we can linearize the equation (G.0.1) with respect to the imaginary part, obtaining the following expressions:

$$\begin{aligned} S_i &= \sum_{j=1}^N x_j \frac{1}{E - S_j} \\ \Delta_i &= \sum_{j=1}^N x_j \frac{\eta + \Delta_j}{(E - S_j)^2}. \end{aligned} \quad (\text{G.0.2})$$

Now we want to obtain the integral equation corresponding to (G.0.2): the region in which the solution is well defined identifies the localized phase.

From the equations (G.0.2) we get:

$$Q(S, \Delta) = \int \prod_{i=1}^N [dx_i dS_i d\Delta_i P(x_i) Q(S_i, \Delta_i)] \delta\left(S - \sum_{i=1}^N \frac{x_i}{E - S_i}\right) \delta\left(\Delta - \sum_{i=1}^N \frac{x_i(\eta + \Delta_i)}{(E - S_i)^2}\right).$$

We replace now the  $\delta$ -functions by their integral representation in the Fourier space and we also write  $Q(S_i, \Delta_i)$  as the inverse Fourier transform of  $\hat{Q}_2(S_i, k_i)$ , defined as:

$$\hat{Q}_2(S_i, k_i) = \int_{-\infty}^{+\infty} d\Delta_i e^{-ik_i\Delta_i} Q(S_i, \Delta_i). \quad (\text{G.0.3})$$

We have:

$$Q(S, \Delta) = \int \prod_{i=1}^N \frac{dx_i dS_i d\Delta_i dk_i}{2\pi} P(x_i) \hat{Q}_2(S_i, k_i) e^{-ik_1 x_i / (E - S_i)} e^{-ik_2 \eta x_i / (E - S_i)^2} \\ \times e^{i(k_i - k_2 x_i / (E - S_i)^2) \Delta_i} \times \frac{dk_1 dk_2}{(2\pi)^2} e^{i(k_1 S + k_2 \Delta)}. \quad (\text{G.0.4})$$

We can now perform the integration over  $d\Delta_i$ , which gives  $2\pi\delta(k_i - k_2 x_i / (E - S_i)^2)$ , and then integrate over  $dk_i$ , yielding:

$$\hat{Q}(k_1, k_2) = \left[ \int dx dS P(x) \hat{Q}_2 \left( S, \frac{k_2 x}{(E - S)^2} \right) e^{-ik_1 x / (E - S)} e^{-ik_2 \eta x / (E - S)^2} \right]^N, \quad (\text{G.0.5})$$

where  $\hat{Q}(k_1, k_2)$  is the standard double Fourier transform of  $Q(S, \Delta)$ : we have obtained in this way the integral version of the equation (G.0.2).

We can now make an assumption for the asymptotic behavior of  $Q(S, \Delta)$  in the localized phase. Starting from the recursive equation (III.4.2) we have seen in the main text that the real part of the self-energy is a Lévy stable law  $L_{\mu/2}^{C(E), \beta(E)}$  with effective parameters  $C(E)$  and  $\beta(E)$  given by the set of equations (III.4.5). A very similar result holds for the probability distribution of the imaginary part  $Q(\Delta)$ : the only difference with the expressions (III.4.5) is that in this case the parameter  $\beta$  is equal to 1 since all the  $\Im G_i$  are positive. We also know that the joint probability distribution  $Q(S, \Delta)$  is a complex Lévy stable law given by the equation (III.3.5). Since the marginal  $Q(\Delta)$  is obtained integrating over  $S$  the joint probability  $Q(S, \Delta)$ , a reasonable *ansatz* for the behavior of the tails of  $Q(S, \Delta)$  in the localized phase is

$$Q(S, \Delta) \sim \frac{A(S)}{\Delta^{1+m}}. \quad (\text{G.0.6})$$

As observed in [38], the exponent  $m$  is constrained to be  $\geq \mu/2$ , since integrating over  $S$  can only make the decaying of the tails of  $\Delta$  slower. This expression in the Fourier space gives:

$$\hat{Q}_2(S, k) \sim \hat{Q}_2(S, 0) + c|k|^m A(S). \quad (\text{G.0.7})$$

Using the definition (G.0.3),  $Q_2(S, 0)$  is the marginal of  $Q(S, \Delta)$  once we integrate over  $\Delta$ : therefore, as we have shown in section (III.4), it is a Lévy stable law  $L_{\mu/2}^{C(E), \beta(E)}(S)$  with exponent  $\mu/2$  and effective parameters  $C(E)$  and  $\beta(E)$  given by the self-consistent equations (III.4.7). The expression (G.0.5) for  $k_2 = 0$  gives:

$$\hat{L}_{\mu/2}^{C(E), \beta(E)}(k_1) = \left[ \int dx dS P(x) L_{\mu/2}^{C(E), \beta(E)}(S) e^{-ik_1 x / (E - S)} \right]^N. \quad (\text{G.0.8})$$

Using now the asymptotic expansion (G.0.7), the above equation becomes:

$$\hat{L}_{\mu/2}^{C(E), \beta(E)}(k_1) + c|k_2|^\nu \hat{A}(k_1) = \left[ \int dx dS P(x) \left( L_{\mu/2}^{C(E), \beta(E)}(S) + c \left| \frac{k_2 x}{(E - S)^2} \right|^\nu A(S) \right) \right. \\ \left. \times e^{-ik_1 x / (E - S)} e^{-ik_2 \eta x / (E - S)^2} \right]^N. \quad (\text{G.0.9})$$

We proceed now expanding the right hand side of the equation (G.0.9) in powers of  $k_2$  and neglecting all the terms smaller than  $|k_2|^m$ . If we define

$$\begin{aligned} I_1 &= \int dx dS P(x) L_{\mu/2}^{C(E),\beta(E)}(S) e^{-ik_1x/(E-S)}, \\ I_2 &= c \int dx dS P(x) \left| \frac{x}{(E-S)^2} \right|^m A(S) e^{-ik_1x/(E-S)}, \end{aligned} \quad (\text{G.0.10})$$

we can rewrite the equation (G.0.9) as

$$\begin{aligned} \hat{L}_{\mu/2}^{C(E),\beta(E)}(k_1) + c|k_2|^m \hat{A}(k_1) &= (I_1 + |k_2|^m I_2)^N \\ &\simeq I_1^N \left( 1 + N|k_2|^m \frac{I_2}{I_1} \right) = I_1^N + N|k_2|^m I_1^{N-1} I_2. \end{aligned} \quad (\text{G.0.11})$$

Using the equation (G.0.8) and the definition of  $I_1$  above, we note that  $I_1^N = \hat{L}_{\mu/2}^{C(E),\beta(E)}(k_1)$ . As a consequence, up to the lowest order in  $k_2$  we have:

$$\hat{A}(k_1) = N \hat{L}_{\mu/2}^{C(E),\beta(E)}(k_1) \int dx dS P(x) \left| \frac{x}{(E-S)^2} \right|^m A(S) e^{-ik_1x/(E-S)}. \quad (\text{G.0.12})$$

We have to study now the behavior of the kernel of this integral equation. The integral over  $x$  can be performed using the fact that

$$\int_0^\infty dx \frac{e^{ikx}}{x^a} = e^{i\frac{\pi}{2}(1-a)\text{sign}(k)} |k|^{a-1} \Gamma(1-a), \quad (\text{G.0.13})$$

and we obtain:

$$\int_0^\infty dx P(x) |x|^m e^{-ik_1x/(E-S)} = \frac{1}{2N} \Gamma(m-\mu/2) e^{-i\frac{\pi}{2}(m-\mu/2)\text{sign}(k_1(E-S))} \left| \frac{k_1}{E-S} \right|^{\mu/2-m}.$$

Plugging the result above into Eq. (G.0.12) we finally get:

$$\hat{A}(k_1) = \frac{1}{2} \Gamma(m-\mu/2) |k_1|^{\mu/2-m} \hat{L}_{\mu/2}^{C(E),\beta(E)}(k_1) \int_{-\infty}^{+\infty} dS \frac{A(S)}{|E-S|^{m+\mu/2}} e^{-i\frac{\pi}{2}(m-\mu/2)\text{sign}(k_1(E-S))}. \quad (\text{G.0.14})$$

We now replace  $A(S)$  by the inverse Fourier transform of  $\hat{A}(k)$ :

$$A(S) = \int \frac{dk}{2\pi} e^{ikS} \hat{A}(k), \quad (\text{G.0.15})$$

and perform the integral over  $dS$  by separating it into two pieces as follows:

$$\begin{aligned} \int_{-\infty}^{+\infty} dS \frac{e^{ikS}}{|E-S|^{m+\mu/2}} e^{-i\frac{\pi}{2}(m-\mu/2)\text{sign}(k_1(E-S))} &= \\ e^{-i\frac{\pi}{2}(m-\mu/2)\text{sign}(k_1)} \int_{-\infty}^E dS \frac{e^{ikS}}{(E-S)^{m+\mu/2}} &+ e^{i\frac{\pi}{2}(m-\mu/2)\text{sign}(k_1)} \int_E^{+\infty} dS \frac{e^{ikS}}{(S-E)^{m+\mu/2}}. \end{aligned} \quad (\text{G.0.16})$$

We change variable  $E - S \rightarrow z$  in the first integral and  $S - E \rightarrow z$  in the second integral and find:

$$e^{ikE} e^{-i\frac{\pi}{2}(m-\mu/2)\text{sign}(k_1)} \int_0^\infty dz \frac{e^{-ikz}}{z^{m+\mu/2}} + e^{ikE} e^{i\frac{\pi}{2}(m-\mu/2)\text{sign}(k_1)} \int_0^\infty dz \frac{e^{ikz}}{z^{m+\mu/2}}. \quad (\text{G.0.17})$$

Using again Eq. (G.0.13) we finally find:

$$\begin{aligned} \int_{-\infty}^{+\infty} dS \frac{e^{ikS}}{|E-S|^{m+\mu/2}} e^{-i\frac{\pi}{2}(m-\mu/2)\text{sign}(k_1(E-S))} = & \quad (\text{G.0.18}) \\ e^{ikE} \Gamma(1-m-\mu/2) |k|^{m+\mu/2-1} \left[ e^{-i\frac{\pi}{2}(m-\mu/2)\text{sign}(k_1)} e^{-i\frac{\pi}{2}(1-m-\mu/2)\text{sign}(k)} + \right. \\ \left. e^{i\frac{\pi}{2}(m-\mu/2)\text{sign}(k_1)} e^{i\frac{\pi}{2}(1-m-\mu/2)\text{sign}(k)} \right]. \end{aligned}$$

If we plug back this last result into Eq. (G.0.14) we obtain:

$$\begin{aligned} \hat{A}(k_1) = & \frac{1}{2} \Gamma(m-\mu/2) \Gamma(1-m-\mu/2) |k_1|^{\mu/2-m} \hat{L}_{\mu/2}^{C(E),\beta(E)}(k_1) \times & (\text{G.0.19}) \\ & \times \left[ e^{-i\frac{\pi}{2}(m-\mu/2)\text{sign}(k_1)} \int_{-\infty}^{+\infty} \frac{dk}{2\pi} e^{ikE} e^{-i\frac{\pi}{2}(1-m-\mu/2)\text{sign}(k)} |k|^{m+\mu/2-1} \hat{A}(k) \right. \\ & \left. + e^{i\frac{\pi}{2}(m-\mu/2)\text{sign}(k_1)} \int_{-\infty}^{+\infty} \frac{dk}{2\pi} e^{ikE} e^{i\frac{\pi}{2}(1-m-\mu/2)\text{sign}(k)} |k|^{m+\mu/2-1} \hat{A}(k) \right]. \end{aligned}$$

We now define:

$$\begin{aligned} I_+ &= \int_0^{+\infty} \frac{dk}{\pi} e^{ikE} |k|^{m+\mu/2-1} \hat{A}(k), & (\text{G.0.20}) \\ I_- &= \int_{-\infty}^0 \frac{dk}{\pi} e^{ikE} |k|^{m+\mu/2-1} \hat{A}(k), \end{aligned}$$

and we also define  $\hat{A}_+(k_1)$  and  $\hat{A}_-(k_1)$  as the function  $\hat{A}(k_1)$  restricted to the regions  $k_1 > 0$  and  $k_1 < 0$  respectively. Using these definitions we have:

$$\begin{aligned} \hat{A}_+(k_1) &= \frac{1}{2} \Gamma(m-\mu/2) \Gamma(1-m-\mu/2) |k_1|^{\mu/2-m} \hat{L}_{\mu/2}^{C(E),\beta(E)}(k_1) \times (\text{G.0.21}) \\ &\quad \times \left[ \sin\left(\frac{\pi\mu}{2}\right) I_+ + \sin(\pi m) I_- \right], \\ \hat{A}_-(k_1) &= \frac{1}{2} \Gamma(m-\mu/2) \Gamma(1-m-\mu/2) |k_1|^{\mu/2-m} \hat{L}_{\mu/2}^{C(E),\beta(E)}(k_1) \times \\ &\quad \times \left[ \sin(\pi m) I_+ + \sin\left(\frac{\pi\mu}{2}\right) I_- \right]. \end{aligned}$$

Finally, we multiply both  $\hat{A}_+(k_1)$  and  $\hat{A}_-(k_1)$  by  $e^{ik_1 E} |k_1|^{m+\mu/2-1}$  and integrate them over  $dk_1/\pi$ . By defining:

$$\begin{aligned} \ell_+ &= \int_0^{+\infty} \frac{dk_1}{\pi} e^{ik_1 E} |k_1|^{\mu-1} \hat{L}_{\mu/2}^{C(E),\beta(E)}(k_1), & (\text{G.0.22}) \\ \ell_- &= \int_{-\infty}^0 \frac{dk_1}{\pi} e^{ik_1 E} |k_1|^{\mu-1} \hat{L}_{\mu/2}^{C(E),\beta(E)}(k_1), \end{aligned}$$

we finally find:

$$\begin{aligned} I_+ &= \frac{1}{2} \Gamma(m - \mu/2) \Gamma(1 - m - \mu/2) L_+ \left[ \sin\left(\frac{\pi\mu}{2}\right) I_+ + \sin(\pi m) I_- \right] \text{(G.0.23)} \\ I_- &= \frac{1}{2} \Gamma(m - \mu/2) \Gamma(1 - m - \mu/2) L_- \left[ \sin(\pi m) I_+ + \sin\left(\frac{\pi\mu}{2}\right) I_- \right]. \end{aligned}$$

Using the specific form of  $\hat{L}_{\mu/2}^{C(E),\beta(E)}$  it is easy to show that  $L_-^* = L_+$ . The linear system above only have non-trivial solutions different from zero if the determinant of the matrix of the coefficients vanishes. Thus, the condition to have a non-trivial solution compatible with our ansatz of the asymptotic behavior of  $Q(S, \Delta)$  is:

$$K_{m,\mu}^2 \ell_+ \ell_- \left[ s_\mu^2 - s_m^2 \right] - K_{m,\mu} (\ell_+ + \ell_-) s_\mu + 1 = 0, \quad \text{(G.0.24)}$$

where we have used the following definitions:

$$\begin{aligned} K_{m,\mu} &= \frac{\mu}{2} \Gamma\left(m - \frac{\mu}{2}\right) \Gamma\left(1 - m - \frac{\mu}{2}\right), \\ s_\mu &= \sin\left(\frac{\pi\mu}{2}\right), \\ s_m &= \sin(\pi m). \end{aligned}$$

We have obtained in this way the equation (III.4.13) of the main text.



# List of Figures

I.1	The figure shows four localized wave-function for a disordered two dimensional material. The image is by Yang-Zhi Chou and Matthew Foster (Rice University) [53]. . . . .	3
I.2	The localized states appear first in the tails of the spectrum, as we expect intuitively. For a fixed value of the disorder $W < W_c$ , by varying the Fermi energy with respect to the mobility edge, a metal-insulator transition occurs in the system. . . . .	4
I.3	Qualitative sketch of the phase diagram of the Anderson model in the $W$ - $E$ plane. For each value of the disorder $W$ there are two symmetric mobility edges, and when the disorder is increased over a critical value $W_C$ all the spectrum is localized. The dashed lines indicate the boundaries of the spectrum, beyond which the density of states is zero. . . . .	5
I.4	The wave going from A to B interferes constructively with the one going from B to A: the interference effects enhance the probability of backscattering. The figure is taken from [57]. . . . .	6
I.5	The average value of the local density of states $\langle \rho_i \rangle$ can not be used as order parameter for Anderson Localization: as shown in blue in the plot, this quantity is regular and finite in both the extended and the localized phase. Instead, since the local density of states develops heavy tails in the localized phase, its typical value is zero in the localized phase and finite in the extended one, as shown in red in the plot, and is actually the good order parameter to consider. . . . .	8
I.6	Renormalization flow for $d = 1$ , $d = 2$ and $d = 3$ . For $d < 2$ the function $\beta(g)$ is always negative and thus there is no phase transition. For $d = 3$ there is a fixed point $g_c$ where $\beta(g_c) = 0$ : this value $g_c$ is associated to the mobility edge. . . . .	11
I.7	The plot shows the level spacing distribution $p(s)$ in the Poisson case and in the case of the Gaussian Orthogonal Ensemble ( $\beta = 1$ ). The two behaviors are typical of the localized phase and of the extended phase respectively. . . . .	15

I.8	Density profile of the atomic matter wave localized by a laser speckle. The waveguide confines the atoms transversely to the $z$ -axis but they are free to travel along the $z$ direction. A laser beam creates a disorder intensity pattern which varies along $z$ . A small Bose-Einstein condensate, initially confined along $z$ is released, and its expansion stops after about 0.5 s. The stationary density profile which emerges at 0.8, 1, and 2 s is plotted, confirming the localization. The image is by [147]. . . . .	19
II.1	Bethe lattice with connectivity $k + 1 = 3$ . . . . .	33
III.1	The plot shows the distribution of the eigenvalues for Lévy matrices with $\mu = 0.5, 1$ and $1.5$ computed numerically by exact diagonalization. The size of the matrices considered is $2^{11} \times 2^{11}$ and we performed averages over 500 samples. We notice the power-law behavior of the tails of the distributions, characterized by an exponent $1 + \mu$ . As $\mu$ is increased the width of the distribution becomes smaller, approaching the semicircle law in the limit $\mu \rightarrow 2$ . . . . .	57
III.2	Phase diagram of Lévy Matrices in the $\mu - E$ plane. The result is obtained solving the equation (III.4.15) for different values of $\mu$ . . . . .	61
III.3	Typical value of the imaginary part of the diagonal elements of the resolvent for $\mu = 0.5$ , and different energies $E$ in the delocalized phase as a function of the iteration in the population dynamics algorithm. We see that, as the mobility edge $E_C \simeq 3.85$ is reached, the stationary value of $\log(\Im G)$ is reached for smaller and smaller values of $\eta$ . . . . .	67
III.4	Phase diagram obtained in Ref. [38] combining analytical and numerical techniques: for $0 < \mu < 1$ the black curve delimits a region on the left of the $\mu - E$ plane in which eigenstates are localized both following the analytical criterium based on the analysis of the recursion equation for the resolvent, i.e. $\langle \Upsilon_{1/2} \rangle < \infty$ in the thermodynamic limit, and looking numerically at the behavior of the IPR, which stays finite for $N \rightarrow \infty$ . The central region of the phase diagram, delimited by the black curve on the left and by the blue one on the right, is characterized by a mixed behavior: the states are delocalized from the analysis of $\langle \Upsilon_{1/2} \rangle$ , which tends to infinity in the thermodynamic limit, but the numerical study of the IPR shows that $\langle \Upsilon_2 \rangle$ remains finite for $N \rightarrow \infty$ . On the right of the blue curve the states are delocalized both from the numerical observation of the IPR ( $\langle \Upsilon_2 \rangle \rightarrow 0$ for $N \rightarrow \infty$ ) and from the analysis of $\langle \Upsilon_{1/2} \rangle$ , which is infinite in the thermodynamical limit. The numerical study of the distribution of the level spacing $P(s)$ suggests that in the mixed phase a non-universal behavior, intermediate between the GOE-like and the Poisson-like limits emerges. The Poisson-like and the GOE-like behavior characterize instead the localized phase (in black) and the delocalized one (in red) respectively. . . . .	69

III.5 Summary of the analytical results obtained through the computation of the mobility edge, the supersymmetric method and the Dyson Brownian motion argument: for  $1 < \mu < 2$  all states are delocalized for any value of energy in the spectrum, and the system has GOE statistics. For  $0 < \mu < 1$ , there is a critical energy  $E^*(\mu)$  for any value of  $\mu$  separating localized and extended energy in the spectrum. The level statistics is Poisson-like in the localized phase and GOE-like in all the extended phase. . . . . 76

III.6 Gap ratio  $\langle r \rangle$  (top panel) and typical value of the overlap  $q^{\text{typ}}$  (bottom panel) for different system sizes for  $\mu = 1.5$ : the system tends towards the GOE limit, represented by the red dashed curve, even if we cannot observe full convergence for high value of energy with the system sizes considered. . . . . 77

III.7 Probability distribution of the gap ratio  $r$  for different values of energy for  $\mu = 1.5$ : the full convergence towards the GOE limit is observed only for small energies, but it is clear that the system evolves towards this limit for increasing size. . . . . 78

III.8 Wavefunction statistics for  $\mu = 1.5$  for different system sizes and  $E = 0.024$ . The distribution has the stretched exponential behavior (III.9.2), represented by the black dashed curve up to value of  $Nw$  of order one: for larger value of  $Nw$  the distribution is broader than in the GOE case. 80

III.9 Exponents  $\beta$  (continuous lines) and  $\beta'$  (dashed lines) describing the scaling with  $N$  of the typical value of the Inverse Participation Ratio and of the support set as a function of the energy for  $\mu = 1.5$ . . . . . 81

III.10  $\ln(q^{\text{typ}}/q_{\text{GOE}}^{\text{typ}})$  as a function of the energy  $E$  for different system sizes for  $\mu = 0.5$ . . . . . 83

III.11 Exponents  $\beta$  (continuous lines) and  $\beta'$  (dashed lines) describing the scaling with  $N$  of the typical value of the Inverse Participation Ratio and of the support set as a function of the energy for  $\mu = 0.5$ . . . . . 85

III.12 The typical value of the overlap  $q$  is plotted for different energies belonging to the crossover region as a function of the characteristic size: this defines a characteristic length  $N_m$  which governs finite size scaling effects. . . . . 86

III.13 Probability distribution of the gap ratio for  $\mu = 0.5$ , for different system sizes, and for four different values of the energy. The Poisson and GOE counterparts of  $\Pi(r)$  are also shown. Top-left panel:  $E = 0.016$ ; The entire probability distribution is described by the GOE. Top-right panel:  $E = 1.25$ ;  $\Pi(r)$  evolves towards the GOE distribution as  $N$  is increased, although we are not able to observe full convergence. Bottom-left panel:  $E = 2.28$ ;  $\Pi(r)$  seems to be described by a  $N$ -independent non-universal distribution. Bottom-right panel:  $E = 7.68$ ;  $\Pi(r)$  converges to the Poisson distribution for large  $N$ . . . . . 87

III.14  $\log N'_m(E) = -\log(\Im G_{ii}^{\text{typ}} \rho(E)) = -\langle \log \Im G_{ii} \rangle - \log(\langle \Im G \rangle / \pi)$  as a function of  $E$  for  $\mu = 0.5$ . . . . . 88

III.15  $\ln N'_m(E)$  as a function of  $\ln N_m(E)$ . . . . . 89

III.16	Marginal probability distribution of $\ln \Im G$ for different values of the imaginary regulator $\eta$ and for $E = 1.25$ , showing convergence to a stationary $\eta$ -independent distribution for small enough $\eta$ . . . . .	90
III.17	Marginal probability distribution of $\ln \Im G$ for different values of the imaginary regulator $\eta$ and for $E = 5.5$ . In the localized phase the limit $\eta \rightarrow 0^+$ is singular: almost all values of $\Im G_{ii}$ are of order $\eta$ , except extremely rare events described by heavy power-law tails with an exponent $1 + m = 3/2$ whose coefficient vanishes as $\sqrt{\eta}$ . . . . .	91
III.18	Marginal probability distribution of $\ln \Im G$ for different values of the imaginary regulator $\eta$ and for $E = 3.25$ , in the crossover phase. For $\eta > 10^{-13}$ the system behaves as it was localized and non ergodic, showing “singular” power-law tails with an exponent $1 + m$ with $1/2 \lesssim m < 1$ and a cut-off in $\Im G = 1/\eta$ . Convergence to a stationary non-singular distribution is achieved for $\eta < 10^{-13}$ . . . . .	92
III.19	Wavefunction statistics for $\mu = 0.5$ for different system sizes and $E = 0.016$ . For very small values of $Nw$ the distribution has the power-law behavior with exponent $1/2$ corresponding to the limit of small weights of the Porter-Thomas distribution. For larger $Nw$ , until values of $O(1)$ , the distribution still exhibits power-law behavior but with an exponent $(1 + \mu)/2$ . . . . .	93
III.20	Wavefunction statistics for $\mu = 0.5$ in the crossover region ( $E = 1.25$ ) for different system sizes: the limit of small weights coincides with the one of the Porter-Thomas distribution. For intermediate value of $Nw$ we have a power-law behavior with exponent $(1 + \mu)/2$ , while the tails of the distribution seem to have a power-law shape as in the localized phase, but the fit get worse increasing the system size. . . . .	94
III.21	Wavefunction statistics for different system sizes for $\mu = 0.5$ in the deeply localized phase ( $E = 7.68$ ): the limit of extremely small weights is the same as that of the Porter Thomas distribution, with an exponent $1/2$ . The regime of intermediate value of $Nw$ is characterized by a power-law tail with an exponent $(1 + \mu)/2$ , while the tails of the distribution also exhibit a power-like behavior with an exponent $1 + (\mu/2)$ . . . . .	95
III.22	Analysis of multifractal spectrum $f(\alpha)$ for different energy and different system sizes. For small energies (top-left panel) $f(\alpha)$ evolves towards a $\delta$ -function concentrated in $\alpha = 1$ . In the crossover region (top-right panel and bottom-left panel) the curves corresponding to different sizes cross at a point $\alpha < 1$ , which however drifts with increasing $N$ : this effect can be studied in a similar way as we have analyzed the behavior of $q^{typ}$ and $\langle r \rangle$ . In the deeply localized phase (bottom-right panel), $f(\alpha)$ becomes broader and seems to converge to a $N$ -independent distribution. . . . .	98
III.23	Characteristic length extracted from the analysis of the multifractal spectrum $f(\alpha)$ and compared with the characteristic length $N_m$ obtained by the analysis of the overlap $q^{typ}$ . . . . .	99

- IV.1  $\langle \ln \text{Im}G(x) \rangle$  as a function of  $x$  in 6 dimensions, for  $L = 6$  and for several values of the disorder, showing that  $\xi_{1d}$  can be measured from Eq. (IV.1.4) by linear fitting of the data at large enough  $x$ . . . . . 104
- IV.2 Left panel:  $\lambda_{1d}$  as a function of the disorder  $W$  for several system sizes  $L$  from 2 to 18 for  $d = 4$ . The vertical dashed line spots the position of the critical point,  $W_c \simeq 34.5$ . Top-right panel: Finite size scaling of the same data for  $L$  from 10 to 18, showing data collapse for  $\nu \simeq 1.11$ . Bottom-right panel:  $\psi f_1 = (\lambda_{1d} - f_\infty)/L^y$  as a function of the scaling variable  $(W - W_c)L^{1/\nu}$  for different sizes  $L$  from 2 to 7, showing data collapse for the same value as before of  $W_c$  and  $\nu$  and for  $y \simeq -1$ . . . . . 106
- IV.3 Left panel:  $\lambda_{1d}$  as a function of the disorder  $W$  for several system sizes  $L$  from 2 to 9 for  $d = 5$ . The vertical dashed line spots the position of the critical point,  $W_c \simeq 57.5$ . Top-right panel: Finite size scaling of the same data for  $L$  from 6 to 9, showing data collapse for  $\nu \simeq 0.96$ . Bottom-right panel:  $\psi f_1 = (\lambda_{1d} - f_\infty)/L^y$  as a function of the scaling variable  $(W - W_c)L^{1/\nu}$  for different sizes  $L$  from 2 to 6, showing data collapse for the same value as before of  $W_c$  and  $\nu$  and for  $y \simeq -1.2$ . . . . . 107
- IV.4 Left panel:  $\lambda_{1d}$  as a function of the disorder  $W$  for several system sizes  $L$  from 2 to 6 for  $d = 6$ . The vertical dashed line spots the position of the critical point,  $W_c \simeq 83.5$ . Top-right panel: Finite size scaling of the same data for  $L$  from 4, 5 and 6, showing data collapse for  $\nu \simeq 0.84$ . Bottom-right panel:  $\psi f_1 = (\lambda_{1d} - f_\infty)/L^y$  as a function of the scaling variable  $(W - W_c)L^{1/\nu}$  for different sizes  $L$  from 2 to 5, showing data collapse for the same value as before of  $W_c$  and  $\nu$  and for  $y \simeq -1.4$ . . . . . 109
- IV.5  $\langle r \rangle$  (top-left) and  $q^{typ}$  (bottom-left) as a function of the disorder  $W$  for several system sizes  $L$  from 4 to 30 for  $d = 3$ . The horizontal dashed lines correspond to the reference GOE and Poisson asymptotic values. The vertical dashed line spots the position of the Anderson Localization transition,  $W_c \simeq 16.35$ . Finite size scaling of the same data (top and bottom-right panels) showing data collapse obtained for  $\nu \simeq 1.57$ . Finite-size corrections to Eq. (IV.1.10) are observed at small sizes (open symbols), and can be described by Eq. (IV.1.8) with  $y \simeq -1$ . 111
- IV.6  $\langle r \rangle$  (top-left) and  $q^{typ}$  (bottom-left) as a function of the disorder  $W$  for several system sizes  $L$  from 3 to 13 for  $d = 4$ . The horizontal dashed lines correspond to the reference GOE and Poisson asymptotic values. The vertical dashed line spots the position of the Anderson Localization transition,  $W_c \simeq 34.5$ . Finite size scaling of the same data (top and bottom-right panels) showing data collapse obtained for  $\nu \simeq 1.11$ . Finite-size corrections to Eq. (IV.1.10) are observed at small sizes (open symbols), and can be described by Eq. (IV.1.8) with  $y \simeq -1$ . . . . . 113

- IV.7  $\langle r \rangle$  (top-left) and  $q^{typ}$  (bottom-left) as a function of the disorder  $W$  for several system sizes  $L$  from 3 to 8. The horizontal dashed lines correspond to the reference GOE and Poisson asymptotic values. The vertical dashed line spots the position of the Anderson Localization transition,  $W_c \simeq 57.5$  for  $d = 5$ . Finite size scaling of the same data (top and bottom-right panels) showing data collapse obtained for  $\nu \simeq 0.96$ . Finite-size corrections to Eq. (IV.1.10) are observed at small sizes (open symbols), and can be described by Eq. (IV.1.8) with  $y \simeq -1.2$ . . . . . 114
- IV.8 Left panel:  $\langle r \rangle$  as a function of the disorder  $W$  for several system sizes  $L$  from 2 to 6 for  $d = 6$ . The horizontal dashed lines correspond to the reference GOE and Poisson asymptotic values. The vertical dashed line spots the position of the Anderson Localization transition,  $W_c \simeq 83.5$ . Top-right panel: Finite size scaling of the same data for the largest system sizes only, showing data collapse for  $\nu \simeq 1.19$ . Bottom-right panel:  $\psi g_1 = (\langle r \rangle - g_\infty)/L^y$  as a function of the scaling variable  $(W - W_c)L^{1/\nu}$  for different sizes  $L$  from 2 to 5, showing a reasonably good data collapse for the same value as before of  $W_c$  and  $\nu$ , and for  $y \simeq -1.4$ . 115
- IV.9 Left panel: Flowing fractal exponent  $\beta$  describing the scaling of the typical value of the IPR with the system size for  $d = 4$ . The vertical dashed black line corresponds to the critical disorder  $W_c \simeq 34.5$ . Right panel: Finite size scaling of the same data showing a reasonably good data collapse obtained for  $\nu \simeq 1.11$ . Strong finite-size corrections to the one-parameter scaling are observed at small sizes (open symbols), and can be described by Eq. (IV.1.8) with  $y \simeq -1$ . . . . . 117
- IV.10 Sketch of the SDRG decimation procedure for a site (top), and a bond (bottom) transformation. Dotted blue lines represent pre-existing hopping amplitudes before decimation. Solid blue lines represent new or renormalized bonds. The on site energies of all the neighbors of the decimated sites (blue circles) are renormalized as well. . . . . 118
- IV.11 Quasi-1d dimensionless localization length,  $\lambda_{1d}$ , obtained using the SDRG procedure for different values of  $k_{\max}$ , at the Anderson Localization critical point,  $W_c \simeq 83.5$ , in 6 dimensions, and for  $L = 3$  (blue circles) and  $L = 6$  (red squares). The horizontal blue (resp., red) solid and dashed lines corresponds to the average value of  $\lambda_{1d}$  and its fluctuations computed using the transfer matrix method for  $L = 3$  (resp.,  $L = 6$ ), showing that for  $k_{\max} \gtrsim 240$  the approximate SDRG results converge, within our numerical accuracy, to the exact values. . . . . 120

IV.12 Bottom-left and bottom-right panels: The quasi-stationary distributions  $R_{\tau_*}(t)$  and  $Q_{\tau_*}(\epsilon)$  at the Anderson Localization critical points in dimensions from 3 to 6. The system size is  $L = 33$  in  $3d$ ,  $L = 14$  in  $4d$ ,  $L = 8$  in  $5d$ , and  $L = 6$  in  $6d$ , in such a way that the total number of sites is approximately the same,  $N \sim 4 \cdot 10^4$ , in all dimensions. The quasi-stationary state is reached for a RG time  $\tau_*$  such that the number of sites left in the system are approximately 1/8 of the initial ones in  $3d$ , 1/16 in  $4d$ , 1/26 in  $5d$ , and 1/40 in  $6d$ . The value of  $k_{\max}$  is set to 360 in all dimensions. Top-panel: The same data of the bottom-left panel plotted in a log-log scale, showing the power law behavior of  $R_{\tau_*}(t) \sim t^{-\gamma}$  with  $\gamma \simeq 2$  (black dashed line), for  $t$  smaller than a cut-off of  $O(1)$ . . . . 123

IV.13 Numerical values of the inverse of the critical exponent  $\nu$  as a function of  $1/d$  in dimensions from 3 to 6 (blue circles), showing a smooth behavior interpolating from  $\nu \rightarrow \infty$  in  $d = 2$  to  $\nu = 1/2$  in  $d \rightarrow \infty$  [166]. The turquoise dashed line shows the predictions of the self-consistent theory of [174], with  $d_u = 4$ . The dashed-dotted magenta line corresponds to the lower bound  $\nu \geq 2/d$  provided by the Harris criterion [171]. The red solid line shows the dimensional dependence of  $\nu$  obtained from a perturbative analysis of the NL $\sigma$ M to five-loops in  $\epsilon = d - 2$  [88, 89], given by equation. (IV.3.1). . . . . 124

IV.14 Dimensional dependence of  $\langle r_c \rangle$  (top-left panel),  $q_c^{typ}$  (bottom-left panel),  $(\lambda_{1d})_c$  (top-right panel), and  $\beta_c$  at the Anderson Localization critical point as a function of  $1/d$ . The dashed horizontal red lines correspond to the reference GOE value, while the dashed black one to the Poisson value. . . . . 126

IV.15 Critical value of the disorder strength,  $W_c$  divided by  $4(2d - 1)$ , as a function of  $1/\log(2d - 1)$ . The dashed black lines corresponds to the asymptotic exact behavior on tree-like structures in the large connectivity limit. . . . . 127

IV.16 Re-scaled singularity spectrum  $f(\alpha)/d$  as a function of  $\alpha/d$  at the AL critical point in dimensions from 3 to 5. The dashed black line shows  $f(\alpha)$  obtained at the Anderson transition of the Anderson model on random regular graphs of connectivity 3. . . . . 129

A.1 Definition of amplitudes  $A_1, A_2, B_1, B_2$ . . . . . 135

A.2 Sketch of a quasi-one dimensional system with cross section  $L^{(d-1)}$  propagating along the  $x$  direction. . . . . 136

B.1 Multifractal electron wave-function. The figure is from <https://www.int.kit.edu/918.php>. . . . . 142

B.2 Plot of the multifractal spectrum  $f(\alpha)$ . In the metallic phase  $f(\alpha)$  is concentrated at  $\alpha = d$ . At the critical point it acquires a finite width, with a maximum which shift to  $\alpha > d$ . . . . . 143



# Bibliography

- [1] F. Bloch, Z. Phys. **52**, 555 (1928).
- [2] P. W. Anderson, Phys. Rev. **109**, 1492 (1958).
- [3] N. F. Mott and W. D. Twose, Adv. Phys. **10**, 107 (1961).
- [4] R. E. Borland, Proc. R. Soc. London A **274**, 529 (1963).
- [5] V. L. Berezinskii, Sov. Phys.-JETP **38**, 620 (1974).
- [6] F. J. Wegner, Z. Phys. B **25**, 327 (1976).
- [7] E. Abrahams, P. W. Anderson, D. Licciardello, and T. V. Ramakrishnan, Phys. Rev. Lett. **42**, 673 (1979).
- [8] R. Abou-Chacra, P. W. Anderson, and D. J. Thouless, J. Phys. C: Solid St. Phys. **6**, 1734 (1973).
- [9] F. J. Wegner, Z. Phys. B **35**, 207 (1979).
- [10] A. MacKinnon and B. Kramer, Phys. Rev. Lett. **47**, 1546 (1981).
- [11] B. Kramer, M. Schreiber, and A. MacKinnon, Z. Phys. B **56**, 297 (1984).
- [12] M. Schreiber, B. Kramer, and A. MacKinnon, J. Phys. C: Solid St. Phys. **17**, 4111 (1984).
- [13] B. Kramer, K. Broderix, A. MacKinnon, and M. Schreiber, Physica A **167**, 163 (1990).
- [14] B. I. Shklovskii, B. Shapiro, B. R. Sears, P. Lambrianides, and H. B. Shore, Phys. Rev. B **47**, 11487 (1993).
- [15] E. Hofstetter and M. Schreiber, Phys. Rev. B **48**, 16979 (1993).
- [16] I. K. Zharekeshev and B. Kramer, Phys. Rev. B **51**, 17239 (1995).
- [17] I. K. Zharekeshev and B. Kramer, Phys. Rev. Lett. **79**, 717 (1997).
- [18] I. K. Zharekeshev and B. Kramer, Ann. Phys. (Leipzig) **7**, 442 (1998).
- [19] I. Varga, E. Hofstetter, M. Schreiber, and J. Pipek, Phys. Rev. B **52**, 7783 (1995).

- [20] A. Rodriguez, L. J. Vasquez, K. Slevin, and R. A. Römer, *Phys. Rev. Lett.* **105**, 046403 (2010).
- [21] A. Rodriguez, L. J. Vasquez, K. Slevin, and R. A. Römer, *Phys. Rev. B* **84**, 134209 (2011).
- [22] M. Schreiber and H. Grussbach, *Phys. Rev. Lett.* **67**, 607 (1991).
- [23] M. Janssen, *Int. J. Mod. Phys. B* **8**, 943 (1994).
- [24] H. Grussbach and M. Schreiber, *Phys. Rev. B* **51**, 663 (1995).
- [25] L. J. Vasquez, A. Rodriguez, and R. A. Römer, *Phys. Rev. B* **78**, 195106 (2008).
- [26] M. V. Berry and M. Tabor, *Proc. R. Soc. London A* **356**, 375 (1977).
- [27] O. Bohigas, M. J. Giannoni, and C. Smith, *Phys. Rev. Lett.* **52**, 1 (1984).
- [28] M. Srednicki, *Phys. Rev. E* **50**, 888 (1994).
- [29] D. E. Logan and P. G. Wolynes, *J. Chem. Phys.* **93**, 4994 (1990).
- [30] A. D. Mirlin and Y. V. Fyodorov, *Nucl. Phys. B* **366**, 507 (1991).
- [31] A. D. Mirlin and Y. V. Fyodorov, *J. Phys. A: Math. Gen.* **24**, 2273 (1991).
- [32] A. D. Mirlin and Y. V. Fyodorov, *Phys. Rev. Lett.* **67**, 2049 (1991).
- [33] A. D. Mirlin and Y. V. Fyodorov, *J. Phys. I France* **2**, 1571 (1992).
- [34] K. B. Efetov, *Sov. Phys.-JETP* **61**, 606 (1985).
- [35] K. B. Efetov, *Sov. Phys.-JETP* **65**, 360 (1987).
- [36] M. R. Zirnbauer, *Phys. Rev. B* **34**, 6394 (1986).
- [37] M. R. Zirnbauer, *Nucl. Phys. B* **265**, 375 (1986).
- [38] P. Cizeau and J.-P. Bouchaud, *Phys. Rev. E* **50**, 1810 (1994).
- [39] G. Biroli, A. C. Ribeiro-Teixeira, and M. Tarzia, *arXiv:1211.7334* (2012).
- [40] A. De Luca, A. Scardicchio, V. E. Kravtsov, and B. L. Altshuler, *arXiv:1401.0019* (2013).
- [41] A. De Luca, B. L. Altshuler, V. E. Kravtsov, and A. Scardicchio, *Phys. Rev. Lett.* **113**, 046806 (2014).
- [42] K. Tikhonov, A. Mirlin, and M. Skvortsov, (2016), *arXiv:1604.05353*.
- [43] K. S. Tikhonov and A. D. Mirlin (2016), *arXiv:1608.00331* .
- [44] B.L.Altshuler, E.Cuevas, L.B.Ioffe, and V.E.Kravtsov (2016), *arXiv:1605.02295*.
- [45] B. L. Altshuler, L. B. Ioffe, and V. E. Kravtsov (2016), *arXiv:16010.00758*.

- [46] I. García-Mata, O. Giraud, B. Georgeot, J. Martin, R. Dubertrand, and G. Lemarié (2016), arXiv:1609.05857.
- [47] B. L. Altshuler, Y. Gefen, A. Kamenev, and L. Levitov, *Phys. Rev. Lett.* **78**, 2803 (1997).
- [48] D. M. Basko, I. L. Aleiner, and B. L. Altshuler, *Annals of Physics* **321**, 1126 (2006).
- [49] A. Sommerfeld, *Naturwissenschaften* **15**, 825 (1927).
- [50] A. Einstein, *Annalen der Physik* **17**, 549 (1905).
- [51] E. Akkermans and G. Montambaux, Mesoscopic Physics of Electrons and Photons (2007).
- [52] G. Feher, *Phys. Rev.* **114**, 1219 (1959).
- [53] Y. Z. Chou and M. Foster, “<http://news.rice.edu/2016/01/21/matthew-foster-wins-nsf-career-award-2>,” (2016).
- [54] I. M. Lifshitz, *Sov. Phys. Uspekhi* **7**, 549 (1965).
- [55] R. P. Feynman, *Rev. Mod. Phys.* **20**, 367 (1948).
- [56] L. P. Gorkov, A. I. Larkin, and D. E. Khmel'nitskii, *JETP Lett.* **30**, 228 (1979).
- [57] A. Lagendijk, B. Van Tiggelen, and D. S. Wiersma, “Fifty years of anderson localization,” *Phys. Today* **62**, 24 (2009).
- [58] M. Aizenman and S. Molchanov, *Comm. in Math. Phys.* **157**, 245 (1993).
- [59] J. T. Edwards and D. J. Thouless, *J. Phys. C: Solid St. Phys.* **5**, 807 (1972).
- [60] D. Licciardello and D. J. Thouless, *J. Phys. C* **8**, 4157 (1975).
- [61] P. Marcoš, *Acta Physica Slovaca* **56**, 561 (2006).
- [62] M. L. Metha, Random Matrices and the Statistical Theory of Energy Levels (1967), new york: academic ed.
- [63] K. Ishii, *Progr. Theor. Phys. Suppl.* **53**, 77 (1973).
- [64] B. Derrida, K. Mecheri, and J. L. Pichard, *J. Physique* **48**, 733 (1987).
- [65] J. L. Muttalib, K. A. ad Pichard and S. A. D., *Phys. Rev. Lett.* **59**, 2475 (1987).
- [66] S. Feng and J. L. Pichard, *Phys. Rev. Lett.* **63**, 753 (1991).
- [67] A. Comtet, C. Texier, and Y. Tourigny, *J. Phys. A: Math. Teor.* **46**, 254003 (2013).
- [68] S. A. Molcanov, *Math USSR Izv.* **12**, 69 (1978).

- [69] H. Kunz and B. Souillard, *Commun. Math. Phys.* **78**, 201 (1980).
- [70] F. Delyon, H. Kunz, and B. Souillard, *J. Phys. A: Math. Gen.* **16**, 25 (1983).
- [71] B. Kramer and A. MacKinnon, *Rep. Progr. Phys.* **56**, 1469 (1993).
- [72] E. Abrahams and T. V. Ramakrishnan, *J. Non-Cryst. Solids* **35**, 15 (1980).
- [73] E. Abrahams and T. V. Ramakrishnan, *Phil. Mag.* **42**, 827 (1980).
- [74] D. J. Thouless, *Phys. Rev. Lett.* **39**, 1167 (1977).
- [75] D. J. Thouless, *Solid State Commun.* **34**, 683 (1980).
- [76] P. W. Anderson, E. Abrahams, and T. V. Ramakrishnan, *Phys. Rev. Lett.* **43**, 718 (1979).
- [77] B. L. Altshuler and Aronov, Electron-Electron Interactions in Disordered Systems (Efros, A. L. and Pollak, M., 1985).
- [78] G. M. Minkov, A. V. Rut, O. E. ad Germanenko, A. A. Sherstobitov, B. N. Zvonkov, E. A. Uskova, and A. A. Birukov, *Phys. Rev. B* **64**, 193309 (2001).
- [79] G. J. Dolan and G. D. Osheroff, *Phys. Rev. Lett.* **43**, 721 (1979).
- [80] S. Kobayashi, F. Komori, Y. Ootuka, and W. Sasaki, *J. Phys. Soc. Japan* **49**, 1635 (1980).
- [81] M. E. Fisher and K. F. Wilson, *Phys. Rev. Lett.* **28**, 548 (1972).
- [82] K. B. Efetov, A. I. Larkin, and D. E. Khmel'nitskii, *Sov. Phys.-JETP* **52**, 568 (1980).
- [83] K. Jüngling and R. Oppermann, *Z. Phys. B: Condens. Matter* **38**, 93 (1980).
- [84] L. Schaefer and F. J. Wegner, *Z. Phys. B: Condens. Matter* **38**, 113 (1980).
- [85] K. B. Efetov, *Adv. Phys.* **32**, 53 (1983).
- [86] K. B. Efetov, Supersymmetry in Disorder and Chaos (Cambridge, England, 1997).
- [87] K. B. Efetov, *Zh. Eksp. Teor. Fiz.* **82**, 872 (1982).
- [88] F. J. Wegner, *Nucl. Phys. B* **316**, 623 (1989).
- [89] S. Hikami, *Phys. Rev. B* **24**, 2671 (1981).
- [90] M. Schreiber and H. Grussbach, *Phys. Rev. Lett.* **76**, 1687 (1996).
- [91] K. Slevin and T. Ohtsuki, *Phys. Rev. Lett.* **82**, 382 (1999).
- [92] K. Slevin and T. Ohtsuki, *New. J. Phys.* **16**, 015012 (2014).

- [93] F. J. Wegner, *Z. Phys. B* **36**, 209 (1980).
- [94] C. Castellani and L. Peliti, *J. Phys. A* **19**, L429 (1986).
- [95] F. J. Wegner, *Nucl. Phys. B* **280**, 210 (1987).
- [96] A. Mildenberger, F. Evers, and A. D. Mirlin, *Phys. Rev. B* **66**, 033109 (2002).
- [97] S. N. Evangelou and T. Ziman, *J. Phys. C* **20**, L235 (1987).
- [98] T. Ando, *Phys. Rev. B* **40**, 5325 (1989).
- [99] A. D. Mirlin, Y. Fyodorov, D. F.-M., J. Quezada, and T. H. Seligman, *Phys. Rev. E* **54**, 3221 (1996).
- [100] F. Evers and A. D. Mirlin, *Phys. Rev. Lett.* **84**, 3690 (2000).
- [101] A. D. Mirlin, *Phys. Rep.* **326**, 259 (2000).
- [102] A. D. Mirlin and F. Evers, *Phys. Rev. B* **62**, 7920 (2000).
- [103] V. E. Kravtsov, I. M. Khaymovich, E. Cuevas, and M. Amini, *New. J. Phys.* **17**, 122002 (2015).
- [104] D. Facchetti, P. Vivo, and G. Biroli, *Eur. Phys. Lett.* **115**, 47003 (2016).
- [105] E. P. Wigner, *Proc. Cambr. Philos. Soc.* **50**, 790 (1951).
- [106] M. L. Mehta, Random Matrices (Elsevier-Academic Press, New York, 2004), 3rd ed.
- [107] S. N. Majumdar, “Random matrices, the ulam problem, directed polymers & growth models, and sequence matching,” in “Les Houches Summer School on Complex Systems,” (2006).
- [108] T. Guhr, A. Mueller-Groeling, and H. A. Weidenmueller, *Phys. Rep.* **299**, 189 (1998).
- [109] A. J. Bray and G. J. Rodgers, *Phys. Rev. B* **52**, 11461 (1988).
- [110] J.-Y. Fortin, *J. Phys. A: Math. Gen.* **52**, L57 (2005).
- [111] E. Telatar, *Eur. Trans. Telecommun.* **10**, 585 (1999).
- [112] L. Laloux, P. Cizeau, B. J.-P., and M. Potters, *Phys. Rev. Lett.* **83**, 1467 (1999).
- [113] F. Luo, P. Srimani, and J. Zhou, Handbook of Data Intensive Computing (2011).
- [114] F. J. Dyson, *Commun. Math. Phys.* **19**, 235 (1970).
- [115] M. L. Mehta, *Commun. Math. Phys.* **20**, 245 (1971).
- [116] E. Wigner, *Ann. of Math.* **62**, 548 (1955).

- [117] K. Johansson, *Commun. Math. Phys.* **215**, 683 (2001).
- [118] L. Erdos, J. A. Ramirez, B. Schlein, and H.-T. Yau (2009), arXiv:0905:2089.
- [119] L. Erdos, S. Péché, J. Ramirez, B. Schlein, and H.-T. Yau, *Comm. Pure Appl. Math.* **63**, 895 (2010).
- [120] T. Tao and V. Vu (2009), arXiv:0906.0510.
- [121] L. Erdos, H.-T. Yau, and J. Yin (2010), arXiv:1001.3453.
- [122] A. Knowles and J. Yin (2011), arXiv:1102.0057.
- [123] L. Erdos, B. Schlein, and H.-T. Yau (2008), arXiv:0803.0542.
- [124] L. Erdős, B. Schlein, and H.-T. Yau (2007), arXiv:0711.1730.
- [125] L. Erdos, B. Schlein, and H.-T. Yau (2008), arXiv:0811.2591.
- [126] L. Erdos, H.-T. Yau, and J. Yin (2010), arXiv:1007.4652.
- [127] J. Frölich and T. Spencer, *Commun. Math. Phys.* **88**, 151 (1983).
- [128] J. Frölich, F. Martinelli, E. Scoppola, and T. Spencer, *Commun. Math. Phys.* **101**, 21 (1985).
- [129] N. Minami, *Commun. Math. Phys.* **177**, 709 (1996).
- [130] A. Elgart, *Duke Math. J.* **146**, 331 (2009).
- [131] A. Klein, *Math. Res. Lett.* **1**, 399 (1994).
- [132] M. Aizenman, R. Sims, and S. Warzel, *Commun. Math. Phys.* **264**, 371 (2006).
- [133] R. Froese, D. Hasler, and W. Spitzer, *J. Funct. Anal.* **230**, 184 (2006).
- [134] A. Kaneko and T. Ohtsuki, *J. Phys. Soc. Jpn.* **68**, 1488 (1999).
- [135] F. Milde, R. A. Römer, and M. Schreiber, *Phys. Rev. B* **61**, 6028 (2000).
- [136] V. Oganesyan and D. A. Huse, *Phys. Rev. B* **75**, 155111 (2007).
- [137] M. V. Berry, *Proc. R. Soc. London A* **400**, 229 (1985).
- [138] A. V. Andreev, O. Agam, B. D. Simons, and B. L. Altshuler, *Phys. Rev. Lett.* **76**, 3947 (1996).
- [139] R. Nandkishore and D. A. Huse, *Ann. Rev. Cond. Mat. Phys.* **6**, 15 (2015).
- [140] P. Cain, R. A. Römer, and M. Schreiber, *Ann. Phys. (Leipzig)* **8**, SI-33 (1999).
- [141] B. Bulka, B. Kramer, and A. MacKinnon, *Z. Phys. B: Condens. Matter* **60**, 13 (1985).

- [142] A. G. Aronov, V. E. Kravtsov, and I. V. Lerner, *Phys. Rev. Lett.* **74**, 1174 (1995).
- [143] Y. Ueoka and K. Slevin, *J. Phys. Soc. Jpn.* **83**, 084711 (2014).
- [144] A. M. García-García and E. Cuevas, *Phys. Rev. B* **75**, 174203 (2007).
- [145] G. A. Thomas and M. A. Paalannen, Localisation Interaction and Transport Phenomena, vol. 61 of Springer Series in Solid State Science (Berlin:Springer, 1985).
- [146] S. Katsumoto, Localisation 1990 (Bristol: Insistute of Physics, 1991).
- [147] A. Aspect and M. Inguscio, “Anderson localization of ultracold atoms,” *Physics Today* **62**, 30 (2009).
- [148] G. Bergmann, *Phys. Rep.* **107**, 1 (1984).
- [149] E. N. Economou and C. M. Soukoulis, *Phys. Rev. B* **40**, 7977 (1989).
- [150] P. Sheng and Y.-C. Zhang, *Phys. Rev. Lett.* **57**, 1878 (1986).
- [151] M. Störzer, P. Gross, C. M. Aegerter, and G. Maret, *Phys. Rev. Lett.* **96**, 063904 (2006).
- [152] T. Schwartz, G. Bartal, S. Fishman, and B. Segev, *Nature (London)* **446**, 52 (2007).
- [153] C. Dembowski, H. D. Gräf, R. Hofferbert, H. Rehfeld, A. Richter, and T. Weiland, *Phys. Rev. E* **60**, 3942 (1999).
- [154] P. Wiersma, D. S. ad Bartolini, A. Lagendijk, and R. Righini, *Nature* **390**, 671 (1997).
- [155] H. Hu., A. Strybulevych, J. H. Page, S. E. Skipetrov, and B. A. Van Tiggelen, *Nat. Phys.* **4**, 945 (2008).
- [156] G. Casati, B. V. Chirikov, F. M. Izrailev, and J. Ford, Stochastic Behaviour in classical and Quantum Hamiltonian Systems, vol. 93 of Lecture Notes in Physics (1979), springer, new york ed.
- [157] S. Fishman, D. R. Grempel, and R. E. Prange, *Phys. Rev. Lett.* **49**, 509 (1982).
- [158] F. L. Moore, J. C. Robinson, C. Bharucha, P. E. Williams, and M. G. Raizen, *Phys. Rev. Lett.* **73**, 2974 (1994).
- [159] J. Billy, V. Josse, Z. Zuo et al., *Nature* **453**, 891 (2008).
- [160] G. Roati, C. D’Errico, L. Fallani et al., *Nature* **453**, 895 (2008).
- [161] G. Casati, I. Guarneri, and D. L. Shepelyansky, *Phys. Rev. Lett.* **62**, 345 (1989).
- [162] J. Chabé, G. Lemarié, D. Grémaud et al., *Phys. Rev. Lett.* **101**, 255702 (2008).

- [163] G. Lemarié, D. Grémaud, and D. Delande, *Europhys. Lett.* **87**, 37007 (2009).
- [164] F. Jendrzejewski, A. Bernard, K. Müller *et al.*, *Nature Physics* **8**, 398 (2012).
- [165] S. S. Kondov, W. R. McGehee, J. J. Zirbel, and B. De Marco, *Science* **334**, 66 (2011).
- [166] A. D. Mirlin and Y. Fyodorov, *Phys. Rev. Lett.* **72**, 526 (1994).
- [167] A. D. Mirlin and Y. Fyodorov, *J. Phys. I* **4**, 655 (1994).
- [168] C. Castellani, C. Di Carlo, and L. Peliti, *J. Phys. A* **19**, L1099 (1986).
- [169] D. J. Thouless, *Journal of Physics C: Solid State Physics* **9**, L603 (1976).
- [170] T. Lukes, *Journal of Physics C: Solid State Physics* **12**, L797 (1979).
- [171] H. A. and T. Lubensky, *Phys. Rev. B* **23**, 2640 (1981).
- [172] J. Straley, *Phys. Rev. B* **28**, 5393 (1983).
- [173] I. Suslov, *Journal of Experimental and Theoretical Physics Letters* **63**, 895 (1996).
- [174] D. Vollhardt and P. Wölfle, *Phys. Rev. Lett.* **45**, 482 (1980).
- [175] D. Vollhardt and P. Wölfle, *Phys. Rev. B* **22**, 4666 (1980).
- [176] R. Abou-Chacra, P. W. Anderson, and D. J. Thouless, *J. Phys. C* **6**, 1734 (1973).
- [177] S. M. Girvin and M. Jonson, *Phys. Rev. B* **22**, 3583 (1980).
- [178] M. Aizenman and S. Warzel, *J. of the Europ. Math. Soc.* **15**, 1167 (2013).
- [179] M. Aizenman and S. Warzel, *Europhys. Lett.* **96**, 37004 (2011).
- [180] K. B. Efetov, *Zh. Eksp. Teor. Fiz.* **94**, 357–369 (1988).
- [181] K. B. Efetov, *Physica A* **167**, 119 (1990).
- [182] A. D. Mirlin and Y. Fyodorov, *J. Phys. I France* **2**, 1571 (1992).
- [183] E. Tarquini, G. Biroli, and M. Tarzia, *Phys. Rev. Lett.* **116**, 010601 (2016).
- [184] N. F. Mott, *Journal of Non-Crystalline Solids* **1**, 1 (1968).
- [185] N. C. Wormald, “Models of random regular graphs,” in “Surveys in Combinatorics,” , vol. 276, J. D. Lamb and D. A. Preece, eds. (London Mathematical Society Lecture Note Series, 1999), p. 239.
- [186] G. Biroli, G. Semerjian, and M. Tarzia, *Prog. Theor. Phys. Suppl.* **184**, 187 (2010).
- [187] C. Monthus and T. Garel, *J. Phys. A: Math. Teor.* **44**, 145001 (2011).

- [188] F. Evers and A. D. Mirlin, *Rev. Mod. Phys.* **80**, 1355 (2008).
- [189] D. J. Thouless, *J. Phys. C: Solid St. Phys.* **3**, 1559 (1970).
- [190] D. J. Thouless, “Anderson localization in the seventies and beyond,” in “Fifty Years of Anderson Localization,” , E. Abrahams, ed. (2012), chap. 2.
- [191] E. N. Economou, Green’s Functions in Quantum Physics (2006), springer series in solid-state sciences ed.
- [192] D. J. Thouless, *Phys. Rep.* **13**, 1167 (1974).
- [193] D. Weaire and A. R. Williams, *J. Phys. C: Solid St. Phys.* **10**, 1239 (1977).
- [194] M. Mézard, G. Parisi, and M. A. Virasoro, Spin Glass Theory and Beyond, vol. 9 of World Scientific Lecture Notes in Physics (World Scientific Pub Co Inc., 1987).
- [195] M. Mézard and G. Parisi, *Eur. Phys. J. B* **20**, 217 (2001).
- [196] T. Rogers and I. P. Castillo, *Phys. Rev. E* **20**, 012101 (2009).
- [197] F. Pietracaprina, V. Ros, and A. Scardicchio, *Phys. Rev. B* **93**, 054201 (2016).
- [198] V. Bapst, *J. Math. Phys.* **55**, 092101 (2014).
- [199] K. B. Efetov, *Zh. Eksp. Teor. Fiz.* **83**, 33 (1982).
- [200] K. B. Efetov and A. I. Larkin, *Zh. Eksp. Teor. Fiz.* **85**, 764 (1983).
- [201] Berezin, The Method of Second Quantization (New York, 1966).
- [202] L. Erdoős and A. Rényi, *Publ. Math. Debrecen* **6**, 290 (1959).
- [203] L. Erdoős and A. Rényi, *Magyar Tud. Akad. Mat. Kutató Int. Közl.* **5**, 17 (1960).
- [204] L. Viana and A. J. Bray, *J. Phys. C* **18**, 3037 (1985).
- [205] I. Kanter and H. Sompolinsky, *Phys. Rev. Lett.* **58**, 164 (1987).
- [206] G. J. Rodgers and A. J. Bray, *Phys. Rev. B* **37**, 3557 (1988).
- [207] G. J. Rodgers and C. De Dominicis, *J. Phys. A* **23**, 1567 (1990).
- [208] Y. Kim and A. B. Harris, *Phys. Rev. B* **31**, 7393 (1985).
- [209] S. Chandrasekhar, *Rev. Mod. Phys.* **15**, 1 (1943).
- [210] G. E. Uhlenbeck and L. S. Ornstein, *Phys. Rev.* **36**, 823 (1930).
- [211] M. C. Wang and G. Uhlenbeck, *Rev. Mod. Phys.* **17**, 323 (1945).
- [212] P. Bleher and A. Its, *Ann. of Math.* **150**, 185 (1999).
- [213] P. Deift, T. Kriecherbauer, K.-R. McLaughlin, S. Venakides, and X. Zhou, *Comm. Pure Appl. Math.* **52**, 1335 (1999).

- [214] P. Deift, T. Kriecherbauer, K.-R. McLaughlin, S. Venakides, and X. Zhou, *Comm. Pure Appl. Math.* **52**, 1491 (1999).
- [215] L. Pastur and M. Shcherbina, *J. Stat. Phys.* **130**, 205 (2008).
- [216] E. Brézin and S. Hikami, *Nucl. Phys. B.* **479**, 697 (1996).
- [217] E. Brézin and S. Hikami, *Phys. Rev. E* **55**, 4067 (1997).
- [218] T. Tao and V. Vu (2010), arXiv:1005.2901.
- [219] L. Erdos, J. Ramirez, B. Schlein, T. Tao, V. Vu, and H.-T. Yau (2009), arXiv:0904.4400.
- [220] L. Erdos, A. Knowles, H.-T. Yau, and J. Yin (2012), arXiv:1212.0164.
- [221] B. V. Gnedenko and A. N. Kolmogorov, Limit Distributions for Sums of Independent Random Variables (Addison-Wesley, Reading, MA, 1954).
- [222] J.-P. Bouchaud and M. Mézard, Lecture Notes on Complex Systems (2013).
- [223] J. P. Nolan, Stable Distribution - Models for Heavy Tailed Data (Birkäuser, Boston, 2010).
- [224] Z. Burda, J. Zurkiewicz, M. A. Nowak, G. Papp, and I. Zahed, *Phys. Rev. E* **75**, 051126 (2007).
- [225] F. L. Metz, I. Neri, and D. Bollé, *Phys. Rev. E* **82**, 021135 (2010).
- [226] I. Neri, F. L. Metz, and D. Bollé, *J. Stat. Mech.* p. P010101 (2010).
- [227] G. Ben Arous and a. Guionnet, *Comm. in Math. Phys.* **278**, 715 (2008).
- [228] G. Biroli, B. J. P., and M. Potters, *Europhys. Lett.* **78**, 78 (2007).
- [229] A. Auffinger, G. Ben Arous, and S. Péché, *Annales de l'IHP: Probabilités et Statistiques* **45**, 589 (2009).
- [230] C. Bordenave and A. Guionnet, *Probab. Theory and Relat. Fields* **157**, 885 (2013).
- [231] P. Cizeau and B. J. P., *J. Phys. A* **26**, L187 (1993).
- [232] L. Levitov, *Europhys. Lett.* **9**, 83 (1989).
- [233] S. Galluccio, B. J. P., and M. Potters, *Physica (Amsterdam)* **259A**, 449 (1998).
- [234] M. Politi, E. Scalas, D. Fulger, and G. G., *Eur. Phys. J. B* **73**, 13 (2010).
- [235] C. Bordenave and A. Guionnet (2016), arXiv:1603.08845.
- [236] K. Janzen, A. Engel, and M. Mézard, *Eur. Phys. Lett.* **89**, 67002 (2010).
- [237] B. Derrida and H. Spohn, *Journal of Statistical Physics* **51**, 817 (1988).

- [238] B. Derrida, *Physica A Statistical Mechanics and its Applications* **163**, 71 (1990).
- [239] B. Derrida, *Phys. Rev. Lett.* **45**, 79 (1980).
- [240] T. Halpin-Healy and Y.-C. Zhang, *Physics reports* **254**, 215 (1995).
- [241] E. Derrida, B. ad Gardner, *J. Phys. C: Solid St. Phys.* **19**, 2253 (1986).
- [242] Y. Y. Atas, E. Bogomolny, O. Giraud, P. Vivo, and E. Vivo (2013), arXiv:1305:7156.
- [243] C. Porter and R. Thomas, *Phys. Rev.* **104**, 483 (1956).
- [244] C. Monthus (2016), arXiv:1606:03241.
- [245] C. Castellani, C. DI Castro, and L. Peliti, *J. Phys. A: Math. Gen.* **19**, L1099.
- [246] J. H. Mard, J. A. Hoyos, E. Miranda, and V. Dobrosavljevic, *Phys. Rev. B* **90**, 125141 (2014).
- [247] H. J. Mard, J. A. Hoyos, E. Miranda, and V. Dobrosavljevic (2014), arXiv:1412:3793.
- [248] D. S. Fisher, *Phys. Rev. Lett.* **69**, 534 (1992).
- [249] F. Igloy and C. Monthus, *Phys. Rep.* **412**, 277 (2005).
- [250] O. Motrunich, S.-C. Mau, D. A. Huse, and D. S. Fischer, *Phys. Rev. B* **61**, 1160 (2000).
- [251] I. A. Kovacs and F. Igloy, *Phys. Rev. B* **83**, 174207 (2011).
- [252] C. Monthus and T. Garel, *Phys. Rev. B* **80**, 024203 (2009).
- [253] H. Aoki, *J. Phys. C* **13**, 3369 (1980).
- [254] R. Landauer, *IBM J. Res. Dev.* **1**, 223 (1957).
- [255] E. N. Economou and C. M. Soukoulis, *Phys. Rev. Lett.* **46**, 618 (1981).
- [256] M. Azbel, *Phys. Lett. A* **78**, 410 (1980).
- [257] D. S. Fischer and L. P. A., *Phys. Rev. B* **23**, 6851 (1981).
- [258] D. C. Langreth and E. Abrahams, *Phys. Rev. B* **24**, 2978 (1981).
- [259] R. Landauer, *Z. Phys. B* **68**, 217 (1987).
- [260] V. Oseledec, *Trans. Moscow. Math. Soc.* **19**, 197 (1968).
- [261] H. Furstenberg, *Trans. Amer. Math. Soc.* **108**, 377 (1963).
- [262] H. Furstenberg and H. Kesten, *Ann. Math. Statist.* **31**, 457 (1960).

- [263] T. C. Halsey, M. H. Jensen, L. P. Kadanoff, I. Procaccia, and B. I. Shraiman, Phys. Rev. A p. 1141 (1985).
- [264] J. J. M. Verbaarschot and M. R. Zirnbauer, J. Phys. A: Math. Gen. **17**, 1093 (1985).
- [265] L. Levitov, Phys. Rev. Lett. **17**, **64**, 547 (1990) 1093 (1985).

# Synthèse en français

L' étude des propriétés de transport des électrons dans les métaux remonte à la théorie classique de Drude, fondée sur l'idée que les électrons libres interagissent avec les ions positifs occupant les sites du réseau. La découverte de la mécanique quantique et du caractère ondulatoire de l'électron a conduit à la révision de ce modèle classique : l'électron est en fait diffracté par un cristal idéal et sa fonction d'onde correspond à une fonction d'onde de Bloch [1]. La résistance électrique, c'est à dire une conductivité finie, apparaît en conséquence de l'interaction des électrons avec les imperfections du cristal. Le modèle classique de Drude peut encore être utilisé, mais dans ce nouveau contexte l'électron n'interagit pas avec les ions mais avec les impuretés. Dans cette description, le libre parcours moyen du mouvement diffusif de l'électron est réduit lorsque la concentration des impuretés augmente et la conductivité diminue donc. La découverte que, au-delà d'une certaine quantité critique du désordre dans le système, la diffusion n'est pas juste réduite mais peut être complètement supprimée est due à Anderson [2] il y a presque soixante ans. Lorsque le désordre dépasse une valeur critique, la fonction d'onde de l'électron cesse d'être délocalisée sur tout l'espace du réseau et devient une onde stationnaire confinée dans l'espace et localisée de façon exponentielle autour d'un centre. L'idée d'Anderson fut révolutionnaire à l'époque et elle a été à l'origine d'une nouvelle vision de la transition métal-isolant : la phase isolante dans le modèle d'Anderson n'est pas due au remplissage des bandes mais à la formation de "pièges" pour l'électron dans le réseau à cause de la présence du désordre.

Comme Anderson l'avait déjà remarqué, la localisation dépend de la dimension du système. À une dimension il a été montré par Mott et Twose que tous les états sont localisés quel que soit l'importance du désordre [3] et ce résultat a été en suite confirmé par d'autres auteurs [4, 5]. La théorie de la localisation a beaucoup progressé pendant les années 70 : le succès des arguments d'échelle dans la description des transitions de phase continues dans d'autres domaines de la physique statistique [81] a suggéré l'utilisation du même type d'arguments dans l'étude de la transition de localisation d'Anderson. D'abord proposée par Wegner [6], la théorie d'échelle a en suite été développée par [7] : un paramètre d'échelle adimensionné qui relie la dépendance de la constante de diffusion de l'électron à la taille du système a été introduit, ainsi que une longueur d'échelle qui tend vers zero lorsqu'on s'approche de la transition a été donc définie. Avec ce type d'arguments il a été établi qu' à une et deux dimensions tous les états sont localisés, tandis qu' en dimension  $d \geq 3$ , une énergie critique qui sépare les états délocalisés des états localisés apparaît dans le spectre. Au-delà d'une valeur critique du désordre, qui dépend de la dimension du système, tous les états deviennent localisés. La théorie d'échelle établit donc que  $d = 2$  est la dimension

critique inférieure. Le comportement en dimension 2 a été débattu pendant longtemps : dans les systèmes à deux dimensions la longueur de localisation est extrêmement grande quand le désordre est peu important, et pour cette raison le système se comporte, dans les simulations numériques et les expériences, comme s’il était délocalisé. L’analyse de systèmes trop petits a donc conduit, dans plusieurs travaux, à l’identification, à tort, d’une transition aussi en dimension  $d = 2$  [71]. En effet, le seul signe de la localisation qui peut être observé en dimension deux dans les expériences et les simulations est dans les anomalies par rapport au comportement classique de la conductivité dues à des processus d’interférences quantiques, et qui sont connues pour être des corrections de *localisation faible*.

La formulation de la théorie d’échelle de la localisation d’Anderson représente un grand pas en avant dans la compréhension de ce phénomène, et elle a reçu des bases solides avec la description de la transition en termes d’un modèle  $\sigma$ -non linéaire, introduit par Wegner [9], qui est cependant insoluble dans la plupart des cas d’intérêt, comme en trois dimensions. Dans sa formulation originale, la moyenne sur le désordre est calculée en utilisant la méthode des répliques [9, 82, 83, 84]. Par la suite, une formulation alternative fondée sur une méthode supersymétrique, qui combine des degrés de liberté fermioniques et bosoniques, a été proposée par Efetov [85, 86, 87]. Au niveau perturbatif les deux techniques sont équivalentes, mais la formulation supersymétrique présente l’avantage de permettre des calculs non-perturbatifs, qui donnent des résultats pour la statistique des niveaux d’énergie et des coefficients des vecteurs propres. Puisque  $d = 2$  est la dimension critique inférieure, il est possible, par une approche du groupe de renormalisation en  $d = 2 + \epsilon$ , d’obtenir une estimation du désordre critique et de l’exposant critique  $\nu$  qui décrit la divergence de la longueur de localisation lorsque l’on se rapproche du point critique [88, 89]. Cependant, ce développement donne des résultats qui sont en accord avec les simulations numériques seulement dans la limite  $\epsilon \rightarrow 0$ . En dimension trois ( $\epsilon = 1$ ), le calcul de  $\nu$  à deux boucles donne le résultat  $\nu \simeq 1$ , tandis que l’estimation des simulations numériques est  $\nu = 1.58 \pm 0.01$  [91, 92, 14, 15, 16, 17, 18, 19, 20, 21]. Le résultat du calcul à quatre boucles s’éloigne encore plus de l’estimation numérique. Cependant, ce développement reste un outil important, qui capture certaines propriétés de la transition, comme la multifractalité des fonctions d’onde au point critique [93, 94].

Presque à la même époque que la première formulation de la théorie de “scaling”, Abou-Chacra, Anderson et Thouless obtinrent un résultat important, en résolvant analytiquement le modèle d’Anderson sur le réseau de Bethe [8]. Le résultat principal de ce travail est une équation auto-consistante qui donne le “mobility edge”, en montrant que les boucles ne sont pas nécessaires pour la localisation de l’électron. L’importance des modèles sur des structures en arbre est généralement liée au fait que, grâce à l’absence de boucles, ces modèles capturent le comportement du système dans la limite de dimension infinie. Pour cette raison, le problème de la localisation d’Anderson sur le réseau de Bethe a été largement étudié dans la littérature: en particulier, le comportement critique a été analysé avec le formalisme supersymétrique, à la fois dans la version “tight-binding” du modèle d’Anderson [30, 31, 32, 33] et dans celle du modèle  $\sigma$  [34, 35, 36, 37].

Le lien entre la localisation d’Anderson et les matrices aléatoires est particulièrement intéressant. Ces dernières constituent un domaine de recherche indépendant

développé depuis les années 50, et qui concerne notamment la caractérisation des propriétés des valeurs propres et des vecteurs propres de différents types de matrices dont les éléments sont extraits au hasard à partir de certaines distributions de probabilité. Après avoir été introduites en tant qu'outil pour l'étude des propriétés spectrales des atomes très lourds [105], les matrices aléatoires ont en suite été utilisées avec succès dans des nombreux contextes, en physique et dans d'autres disciplines [106, 107, 108]. La diffusion dans les graphiques aléatoires [109, 110], les communications sans fil [111], le risque financier [112] ou la biologie [113] en sont des exemples. La plupart des résultats sur les matrices aléatoires ont été fournis pour les trois ensembles gaussiens, qui comprennent les matrices dont les éléments sont des variables aléatoires Gaussiennes indépendantes et identiquement distribuées: en particulier, les matrices symétriques réelles constituent l'ensemble GOE ("Gaussian Orthogonal Ensemble"), les matrices hermitiques complexes l'ensemble GUE ("Gaussian Unitary Ensemble"), tandis que les matrices auto-adjointe de quaternions appartiennent à l'ensemble GSE ("Gaussian Symplectic Ensemble"). Grâce à l'invariance par rotation de la distribution des éléments, des résultats analytiques sont disponibles pour de telles classes de matrices: en particulier la densité des états converge vers la loi du demi-cercle de Wigner et il est possible de calculer analytiquement la fonction de corrélation à deux points des valeurs propres (même si une expression finale n'est disponible que dans le cas GUE). L'expression de cette fonction de corrélation tient compte des fortes corrélations entre les valeurs propres, caractéristique des ensembles gaussiens. De plus, l'invariance par rotation assure également que dans le cas gaussien les vecteurs propres sont délocalisés.

La grande polyvalence de la théorie des matrices aléatoires repose sur la conjecture de l'universalité : les propriétés des ensembles gaussiens sont ainsi supposé valables pour une très grande classe de matrices aléatoires, en particulier pour les matrices de Wigner, qui sont des matrices dont les éléments sont distribués de façon indépendante et identique, avec variance finie. L'idée que seulement quelques caractéristiques déterminent la classe d'universalité, et donc que les propriétés des valeurs propres et des vecteurs propres des matrices aléatoires sont indépendantes d'une distribution de probabilités particulière, permet de relier l'étude des matrices aléatoires à différents problèmes physiques et en particulier au comportement des systèmes électroniques désordonnés. Le lien avec l'étude de la transition de localisation d'Anderson est particulièrement fort, puisque l'Hamiltonien d'Anderson peut être considéré comme une matrice aléatoire, avec une partie hors-diagonale déterministe et une partie aléatoire diagonale: cette matrice appartient à une classe plus générale de matrices aléatoires que l'ensemble de Wigner, composé par des matrices avec des éléments indépendants mais non identiquement distribués, et elles peuvent également être vues comme un opérateur de Schrödinger avec un potentiel aléatoire sur chaque site. Une conjecture d'universalité pour ce type de matrices établit qu'il existe deux régimes différents en fonction de la force du désordre et de l'énergie: dans le régime de fort désordre les vecteurs propres sont localisés et les statistiques des gaps d'énergie sont de type Poisson, tandis que pour désordre suffisamment faible les vecteurs propres sont délocalisés et les statistiques des gaps d'énergie sont les mêmes que pour les matrices GOE. Cette relation entre la localisation d'Anderson et les matrices aléatoires fournit d'une part un outil permettant de calculer numériquement le diagramme de phase [15, 16, 19, 134, 135], en analysant le comportement des statistiques des niveaux

d'énergie, et d'autre part d'établir un lien avec les concepts d'ergodicité et de chaos quantique. En particulier, des conjectures distinctes dues à Barry et Tabor [26] et à Bohigas, Giannoni et Smith [27] établissent respectivement que les systèmes quantiques intégrables ont des statistiques des niveaux d'énergie poissoniennes et que les systèmes ergodiques quantiques non intégrables présentent des distributions des niveaux d'énergie GOE: dans ce contexte la transition de localisation peut être considérée non seulement comme localisation dans l'espace réel mais aussi comme localisation dans l'espace des configurations. Ces conjectures peuvent être comprises dans la limite semi-classique [137, 138]: pour  $\hbar \rightarrow 0$ , les fonctions d'onde d'un système quantique non intégrable s'étendent sur l'ensemble de l'espace de configuration donné par la surface microcanonique alors que pour les systèmes quantiques intégrables ils restent localisés.

Malgré presque soixante ans de recherche intense après les premiers travaux d'Anderson, l'étude de la localisation d'Anderson reste un domaine avec divers problèmes non résolus. En particulier, il n'existe encore (presque) aucune approche analytique disponible loin de la dimension critique inférieure : en effet, le développement perturbatif en dimension  $d + \epsilon$  est capable de capturer les propriétés critiques du phénomène seulement dans une région très proche de la dimension critique inférieure. Les approches analytiques au-delà de cette région proche de  $d = 2$  sont en général difficiles, d'une part à cause de l'absence de petits paramètres, puisque l'énergie critique est du même ordre que la largeur de bande déjà dans les systèmes tridimensionnels. D'autre part, une autre cause de ces difficultés est la nature non conventionnelle du paramètre d'ordre de la transition de localisation, puisqu'il s'agit de la densité locale des états, dont la distribution de probabilité a une décroissance lente dans la phase isolante.

En conséquence de ces difficultés rencontrées dans les approches analytiques, les méthodes numériques sont encore très importantes pour la compréhension du phénomène. La plupart des résultats numériques sont disponibles en trois dimensions: de nombreux auteurs ont analysé des quantités relatives aux propriétés de transport [10, 11, 12, 13, 140, 91, 92] et aux statistiques des niveaux [14, 15, 16, 17, 18, 19] d'énergie et des statistiques des coefficients des vecteurs propres [20, 21, 22, 23, 24, 25]. Le comportement de ces observables est en général étudié pour différentes tailles du système et diverses analyses d'échelle sont effectuées. Pour les systèmes à symétrie orthogonale, l'estimation la plus précise de l'exposant critique  $\nu$  décrivant la divergence de la longueur de localisation est  $\nu = 1,58 \pm 0,01$  [91, 92, 14, 15, 16, 17, 18, 19, 20, 21]. Moins de résultats sont disponibles dans des dimensions plus élevées: en particulier, peu de résultats récents en dimension 4 et 5 [143] étudient seulement les propriétés de transport. Très peu de résultats sont connus sur les statistiques des niveaux d'énergie au-dessus de la dimension trois [144], et aucun résultat n'est disponible sur les propriétés de transport au-dessus de  $d = 5$ . La raison en est l'augmentation rapide des temps de calcul des algorithmes avec la taille du système, qui est responsable des limitations sévères sur les tailles des systèmes qui peuvent être simulés lorsque la dimension est grande aimentée.

Pour toutes ces raisons, la détermination des propriétés critiques en grande dimension reste un problème ouvert, ainsi que l'existence d'une dimension critique supérieure  $d_u$ . À ce propos, plusieurs observations semblent indiquer que  $d_u$  est peut être infinie [166, 167, 144, 168], mais d'autres hypothèse proposent  $d_u = 4, 6$  et  $8$  [169, 170, 171, 172, 173, 174, 175].

Une autre question importante est la relation avec la limite de dimension infinie, correspondant à la localisation d'Anderson sur des structures en arbre [8], et à d'autres modèles de matrices aléatoires avec interactions à longue portée, comme les matrices de Lévy [183], qui sont des matrices avec des éléments distribués de façon identique et indépendante avec une loi de probabilité de Lévy (décroissante en loi de puissance). Comme nous l'avons déjà mentionné, le comportement du modèle d'Anderson sur des structures en arbre a été largement étudié dans la littérature et constitue l'un des rares modèles pour lesquels des résultats analytiques peuvent être fournis [34, 35, 36, 37, 30]. Les propriétés de la phase délocalisée de ce type de structure sont toutefois très inhabituelles: dans les simulations numériques, le système présente un comportement fortement non-ergodique dans une grande région, même loin du point critique. Cet effet, observé pour la première fois dans la réf. [39], où l'analyse se concentre principalement sur les statistiques des niveaux d'énergie, a ensuite été observé dans des travaux ultérieurs analysant les statistiques des fonctions d'onde dans la phase délocalisée [40, 41]. Le comportement inhabituel de ces observables rend l'analyse des données non triviale et a suggéré l'existence d'une phase intermédiaire, délocalisée mais non ergodique. Il s'avère cependant difficile d'établir si un tel comportement inhabituel est le signe d'une transition de phase intermédiaire réelle. Cela pourrait être plutôt la conséquence d'effets très importants de taille finie qui généreraient une grande région de "crossover" dans laquelle le volume de corrélation est plus grand que les tailles du système accessibles. De plus, l'existence d'une phase intermédiaire délocalisée non ergodique serait en conflit avec les résultats qui s'appuient sur le formalisme supersymétrique et qui établissent que la phase délocalisée est ergodique.

Le comportement inhabituel observé dans la phase délocalisée des modèles en arbre semble être présent également dans d'autres modèles de matrices aléatoires avec interactions à longue portée comme les matrices de Lévy, pour lesquelles la question de l'existence d'une phase mixte intermédiaire a été ouverte depuis le travail fondateur de Cizeau et Bouchaud [38]. L'étude des matrices de Lévy est un sujet mathématique intéressant: elles constituent une classe d'universalité plus grande que celle qui est habituellement traitée dans la théorie des matrices aléatoires. De plus, puisqu'une grande variété de distributions en physique et dans d'autres disciplines présentent des décroissances en loi de puissance, elles apparaissent dans des contextes différents, qui s'étendent des modèles de verres de spins avec des interactions RKKY [231] et des systèmes électroniques désordonnés [232] à l'étude des corrélations dans des grands ensembles de données [234]. Les matrices de Lévy présentent un comportement plus riche que les matrices habituellement considérées dans la théorie des matrices aléatoires: l'une de leurs caractéristiques les plus intéressantes, qui les relie à l'étude de la localisation d'Anderson, est la présence d'une énergie critique dans le spectre de leurs valeurs propres, qui sépare les états délocalisés de ceux localisés. D'une part cet ensemble de matrices présente une structure complètement connectée qui permet un traitement analytique. D'autre part, en raison de la loi à décroissance lente des éléments, les matrices de Lévy se comportent comme des matrices creuses, et elles peuvent en effet être considérées comme la limite de très grande connectivité d'une structure en arbre (plus précisément un graphe de Erdős- Rényi) dans un bain constitué de petits termes de type gaussien. La similarité avec le comportement du modèle d'Anderson sur une structure en arbre apparaît également dans les caractéristiques inhabituelles de la

phase délocalisée: dans les matrices de Lévy, comme mentionné ci-dessus, le problème de l'existence d'une phase intermédiaire non-ergodique était ouvert depuis le premier travail sur le sujet [38], et c'est là une des raisons qui nous ont poussés à étudier ce type de modèle.

Les modèles qui sont représentatifs du comportement en dimension très grande de la localisation d'Anderson, comme les structures en arbre ou les matrices de Lévy, ont reçu une attention renouvelée ces dernières années en raison de leur relation avec le phénomène connu sous le nom de "Many Body Localization", une transition de phase qui a lieu quand on tient compte des interactions entre électrons: en effet, Basko, Aleiner et Altshuler [48] ont montré que si la fonction d'onde de l'électron est localisée au niveau de la surface de Fermi, et si la température est inférieure à une certaine température critique  $T_c$ , alors l'interaction électron-électron ne peut à elle seule restaurer une conductivité finie et le système reste isolant. En revanche, au-delà de la température critique  $T_c$ , la conductivité est finie. Exactement à  $T_c$ , le système subit une transition de phase, appelée "Many Body Localization" (MBL). Pour décrire ce phénomène, la description de la transition en termes de rupture de l'ergodicité est particulièrement significative : en effet, il s'agit d'un nouveau type de transition de phase entre une phase ergodique à haute température, et une phase non ergodique à basse température (un verre purement quantique), dans laquelle les états propres conservent une certaine mémoire des conditions initiales locales. Ce phénomène se produit dans des systèmes quantiques isolés en interaction, et en particulier pour des électrons désordonnés, mais a également été étudié de manière indépendante dans [29] pour expliquer la transition ergodique quantique de molécules complexes. La MBL peut être vue comme une localisation dans l'espace de Fock des déterminants de Slater, qui joue le rôle de sites de réseau dans un modèle d'Anderson "tight-binding" à une particule. Le problème d'un grand nombre  $N$  de particules interagissant sur un réseau en dimension finie est donc interprété comme un problème de localisation d'une particule sur un réseau de très grande dimension. L'étude de la seule localisation d'Anderson à une particule en grande dimension se révèle donc particulièrement intéressante également par rapport à la MBL. Dans les systèmes présentant une transition MBL, l'existence d'une phase non-ergodique délocalisée intermédiaire a été suggérée [47]: dans le langage de la MBL, c'est une phase dans laquelle la thermalisation et l'ergodicité ne sont possibles que dans certaines sous-régions de l'espace des configurations.

La question de l'existence d'une phase intermédiaire délocalisée et non ergodique pour le modèle d'Anderson en grande dimension est un problème largement débattu qui a été à l'origine de nombreuses discussions au cours des dernières années et qui reste encore un sujet de recherche actif. De plus, l'origine de ce comportement non-ergodique dans une région d'une telle taille dans la phase délocalisée tel qu'il a été observé dans les simulations numériques, reste inconnue.

L'objectif de cette thèse est d'investiguer le comportement de la localisation d'Anderson en grande dimension. Dans la première partie nous étudions les matrices de Lévy. Nous établissons l'équation qui détermine la transition de localisation et nous obtenons le diagramme de phase. Nous investiguons en suite le comportement inhabituel de la phase délocalisée. Avec des arguments basés sur la méthode supersymétrique et sur le mouvement brownien de Dyson, nous montrons que la distribution des écarts entre valeurs propres est la même que dans le cas GOE dans toute la phase délocalisée et

elle est de type Poisson dans la phase localisée. Notre analyse numérique confirme ce résultat, valable dans la limite thermodynamique, et fournit des informations sur le comportement d'autres quantités comme la statistique des vecteurs propres. De plus, les résultats numériques révèlent que l'échelle caractéristique qui gouverne les effets de taille finie diverge beaucoup plus vite qu'une loi de puissance quand on s'approche de la transition, et elle est déjà très grande loin du point critique.

Dans la seconde partie nous étudions numériquement le comportement du modèle d'Anderson en dimension de 3 à 6 en utilisant la méthode de la matrice de transfert, la diagonalisation exacte, et une technique approximée de Groupe de Renormalisation pour fort désordre. Les résultats suggèrent que la dimension critique supérieure de la localisation d'Anderson est infinie. Nous discutons aussi les implications possibles de ce scénario sur le comportement inhabituel de la phase délocalisée des modèles représentatifs de la limite de dimension infinie, comme les matrices de Lévy et le modèle d'Anderson sur des structures en arbre.



**Titre : Localisation d'Anderson sur des réseaux en grande dimension**

**Mots-clés :** Transition de Localisation, Matrices aléatoires, Transitions de phase, Matière condensée, Systèmes désordonnés.

**Résumé :** L'objectif de cette thèse est d'investiguer le comportement de la localisation d'Anderson en grande dimension. Dans la première partie nous étudions les Matrices de Lévy, un modèle de matrices aléatoires avec interactions à longue portée qui présente une forte analogie avec le problème de la localisation d'Anderson sur des structures en arbre, représentatives du comportement en dimension infinie. Nous établissons l'équation qui détermine la transition de localisation et nous obtenons le diagramme de phase. Nous investiguons en suite le comportement inhabituel de la phase délocalisée. Avec des arguments basés sur la méthode supersymétrique et sur le mouvement brownien de Dyson, nous montrons que la distribution des écarts entre valeurs propres est la même que dans le cas GOE dans toute la phase délocalisée et elle est de type Poisson dans la phase localisée. Notre analyse numérique confirme ce résultat, valable dans la limite thermodynamique, et fournit des informations sur le comportement d'autres quantités comme la statistique des vecteurs propres. De plus, les résultats numériques révèlent que l'échelle caractéristique qui gouverne les effets de taille finie diverge beaucoup plus vite qu'une loi de puissance quand on s'approche de la transition, et elle est déjà très grande loin du point critique.

Dans la seconde partie nous étudions numériquement le comportement du modèle d'Anderson en dimension de 3 à 6 en utilisant la méthode de la matrice de transfert, la diagonalisation exacte, et une technique approximée de Groupe de Renormalisation pour fort désordre. Les résultats suggèrent que la dimension critique supérieure de la localisation d'Anderson est infinie. Nous discutons aussi les implications possibles de ce scénario sur le comportement inhabituel de la phase délocalisée des modèles représentatifs de la limite de dimension infinie, comme les matrices de Lévy et le modèle d'Anderson sur des structures en arbre.



**Title :** Anderson Localization in high dimensional lattices

**Keywords :** Localization Transition, Random Matrices, Phase Transitions, Condensed Matter, Disordered Systems.

**Abstract :** In this thesis, we investigate the behavior of Anderson Localization in high dimension. In the first part we study Lévy Matrices (LMs), a Random Matrix model with long-range hopping presenting strong analogy with the problem of Anderson Localization on tree-like structure, representative of the limit of infinite dimensionality. We establish the equation determining the localization transition and obtain the phase diagram. We investigate then the unusual behavior of the delocalized phase. Using arguments based on supersymmetric field theory and Dyson Brownian motion we show that the eigenvalue statistics is the same one as of the Gaussian orthogonal ensemble in the whole delocalized phase and is Poisson-like in the localized phase. Our numerical analysis confirms this result, valid in the limit of infinitely large LMs, and provides information on the behavior of other observables like the wave-functions statistics. At the same time, numerical results also reveal that the characteristic scale governing finite size effects diverges much faster than a power law approaching the transition and is already very large far from it. This leads to a very wide crossover region in which the system looks as if it were in a mixed phase.

In the second part we study numerically the behavior of the Anderson Model in dimension from 3 to 6 through exact diagonalization, Transfer Matrix method and an approximate Strong Disorder Renormalization Group technique. The results we find suggest that the upper critical dimension of Anderson Localization is infinite. Finally, we discuss the possible implications of this scenario on the anomalous behavior of the delocalized phase of models representative of the limit of infinite dimension, like Lévy Matrices and the Anderson model on tree-like structures.

